THE UNIVERSITY OF ASTON IN BIRMINGHAM.

A STUDY OF ELECTROSTATIC CHARGED PARTICLE OSCILLATORS.

Thesis submitted for the degree of

DOCTOR OF PHILOSOPHY

by

Gordon James Rushton.

Department of Physics.

May 1972.

Synopsis.

There are various low pressure devices that use a combination of electrostatic and magnetic fields or electrostatic fields alone, in order to produce long electron trajectories and hence efficient gas phase ionisation. A critical review of these is given in the first chapter.

The purpose of this work was to study the properties of the twin wire electrostatic charged particle oscillator, which is a new device that is capable of producing extremely long electron path lengths. However, previous work had shown that a self-maintained discharge cannot be operated below about 10^{-6} torr. Experiments are described which show how the performance of the oscillator is affected by such factors as anode diameter, anode separation and cathode material. The influence of an externally applied magnetic field upon the performance of the oscillator was also investigated and it is now believed that the low pressure limit of the device is due to the influence of the earth's magnetic field. At higher pressures, the presence of the earth's magnetic field is unimportant and the use of the oscillator as a low pressure ion source is discussed. This is shown to be particularly suitable for ion etching of both electrically conducting and non-conducting materials.

In order to extend the low pressure limit of the oscillator, electrons were injected into the device using a thermionic filament. With this form of electron injection, it was found that there are two principal modes of operation, the "orbiting mode" and the "oscillating mode". Both modes give efficient gas phase ionisation. This method of electron injection into the orbiting mode has been utilised to produce a new high sensitivity thermionic ionisation gauge, which has a low pressure limit due to X-rays in the region of 10^{-12} torr.

Index.

Chapter 1.	The Production of Efficient Gas Phase Ionisation.	Page.
1.1.	Introduction.	1.
1.2.	Use of combined electrostatic and magnetic fields.	1.
1.2.1.	Cold cathode devices.	1.
1.2.2.	Thermionic cathode devices.	7.
1.3.	Use of purely electrostatic fields.	9.
1.3.1.	Low sensitivity electrostatic devices.	9.
1.3.2.	The orbitron.	11.
1.3.3.	The twin wire electrostatic charged particle oscillator.	17.
Chapter 2.	Investigation of the Thermionic Twin Wire Oscillator.	
2.1.	Introduction.	25.
2.2.	Experimental equipment.	25.
2.2.1.	Design of the experimental oscillator.	25.
2.2.2.	The electrical circuit.	26.
2.2.3.	The high vacuum system.	27.
2.3.	Effects of changes in the collector electrode geometry.	28.
2.4.	The orbiting electron theory.	29.
2.5.	Modes of operation in the thermionic twin wire oscillator.	31.
2.6.	Discussion.	36.

Chapter 3. The Electron-orbit Ionisation Gauge.

3.1. Introduction. 38.

3.2. The electron-orbit ionisation gauge in high vacuum. 38.

3.2.1. Description of the gauge. 38.

3.2.2. Experimental results. 39.

3.2.3. Variation of the length of the gauge and the position of the filament. 41.

3.2.4. Ion losses. 42.

3.3. The electron-orbit ionisation gauge in ultra high vacuum. 43.

3.3.1. Description of the gauge. 43.

3.3.2. The ultra high vacuum system. 44.

3.3.3. Experimental results and discussion. 44.

3.3.4. Reduction of the electron space-charge. 48.

3.4. Discussion. 52.

Chapter 4. Investigation of the Cold Cathode Twin Wire Oscillator.

4.1. Introduction. 54.

4.2. Experimental equipment. 54.

4.2.1. Design of the oscillator. 54.

4.2.2. The electrical circuit. 54.

4.3. The current - voltage characteristics. 55.

4.4. The effects of variation of anode separation and anode diameter. 57.

4.5. The influence of electron yield from the collector electrode. 61.

4.6. Discussion. 62.

Chapter 5. The Influence of Magnetic Fields upon the Performance of the Oscillators.

5.1.	Introduction.	63.
5.2.	The influence of magnetic fields on the cold cathode twin wire oscillator.	63.
5.3.	The influence of magnetic fields on the thermionic oscillators.	68.
5.4.	Discussion.	69.

Chapter 6. The Improved Ion Source.

6.1.	Introduction.	72.
6.2.	Description and performance of the improved ion source.	72.
6.3.	The radial distribution of positive ions emerging from the discharge.	74.
6.4.	Current density of the ion beam.	75.
6.5.	Energy distribution of the ion beam.	77.
6.6.	Examples of ion etching using the improved ion source.	81.
6.7.	Small volume ion sources.	82.
6.8.	Multiple and wide beam ion sources.	83.
6.9.	Discussion.	85.

Chapter 7. Conclusions and Suggestions for Future Work. 87.

Appendices. 1 - 6.

List of Figures.

List of Symbols.

References.

CHAPTER 1.

THE PRODUCTION OF EFFICIENT GAS PHASE IONISATION.

1.1. Introduction.

The main secondary process in vacuum devices such as ionisation gauges, ion pumps and ion sources is the ionisation of neutral gas molecules by electron bombardment. These primary electrons may originate from a thermionic source or from background radiation. The efficiency of the ionisation process depends upon a number of factors such as the energy of the primary electrons and the nature of the gas molecules. However, the number of ions produced per electron is also dependent upon the total path length of the electron. In many applications it is desirable to have this as large as possible and this is done by constraining the electrons in either an electrostatic field alone or in a combination of electrostatic and magnetic fields. This increase in efficiency of the ionisation process enables vacuum ionisation devices to be usefully operated at lower pressures. The purpose of this chapter is to review the methods of producing these long electron path lengths.

1.2. Use of combined electrostatic and magnetic fields.

1.2.1. Cold cathode devices.

In order that a cold cathode discharge may be self-maintained, a new electron must be introduced into the discharge when any electron is captured at the anode. This new electron can be produced by one of several mechanisms, such as by ejection from the cathode surface due to positive ion bombardment or by ionising collisions of primary electrons with neutral gas molecules producing secondary electrons

from the gas phase. For either of these processes to occur, the production of positive ions either before or after the event is required. Photons produced from excited molecules returning to lower energy states can provide photo-electric emission from the cathode surface when they fall upon it. The photo-ionisation of neutral gas molecules can be ignored at low pressures due to the small ionisation cross-section involved. Electron emission from the cathode can also occur due to the arrival of metastable atoms at the cathode surface. If the total average path length of the electrons, from their introduction into the discharge to their arrival at the anode, is less than the mean free path between ionising collisions with neutral gas molecules at that pressure, then the discharge will eventually cease. With normal cold cathode glow discharges, this occurs at pressures in the region of 10^{-3}torr. The production of a cold cathode discharge at pressures below about 10^{-3}torr was first accomplished by Penning[1].

Penning[1] used a strong magnetic field to extend the total electron path lengths between cathode and anode and so increased the ionisation current to a measurable level at pressures below 10^{-3}torr. The anode was in the form of a loop and two metal cathode plates were positioned above and below the anode as illustrated in Figure 1.1.

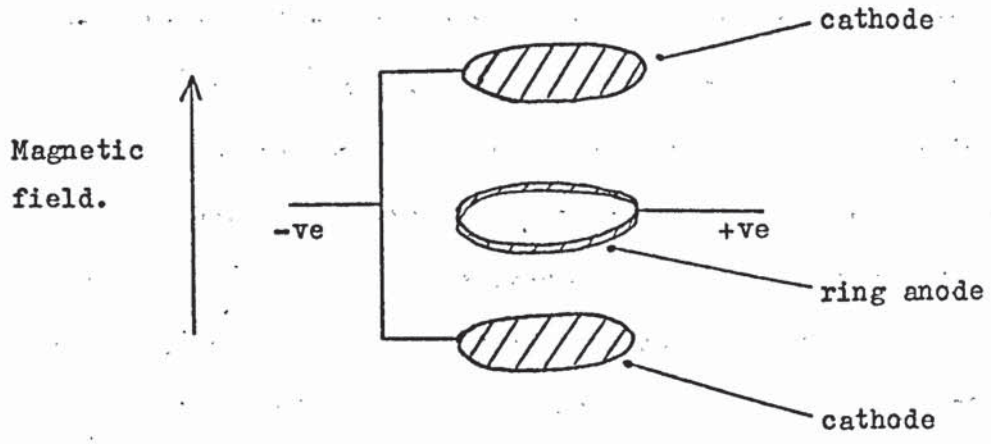

Figure 1.1. Electrode structure for the Penning discharge.

The magnetic field is typically of 0.05 to 0.15 webers m^{-2} and a voltage of about +2 kV is applied to the anode. Secondary electrons produced at either of the cathodes by positive ion bombardment, are trapped by the magnetic field lines and so oscillate through the ring anode rather than travel directly to it. The electron paths are helical due to the action of the magnetic field and the electrons execute extremely long total path lengths, travelling through the ring anode several times before being collected by the anode. Thus, the discharge can be self-maintained down to pressures of about 10^{-5} to 10^{-6} torr, which is two or three orders less than with no magnetic field. In a later development by Penning and Nienhuis[2], the ring anode was replaced by a cylindrical anode which extended almost to the cathodes. Thus, the discharge was virtually enclosed in a box which not only extended the discharge to below 10^{-7} torr but removed some of the discharge instabilities often observed with the ring anode. Due to their large mass compared with the electrons, the positive ions formed in the discharge are relatively unaffected by the presence of the magnetic field and so travel directly to the cathodes.

As the discharge current between the electrodes in a gaseous discharge is dependent upon pressure, it can be used as a measure of the pressure inside a vacuum system. The basic Penning discharge has been successfully used for many years as a vacuum gauge in the pressure range of 10^{-3} to 10^{-6} torr. With the modified cylindrical anode as described by Penning and Nienhuis[2], the discharge can be maintained to very low pressures, but there may be a considerable delay before the discharge strikes. This can be overcome in the manner described by McIlwraith[3], in which a hot filament is used to initiate the discharge. This is the basis of the cold cathode Trigger gauge as investigated by for example, Chernatony and Crawley[4]. They reported sensitivities of 1 amp $torr^{-1}$ for such a gauge.

Improved low pressure characteristics are obtained in the magnetron cold cathode ionisation gauge (Redhead[5]) and also in the inverted magnetron cold cathode ionisation gauge (Hobson and Redhead[6]). A cutaway drawing of the inverted magnetron gauge is shown in Figure 1.2.

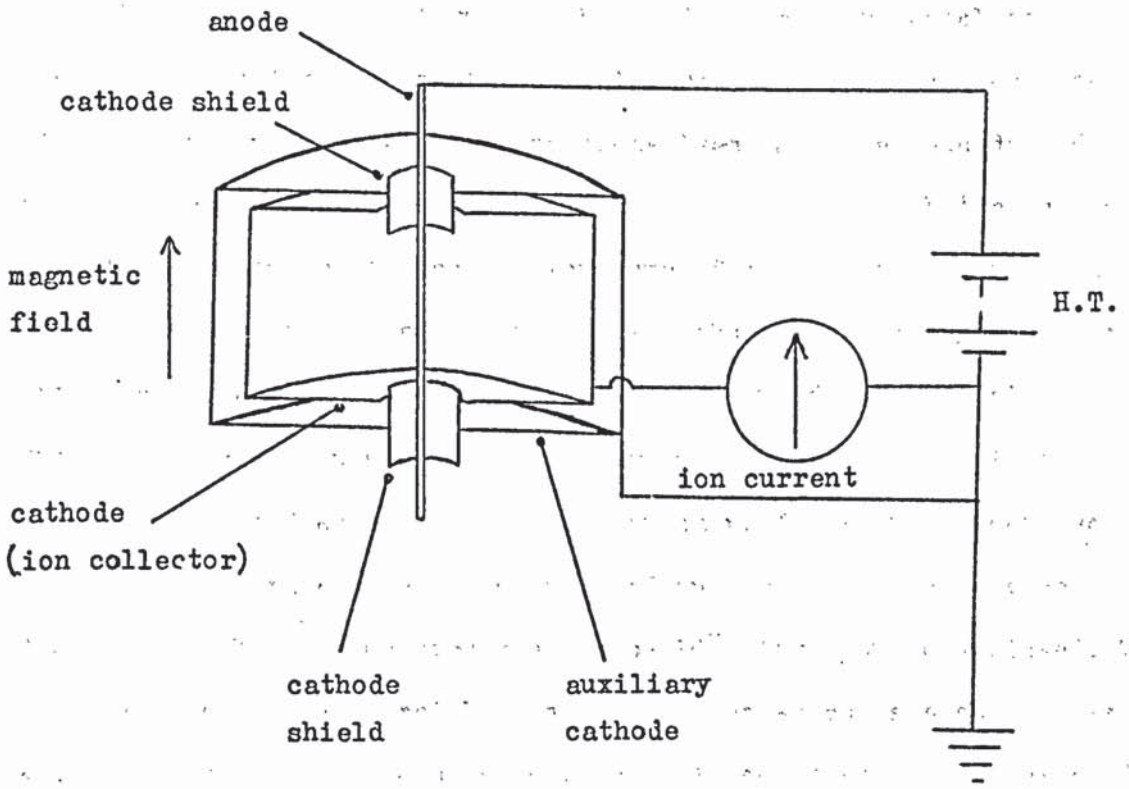

Figure 1.2. Cutaway diagram of the inverted magnetron gauge.

The cathode is a short cylinder of about 3 cm in diameter with its axis parallel to a magnetic field of about 0.2 webers m^{-2}. The anode is a 1 mm diameter rod passing axially through holes in the cathode and is at about +6 kV with respect to the cathode. An auxiliary cathode surrounds the ion collecting cathode and it is grounded directly. This acts as an electrostatic shield against external disturbances. The cathode shield cylinders extend up into the ion collecting cathode and prevent the end-plates of the ion collector from being exposed to high electric fields.

These shield cylinders also provide the field emission current to initiate the discharge at low pressures. The gauge operates on the basic Penning principle and a sensitivity of 1 amp torr^{-1} was reported by Hobson and Redhead[6], giving it a useful operating range from about 10^{-3} torr down to the region of 10^{-12} torr.

The positive ions formed within a discharge are accelerated towards the cathode by the electrostatic field. Due to their acquired kinetic energy, the ions are able to bury themselves into the cathode and so be removed from the gas phase. Thus, a discharge will exhibit a pumping action which can be utilised in ion pumps for producing ultra high vacuum. Obviously long electron path lengths are necessary in order to obtain a large amount of ionisation to give an adequate pumping speed. The Penning and Nienhuis[2] electrode arrangement with the cylindrical anode can be used as a simple diode ion pump. In order to increase the pumping speed, many such cells are used in a single pump body as described by Hall[7], and pressures below 10^{-9} torr can be achieved. The cathodes are made of a metal such as titanium which is a chemically active material known as a getter. The cathode material is sputtered onto the pump walls due to the positive ion bombardment of the cathode surface. Chemically active gases readily combine with this sputtered material and thus are removed from the gas phase. The inert gases will not combine with this sputtered material and can only be removed from the gas phase by ion burial into the cathode. The main disadvantage of the diode sputter-ion pump is that the removal of cathode material by positive ion bombardment may release gas molecules that have been buried into the cathode previously. Many attempts have been made to overcome this instability in ion pumps, amongst them being the slotted cathode diode ion pump (Jepson et al[8]) and the triode ion pump (Brubaker[9]). More recently, the magnetron ion gauge principle as described by Redhead[5] has been applied to an ion pump (Andrew et al[10]) which gives

improved inert gas pumping, as the inert gas ions are pumped at regions in which there is less bombardment by energetic ions.

At pressures in the region of 10^{-1} torr, D.C. glow discharges have been used as ion sources for surface etching and thinning of metallographic specimens with argon ions. With non-conducting specimens, a charge build-up occurs on the specimen surface when using a D.C. glow discharge. In order to overcome this, R.F. discharges are often used to etch non-conducting materials such as biological specimens as described by Stuart et al [11]. However, most of these ion sources consume a considerable amount of gas and power and do not produce a directed beam of ions. They also have to be run at comparatively high pressures and this can lead to surface contamination. In differentially pumped ion sources, an intense discharge can be produced in a constricted region as described by Lamar et al[12]. The discharge region is a region of relatively high pressure and the ions produced are allowed to exit through a small aperture into an adjacent chamber containing the specimen. This specimen chamber is maintained at a relatively low pressure in the region of 10^{-5} torr. To accomplish this, large pumping systems are required in order to maintain the specimen chamber at this pressure. More efficient ion sources in which longer electron path lengths are obtained, can be operated at lower pressures. These use smaller quantities of gas and can be used in conjunction with much smaller pumping systems. The Penning discharge can be used as an ion source by allowing ions formed in the cold cathode discharge to pass through an aperture in one of the cathodes. Such an ion source in one of its simplest forms is described by Barnett et al[13]. Ion beam current densities of 100 $\mu A\ cm^{-2}$ or more can be easily achieved from the Penning ion source making it suitable for the ion etching and thinning of specimens.

1.2.2. Thermionic cathode devices.

The use of a magnetic field to extend electron path lengths can be applied to discharge devices which have a thermionic source of electrons. With a thermionic cathode, there is a continual supply of electrons and it no longer depends upon ion bombardment of the cathode surface to liberate electrons. Houston[14] added a short tungsten filament just in front of one of the cathode plates in the Penning and Nienhuis[2] electrode structure. With an applied potential difference of 1 kV and a magnetic field of 0.17 webers m^{-2}, stable operation was obtained down to pressures below 10^{-8} torr with an emission current from the filament of only 10^{-7} amps.

When operating an ionisation gauge with constant electron emission from a thermionic cathode, there is a low pressure limit which is set by the existence of a residual current to the ion collector which is independent of pressure. This residual current is due to soft X-rays which are generated by the low energy electrons striking the anode. These X-rays produce photo-electric emission when they reach the ion collector and the resulting loss of electrons cannot be distinguished from the collection of positive ions. Hence, this gives rise to a pressure independent residual current and the low pressure limit is when this residual current is equal to the true ion current. An anomalous ion current can be caused by the electron bombardment of the gauge anode. Adsorbed gas molecules can be desorbed from the anode as ions and so give rise to an ion current that is dependent upon the cleanliness of the anode. Increasing the gauge sensitivity by increasing the electron path lengths in the discharge, may reduce the X-ray limit due to the increased number of ions produced at a given electron emission. Furthermore, the electron emission may be reduced when the sensitivity is increased, so reducing the ion desorption, outgassing from the gauge electrodes and the degree of dissociation of the gas molecules at the hot filament.

In the Lafferty gauge[15], the extended electron path lengths are achieved by use of a magnetic field as shown in Figure 1.3.

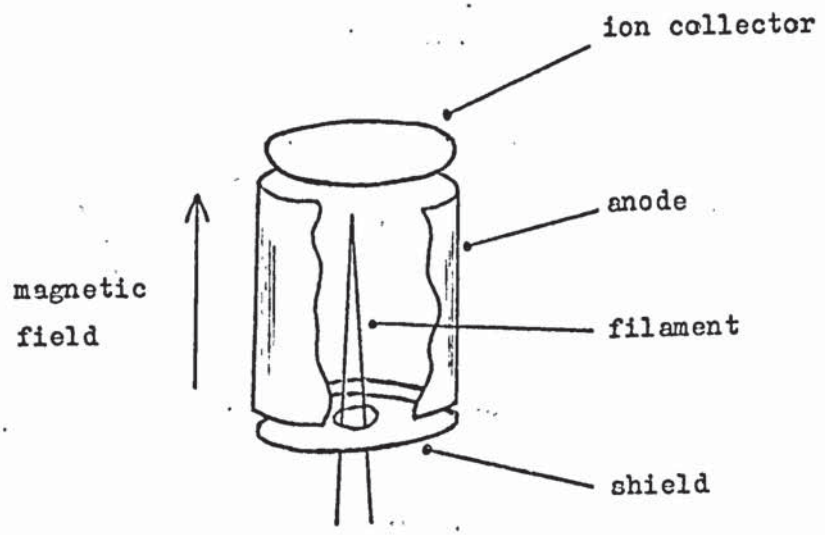

Figure 1.3. The Lafferty gauge.

In this hot cathode magnetron ionisation gauge, a hairpin thermionic filament is mounted along the axis of a cylindrical anode. Two end-plates for the anode are used which are maintained at negative potentials with respect to the filament. One end-plate acts as the ion collector and the other as a shield. The anode is maintained at +300 volts, the ion collector at -45 volts and the shield at -10 volts with respect to the filament, together with a magnetic field of 0.025 webers m^{-2}. The electrons emitted from the filament spiral around it due to the axial magnetic field and are eventually collected by the anode. In this gauge the X-ray limit is reduced to about 5×10^{-14} torr. A very low level of electron emission in the range of 10^{-6} to 10^{-9} amps is used to ensure stable operation and also to prevent swamping of the ion current by the random high energy electrons which are generated in this device.

In the Nielsen[16] ion source, the discharge is formed using a hot

filament as a cathode and a cylindrical anode as shown in Figure 1.4.

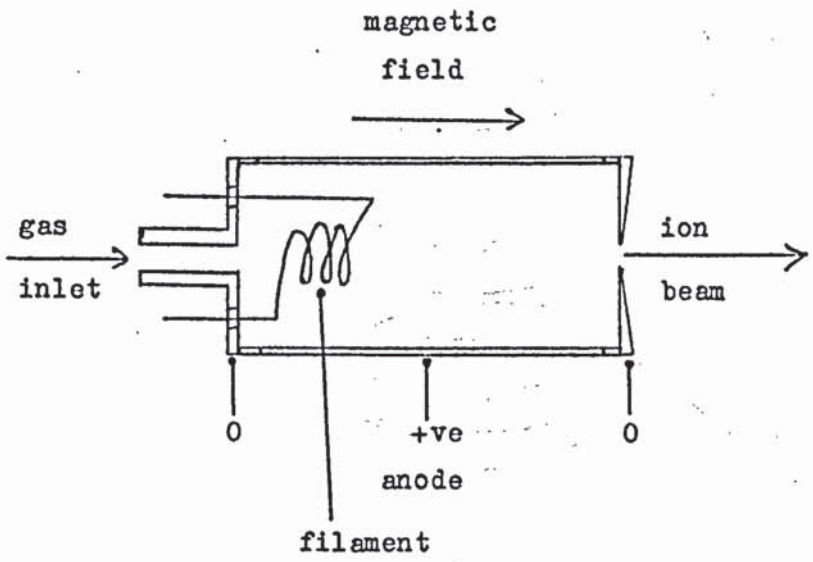

Figure 1.4. The Nielsen ion source.

An axial magnetic field is used to increase the electron path lengths before they reach the anode, in a similar manner to the cold cathode Penning[1] discharge. The total discharge current may be as high as a few amps, making this type of ion source particularly suitable for the doping of semiconductors by ion implantation.

1.3. Use of purely electrostatic fields.

1.3.1. Low sensitivity electrostatic devices.

Various low sensitivity ionisation devices can be used in ultra high vacuum by using a source of electrons supplied from a thermionic filament. The Bayard - Alpert ionisation gauge[17] is a purely electrostatic low sensitivity pressure measuring device. The low pressure limit due to X-rays is generally about 2×10^{-10} torr due to the very small solid angle subtended to the X-rays by the thin wire collector

electrode as illustrated in Figure 1.5.

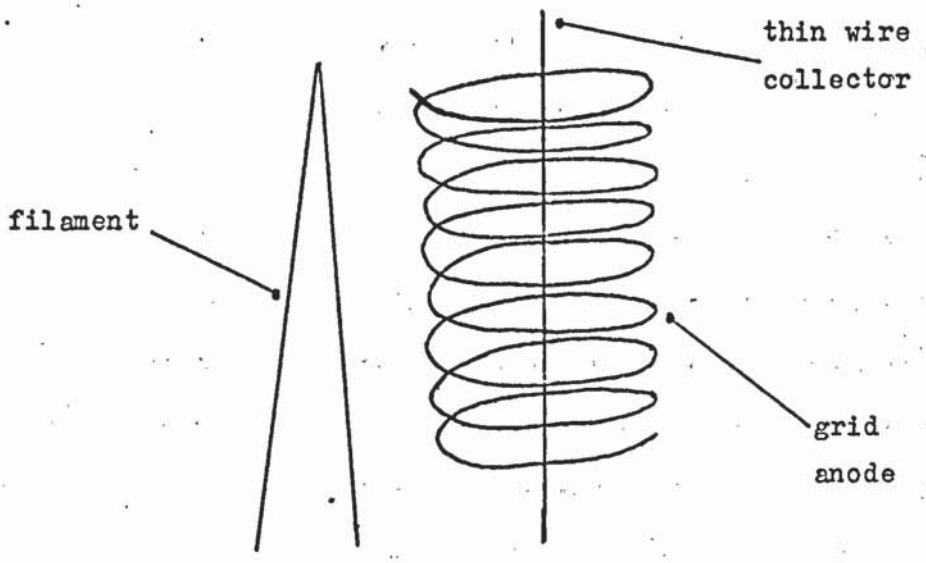

Figure 1.5. The Bayard - Alpert ionisation gauge.

The grid anode is maintained at about +150 volts with respect to the filament and the electrons emitted from the filament oscillate through the grid a number of times giving a total electron path length of a few centimetres, which in turn gives a sensitivity of about 10 $torr^{-1}$. Here the sensitivity S, for a gauge with a thermionic cathode is defined as :-

$$S = \frac{i_p}{i_e} \cdot \frac{1}{p} \quad torr^{-1} \qquad \ldots\ldots\ldots\ldots (1)$$

where i_p is the positive ion current, i_e is the electron current and p is the total gas pressure. In order to obtain a measurable ion current with this low sensitivity, the electron emission current has to be in the region of 100 μA to 10 mA depending upon the operating pressure. Due to this relatively high electron current, ion desorption effects can be very significant if the gauge head is not adequately outgassed.

Several attempts have been made to reduce the low pressure limit due to X-rays of the Bayard - Alpert gauge. One way of doing this is to measure the residual current due to the X-rays. In the modulator gauge described by Redhead[18], an extra collector electrode, called a modulator, is inserted into the Bayard - Alpert type gauge head. By switching the modulator from grid to collector potential, the ion current can be altered without any change in the residual current, so allowing the residual current to be determined. A method of operating a hot cathode ionisation gauge to eliminate the X-ray effect was introduced by Schuemann[19]. Positive ions are extracted from the ionisation region and are collected by an ion collector electrode which is hidden from the direct line of sight of the X-rays. An additional suppressor electrode is located near the ion collector to prevent photo-electrons from leaving the collector electrode.

An electrostatic ion source based on the Bayard - Alpert type ionisation gauge has been described by Khan and Schroeer[20]. This ion gun produces a total beam current of about .1 μA of argon ions with a current density of about 1 to 5 μA cm^{-2} at an argon pressure of 5×10^{-6} torr. Thus, no differentially pumped system is needed to keep the target at a relatively low pressure.

However, extremely long path lengths can be achieved by constraining electrons in electrostatic fields alone. Two such purely electrostatic high sensitivity devices are the orbitron and the twin wire electrostatic charged particle oscillator. As it is these type of high sensitivity devices that are investigated in this work, they will be discussed in some detail in the next two sections.

1.3.2. The orbitron.

In 1962, Gabor[21] described a radial field electrostatic device which gave very long total electron path lengths without the use

of a magnetic field. The device was originally designed as an electrostatic ion pump with a wire anode positioned along the axis of an outer cylindrical ion collector as illustrated in Figure 1.6.

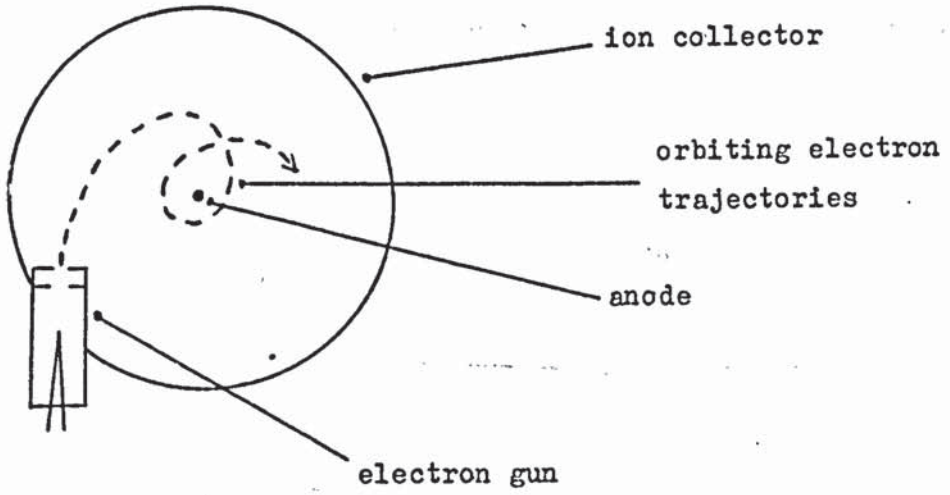

Figure 1.6. The radial field electrostatic ion pump. (After Gabor[21]).

Electrons were injected into the device from an electron gun with sufficient angular momentum to perform orbiting trajectories around the central anode. This enabled them to execute extremely long path lengths within the device before being collected by the anode. In this way, efficient gas phase ionisation occurred and the positive ions produced moved to the collector which was coated with a gettering material.

Herb et al[22] in 1963 and Mourad et al[23] in 1964, reported upon investigations carried out on the orbitron ionisation gauge which is a development of the Gabor[21] principle. The orbitron employs a hot filament at one end of the device to inject the electrons into orbiting trajectories about the central anode. The essential features of the orbitron are illustrated in Figure 1.7. The filament is mounted on two supports, with one of these supports acting as a shield post to prevent electrons emitted from the filament going straight to the anode. Applying a suitable

positive bias voltage V_B to the filament with respect to the collector electrode, creates a field distortion that ejects the electrons into orbits about the anode which is held at several hundred volts above earth potential. Again very long electron path lengths are obtained and the positive ions formed by electron collisions with neutral gas molecules, travel to the collector electrode which is maintained at earth potential.

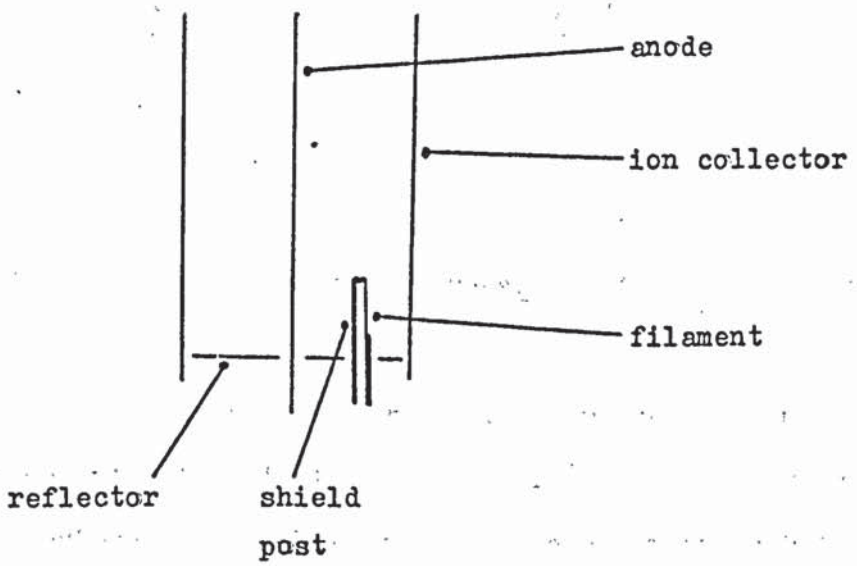

Figure 1.7. The orbitron ionisation gauge.

If b is the radius of the collector electrode, a is the radius of the anode, r is the radial position of an electron and V_A is the potential of the anode, then the potential V(r) at r is given by :-

$$V(r) = V_A \frac{\ln(b/r)}{\ln(b/a)} \qquad \ldots\ldots\ldots\ldots (2).$$

Using the expression in equation (2) for the radial electrostatic field in the orbitron, Hooverman[24] has shown that with appropriate angular momentum, the electrons are capable of travelling in orbiting type motion

about the anode and has determined the electron trajectories within the orbitron. Typical electron trajectories are illustrated in Figure 1.8.

Figure 1.8. Electron trajectories. (After Hooverman[24]).

The electron trajectory in Figure 1.8(a) represents an orbit of higher angular momentum than that of Figure 1.8(b). Trajectories of this nature can be simulated on a rubber model analogue of the orbitron. This analogue consists of a rubber sheet stretched across a circular frame to simulate the collector electrode. A metal rod is pressed into the rubber to simulate the anode and the depth of depression into the rubber is analogous to the anode potential V_A. The electron trajectories are simulated by rolling ball bearings on the surface of the rubber. The use and some of the limitations of rubber model analogues are discussed by White and Perry[25]. In the theoretical analysis by Hooverman[24], no account was taken of electron motion in the axial direction of the orbitron or of the potential disturbance due to the positive bias voltage V_B on the filament.

It was reported by Meyer and Herb[26] and by Gammon[27], that the sensitivity S, of the orbitron depended critically upon the value of V_B

placed upon the filament. This gave rise to undesirable ion collector current instabilities in the bias characteristics as illustrated in Figure 1.9. Gammon[27] reported observing these instabilities at pressures of 10^{-5} torr and above.

Figure 1.9. Variation of sensitivity with the ratio V_B/V_A. (After Gammon[27]).

Meyer and Herb[26] reported instabilities at lower pressures with "dips" to negative values of sensitivity, which were not present in the instabilities reported by Gammon[27]. The sensitivities reported by Gammon[27] were in the region of 10^3 to 10^4 $torr^{-1}$, whereas Meyer and Herb[26] reported sensitivities higher than 10^5 $torr^{-1}$. Meyer and Herb[26] attributed their ion current instabilities to some electrons gaining sufficient energy to enable them to reach the ion collector electrode. They proposed three ways in which electrons might gain this energy - namely from their thermal energies at the filament, from an R.F. field and thirdly by electron - electron collisions. They considered that the electron - electron scattering was the most probable process by which electrons gained the

energy necessary to reach the collector electrode. Gammon[27] attributed the ion current instabilities that he observed, to electron interaction with the field distortion around the filament. He also suggested that the instabilities observed by Meyer and Herb[26] in their very high sensitivity devices may be due to the same process. Electron interaction with the field distortion around the filament will occur if the electron trajectory closes on itself at the position of the filament and if by this time the electron has not drifted away from the plane of the filament along the axial direction of the orbitron.

Thus, although the field distortion around the filament is necessary to inject the electrons into the orbitron, it is undesirable after the electrons are in flight. A possible way to overcome this problem is to inject the electrons into the device from an electron gun as originally suggested by Gabor[21]. This method was tried with some success by Fitch et al[28]. They obtained smooth bias characteristics for their gauge whilst obtaining sensitivities in the region of 10^4 $torr^{-1}$, but with their design only about 10% of the filament emission was injected into the main gauge envelope. This necessitated operating the filament at an undesirably high temperature.

Attempts have been made to reduce the X-ray limit of orbitron type devices by introducing further electrodes. A spiral electrode was introduced into the orbitron by Gosselin et al[29], in order to suppress secondary electron emission from the ion collector. They reported a low pressure limit in the region of 10^{-12} torr for such a design of orbitron gauge.

Douglas et al[30] and later Bills[31] reported upon the performance of the orbitron when applied as the ioniser in electrostatic getter ion pumps. Due to the high sensitivity of the orbitron, high pumping speeds could be expected. However, the sticking probability for the ions at the

collector is often low, due to the ions having insufficient energy to be trapped efficiently by ion burial at the collector. In the radial field ion pumps described by Bills[31], a grid electrode is placed coaxially between the central anode and the collector electrode. This grid electrode is kept at a positive potential with respect to the earthed collector electrode, and serves to accelerate the ions that pass through it providing them with sufficient kinetic energy to bury themselves deeply in a layer of titanium on the collector surface.

1.3.3. The twin wire electrostatic charged particle oscillator.

The twin wire electrostatic charged particle oscillator[32] consists essentially of two positively charged anode wires, symmetrically disposed about the axis of a cylindrical collector electrode as illustrated in Figure 1.10 which shows the xy plane of the oscillator.

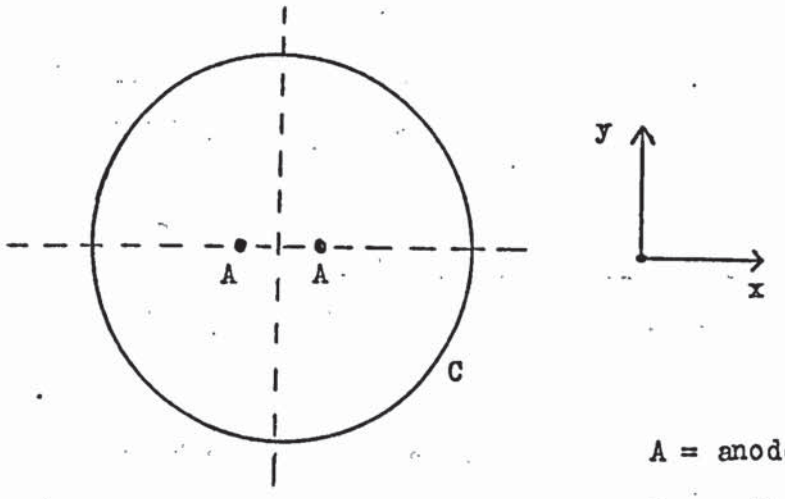

Figure 1.10. Schematic diagram of the twin wire oscillator in the xy plane.

With this arrangement, the electrostatic field is similar in shape to that in the orbitron except in the vicinity of the anodes, where there

is a saddle-point midway between the anodes. Although the saddle-point is a point of unstable equilibrium, electrons can oscillate through it in stable trajectories along the general direction of the y axis of the oscillator. Oscillatory trajectories of this type have been demonstrated on a rubber model analogue of the twin wire oscillator by McIlraith[32, 33].

Using digital computer techniques, McIlraith[33] investigated the trajectories followed by a particle attracted by a pair of isolated poles by making use of the calculated field strength at any point. For a pair of infinitely long anodes at a separation of 2d and with a charge of +q per unit length, the potential at a point P(x,y), relative to the saddle-point at the origin (Figure 1.11), is given by :-

$$-V_{xy} = \frac{q}{2\pi\epsilon\epsilon_o} \ln d^2 - \frac{q}{2\pi\epsilon\epsilon_o} (\ln r_1 + \ln r_2)$$

$$= \frac{q}{4\pi\epsilon\epsilon_o} \ln \left[\frac{d^4}{r_1^2 \; r_2^2} \right]$$

$$= \frac{q}{4\pi\epsilon\epsilon_o} \ln \left[\frac{d^4}{(y^2 + (x - d)^2)(y^2 + (x + d)^2)} \right] \qquad \ldots\ldots\ldots(3)$$

where ϵ is the dielectric constant which is unity for vacuum and ϵ_o is the permitivity of free space.

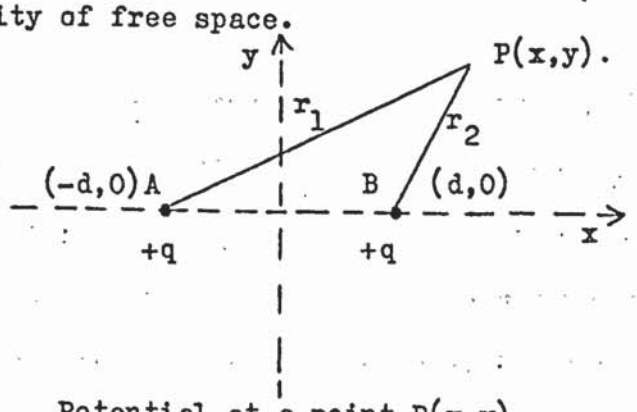

Figure 1.11. Potential at a point P(x,y).

Differentiating equation (3) with respect to x and y, then the field E_x in the x direction is given by :-

$$E_x = \frac{-q}{4\pi\epsilon\epsilon_o} \cdot \frac{4x(x^2 + y^2 - d^2)}{(y^2 + (x + d)^2)(y^2 + (x - d)^2)} \qquad \ldots\ldots(4)$$

and in the y direction :-

$$E_y = \frac{-q}{4\pi\epsilon\epsilon_o} \cdot \frac{4y(x^2 + y^2 + d^2)}{(y^2 + (x + d)^2)(y^2 + (x - d)^2)} \qquad \ldots\ldots(5).$$

Thus, we see in equation (4) that $E_x = 0$ for $x = 0$ and also for $x^2 + y^2 = d^2$. Thus, there is no resultant force in the x direction for an electron anywhere on the y axis, or on the circle with AB as its diameter. Inside this circle, the force F_x in the x direction is away from the y axis while outside the circle, F_x is towards the y axis. The force F_y on an electron is always towards the x axis. Now from equations (4) and (5) :-

$$\frac{E_y}{E_x} = \frac{y}{x} \cdot \frac{x^2 + y^2 + d^2}{x^2 + y^2 - d^2}$$

$$\longrightarrow \frac{y}{x} \qquad \text{when } x^2 + y^2 \gg d^2.$$

Thus, at large distances r_1 and r_2 from the anodes, the field lines radiate from the saddle-point at the origin O. Hence, the accelerating force on an electron will be towards the saddle-point when $x^2 + y^2 \gg d^2$.

An experimental twin wire oscillator was constructed by Thatcher[34] using a stainless steel collector electrode. The tungsten anode wires

had to be spring loaded in order to prevent them from bowing when being heated by the bombarding electrons. Due to the drift velocities of the electrons along the z axis of the oscillator, plane end-plates had to be employed on the collector electrode as illustrated in Figure 1.12, in order to maintain a cold cathode discharge. These end-plates were maintained at the collector potential and served to reflect the electrons back along the z axis of the oscillator to prevent them from drifting out of the ends of the oscillator.

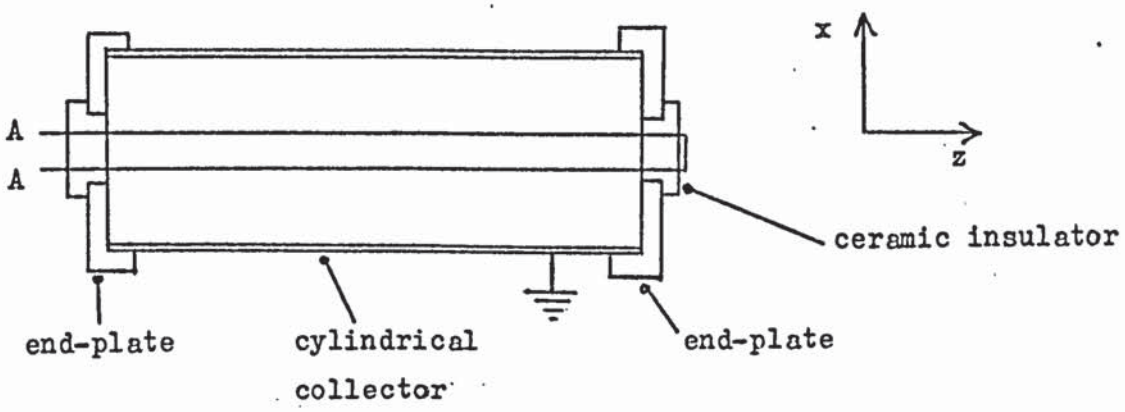

A = anode wires (spring loaded).

Figure 1.12. Schematic diagram of the twin wire oscillator in the xz plane.

It was found that the discharge was contained in a Figure of "8" region in the xy plane, producing two ion etched regions on the inside surface of the collector electrode as shown in Figure 1.13.

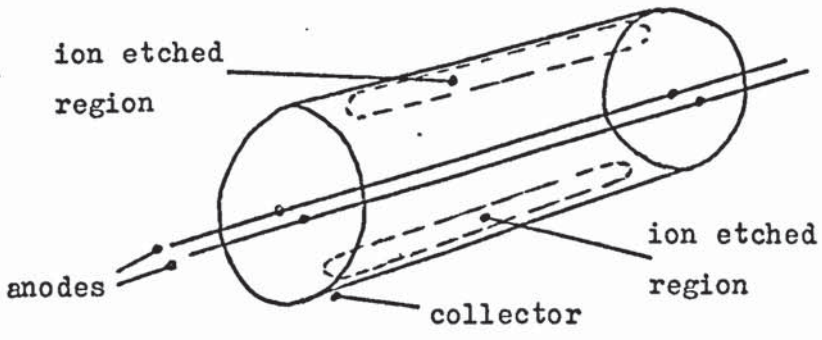

Figure 1.13. The ion etched regions on the collector surface.

The threshold voltage at which the cold cathode discharge would strike, was found to be pressure dependent. McIlraith[35] suggested that this could be accounted for by assuming that the total electron path length $\bar{l}$ in the oscillator is finite in the absence of all particles. Thus, the condition for a self-sustained discharge is :-

$$l_i \leqslant \bar{l}$$

where l_i is the distance an electron must travel to produce a useful ionising collision. Thus, it can be shown (Thatcher[34]) that :-

$$l_i = \frac{1}{NP\sigma} \leqslant \bar{l}$$

where P is the operating pressure, N is the number of molecules per unit volume at unit pressure and σ is the the ionisation cross-section. Since σ is dependent upon the electron energy, it will also be dependent upon the threshold voltage. Hence, the threshold voltage will vary with pressure.

It was found by Thatcher[34] that for optimum performance of the oscillator, the anode wires should be parallel to each other and symmetrically displaced about the axis of the collector electrode. It had been predicted by McIlraith[36] that the anode diameter should be small and that an optimum ratio for anode diameter to anode separation to collector electrode diameter would be 1 : 10 : 100. Hence, small diameter wire anodes were employed and this led to problems with the anodes burning out when the oscillator was operated at fairly high discharge currents. This was certainly the case when the oscillator was employed as an ion source as first described by Fitch et al[37]. This was done simply by milling a slot into the collector electrode at the intersection with the y axis. Positive ions formed in the discharge travel radially outward towards the collector and those which pass through the slot were allowed

to impinge upon a specimen surface which was to be etched by ion bombardment. Ion beam current densities of about 100 $\mu A\ cm^{-2}$ were obtained with an anode voltage of 6 kV and a pressure of 5×10^{-4} torr. The ion beam was very well collimated in the yz plane and only slightly divergent in the xy plane as would be expected from the nature of the discharge.

However, Thatcher[34] found that it was not possible to maintain the cold cathode discharge below 10^{-6} torr. In order to extend the twin wire oscillator to lower pressures, electrons were injected into the oscillator from a hot "V" shaped filament placed on the y axis (Fitch et al[38]). The filament was biased with a positive voltage V_B with respect to the collector electrode. The variation of sensitivity with the ratio $-V_B/V_A$ is given in Figure 1.14, where the electron emission current i_e from the filament had been kept constant at 1 μA. The vacuum chamber pressure was kept constant at 10^{-6} torr in a residual atmosphere of air.

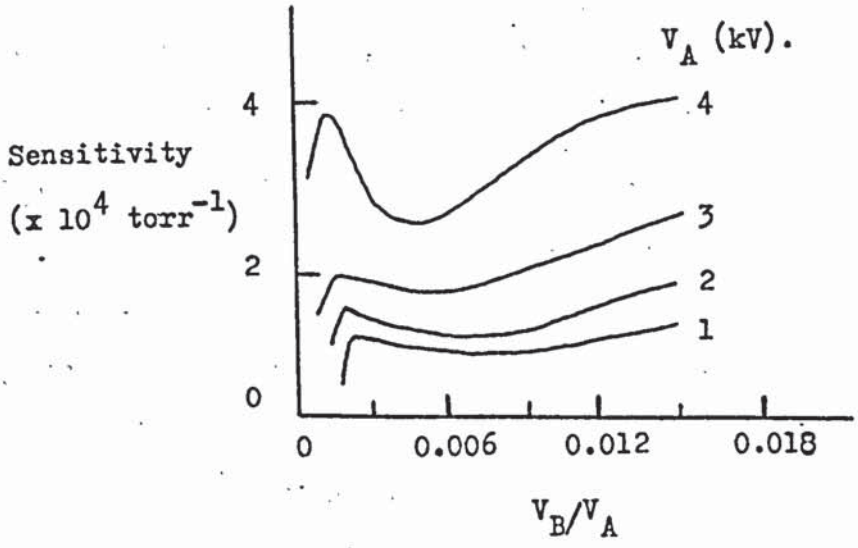

Figure 1.14. The variation of sensitivity with V_B/V_A.

It can be seen, that these bias curves consist essentially of two peaks at low and high values of V_B. Very high sensitivities of almost $10^5 torr^{-1}$ were capable of being achieved and no instabilities in the bias curves were observed as were reported for the orbitron by, for example, Gammon[27]. Thus, the thermionic twin wire oscillator showed promise as a very high sensitivity ionisation gauge, but the solid collector electrode was inadequate for ultra high vacuum conditions in several ways. Firstly, the solid collector cylinder would collect all of the X-rays produced at the anodes by electron bombardment and consequently a large residual secondary electron current would be produced at the collector electrode. The solid collector cylinder was also bulky and in order to reduce the outgassing from the collector, the solid cylinder was replaced by a cage consisting of 16 equally spaced tungsten wires. This would also reduce the number of X-rays intercepted by the collector electrode and so it was believed, lower the low pressure limit of the gauge due to these X-rays.

With this "nude" construction for the thermionic twin wire oscillator, the variation of sensitivity with the ratio V_B/V_A as found by Thatcher[34] is shown in Figure 1.15. The bias characteristics were again smooth with no instabilities, but they now consisted of only a single peak, with sensitivities of the order of 10^3 $torr^{-1}$.

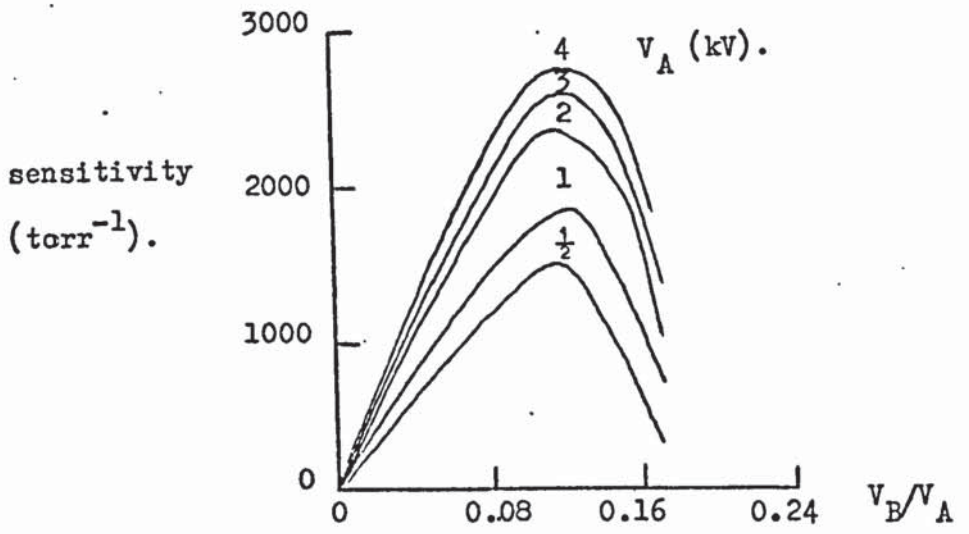

Figure 1.15. The variation of sensitivity with V_B/V_A for the nude oscillator.

A linear variation of collector current i_c with pressure was obtained over the range 10^{-4} torr to the low pressure X-ray limit of 5×10^{-10} torr. The comparatively low sensitivity of the nude gauge was considered to be due to increased ion losses due to the reduced collector area and possibly also due to a decrease in electron path length as a result of electrons interacting with the field distortions associated with the open collector electrode.

In the next two chapters, experiments will be described which were undertaken to study the consequences of the field distortions around the thermionic filament and the open collector. Experiments described in the later chapters are concerned with the study of the factors limiting the low pressure limit of the cold cathode oscillator.

CHAPTER 2.

INVESTIGATION OF THE THERMIONIC TWIN WIRE OSCILLATOR.

2.1. Introduction.

In order to determine why the sensitivity found by Thatcher[34] for the nude thermionic twin wire oscillator was relatively low, an experimental thermionic twin wire oscillator was constructed in which the collector electrode geometry could be easily varied. A field plotting technique was used to determine the electrostatic field distributions for the various collector electrode geometries, so allowing the influence upon the electron trajectories of various forms of field distortion at the collector electrode to be investigated.

2.2. Experimental equipment.

2.2.1. Design of the experimental oscillator.

The experimental thermionic twin wire oscillator shown in Figure 2.1 was designed with the collector electrode consisting of 32 tungsten rods of 2 mm diameter. These tungsten rods were positioned in the holes drilled into the "Dural" end-plates on a circle of 5 cm diameter as illustrated in Figure 2.2. The rods could be easily removed in order that the collector electrode geometry could be varied. The anodes were of 0.4 mm diameter tungsten wires at a separation of 0.5 cm and were positioned in and insulated from the end-plates by means of 1.25 cm diameter ceramic bushes. The commercial ceramic used was "Ceramtec" which the manufacturers claim has a resistivity of 10^{14} ohms cm in air at 20°C. Four 4 BA screwed rods were used to tension the two anode wires and also to maintain the distance between the end-plates at 20 cm. These four

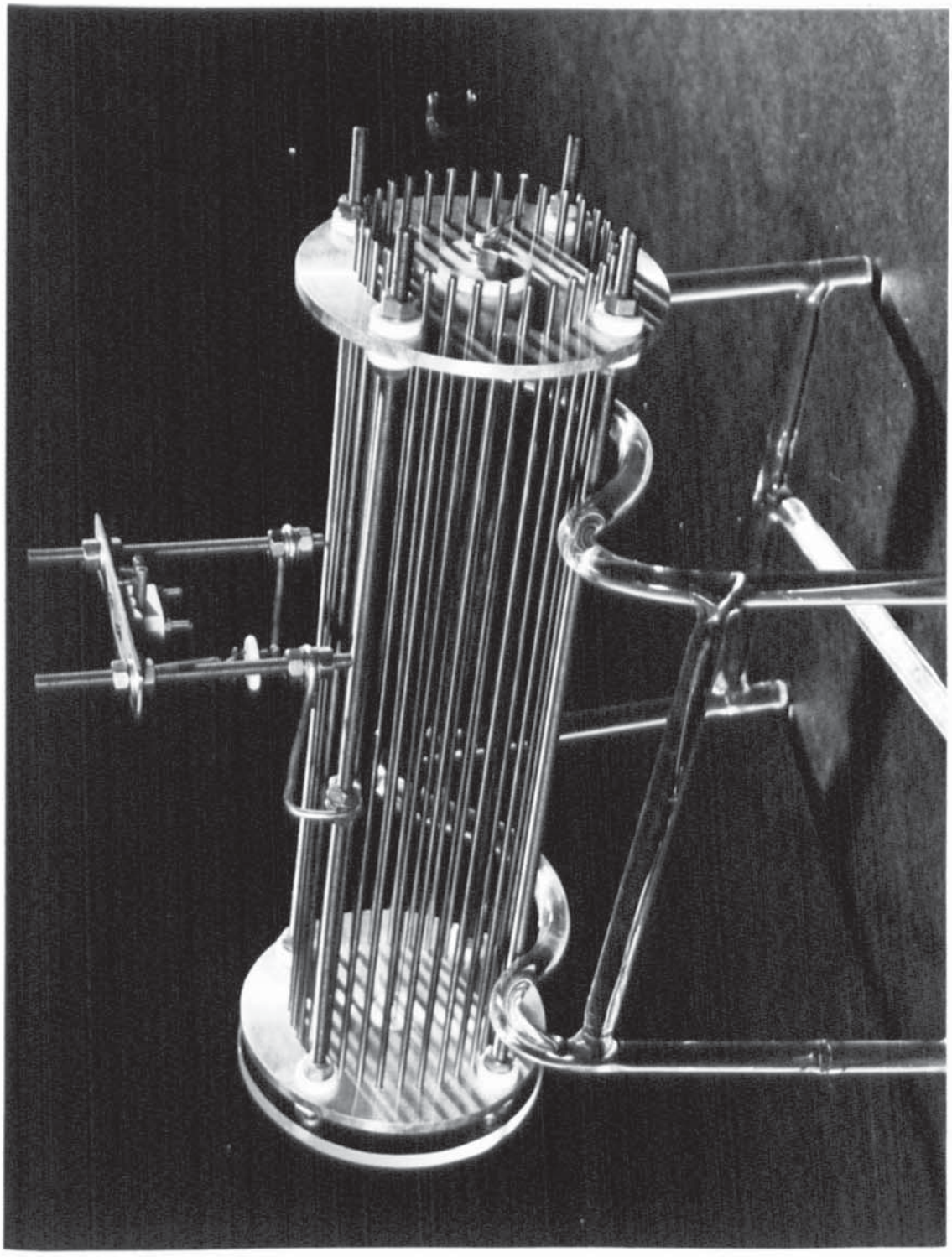

Figure 2.1. The thermionic twin wire oscillator with a collector electrode consisting of 32 tungsten rods.

screwed rods were insulated from the end-plates by P.T.F.E. bushes, in order to prevent them from contributing to the collector electrode area.

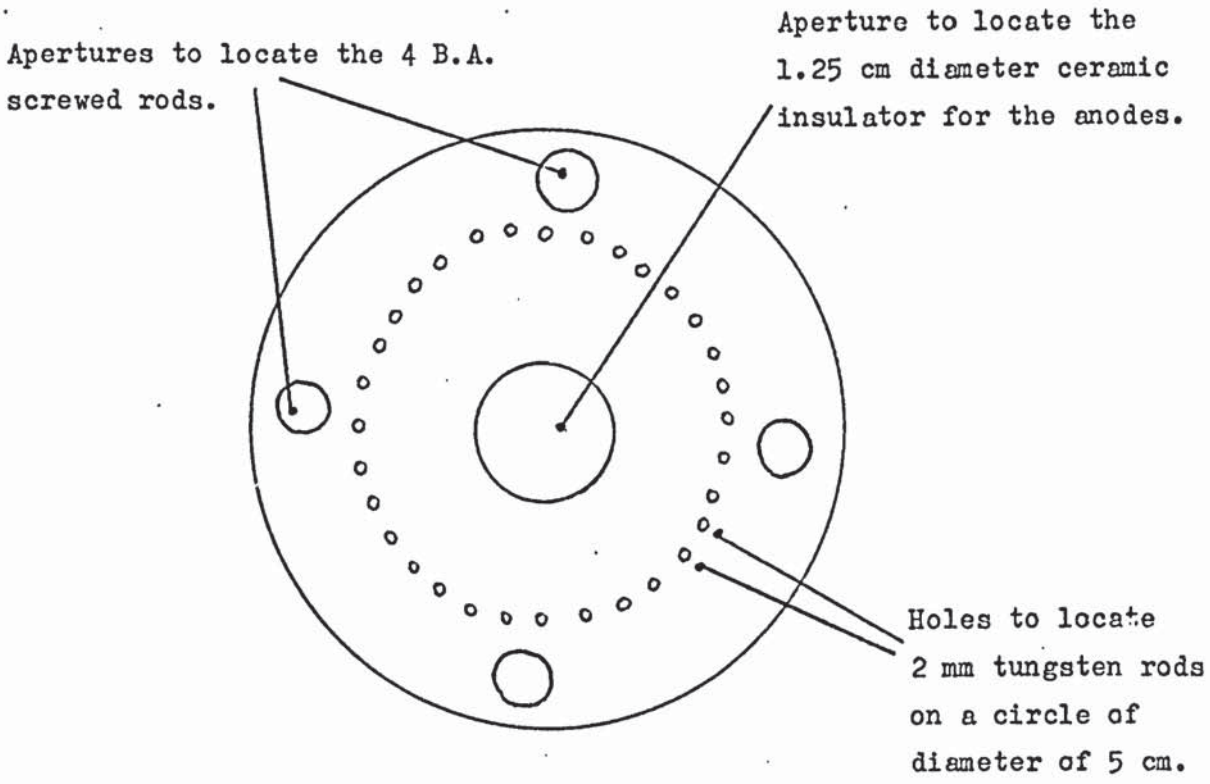

Figure 2.2. End-plate for the twin wire oscillator.

A "V" shaped filament of about 2 mm length was constructed from 0.1 mm diameter tungsten wire. This filament was mounted on two parallel 1 mm diameter tungsten rods and was positioned midway along the length of the cylindrical collector electrode. The filament was mounted in a manner which allowed the filament immersion depth to be varied.

2.2.2. The electrical circuit.

A schematic diagram of the thermionic twin wire oscillator and its associated electrical circuit is given in Figure 2.3. The anode

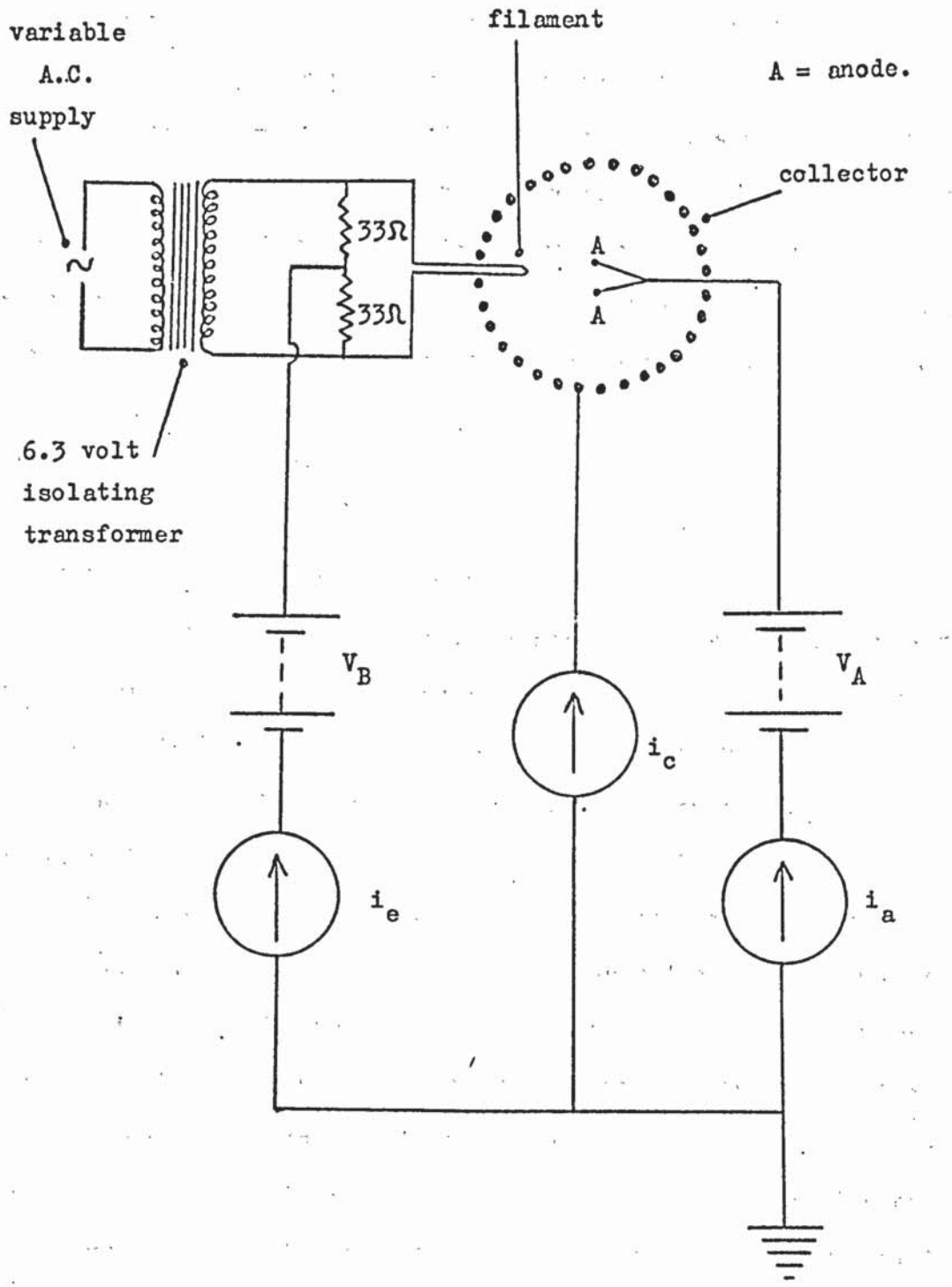

Figure 2.3. Schematic diagram of the twin wire oscillator and the associated electrical circuit.

voltage V_A was varied from 1 to 5 kV using a stabilised H.T. power supply, whilst the collector electrode and end-plates were maintained at earth potential. A D.C. amplifier capable of measuring from 10^{-6} to 10^{-13} amps was used to measure the collector current i_c. A Variac and a 6.3 volt isolating transformer were used for the filament supply. Dry batteries were used for the positive bias voltage V_B on the filament. The bias lead was centre-tapped between two 33 Ω resistors across the transformer secondary winding in order to maintain the tip of the filament at the correct bias voltage. Microammeters capable of measuring from 0.2 μA up to 120 mA, were used to measure the filament emission current i_e and the electron current to the anodes i_a.

2.2.3. The high vacuum system.

Experimental investigations using the thermionic twin wire oscillator described, were carried out in a conventional high vacuum system consisting of a 3" silicone oil diffusion pump, rotary pump and a liquid nitrogen cold trap. The vacuum chamber consisted of a 12" diameter glass bell jar mounted on a 14" diameter steel base-plate containing 2 H.T. and 4 L.T. electrical feedthroughs. The system was capable of achieving pressures down to 10^{-6} torr which were measured by a Penning gauge mounted just above the baffle-valve. The leak-valve was in a similar position facing the Penning gauge. The pressures indicated by the Penning gauge were compared with those indicated by a nude Bayard - Alpert type ionisation gauge (Mullard IOG 13T) by mounting the ionisation gauge in the vacuum chamber. The results of this comparison are given in Appendix 1, and it is the Bayard - Alpert gauge pressures rather than the Penning gauge pressures that were assumed to be the true pressures. Liquid nitrogen was used in the cold trap throughout the investigation and all measurements have been taken using air as the residual atmosphere in the vacuum chamber.

2.3. Effects of changes in the collector electrode geometry.

The filament bias characteristics were obtained by observing the variation of collector current i_c with filament bias voltage V_B, whilst maintaining the current to the anodes i_a constant at 1 μA. It should be noted that it was always i_a rather than i_e that was maintained constant when taking measurements. A constant pressure of 1.4×10^{-5} torr was maintained during the measurements and the characteristics were obtained for values of V_A ranging from 1 to 5 kV. Bias characteristics were obtained for various filament immersion depths D into the oscillator tube. The filament immersion depth is defined as the distance from the tip of the filament to the inside surface of the collector electrode. Bias characteristics for four values of D are given in Figure 2.4.

Two peaks occur in the bias characteristics, one at low values of V_B and the other at high values of V_B, with a sharp emission cut-off occuring at the second peak. With D equal to 0.38 cm, i_c and hence the sensitivity S is greatest with V_B equal to about +6 volts at V_A = 1 kV. It was found that by removing certain rods from the collector electrode, the sensitivity of the device could be drastically reduced.

A cross-sectional scale diagram of the electrode assembly (but excluding the filament) was painted onto Teledeltos resistance paper using a conducting paint consisting of a dispersion of silver in methyl isobutyl ketone. These painted electrodes were energised by a Servomex field plotter and the equipotential lines of the electrostatic field were plotted for several collector electrode configurations. Four of these field plots are reproduced in Figure 2.5, namely the 32 rod, 28 rod(a), 28 rod(b) and 20 rod collector electrodes. The equipotentials are expressed as a percentage of the anode voltage V_A. The saddle-point occurs at between 70% and 80% of V_A. It was found that the 32 rod collector configuration gave very high sensitivities, with the maximum sensitivity

(a).

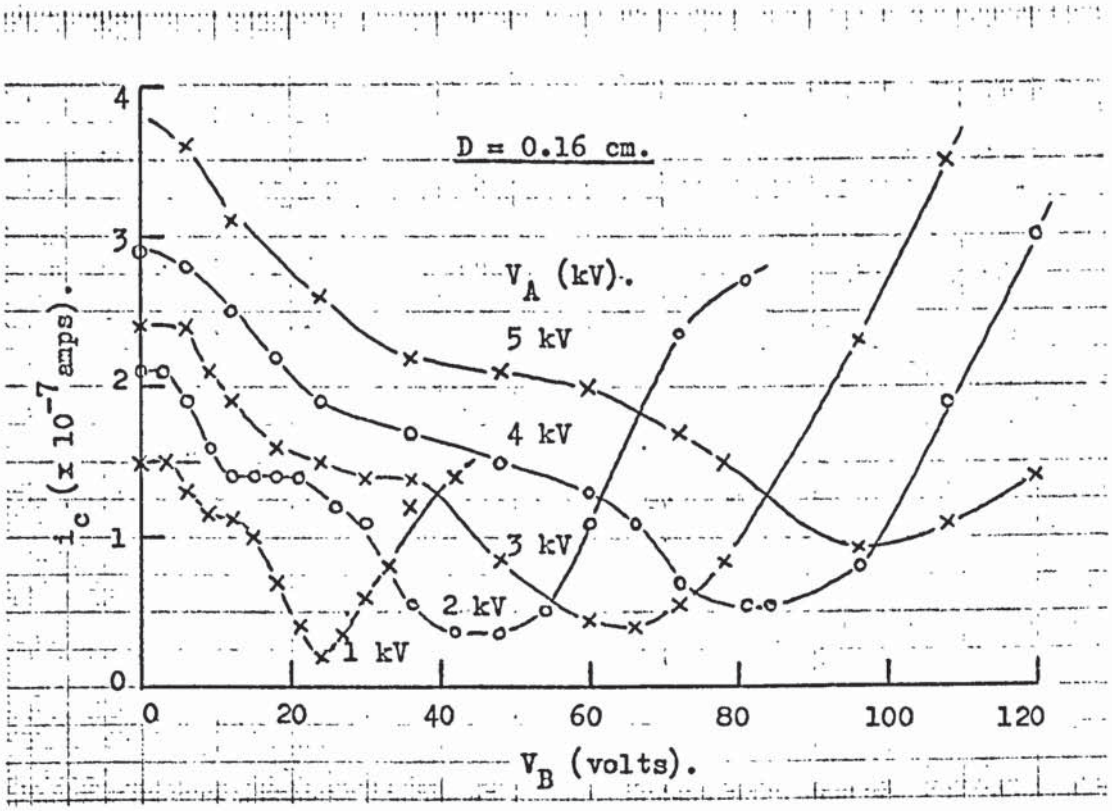

(b).

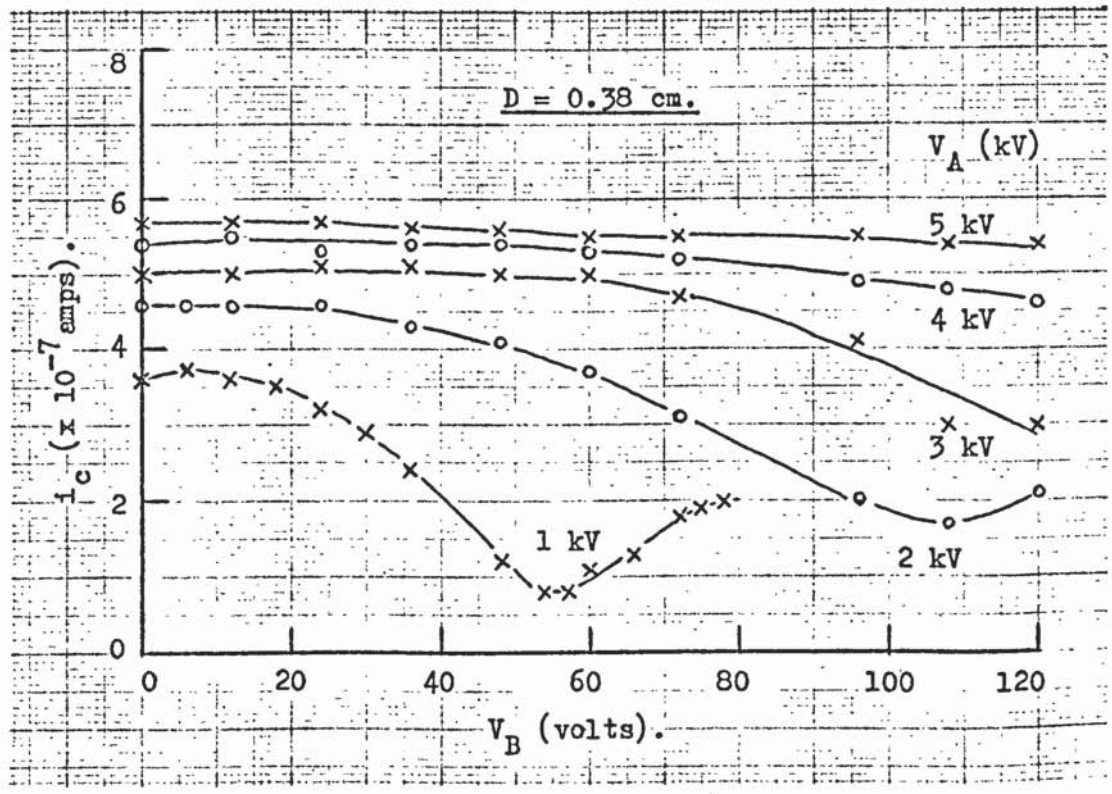

Figure 2.4. The variation of collector electrode current with filament bias voltage in the twin wire oscillator.

(c).

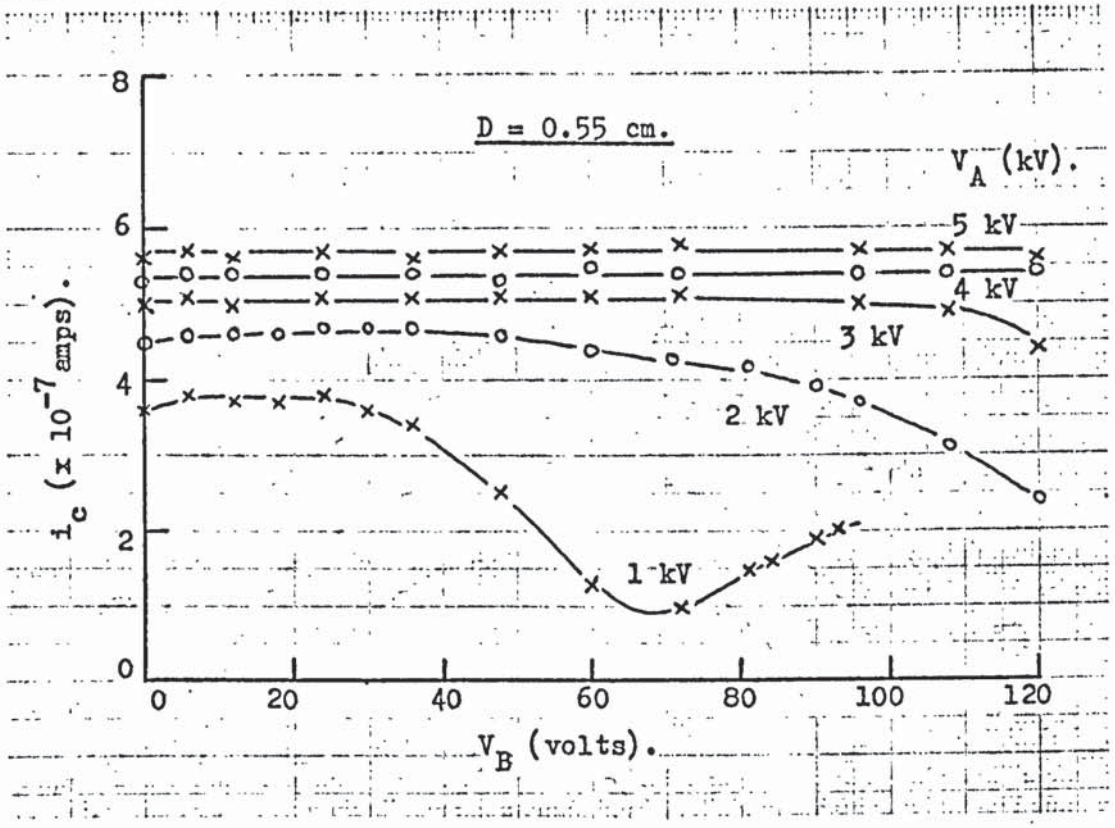

(d).

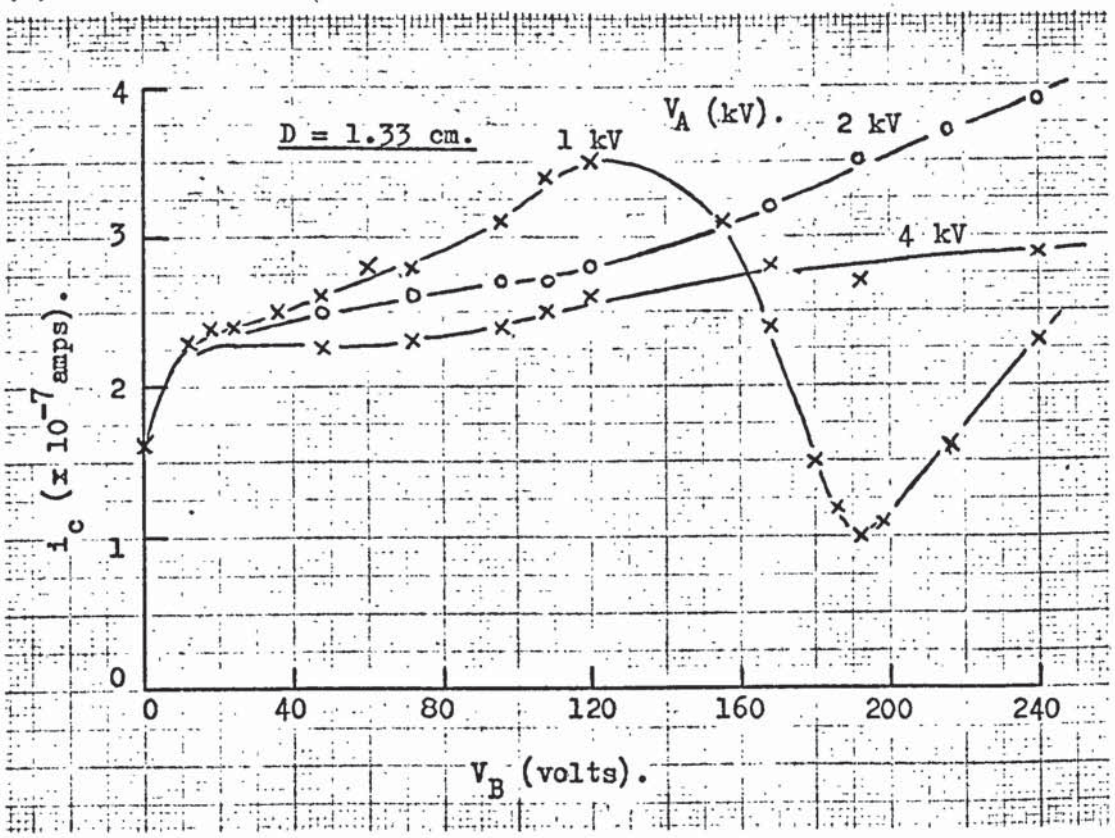

Figure 2.4. (continued).

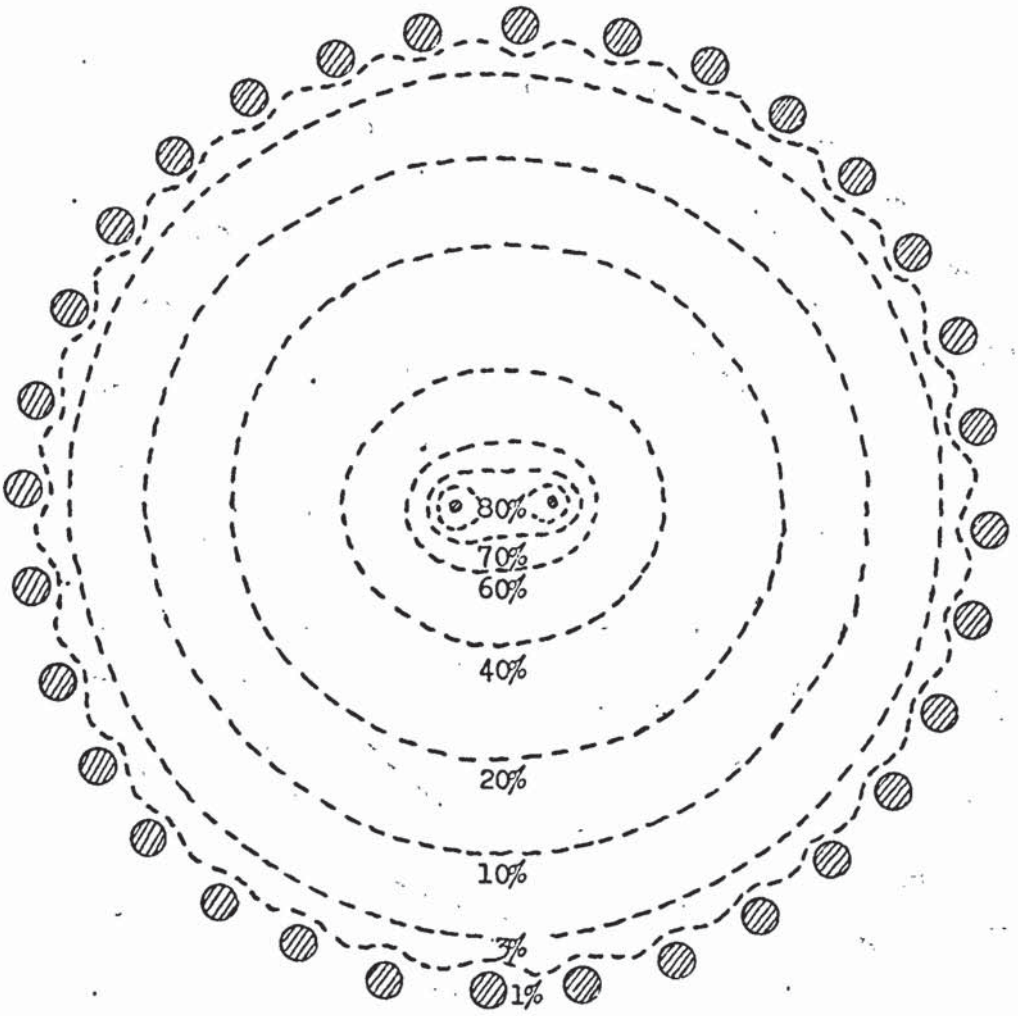

Figure 2.5(a). The distribution of the lines of equipotential in the 32 rod collector electrode.

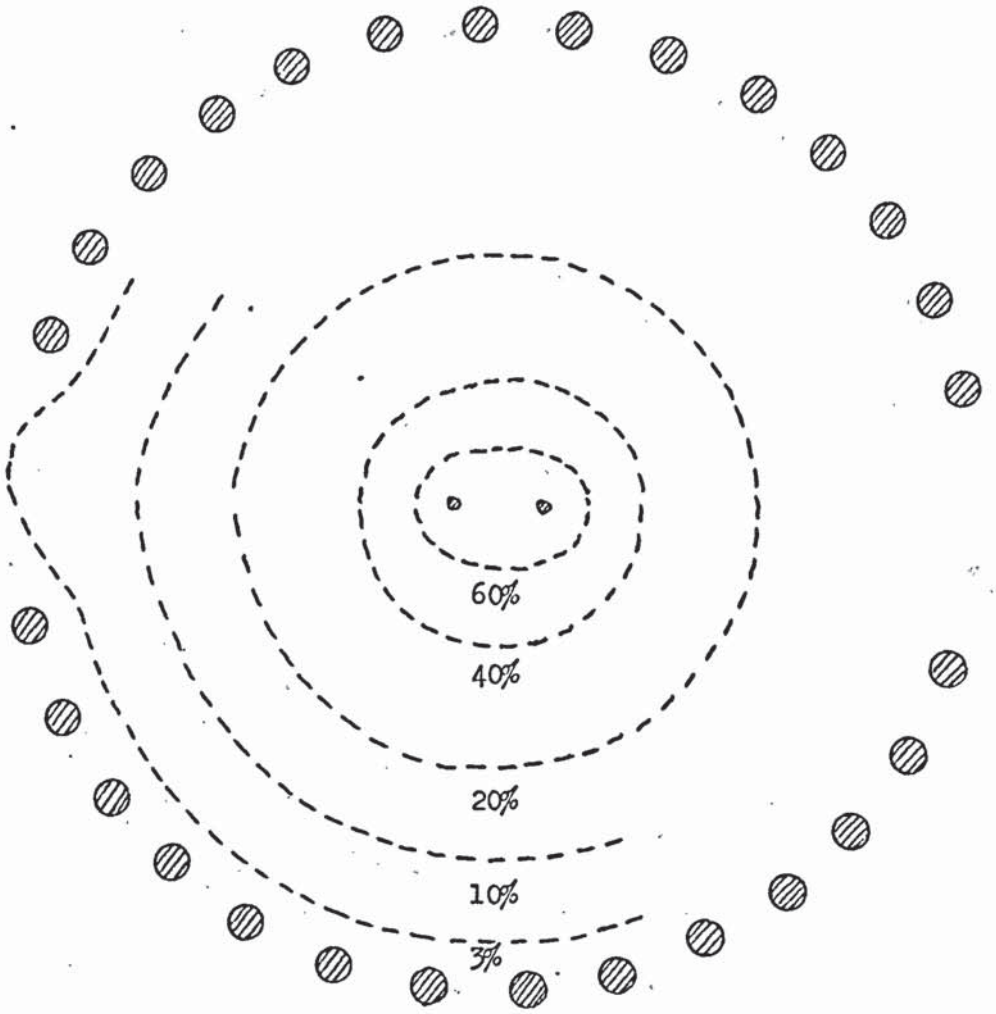

Figure 2.5(b). The distribution of the lines of equipotential in the 28 rod(a) collector electrode.

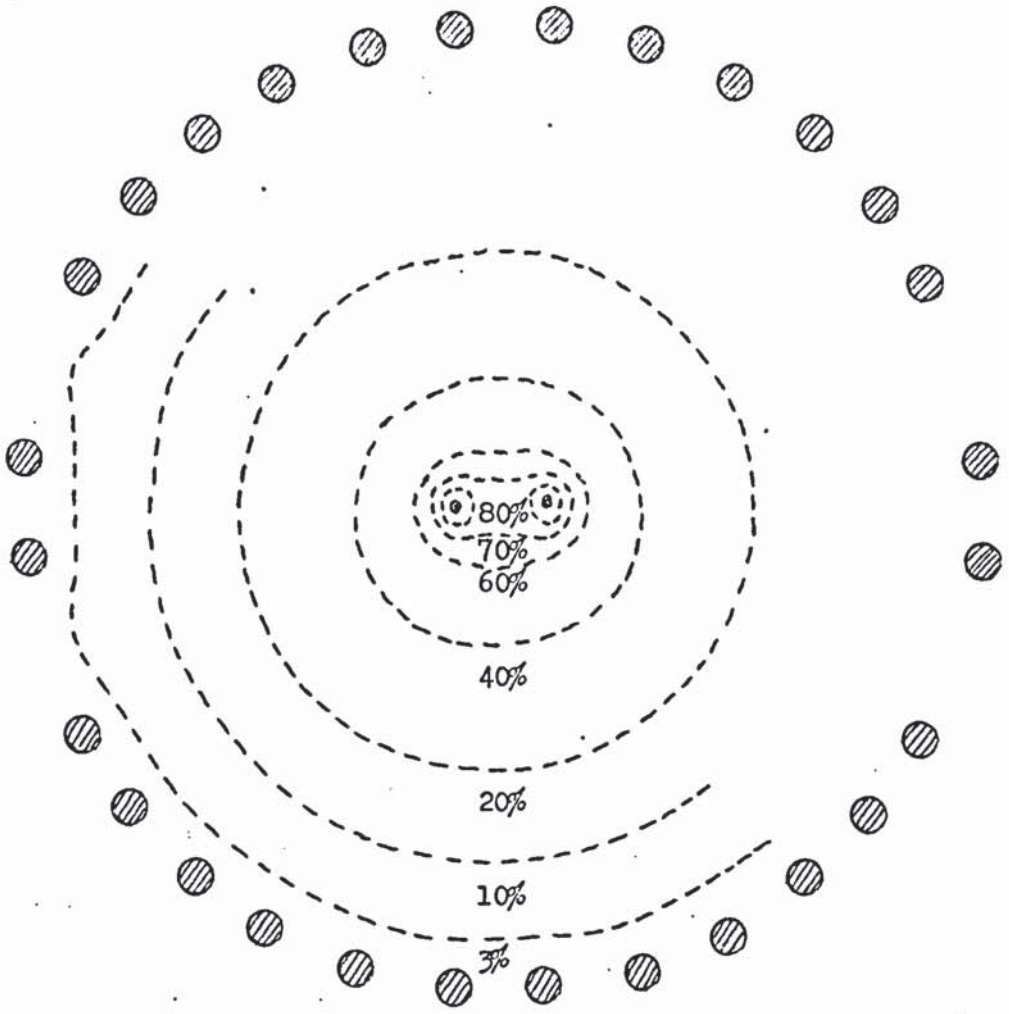

Figure 2.5(c). The distribution of the lines of equipotential in the 28 rod(b) collector electrode.

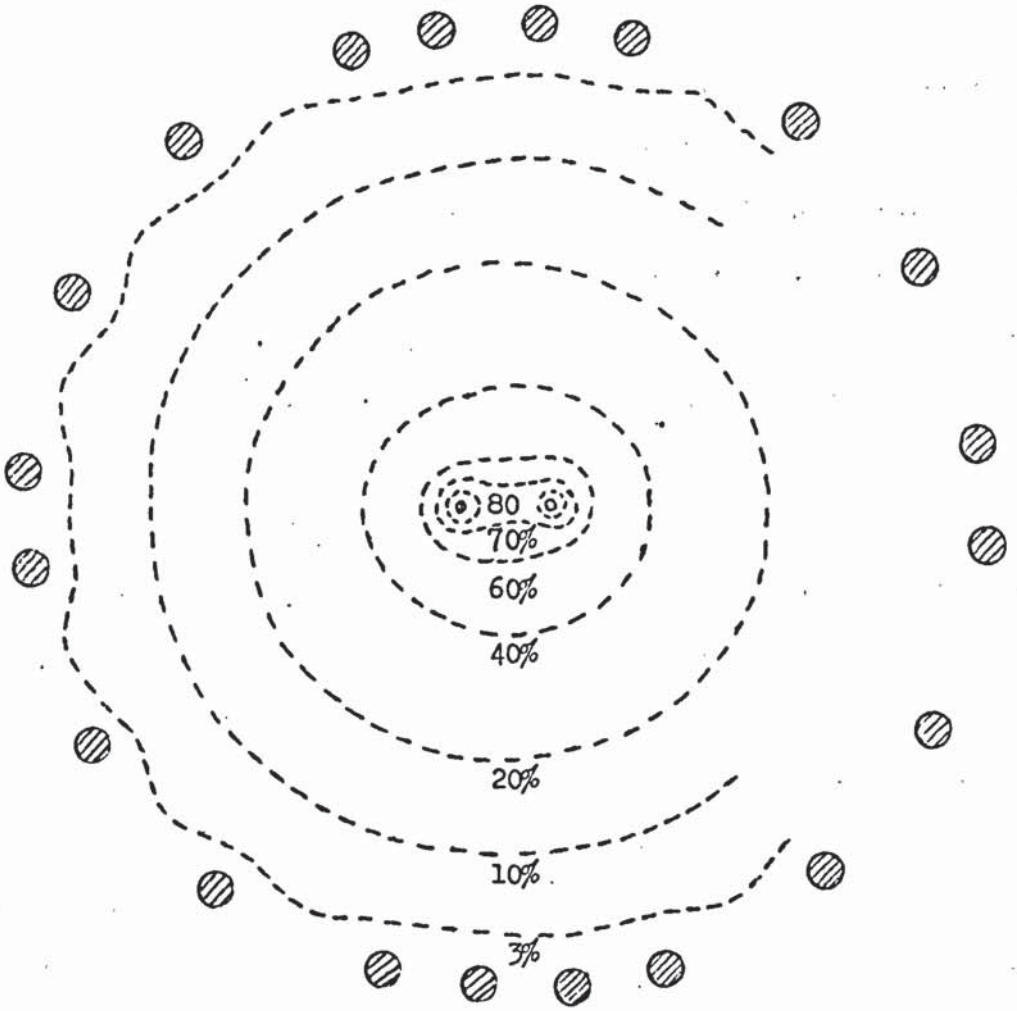

Figure 2.5(d). The distribution of the lines of equipotential in the 20 rod collector electrode.

being obtained with V_B at approximately +6 volts when V_A = 1kV. However, with these filament bias conditions, the presence of two double spaces in the 28 rod(a) collector reduced the sensitivity S more than did the use of the 28 rod(b) collector with four single spaces in it. In fact, the presence of the two double spaces in 28 rod(a) was more detrimental to the performance of the device than was the presence of 12 single spaces in the 20 rod collector electrode. The field distortion associated with the double spaces in the 28 rod(a) collector electrode should have had little effect on any electrons that were oscillating between the anodes. It was then suspected that some of the electrons may be orbiting around the twin anodes rather than oscillating between them.

2.4. The orbiting electron theory.

The maximum value of i_c in the low bias voltage peak was obtained when the filament bias potential V_B did not match the anode field potential at the tip of the filament. The resulting field distortion around the filament would probably give the electrons sufficient angular momentum to get them into an orbiting trajectory around the anodes. In this way, the electrons would encounter the field distortions of the 28 rod(a), 28 rod(b) and 20 rod collector geometries. The larger field distortion associated with the double spaces in the 28 rod(a) collector would be more detrimental to the orbiting motion of the electrons than would the distortion of the 12 single spaces in the 20 rod colletor.

In order to verify that the electrons were performing any orbiting motion, metal foil was wrapped around the twin anodes. This would stop any oscillatory motion of the electrons between the anodes, but would still allow any orbiting motion around the anodes. This now produced a device with a single plate anode of $\frac{1}{2}$ cm wide by 20 cm long. The field plot in Figure 2.6 shows that the potential distribution within the device is as might be expected, altered very little by the use of the single

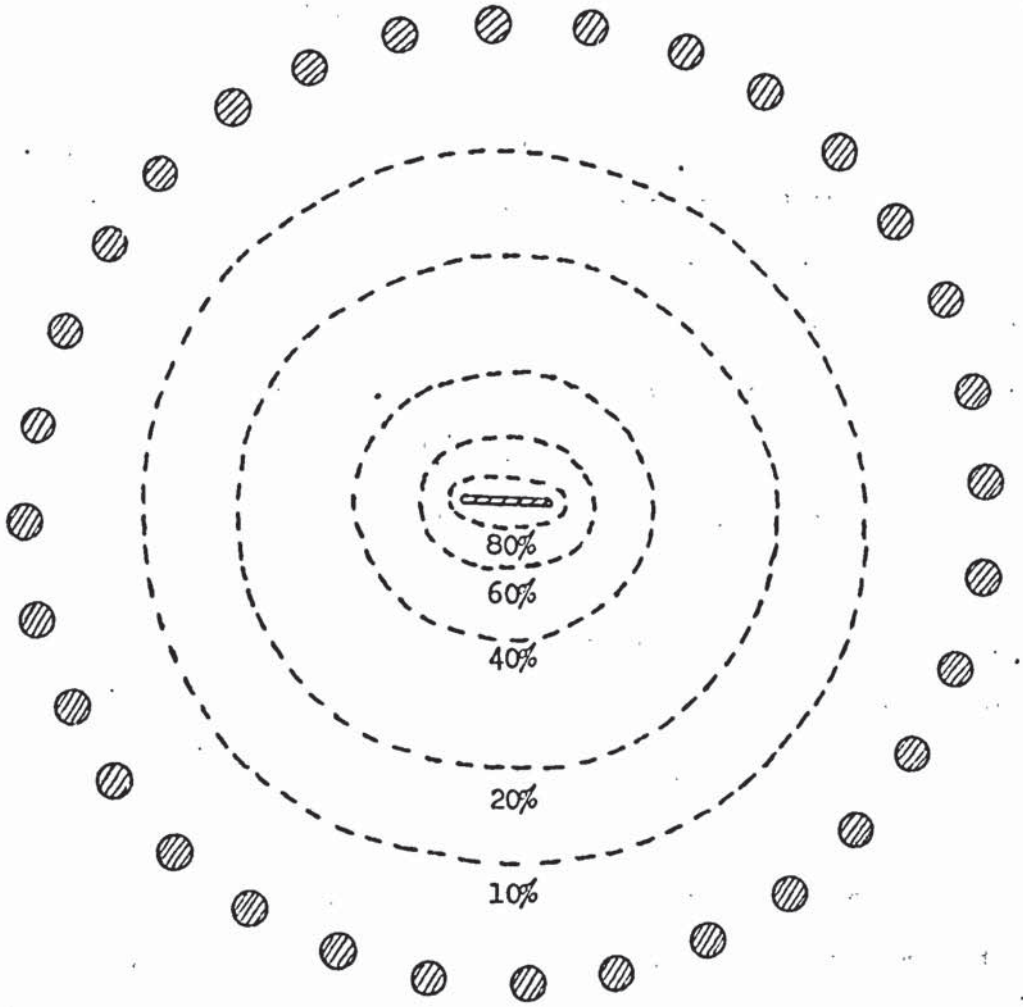

Figure 2.6. The distribution of the lines of equipotential in the single plate anode device.

plate anode. Bias characteristics at a pressure of 1.4×10^{-5} torr were obtained for the single plate anode device for various values of filament immersion depth D and four sets of these are reproduced in Figure 2.7. Large collector currents i_c were obtained with the single plate anode device. The maximum values of i_c with V_A = 1kV were very little different from those obtained for the twin wire oscillator at low values of V_B. However, the variation of the maximum value of i_c with V_A was not so great as with the twin wire device. It was concluded that under the low bias conditions, the majority of electrons were going into orbit around the anodes in the thermionic twin wire oscillator. The bias characteristics obtained for the single plate anode device were of a different form from those for the twin wire oscillator. It can be seen from Figure 2.7 that there is no minimum in the bias characteristics, before emission cut-off is encountered.

The likely variation of the potential distribution at the filament with change in V_B is illustrated in Figure 2.8. For example, consider a filament biased at zero volts with respect to the collector electrode and with its tip at the position of the 100 volt equipotential of the undisturbed anode field. Under these conditions, the electrostatic potential distribution around the filament would be similar to that illustrated in Figure 2.8(a). This field distortion would give the electrons emitted from the sides of the filament, an angular momentum that would be sufficient to put them into orbiting trajectories around the anodes. The electrons emitted from the tip of the filament may go into oscillation between the anodes. As V_B is increased to say +50 volts (Figure 2.8(b)), the area of electron emission from the filament will be reduced as shown by Haine and Einstein[39]. Neglecting the thermal energies of the electrons, electron emission can only take place from the region of the filament in front of the point where the 50 volt equipotential cuts

(a).

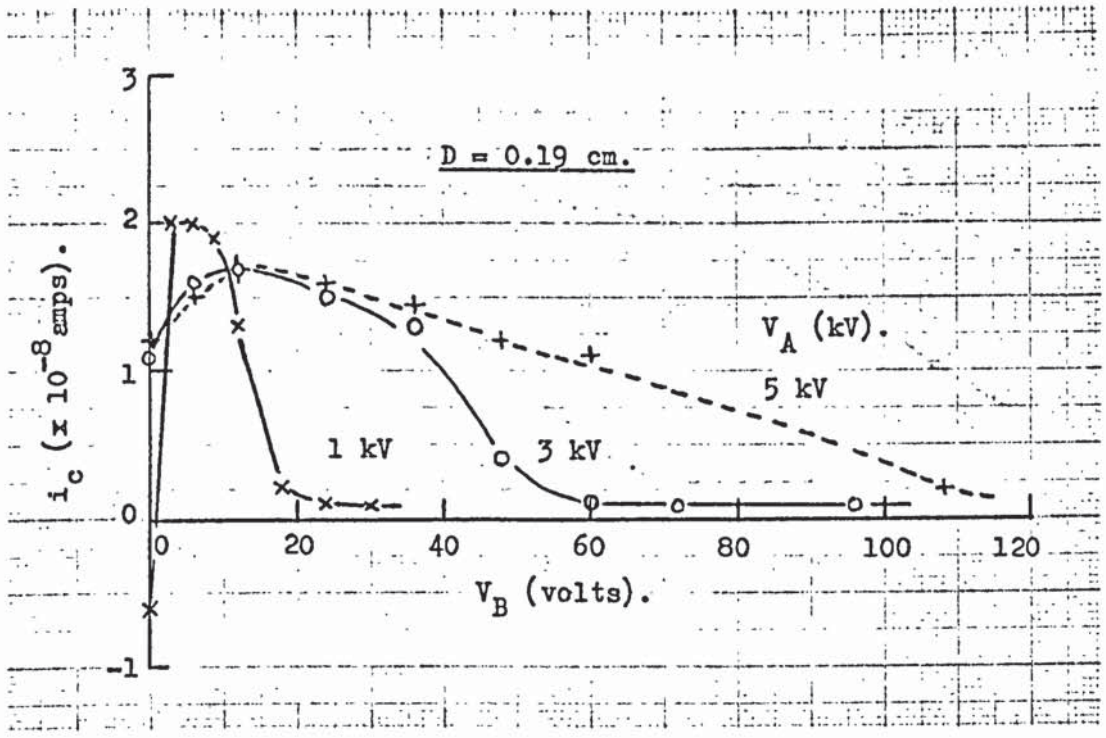

(b).

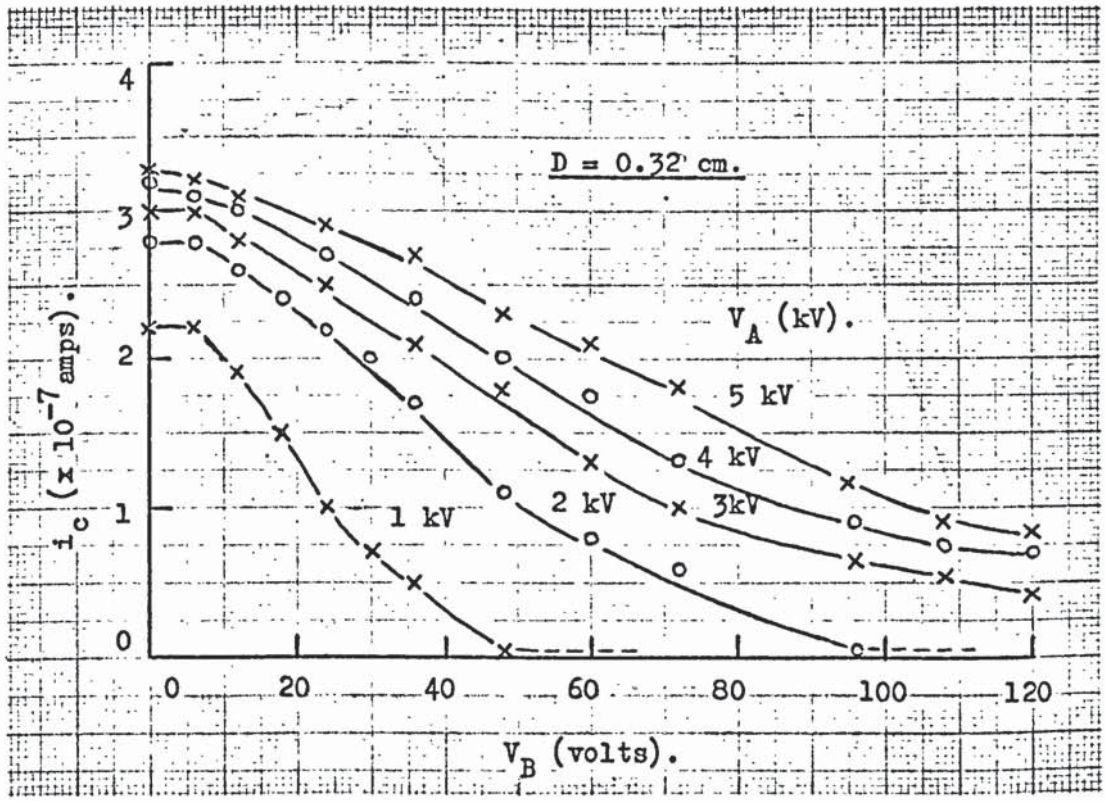

Figure 2.7. The variation of collector electrode current with filament bias voltage in the single plate anode device.

(c).

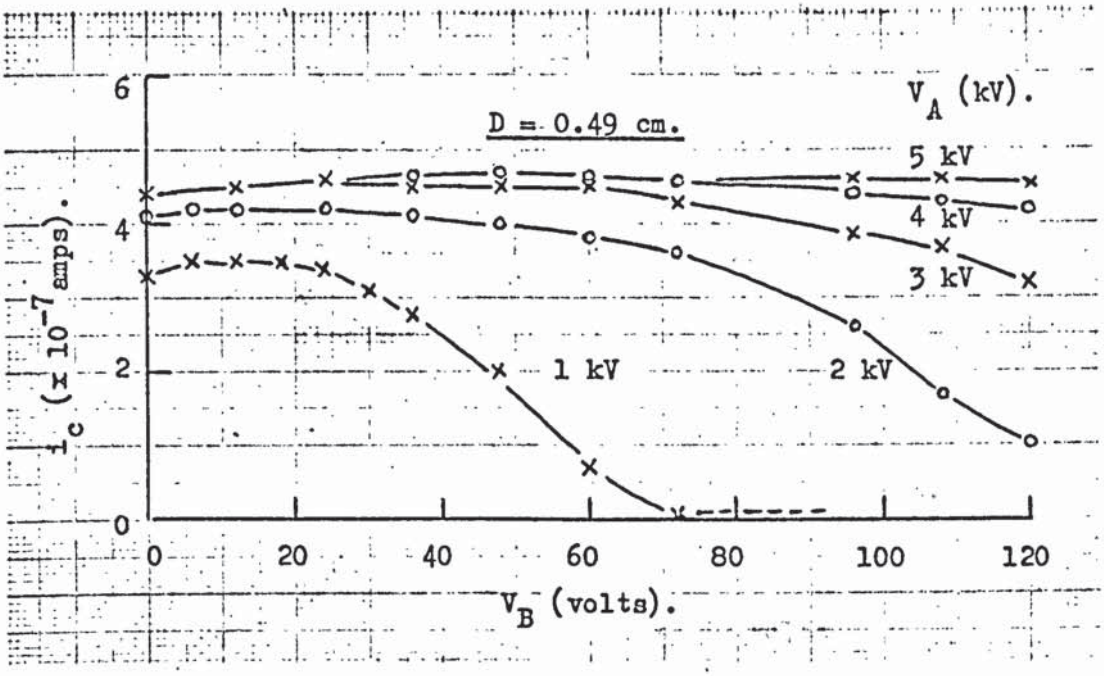

(d).

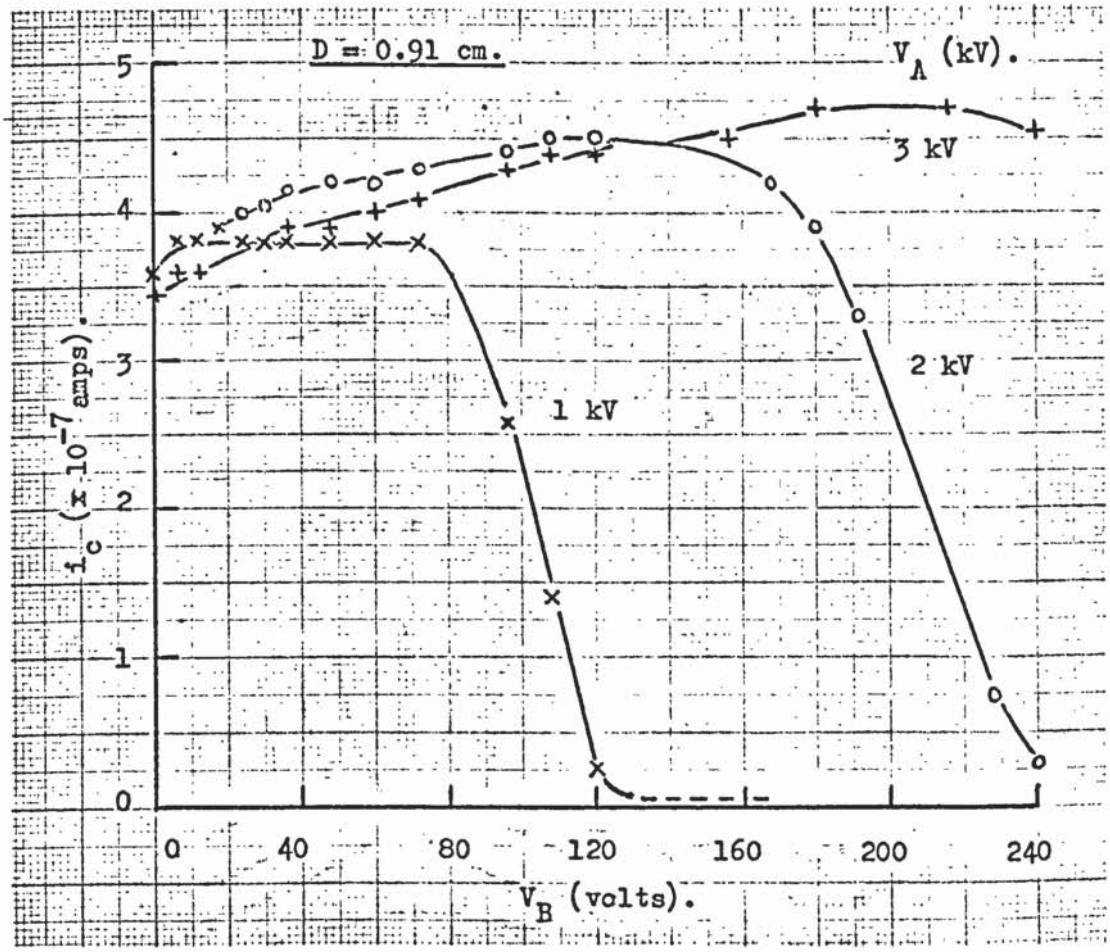

Figure 2.7. (continued).

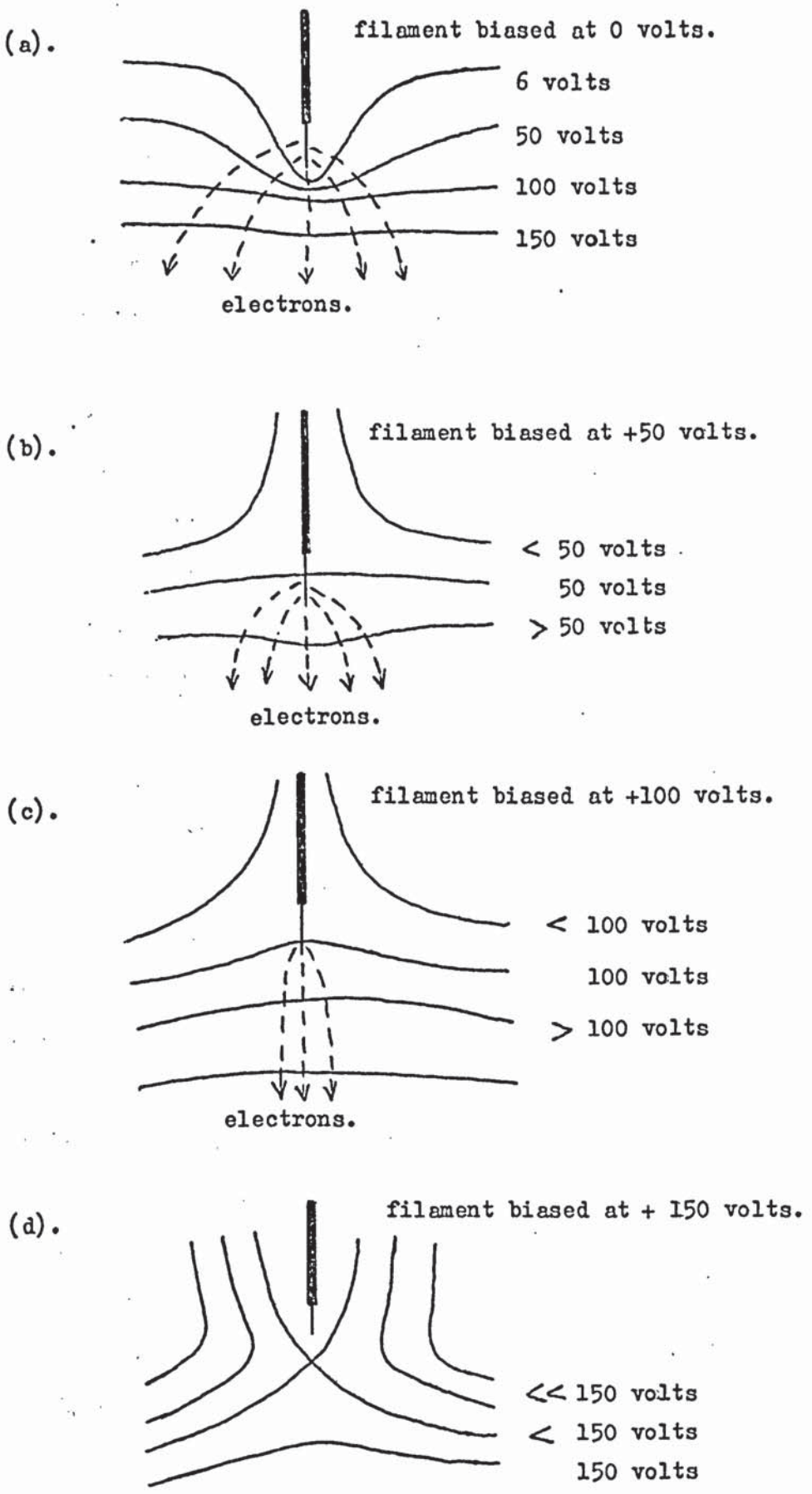

Figure 2.8. The variation of the lines of equipotential in the field around the filament with change in filament bias voltage.

the filament surface. If V_B is increased further to say +100 volts (Figure 2.8(c)), the electron emitting area of the filament will be decreased further and near to cut-off, the region of electron emission would be reduced to only the very tip of the filament. A collimated beam of electrons would be obtained for this condition of bias, making this most suitable for the emitted electrons to oscillate betweem the anodes. Emission cut-off from the filament is obtained when the filament bias V_B is large enough to make the equipotential no longer cut the filament surface and so produce a retarding field at the filament tip (Figure 2.8(d)). Allowing for the thermal energies of the electrons leaving the filament, the value of V_B for emission cut-off would not be much greater than that required for a matched filament bias when the equipotential cuts the very tip of the filament.

2.5. Modes of operation in the thermionic twin wire oscillator.

It was therefore suspected that the peak at high values of V_B in the bias characteristics of the thermionic twin wire oscillator, was due to electrons oscillating between the anodes. To verify this the filament was rotated about the plane of the twin anodes. Bias characteristics were obtained for 0° rotation, 45° rotation and 90° rotation of the filament about the anode plane, as illustrated in Figure 2.9(a). The three curves are given in Figure 2.9(b) and were obtained whilst maintaining V_A at 1 kV, i_a at 1 μA and the pressure at 1.4×10^{-5} torr. The normal form of bias characteristic with two peaks was obtained at 0° rotation of the filament (curve 1). At 45° rotation, i_c was reduced by about 20% at the low values of V_B and at high values of V_B, i_c remained at less than 10^{-8} amps with an emission cut-off at approximately +72 volts bias (curve 3). The same form of bias curve was obtained for the 90° rotation of the filament (curve 2).

Thus, two modes of operation exist in the thermionic twin wire

(a).

0° Rotation. 45° Rotation. 90° Rotation.

(b).

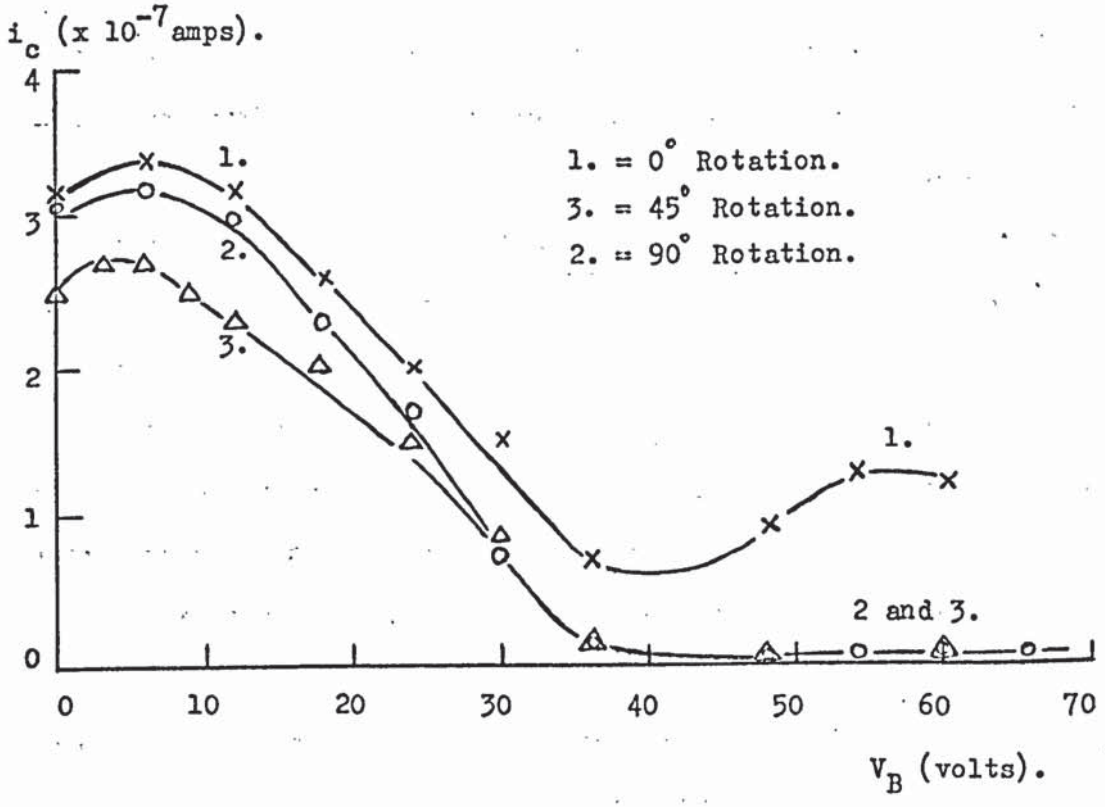

Figure 2.9. The effect of filament rotation about the anode wires.

oscillator, the "orbiting mode" at low values of V_B and the "oscillating mode" at high values of V_B, (Fitch and Rushton[40]). The variation of i_c with V_B for both the twin wire oscillator (solid line) and the single plate anode device (dashed line) is given in Figure 2.10, with V_A = 1 kV, i_a = 1 μA and D at approximately 0.5 cm. In the twin wire oscillator, the peak (a) is due mainly to electrons orbiting around the anodes and as V_B is increased, the accelerating field distortion at the filament is reduced until a minimum at (b) is obtained. There is an increase again to peak (c) due to electrons oscillating between the anodes and a sharp emission cut-off at (c'). In the single plate device case, the peak (a) is due purely to electrons orbiting around the plate anode and no minimum (b) is passed through before an emission cut-off is again obtained at (c'). There is, however, a small difference in height of peak (a) between the twin wire oscillator and the single plate anode device. This difference is due to the electrons emitted from the tip of the filament at low values of V_B, going into oscillation between the anodes in the twin wire oscillator, whereas in the single plate anode device, these electrons go straight to the anode.

At V_A = 1kV, the difference in i_c for the twin wire and single plate anode devices was less than 10% but, in order to determine the actual proportion of electrons that are oscillating between the anodes in the twin wire oscillator under these conditions, a knowledge of the relative ion production efficiencies for the orbiting and oscillating modes is required. Also, in the twin wire oscillator, the orbiting mode peak (a) shows an increase in i_c with increase in V_A whereas with the single plate anode device, the height of the peak (a) was almost independent of change in V_A. This was due to this oscillating mode contribution being dependent upon V_A, whereas the orbiting mode is relatively independent of V_A.

In the orbiting mode, electrons require a sufficiently large

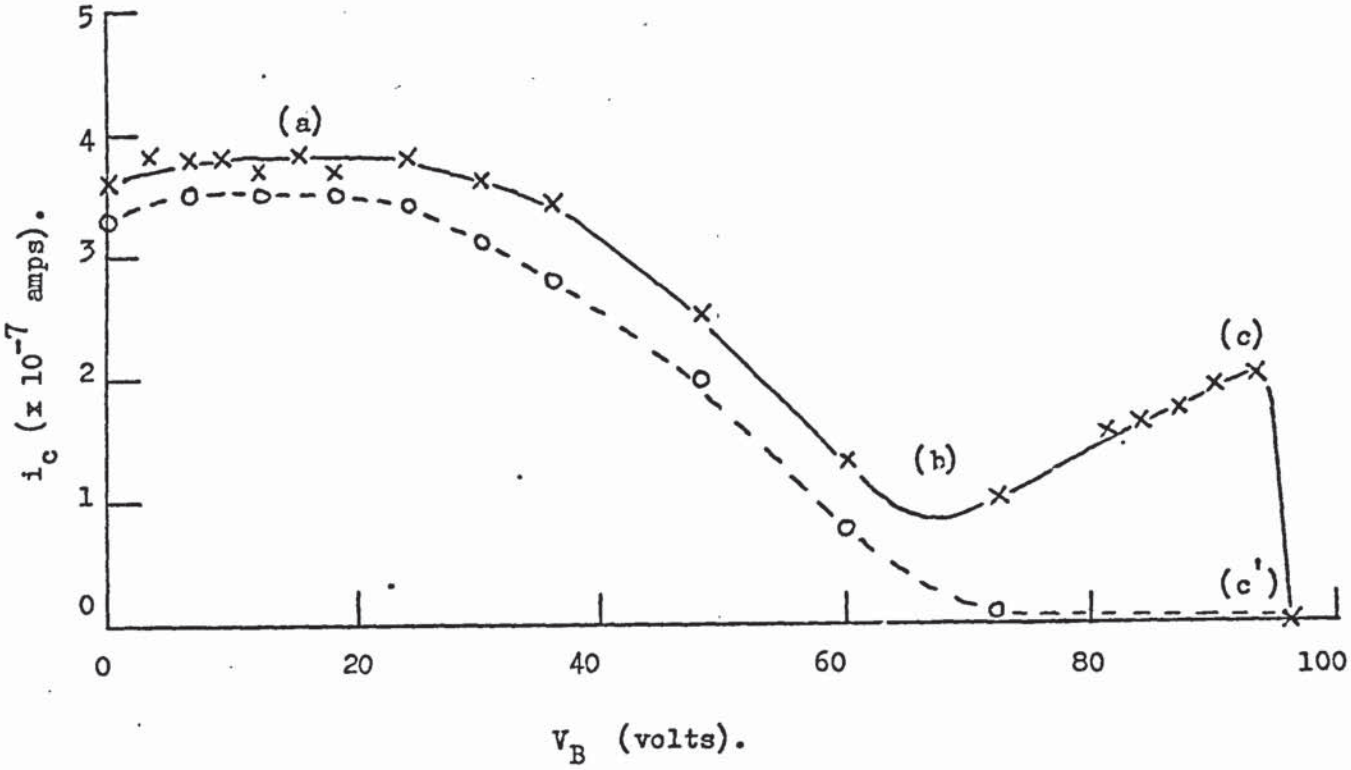

Figure 2.10. Modes of operation in the twin wire oscillator.

angular momentum about the anodes in order to go into an orbiting trajectory. Electrons ejected from the collector electrode by positive ion bombardment and secondary electrons from the gas phase ionisation would not have sufficient angular momentum around the anodes to enable them to go into orbit. Thus, the orbiting mode will be relatively independent of V_A, as the secondary electrons do not contribute to it. However, electrons must not have a large velocity component tangential to the anodes in order to go into the oscillating mode. Thus, electrons ejected from the collector surface by ion bombardment and secondary electrons from the gas phase ionisation will probably go into oscillation if they are produced in the appropriate region near the y axis. Hence, the oscillating mode will be dependent upon V_A as these electrons will gain more energy and so produce more ions and electrons as V_A is increased. The existence of the oscillating electron contribution in the twin wire oscillator when operated under the orbiting mode condition, was demonstrated by an experiment in which two external electrodes A and B were positioned outside the collector electrode of the twin wire oscillator, as illustrated in Figure 2.11(a). Electrode A was positioned on the y axis, opposite the filament and the current collected by electrode A will be dependent upon positive ions produced by both the orbiting mode and the oscillating mode electrons, escaping through the collector. Electrode B was positioned on the x axis at right angles to the filament and the current collected by electrode B will be dependent upon positive ions produced by only the orbiting mode electrons. With $i_a = 1\ \mu A$, the variation of the currents in A and B with V_A was determined. The values of V_B employed were 6, 12, 18, 24 and 30 volts for values of V_A of 1, 2, 3, 4 and 5 kV respectively. These correspond to the peak (a) in Figure 2.10. It can be seen in Figure 2.11(b) that the current B is independent of V_A whereas the current A is dependent upon V_A.

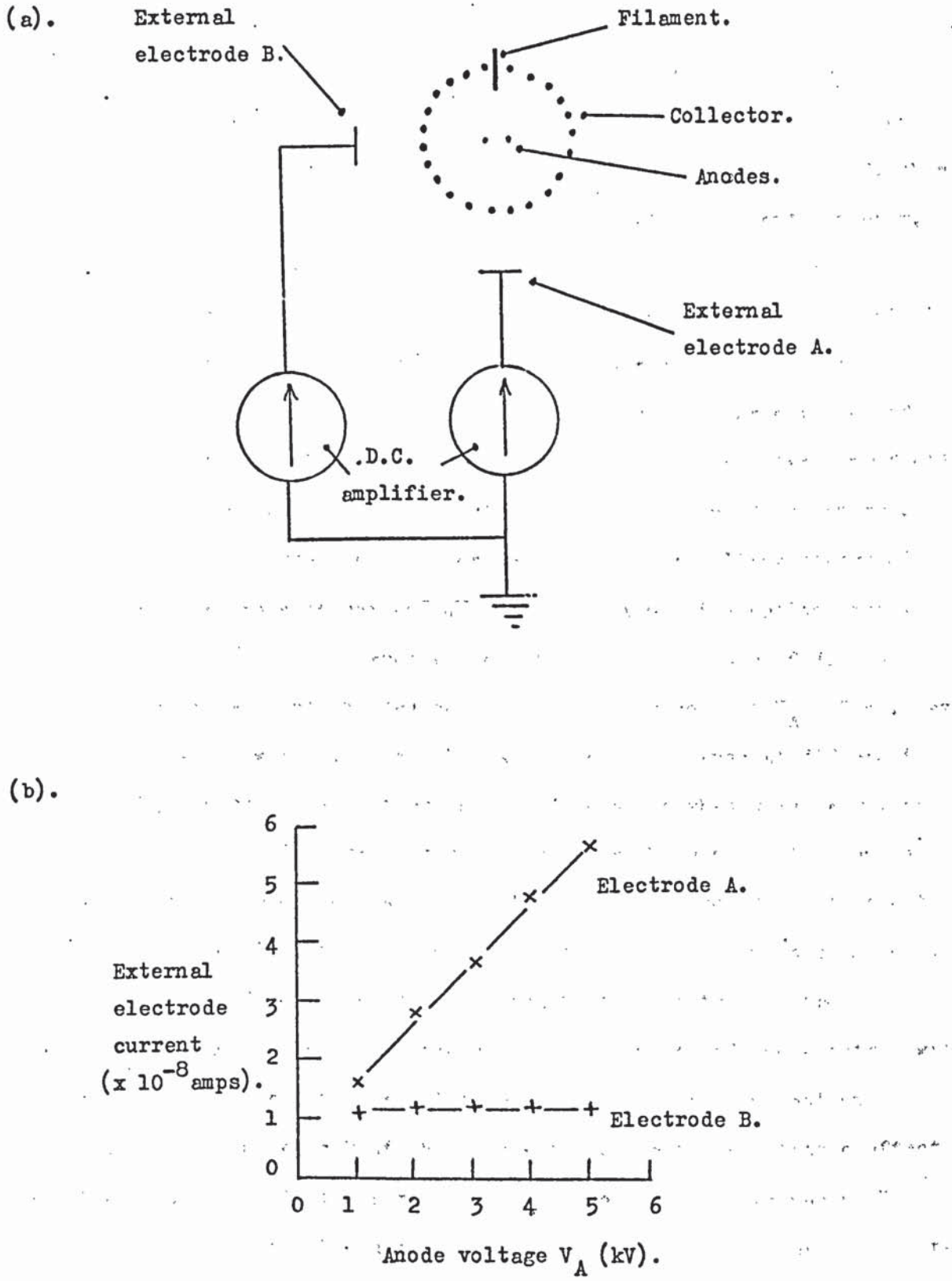

Figure 2.11. Demonstration of the dependence of the oscillating mode upon the anode voltage.

Returning to Figure 2.4(a-d), it can be seen that as the filament immersion depth D is increased, the maximum value of i_c in the orbiting mode peak also increases. This is due to the accelerating field around the filament being insufficient to give many of the electrons sufficient angular momentum about the anodes when D is small. As D is increased, this accelerating field also increases if V_B is maintained constant. However, when D reaches about 0.5 cm, any further increase in D results in no further increase in the maximum value of i_c for the orbiting mode. This is due to the maximum ionisation cross-section of air occuring when the incident electron energy is in the region of 100 eV. At large values of D, as for example when D = 1.33 cm (Figure 2.4(d)), the accelerating field around the filament can give the electrons far more than 100 eV energy. Thus, V_B has to be increased in order to reduce the resulting energy of the orbiting electrons to correspond with the maximum ionisation cross-section for air. Hence, at large values of D and low values of V_B, the ionisation efficiency of the device in the orbiting mode at V_A = 2 kV, may be less than at V_A = 1 kV. This will cause the bias curves at different values of V_A, to cross each other as V_B is increased when D is large, as is the case when D = 0.91 cm (Figure 2.7(d)) for the single plate anode device. It should be noted that the field distortion around the filament determines the initial kinetic energies of the electrons and the anode field will then modify the electron energy further as the electron approaches the anode. Thus, the average kinetic energy of the electron will depend upon the trajectory that it takes during its orbiting motion.

The immersion depth D of the filament appears to have little effect upon the value of i_c in the pure oscillating mode at high values of V_B. This is to be expected, because in the oscillating mode, a large accelerating field around the filament is neither required nor desired. It is for this reason that the pure oscillating mode only occurs at high values of V_B, when a nearly collimated beam of electrons is obtained. The maximum

value of i_c for the oscillating mode is obtained when V_B is near to emission cut-off from the filament. Then the electrons are emitted from only the very tip of the filament which gives the most favourable conditions for a collimated beam of electrons with little velocity component tangential to the anodes.

The variation with D of the maximum ion current i_c obtained on the orbiting mode peak for both the twin wire and single plate anode devices is given in Figure 2.12(a) for V_A = 1kV and in Figure 2.12(b) for V_A = 3kV. This data was obtained at a pressure of 1.4×10^{-5} torr and with i_a = 1 μA. With values of D at 0.5 cm or greater, the orbiting electrons make most of the contribution to i_c. The small difference in i_c between the twin wire oscillator and the single plate anode device is due to those electrons coming off the filament tip and going into oscillation between the anodes in the twin wire oscillator. This oscillating electron contribution increases with V_A and so this difference is greater at V_A = 3 kV than at V_A = 1 kV. However with D less than about 0.5 cm, the contribution from electrons, that at sometime during their trajectories must have passed between the twin wire anodes, increases as D is reduced. When D is less than about 0.2 cm, i_c is very small in the single plate anode device case and so the contribution from orbiting electrons is apparently very small, this being due to the low accelerating field around the filament at these small filament immersion depths. Thus, it seems likely that at these small values of D, the major contribution to i_c in the twin wire oscillator is due to electrons that have insufficient energy to orbit around the anodes continually and so follow a trajectory that eventually takes them between the anodes. Thus, there will probably be a third mode of operation which is predominant at only small values of D in the twin wire oscillator. This third mode could possibly be a composite of the oscillating and orbiting modes, as illustrated in Figure 2.13(a). Complex electron trajectories may arise, such as the Figure of "8" trajectory illustrated. Evidence for

(a).

V_A = 1 kV.

Maximum i_c on the low bias peak ($\times 10^{-7}$ amps).

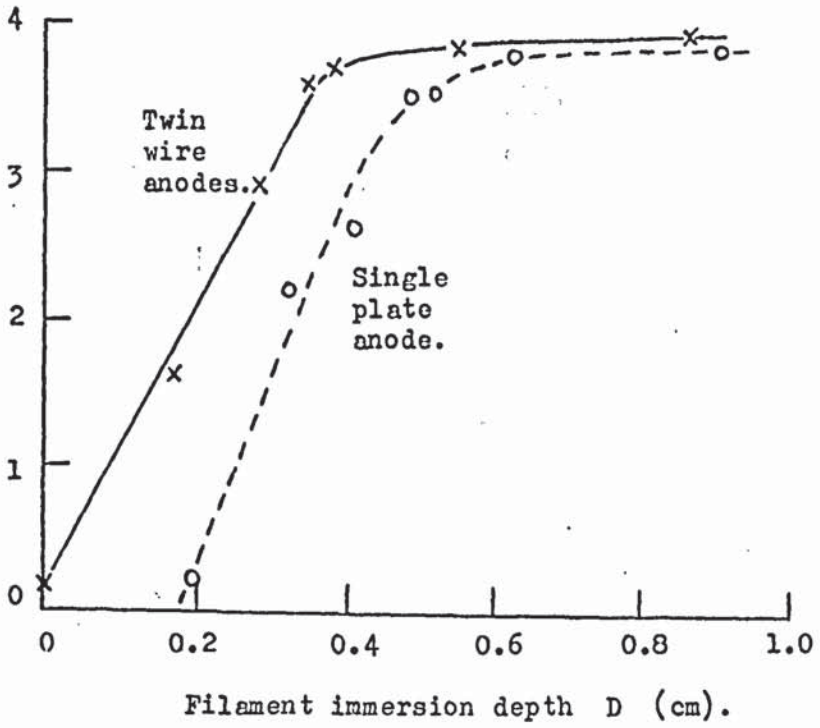

(b).

V_A = 3 kV.

Maximum i_c on the low bias peak ($\times 10^{-7}$ amps).

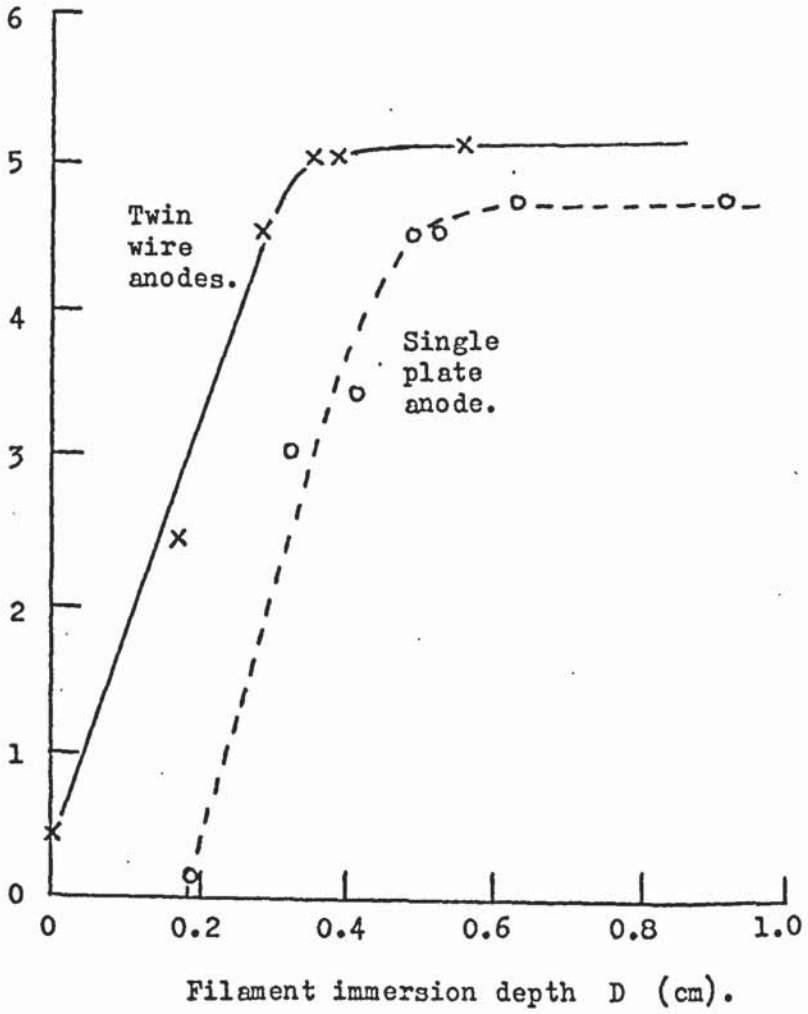

Figure 2.12. Variation of the maximum value of i_c for the orbiting peak with change of filament immersion depth.

(a).

Oscillating mode.

Orbiting mode.

Composite mode.

Figure of "8" trajectory.

(b).

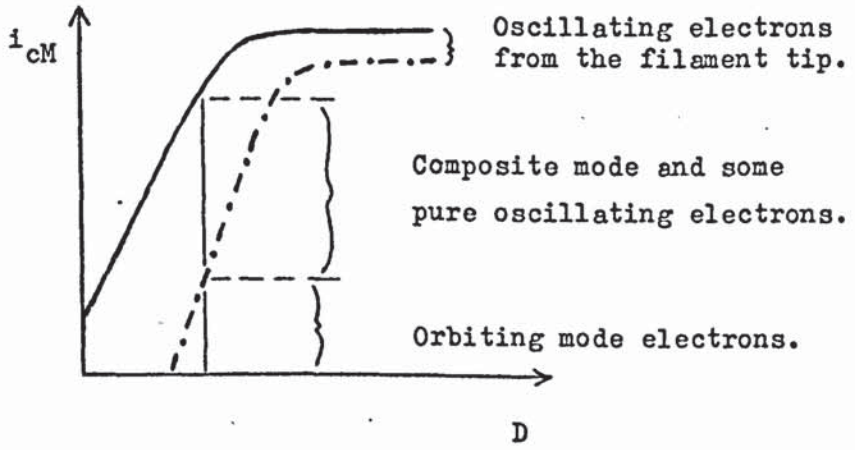

i_{cM} = The maximum ion current obtained on the low bias peak.

D = Filament immersion depth.

———— Twin wire device.

—·—·—·— Plate anode device.

Figure 2.13. Composite electron modes.

the existence of such trajectories has also been obtained when using the rubber model analogue to predict electron trajectories.

The contributions of these various electron modes are summarised in Figure 2.13(b). When D is zero, i_c is most likely due in the twin wire oscillator, to oscillating electrons and perhaps a small contribution from the composite mode. When D is zero in the single plate anode device, i_c is less than 5×10^{-10} amps giving sensitivities less than 100 $torr^{-1}$, indicating that the electrons were going almost immediately to the plate anode.

2.6. Discussion.

It has been shown that with the thermionic twin wire oscillator with the solid cylindrical collector electrode (Fitch et al[38]), the two peaks in the bias characteristics (Figure 1.14) were due to the orbiting and oscillating electron modes. However, the orbiting peak was depressed due to a very small filament immersion depth being used in this device. Similar experiments have been carried out using a solid stainless steel collector electrode, but with larger filament immersion depths. Bias characteristics were obtained that had pronounced orbiting mode and oscillating mode peaks similar to that with the 32 rod collector electrode. The small amount of field distortion at the 1% equipotential in the 32 rod collector (Figure 2.5(a)) appeared to produce little deterioration in the performance of the device.

When operating the twin wire oscillator in the orbiting mode at $V_A = 1$ kV and at a pressure of about 10^{-6} torr, i_a was varied from 1 to 6 μA and i_c was found to vary linearly with i_a in this region. This indicates that the device is not space-charge limited at this pressure. The orbiting mode peak was always very reproducible, though this was not always the case with the oscillating mode peak.

In the bias characteristics of the nude twin wire oscillator as described by Fitch et al[38], the orbiting mode peak is probably depressed due to the field distortion at the nude collector electrode. Hence, the only electrons that can orbit successfully are those which pass near to the anode wires. The oscillating mode peak will also probably be depressed due to the smaller number of secondary electrons liberated from the reduced collector electrode area. This could explain why the bias characteristics for the nude oscillator consist of only a single peak as shown in Figure 1.15. The maximum collector current i_c will occur at a bias voltage V_B where the electrons are both orbiting closely around and oscillating between the anode wires. This value of V_B will not be ideal for either the orbiting nor the oscillating modes and so a relatively low sensitivity is obtained for the nude oscillator.

The thermionic twin wire oscillator with the 32 rod collector electrode, gives very high sensitivities in excess of 10^4 $torr^{-1}$ at 10^{-5} torr, when operated in either the orbiting or the oscillating modes. The sensitivity of the twin wire oscillator was still increasing with decrease in pressure and at 10^{-6} torr when operated in the orbiting mode, sensitivities in excess of 10^5 $torr^{-1}$ were obtained with V_A = 1 kV. In order to maintain i_a at 1 μA, the filament has to be run at a much higher temperature for the oscillating mode than for the orbiting mode. This is due to the restricted area of electron emission from the filament when operated under the high bias voltage conditions. The orbiting mode peak was very smooth and flat at 10^{-5} torr, so that this method of electron injection appeared to be very suitable for an orbitron type device. Thus, the twin wire anodes were replaced by a single wire anode, giving rise to the electron-orbit ion gauge[41, 42]. The performance of this electron-orbit ionisation gauge in both high and ultra high vacuum conditions will be discussed in the next chapter.

CHAPTER 3.

THE ELECTRON - ORBIT IONISATION GAUGE.

3.1. Introduction.

At 10^{-5} torr, the orbiting mode peak in the bias characteristic of the twin wire oscillator shows no sign of any instabilities as reported for the orbitron at similar pressures by for example Gammon[27]. Thus, the twin wire anodes were replaced by a single wire anode positioned along the axis of the cylindrical 32 rod collector electrode, giving rise to the electron-orbit ionisation gauge (Fitch and Rushton[41,42]). Using the "V" shaped filament in this way gives a simple and efficient method of electron injection into this gauge, from which very high sensitivities are obtained.

3.2. The electron-orbit ionisation gauge in high vacuum.

3.2.1. Description of the gauge.

A schematic diagram of the gauge together with its associated electrical circuit is given in Figure 3.1. The construction and materials used for the gauge were identical to those of the thermionic twin wire oscillator described in section 2.2.1, except for the use of a single anode wire. The anode wire was of 0.4 mm diameter tungsten and was positioned along the axis of the collector electrode. The electrical circuit was essentially the same as that described in section 2.2.2 for the thermionic twin wire oscillator. However, the electron emission current i_e from the filament was no longer monitored. An end-on view of the gauge, including the filament and its supports is shown schematically in Figure 3.2. This also shows the potential distribution within the gauge, with the equipotentials again given as a percentage of the anode

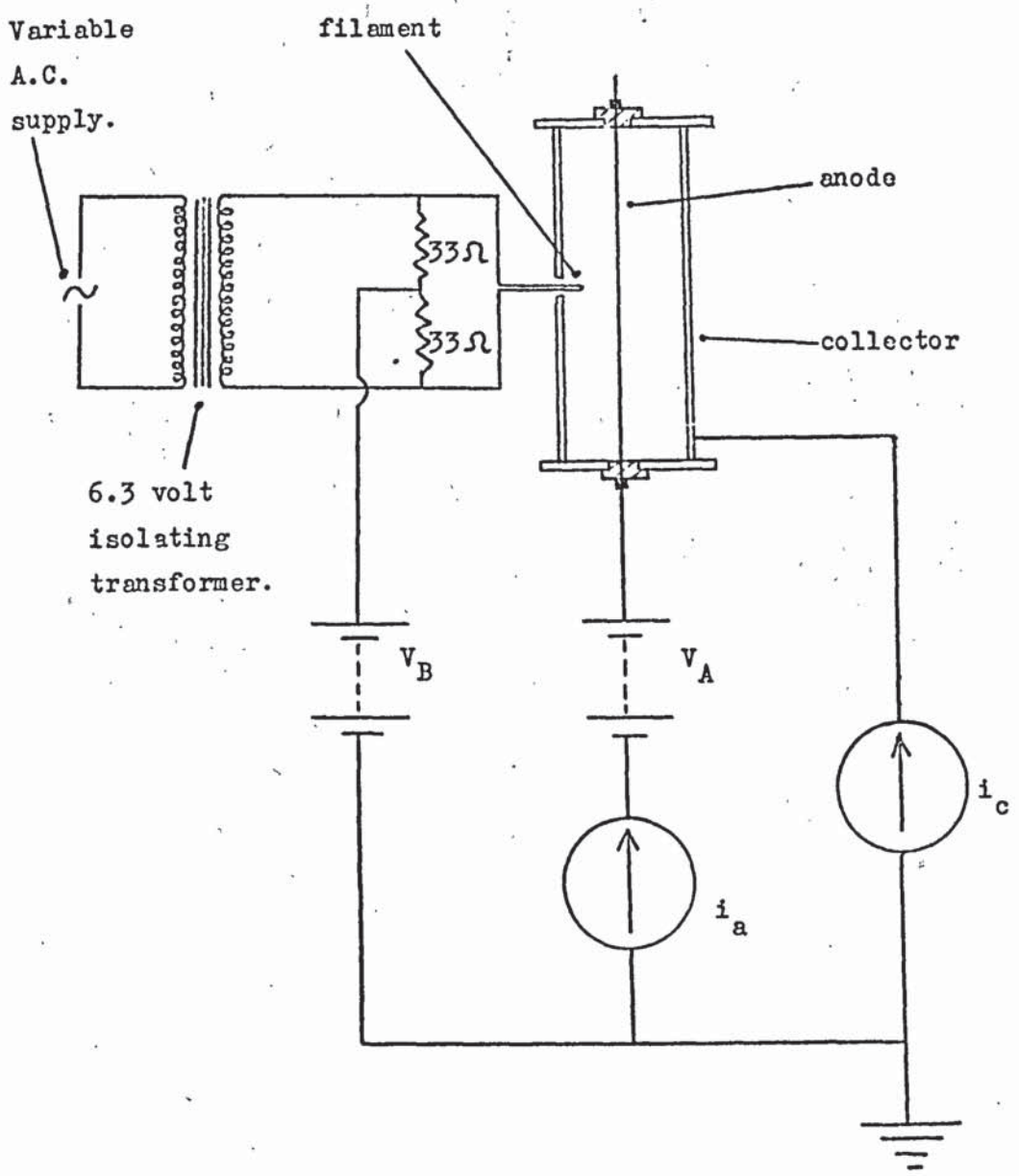

Figure 3.1. The electron-orbit ionisation gauge and its electrical circuit.

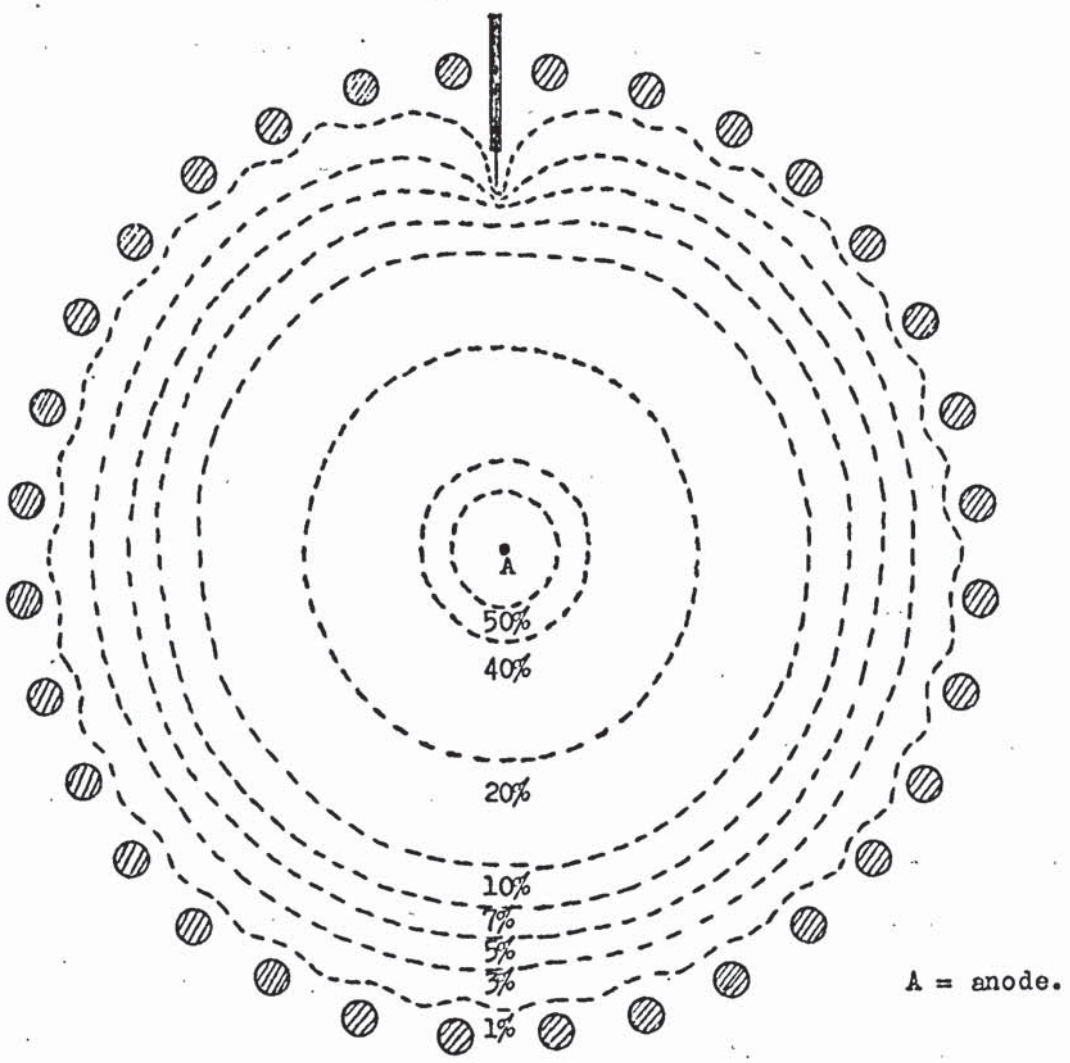

Figure 3.2. The potential distribution inside the electron-orbit ionisation gauge.

voltage V_A. As with the twin wire oscillator, the small amount of distortion of the electrostatic field caused by this 32 rod collector electrode can only be seen for the 1% equipotential line. Figure 3.2 also shows that with the filament and its supports at the same potential as the collector, a small potential disturbance exists around the filament. This potential disturbance is required to inject the electrons into orbiting trajectories about the anode. The gauge was tested down to about 10^{-6} torr in the oil diffusion pumped high vacuum system described in section 2.2.3.

3.2.2. Experimental results.

Bias characteristics of collector current i_c versus bias voltage V_B were obtained for the electron-orbit ionisation gauge whilst maintaining the anode current i_a at 1 μA. The anode voltage V_A was varied from 1 to 5 kV for several values of filament immersion depth D and the pressure was again maintained constant at 1.4×10^{-5} torr. Similar forms of bias curves were obtained as with the single plate anode device. At 10^{-5} torr, higher sensitivities were obtained than with either the twin wire or single plate anode devices. This increase in sensitivity was to be expected as the single wire anode is smaller and produces a true central force field whereas the plate anode only approximates to this field.

The value of the filament immersion depth D was not very critical but was found to be optimum at about 0.5 cm. For much smaller values of D, the accelerating field around the filament was insufficient to inject the majority of the electrons into satisfactory orbiting trajectories. On the other hand, for larger values of D, it was necessary to use high values of V_B to obtain maximum gauge sensitivity. With D = 0.5 cm, it can be seen in Figure 3.3, that i_c varies smoothly with changes in V_B. At a pressure of 1.4×10^{-5} torr, the maximum sensitivity is about

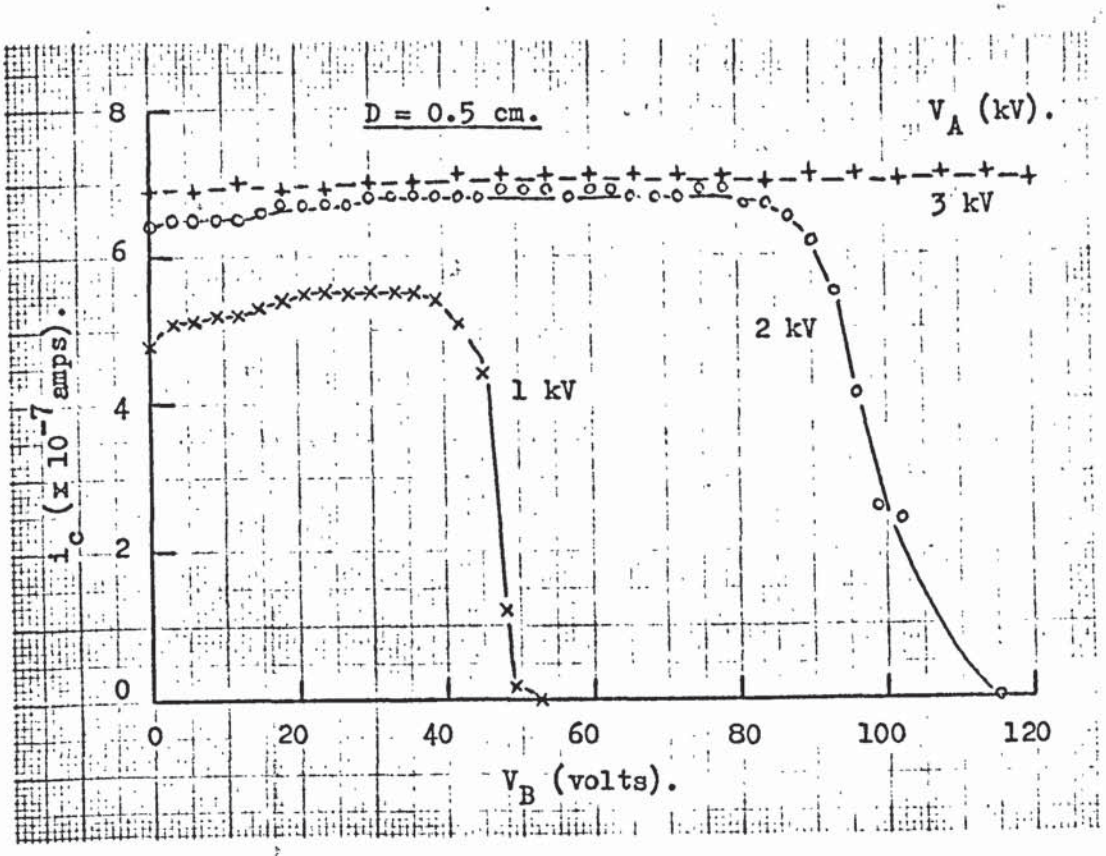

Figure 3.3. The variation of collector electrode current with filament bias voltage at a pressure of 1.4×10^{-5} torr.

4×10^4 $torr^{-1}$ with V_A = 1 kV and V_B = 30 volts; and about 5×10^4 $torr^{-1}$ with V_A = 3 kV and V_B = 90 volts. However, the loss in sensitivity when V_B = 0 is very small for all values of V_A at this pressure. The variation of the gauge sensitivity with pressure for V_A = 1, 2 and 3 kV with V_B = 30, 60 and 90 volts respectively is shown in Figure 3.4. At 1.4×10^{-6} torr, the sensitivity is 1.1×10^5 $torr^{-1}$ for V_A = 1 kV and 2.8×10^5 $torr^{-1}$ for V_A = 3 kV. The sensitivity is shown to increase with decreasing pressure for all values of V_A and has not reached a constant value at 10^{-6} torr. Results in Figure 3.4 indicate that the upper pressure limit of the gauge - that is when the gauge sensitivity is independent of pressure - will be in the region of 10^{-7} torr.

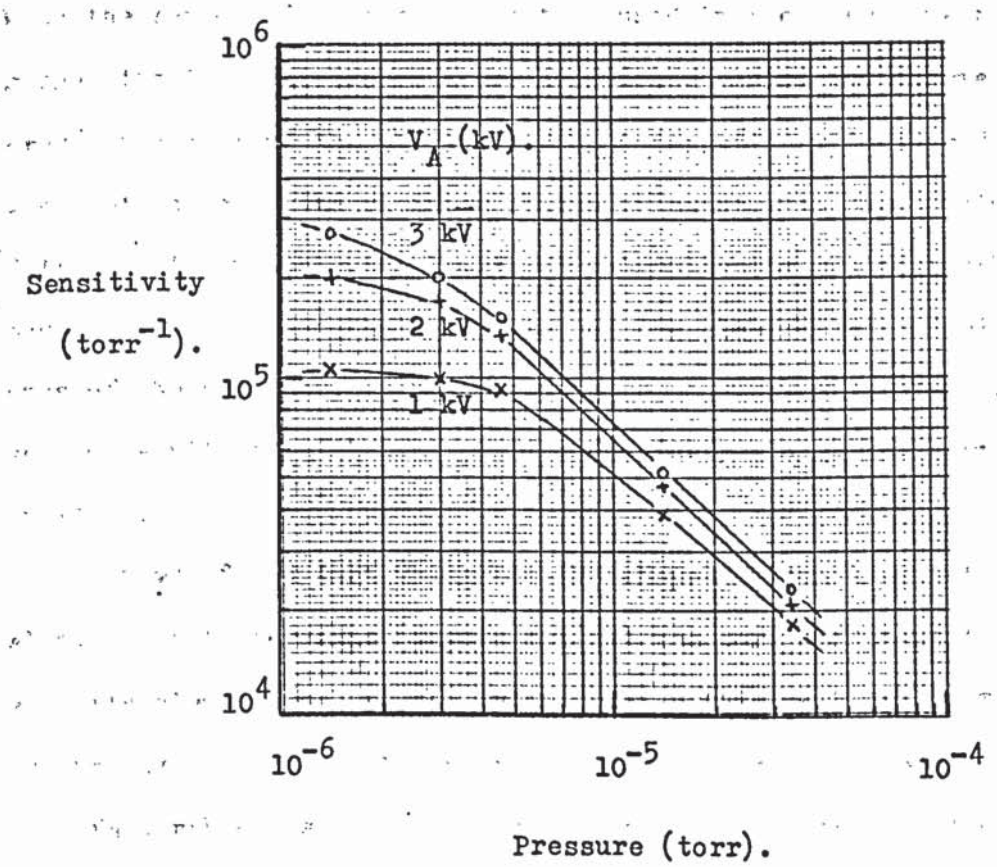

Figure 3.4. The variation of sensitivity with pressure.

3.2.3. Variation of the length of the gauge and the position of the filament.

The length of the gauge was varied from 20 cm downwards when operating at a pressure of about 10^{-5} torr. It was found that there was no significant loss in sensitivity until the length had been reduced to about 5 cm. This is when the collector length is equal to the collector diameter. The plane end-plates are adequate for the reflection of the electrons in the axial direction, as the electrons will be reflected at a distance from the end-plates which is approximately equal to the cylinder radius.

The largest potential disturbance in the orbitron arises from the presence of the filament supports rather than from the filament itself. With the method of electron injection used in the electron-orbit ionisation gauge, the filament supports are positioned behind the filament, so preventing most of the electrons from interacting with this distortion when returning to the vicinity of the filament. The positioning of the filament midway along the length of the collector cylinder makes it possible to have smooth termination of the electrostatic field at both ends of the cylinder. It was for this reason that all future measurements were made with the filament positioned midway along the length of the cylinder.

It was found that using the "V" shaped filament with its plane along the cylinder axis (Figure 3.5(a)) was more efficient than using it with its plane normal to the cylinder axis (Figure 3.5(b)). This was presumably on account of the larger emitting area of the filament being in a favourable position to inject electrons into the orbiting trajectories when the filament was positioned in the manner illustrated in Figure 3.5(a). Thus, all future measurements with the electron-orbit ionisation gauge, involved the use of the filament orientation illustrated in Figure 3.5(a).

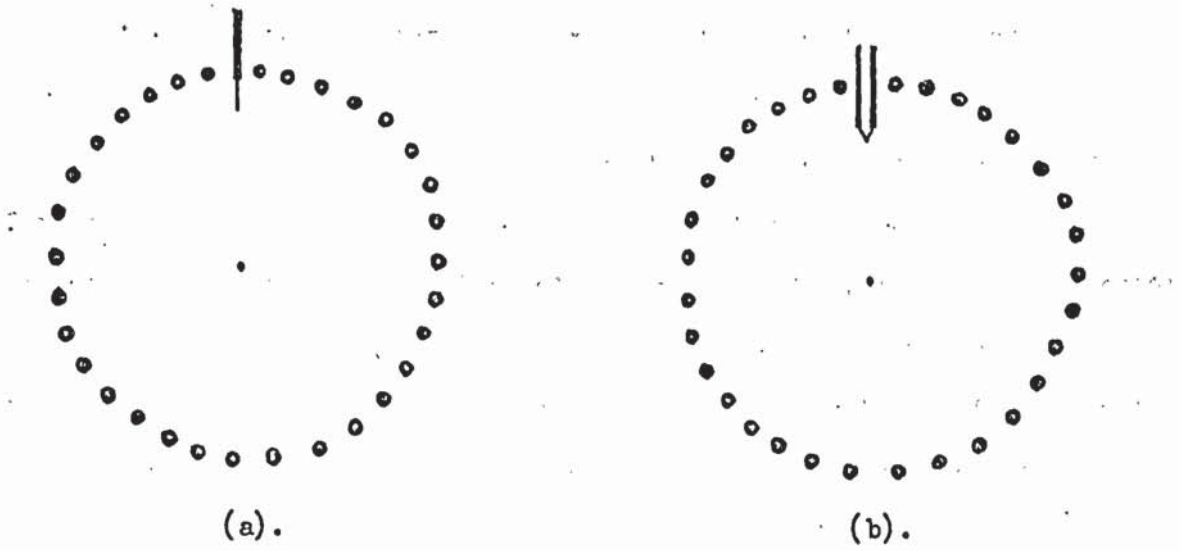

(a). (b).

Figure 3.5. Filament orientations.

3.2.4. Ion losses.

With the twin wire oscillator operated in the orbiting mode, it was found in experiments using a solid cylinder as the collector electrode, that the small amount of field distortion at the 1% equipotential for the 32 rod collector did not seriously influence the electron trajectories. This design did however, provide very good conductance to the vacuum system. The difference in collector currents for the solid cylinder and 32 rod collectors was attributed mainly to ion losses through the 32 rod collector. The ion losses were determined by measuring the electron current leaving the filament i_e, the electron current arriving at the anode i_a and the collector electrode current i_c. Thus, if i_L represents the ion current lost through the collector and neglecting secondary electron emission from the collector, then :-

$$i_L = i_a - i_e - i_c$$

and hence the the fractional loss of collector current is :-

$$\frac{i_L}{i_c + i_L} = \frac{i_a - i_e - i_c}{i_a - i_e}$$

It was found that for V_A = 1 kV, about 15% of the ions are lost through the 32 rod collector electrode. This is less than would be expected from this design of collector which has a 60% open structure. This must be due to some degree of ion focussing arising from the potential distortion around the collector rods. Thus, this open collector electrode structure should offer the advantage of reducing the effects of X-rays produced at the anode and so reduce the X-ray limit of the electron-orbit ionisation gauge when operated in ultra high vacuum conditions.

3.3. The electron-orbit ionisation gauge in ultra high vacuum.

3.3.1. Description of the gauge.

The ultra high vacuum form of the electron-orbit ionisation gauge (Fitch and Rushton[43]) was very similar to the high vacuum device, but was constructed entirely of stainless steel, tungsten and ceramic insulators as illustrated in Figure 3.6. The stainless steel end-plates were of 5 cm diameter and the 2 mm diameter tungsten rods were located in 32 "V" shaped notches around the circumference of the end-plates. Stainless steel cleats were used to secure the tungsten rods to the end-plates. Ceramtec bushes were again used to insulate the anode wire from the end-plates and collector rods. The anode wire was of 0.25 mm diameter tungsten and was positioned along the axis of the gauge cylinder. Due to the independence of gauge sensitivity with gauge length, the overall length of the gauge was reduced to 12.5 cm. The gauge including the 0.1 mm diameter filament and its supports, was mounted on a 6" o.d. conflat flange which was inserted into a stainless steel ultra high vacuum chamber. A filament immersion depth of 0.5 cm was used and a general view of the completed gauge mounted on the flange is given in Figure 3.7. The electrical circuit was essentially the same as given in Figure 3.1, except that the anode voltage was now supplied from H.T. batteries.

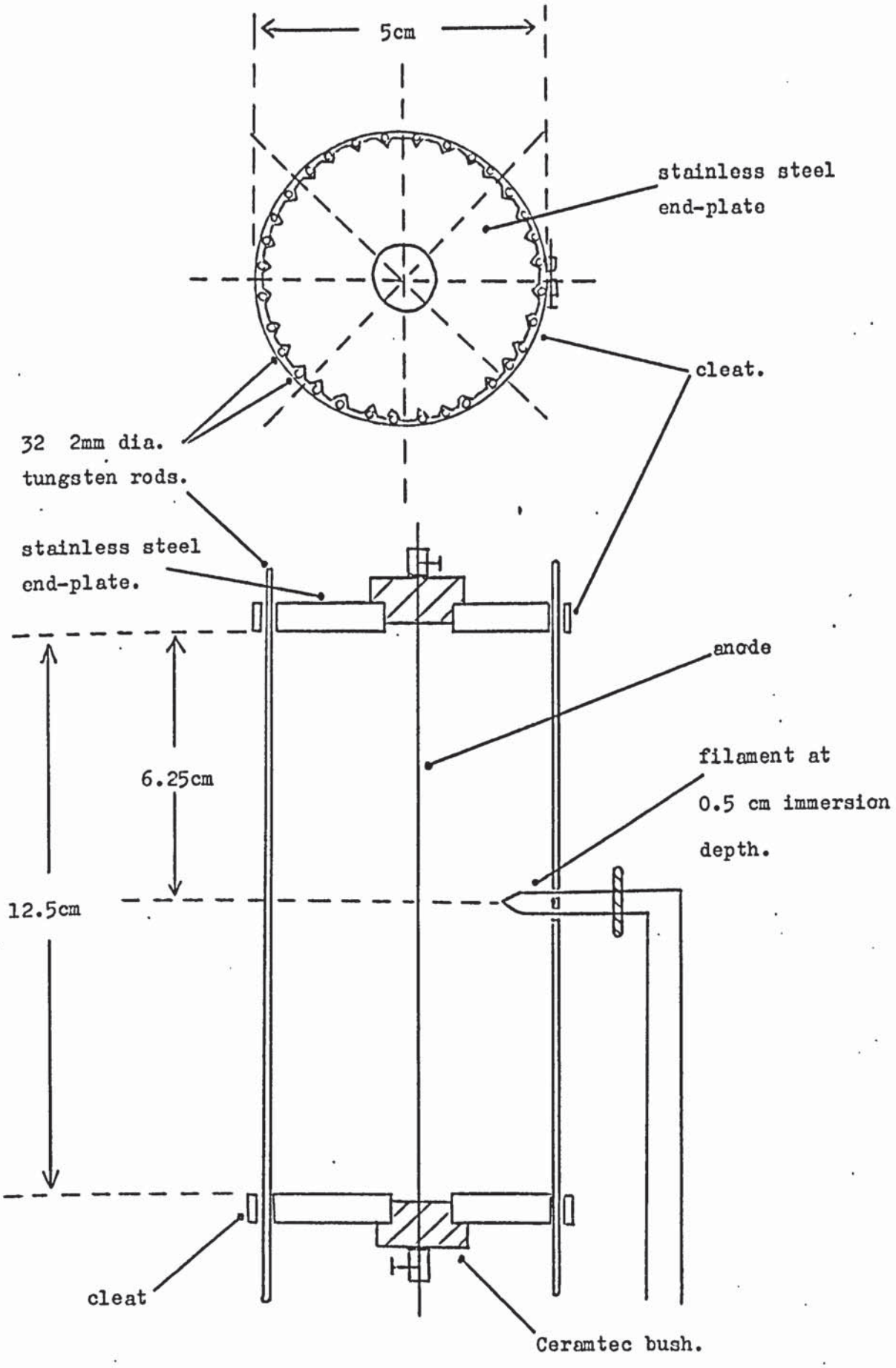

Figure 3.6. Schematic diagram of the electron-orbit ionisation gauge for use in ultra high vacuum.

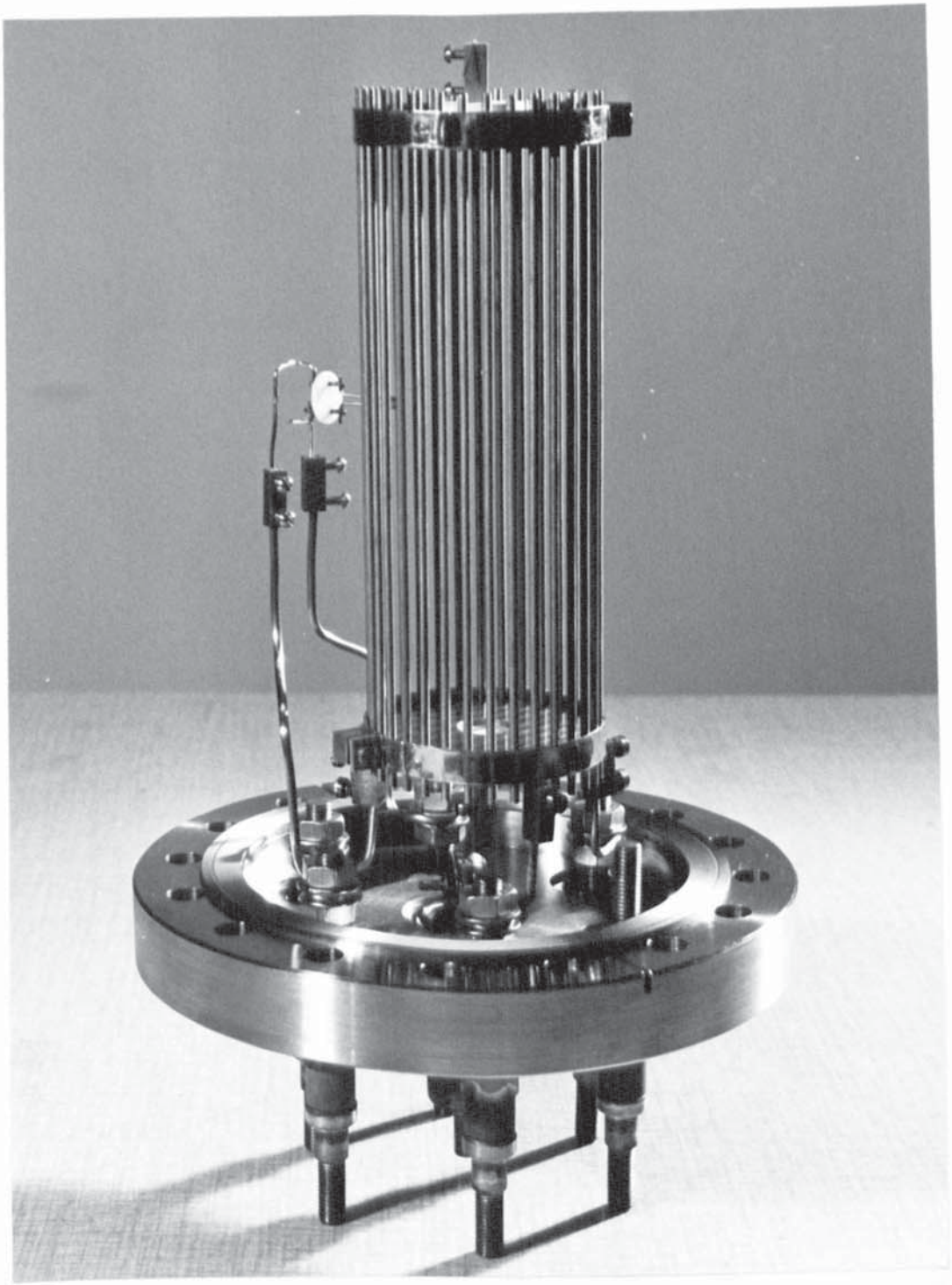

Figure 3.7. The electron-orbit ionisation gauge for use in ultra high vacuum.

3.3.2. The ultra high vacuum system.

A schematic diagram of the ultra high vacuum system is given in Figure 3.8. The system is a standard A.E.I. ultra high vacuum system with a 12" diameter stainless steel vacuum chamber. The system was roughed out to about 10^{-3} torr (as measured by a thermocouple gauge) by two liquid nitrogen cooled zeolite sorption pumps with the isolation valve open. At a pressure of about 10^{-3} torr, the 120 litre sec^{-1} triode ion pump could be operated and the isolation valve then closed. Extra pumping speed was obtained by using a water cooled sublimation pump. The sublimation period was automatically controlled but the cycling time had to be operated manually. Three ovens were used to bake the vacuum chamber and ion pump up to a temperature of 350° C. With this bakeout, pressures in the region of 10^{-11} torr could be achieved. The total gas pressure in the system was measured by both an A.E.I. Trigger gauge and a Mullard IOG 13T ionisation gauge. Partial pressure analysis could also be carried out by use of the Minimass mass spectrometer on the system. The gas pressure in the system could be controlled by pumping against a continual leak via the ultra high vacuum leak valve. Figure 3.9 shows the complete system together with the associated control units for the equipment. On top of the vacuum chamber is a 6" o.d. conflat flange onto which the experiments could be mounted.

3.3.3. Experimental results and discussion.

The bias characteristics for the electron-orbit ionisation gauge with V_A = 1 kV and i_a = 1 μA are given in Figure 3.10 for pressures ranging from 10^{-5} torr to 10^{-8} torr as measured by the Mullard IOG 13T ionisation gauge. A normal bias characteristic with a broad collector current peak was obtained at 10^{-5} torr, as shown in Figure 3.10(a). As the pressure was reduced to 10^{-6} torr, the peak became more critical as shown in Figure 3.10(b), with the maximum of the peak corresponding to the

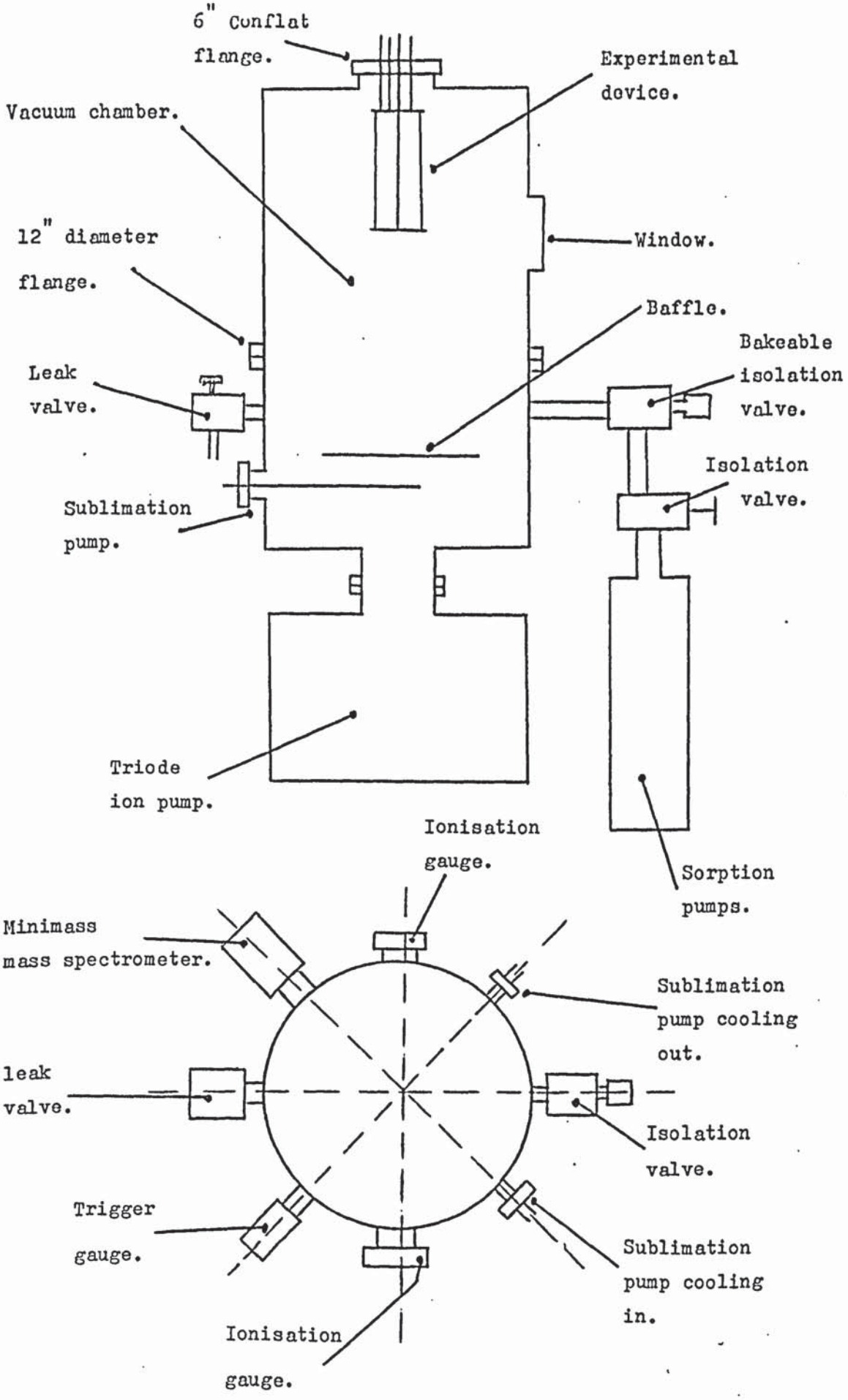

Figure 3.8. Schematic diagram of the ultra high vacuum system.

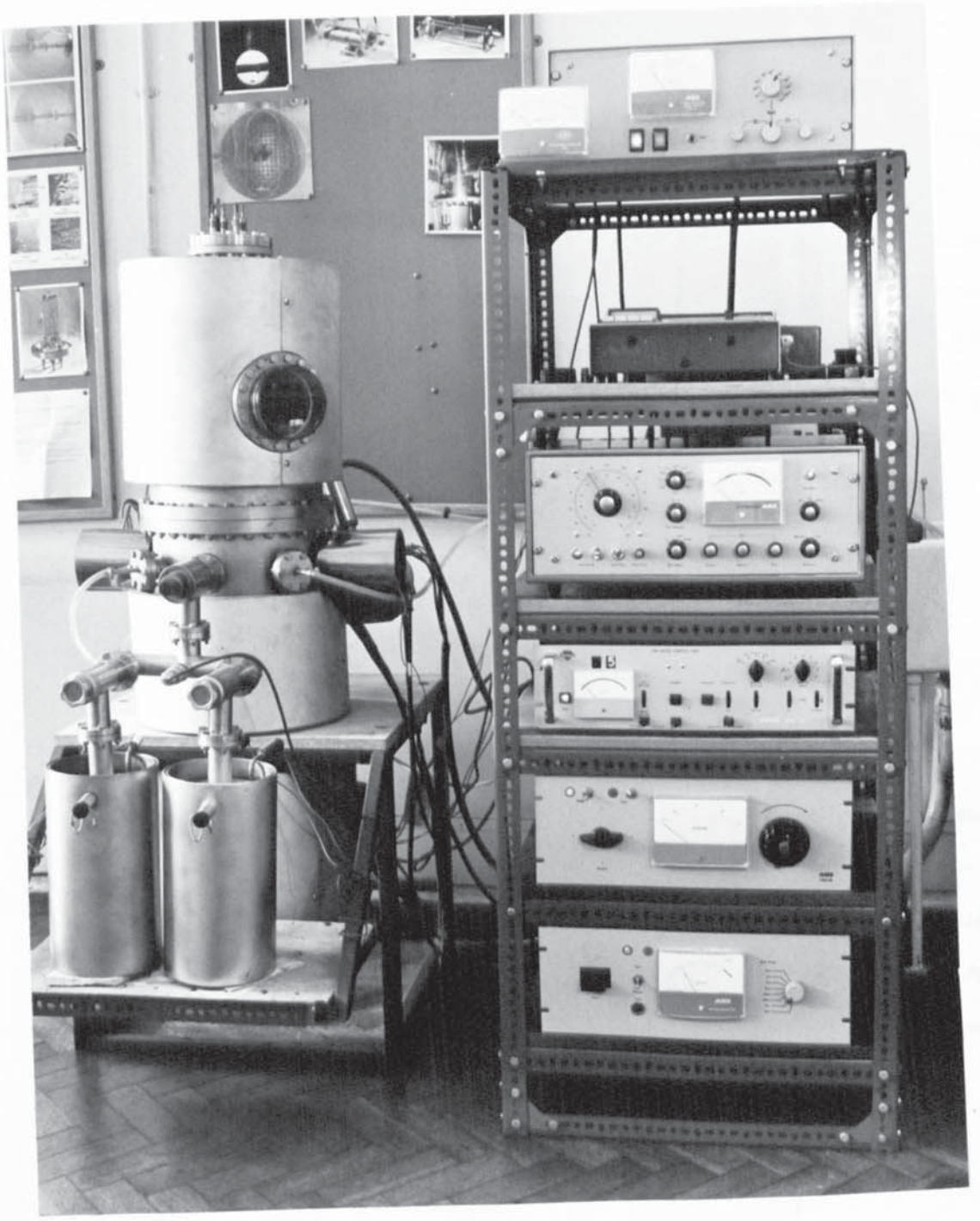

Figure 3.9. The ultra high vacuum system.

electron energies where the maximum ionisation cross-section occurs. However, at 5×10^{-7} torr, the general shape of the characteristic shown in Figure 3.10(c) is similar to that observed at 10^{-6} torr. The maximum sensitivity is 2×10^{5} $torr^{-1}$ at $V_B = +20$ volts. But there is clear evidence of a second peak occuring near this region of maximum sensitivity. Figures 3.10(d), 3.10(e) and 3.10(f) show the form of the characteristics at 10^{-7}, 5×10^{-8} and 10^{-8} torr respectively. It can be seen that as the pressure is reduced, the apparent sensitivity of the gauge also reduces and at 10^{-8} torr, the recorded collector current i_c is negative at nearly all values of V_B. These characteristics were quite reproducible and the positions of the various peaks were always found to occur at a definite value of V_B for any particular pressure.

If we examine the bias characteristic at 10^{-8} torr (Figure 3.10(f)), then at very small values of V_B, some of the electrons are able to reach the collector electrode due to their own thermal energies. In addition some electrons can reach the collector electrode due to the use of A.C. heating of the filament. The A.C. heating superimposes a small alternating voltage of approximately $\pm$ 1.5 volts upon the steady bias voltage V_B. This electron current to the collector is virtually independent of pressure and is therefore negligable at high pressures. Over the region AB, electrons leaving the filament only require to gain a small amount of energy due to the small value of V_B , in order to enable them to reach the collector electrode. Therefore, it is possible that i_a is mainly due to electrons that have travelled relatively short total path lengths, as the long lived electrons will possibly have gained sufficient energy in order to surmount the small potential barrier at low values of V_B and so reach the collector electrode. A possible mechanism by which they gain this excess energy may be by electron-electron collisions as suggested by Meyer and Herb[26] for the orbitron. Thus, at low pressures, this electron current to the collector will be larger than the positive ion current to the

collector, because at these values of V_B , the electron energies will not be near the maximum cross-section for ionisation.

As V_B is increased further, the electrons now require more energy to reach the collector and so the electrons will exist in stable trajectories. At pressures below about 10^{-7} torr, the total electron path lengths are large enough for these electrons to form a significant electron space-charge within the ionising volume. Thus, any further electrons ejected from the filament will tend to be screened from the anode by this space-charge. Electrons leave the filament in random directions and so an equilibrium of the electron space-charge density will not exist. With an imbalance of the electron space-charge density, the electrons tend to move into regions of lower electron density and so acquire kinetic energy and overshoot these regions. The imbalance remains and so the electrons are attracted back and again overshoot, so producing an oscillation of the electron space-charge density. Hence, some electrons will extract a nett energy from the space-charge oscillations, enabling them to reach the collector electrode. This electron space-charge will exist over the range of V_B from B to F. In this region, i_c will be negative due to more electrons than positive ions arriving at the collector electrode, but a peak CDE is obtained which is probably due to the electron energies at this value of V_B, being near to the maximum cross-section for ionisation of the gas molecules.

As V_B is again increased over the region FG, the area of electron emission from the filament will be restricted to the filament tip, thus making the electrons pass very close to the anode. This is a region of high potential gradient in the anode field and more electrons will go straight to the anode. Thus, the effect of the electron space-charge will be reduced and the positive ion current obtained with this bias voltage will predominate over region FG.

The electron space-charge hypothesis is supported by the fact that

(a).

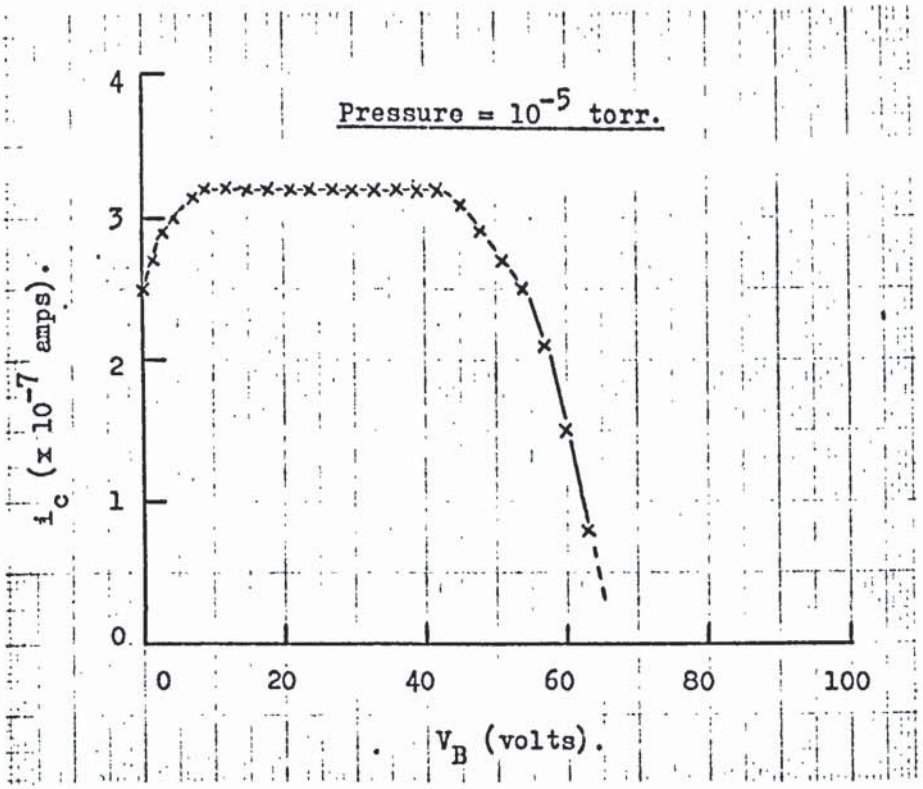

(b).

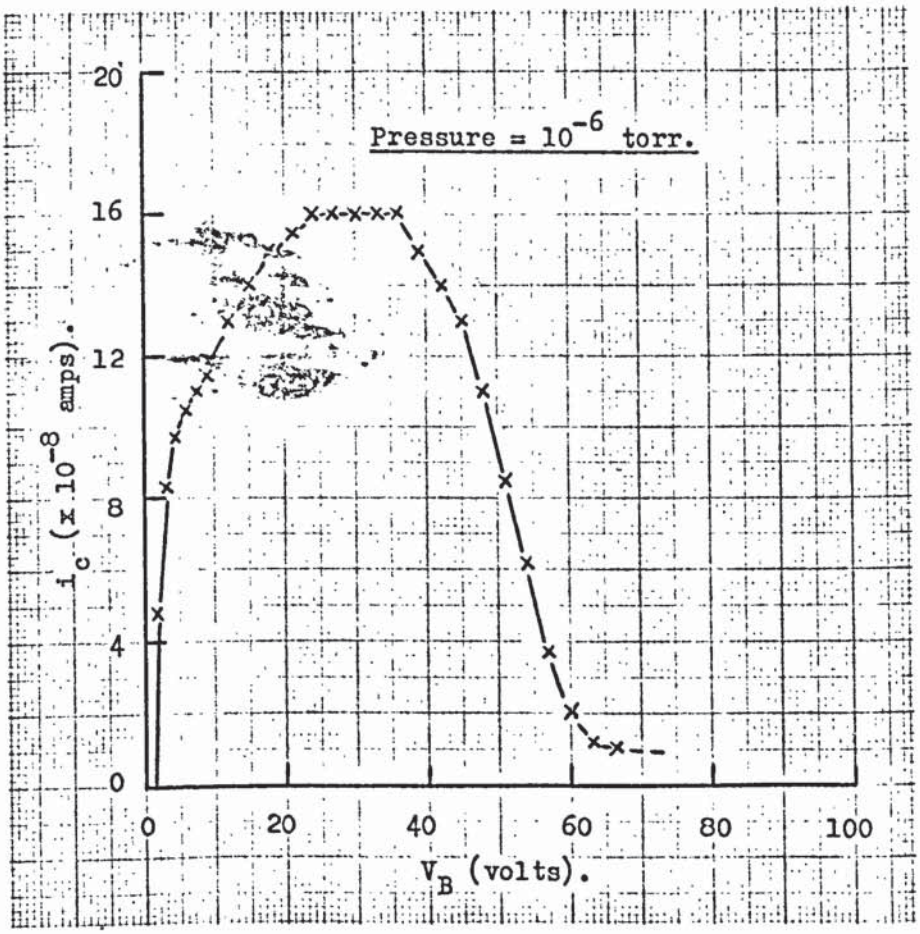

Figure 3.10. The bias characteristics of the electron-orbit ionisation gauge in ultra high vacuum.

(c).

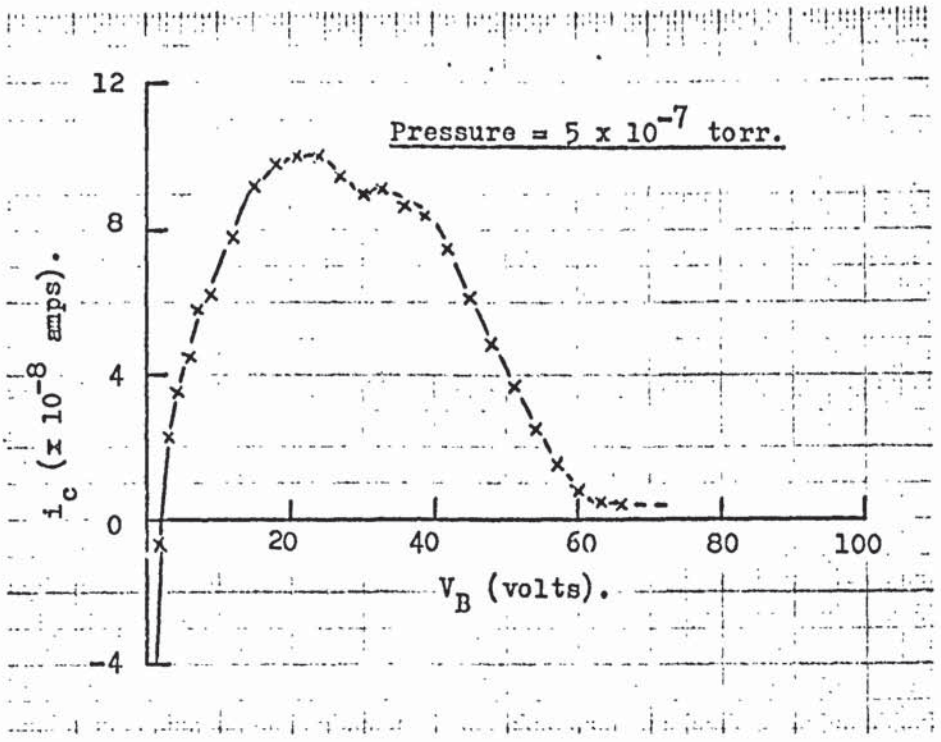

(d).

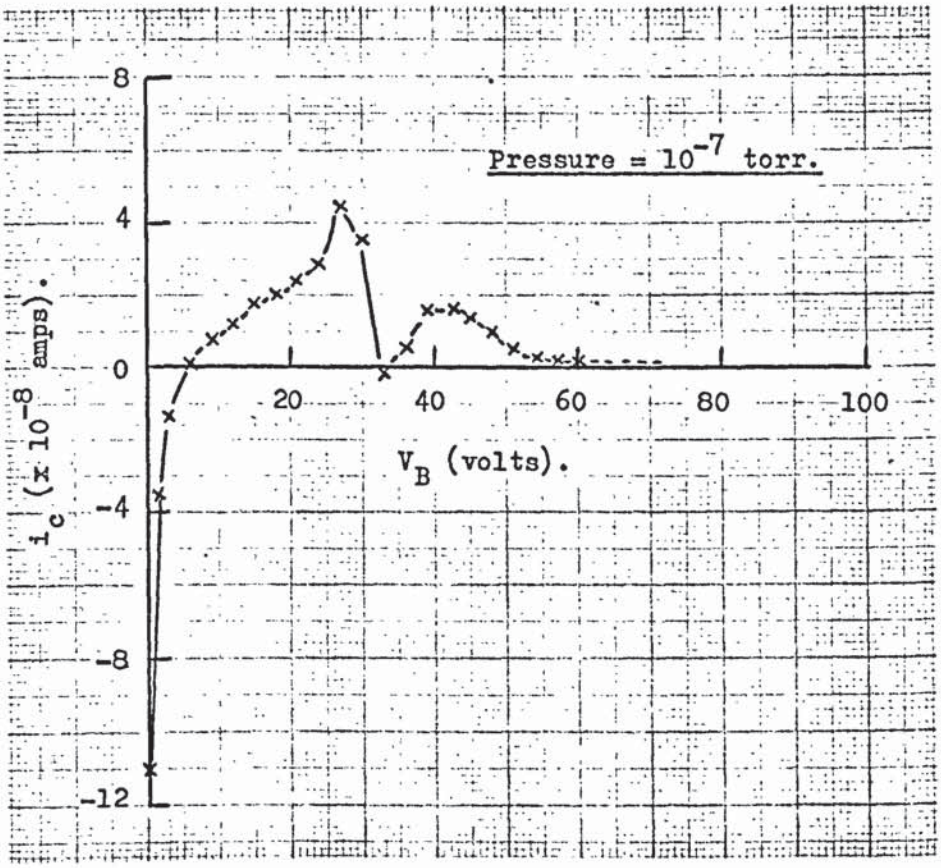

Figure 3.10. (continued).

(e).

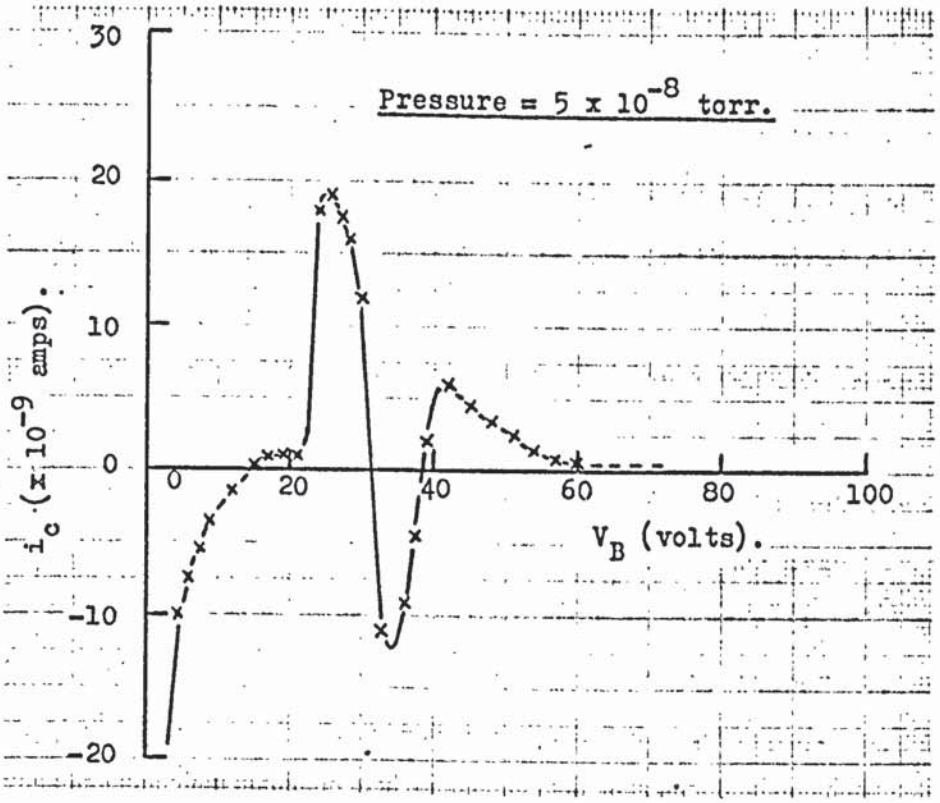

(f).

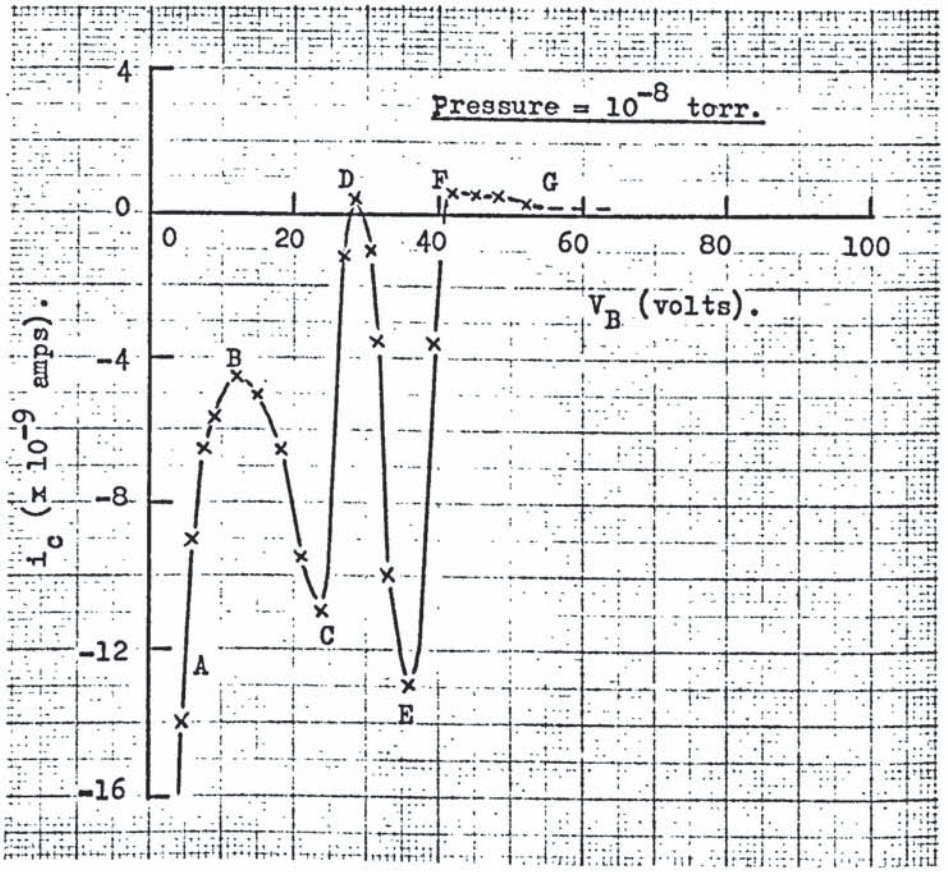

Figure 3.10. (continued).

if the electron emission current from the filament is increased, the electron current to the collector electrode at the minima C and E also increases (that is i_c goes more negative). A further point of interest is that these bias characteristics in Figure 3.10 were obtained without the mass spectrometer magnet being in position. The residual magnetic field in the ultra high vacuum system was of the same order as the stray magnetic field in the laboratory. With the mass spectrometer magnet in its normal position on the mass spectrometer, the leakage magnetic field was large ($> 10^{-4}$ webers m^{-2}) and the bias characteristic at 10^{-8} torr was modified in the manner illustrated in Figure 3.11. Therefore, the application of the magnetic field tends to remove the electrons from the electron space-charge to the anode; thus reducing the electron current to the collector electrode. This makes the positive ion current to the collector obtained at 10^{-8} torr predominate giving rise to a single peak in the bias curve.

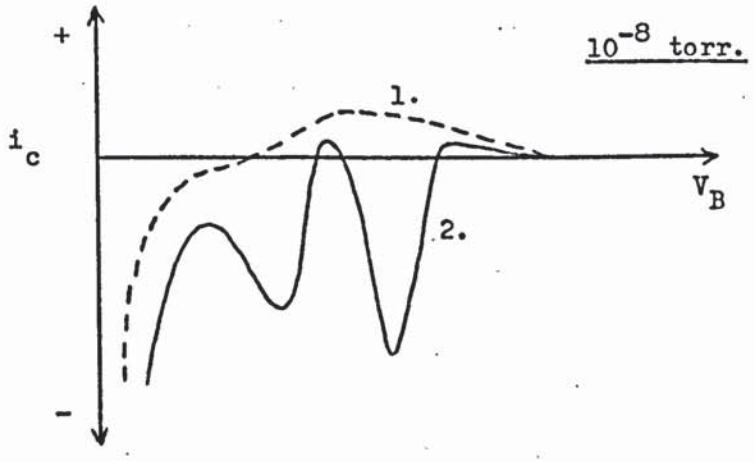

1. Mass spectrometer magnet in position.
2. Mass spectrometer magnet not in position.

Figure 3.11. Modification of the low pressure bias characteristic by the presence of a magnetic field.

The electron energies and trajectories will be modified by the anode field and by the presence of the electron space-charge. The electron mean free path between ionising collisions will be dependent upon pressure and so the extent to which the electron trajectories and energies are modified by the electron space-charge will be dependent upon pressure. This could possibly be the reason why the ion current peak D appears to move to slightly larger values of V_B with decrease in pressure.

With these electron space-charge oscillations present in the bias characteristics, the use of the device as a pressure measuring gauge is limited and attempts were made to overcome these limitations.

3.3.4. Reduction of the electron space-charge.

The bias characteristics given in Figure 3.10 were obtained with the anode current i_a maintained at 1 μA. In order to overcome the electron space-charge limitation of the electron-orbit ionisation gauge, the anode current i_a was reduced to 10^{-7} amps, so reducing the electron density within the ionising volume of the gauge. A D.C. amplifier was now employed to measure i_a and the mass spectrometer magnet was again removed.

The bias characteristics obtained with V_A = 1 kV and $i_a = 10^{-7}$ amps are given in Figure 3.12 for pressures ranging from 10^{-5} to 10^{-9} torr as measured with the Mullard IOG 13T ionisation gauge. With this reduced anode current of 10^{-7} amps, it can be seen that the collector current peak is constant at all pressures at about +36 volts filament bias V_B. No negative values of i_c are present at large values of V_B, indicating that no significant electron space-charge oscillations are present.

Figure 3.13 shows the variation of collector current i_c with pressure for the electron-orbit ionisation gauge operating at V_A = 1 kV, V_B = 36volts and $i_a = 10^{-7}$ amps. The pressures were measured simultaneously with the Trigger gauge and the IOG 13T gauge. As can be seen from the two graphs in Figure 3.13, there is agreement in the pressure values indicated by the

(a).

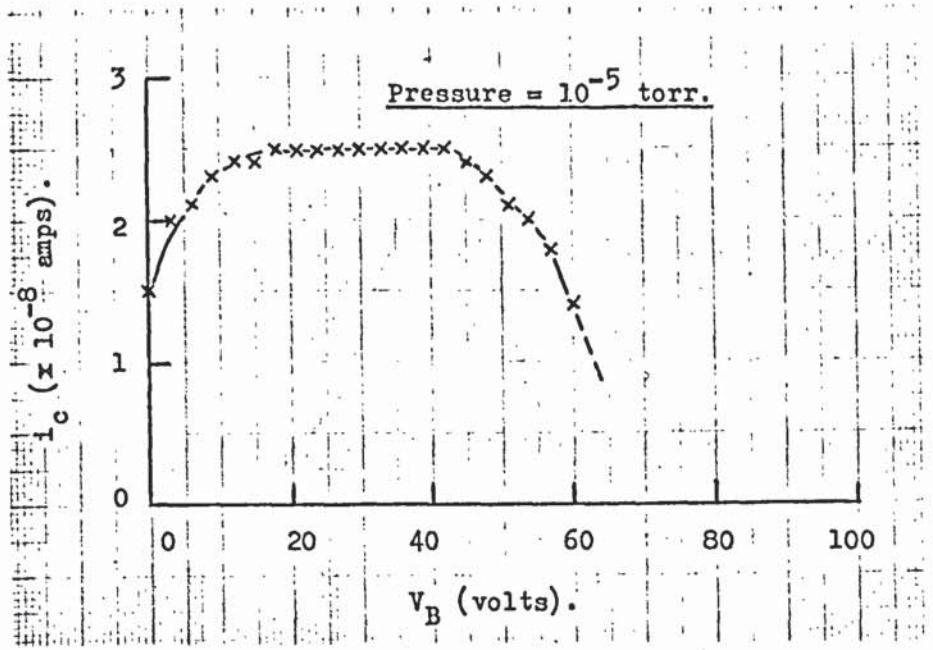

(b).

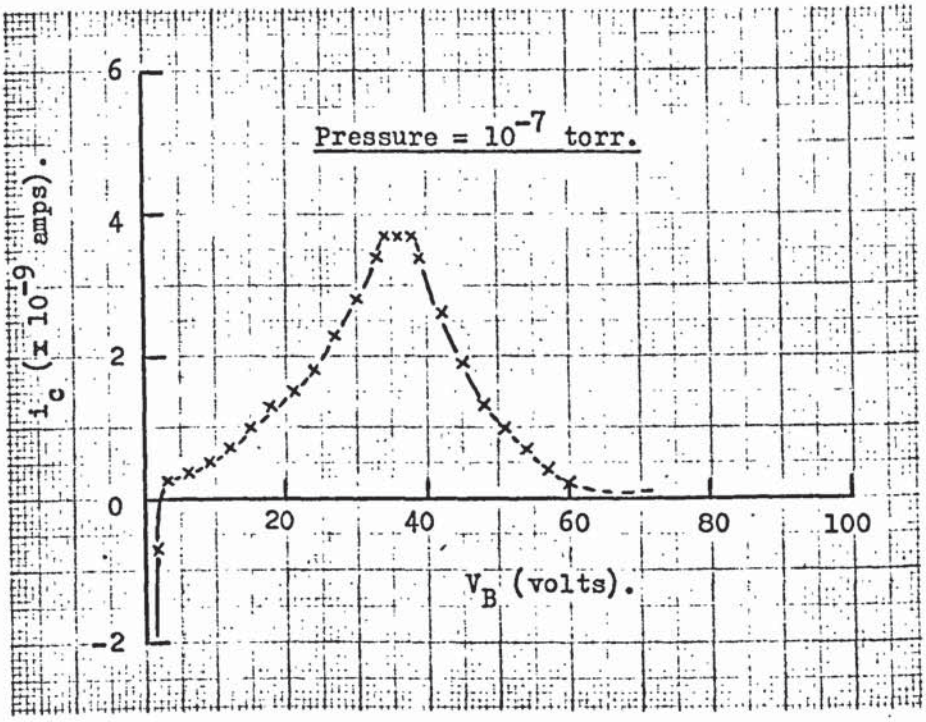

Figure 3.12. The bias characteristics for the electron-orbit ionisation gauge using a reduced electron emission current.

(c).

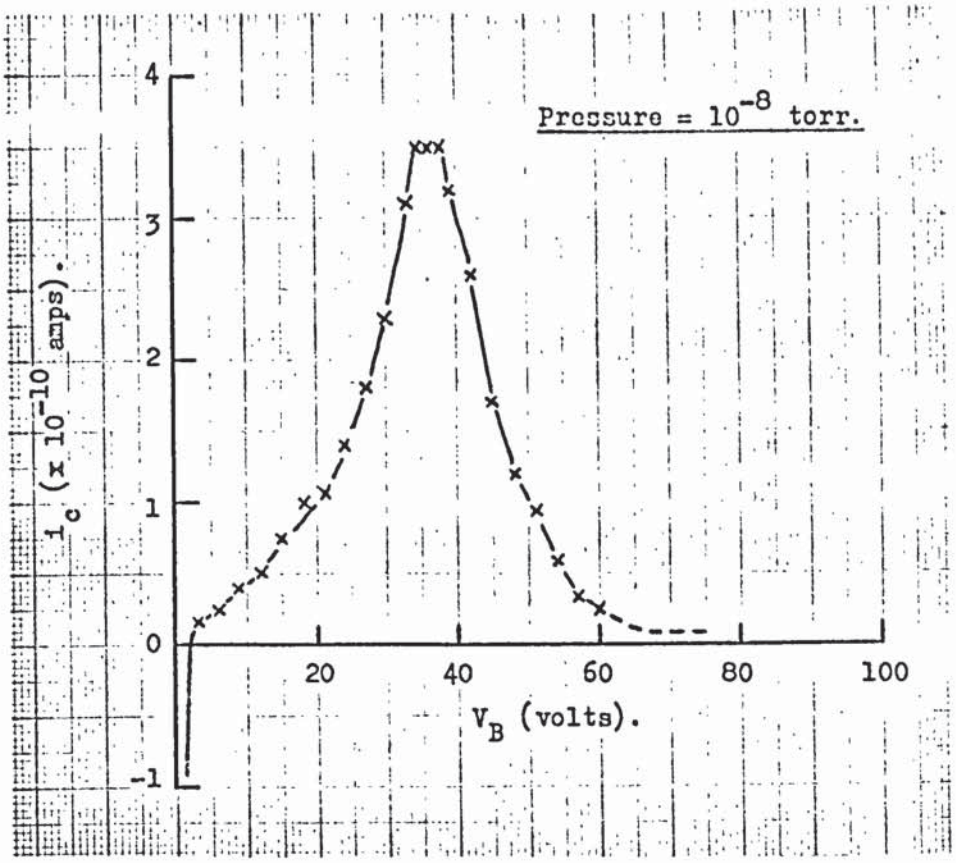

(d).

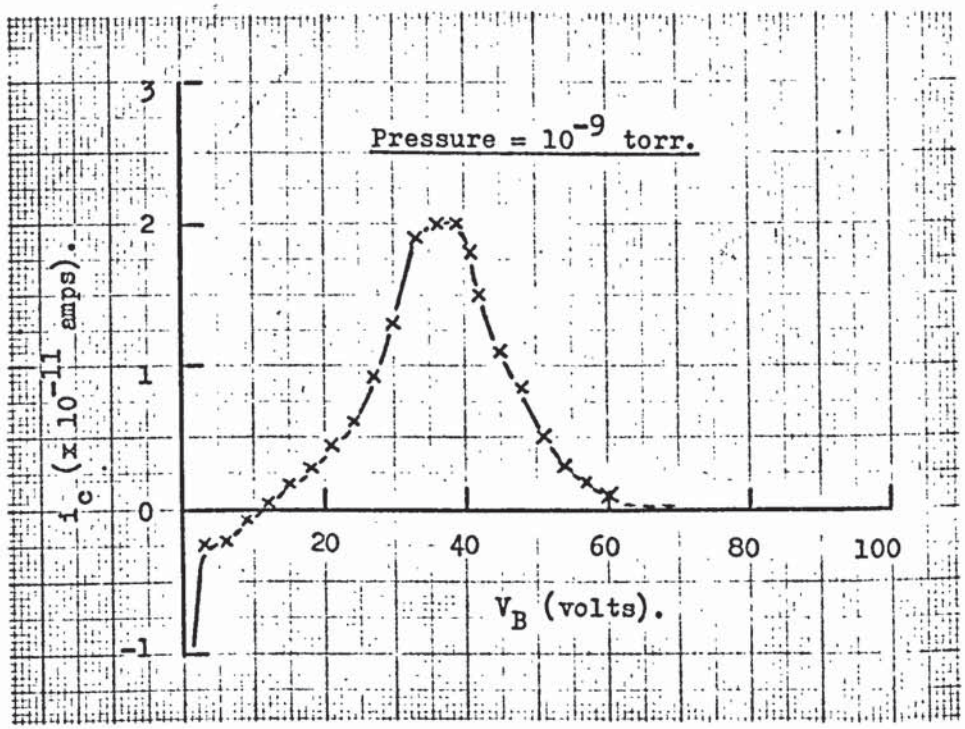

Figure 3.12. (continued).

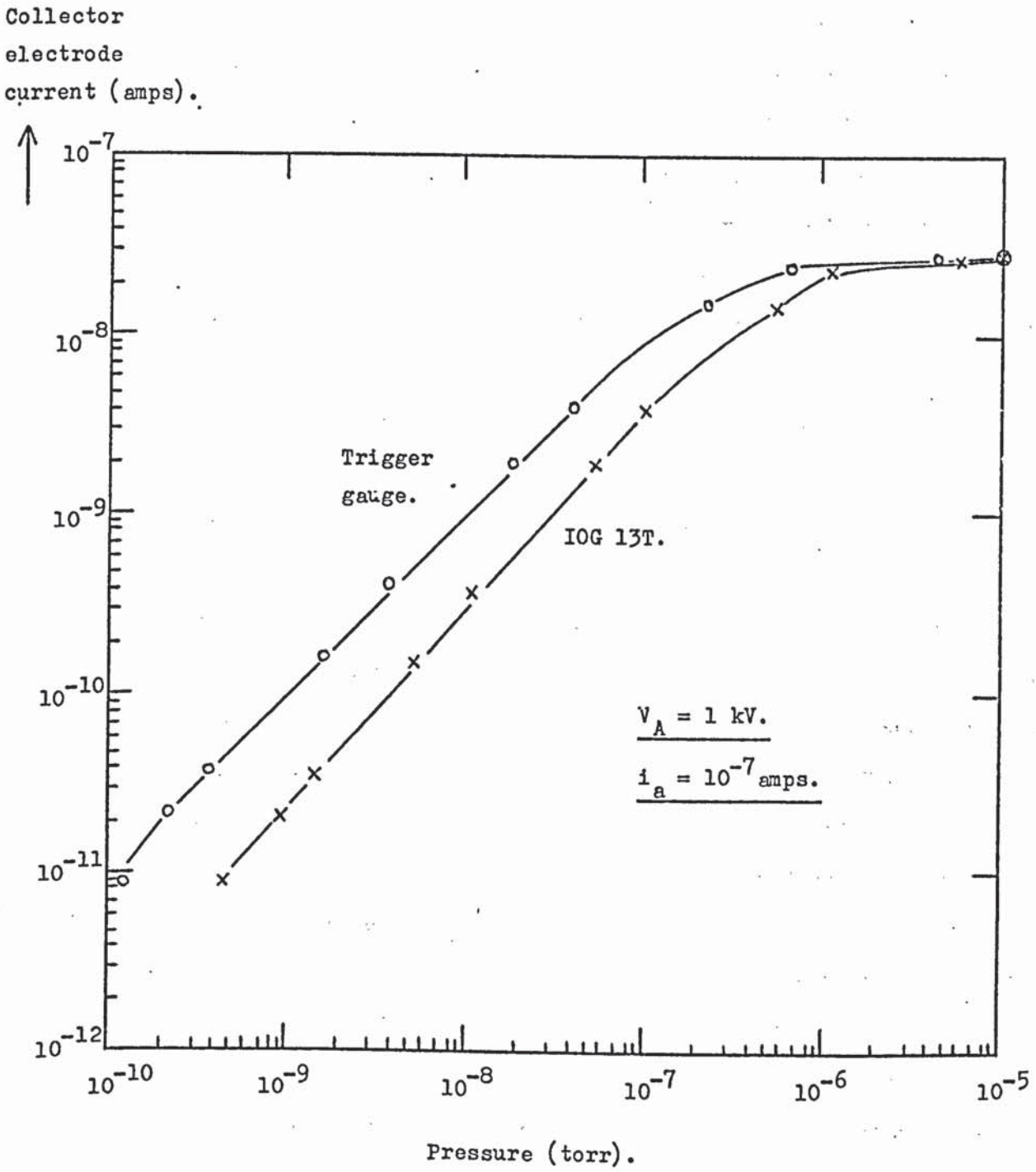

Figure 3.13. The variation of collector current with pressure.

Trigger and IOG 13T gauges at 10^{-5} torr. However, below 10^{-5} torr, a discrepency exists between the two gauges. Thus, the sensitivity of the electron-orbit ionisation gauge will appear to be greater when the pressure is measured with the Trigger gauge rather than the IOG 13T gauge. The high pressure limit for the electron-orbit ionisation gauge is as predicted earlier, in the region of 10^{-7} torr. This high pressure limit is when the average total electron path length in the gauge is limited by electron collisions with gas molecules. Below 10^{-7} torr, there is a fairly linear variation of collector current i_c with pressure.

Figure 3.14 shows the variation of sensitivity of the electron-orbit ionisation gauge with change in pressure as indicated by the IOG 13T gauge. The apparent sensitivity of the gauge when using an anode current of 1 μA, given in Figure 3.14(a), was determined from the maximum positive values of i_c obtained at the peak D in Figure 3.10. With i_a = 1 μA, a maximum sensitivity of about 4.5×10^5 $torr^{-1}$ is obtained at about 10^{-7} torr, but at lower pressures, the apparent sensitivity rapidly decreases due to the electron space-charge limitation. With $i_a = 10^{-7}$ amps, Figure 3.14(b), a maximum sensitivity of nearly 4×10^5 $torr^{-1}$ is obtained in the region of 10^{-7} torr, but at lower pressures the sensitivity does not decrease nearly so rapidly as when i_a = 1 μA. It should be noted that a maximum sensitivity of 10^6 $torr^{-1}$ is obtained for the electron-orbit ionisation gauge, when using the Trigger gauge pressure measurements to determine the sensitivities. Reducing the emission current from the filament has the desired effect of reducing the electron space-charge oscillations.

It can be shown (Dushman[44]) that :-

$$I_p = \text{ð}\, \bar{l}\, n\, I_e \qquad \ldots\ldots\ldots\ldots (6)$$

where $\bar{l}$ is the average total path length of the electrons before collection by the anode, I_p is the positive ion current produced in the device, ð is

(a).

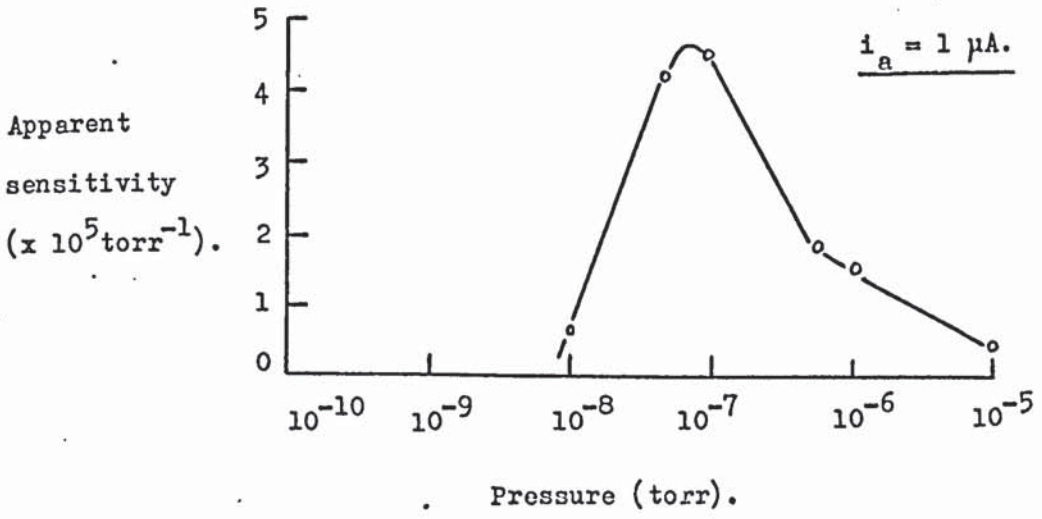

(b).

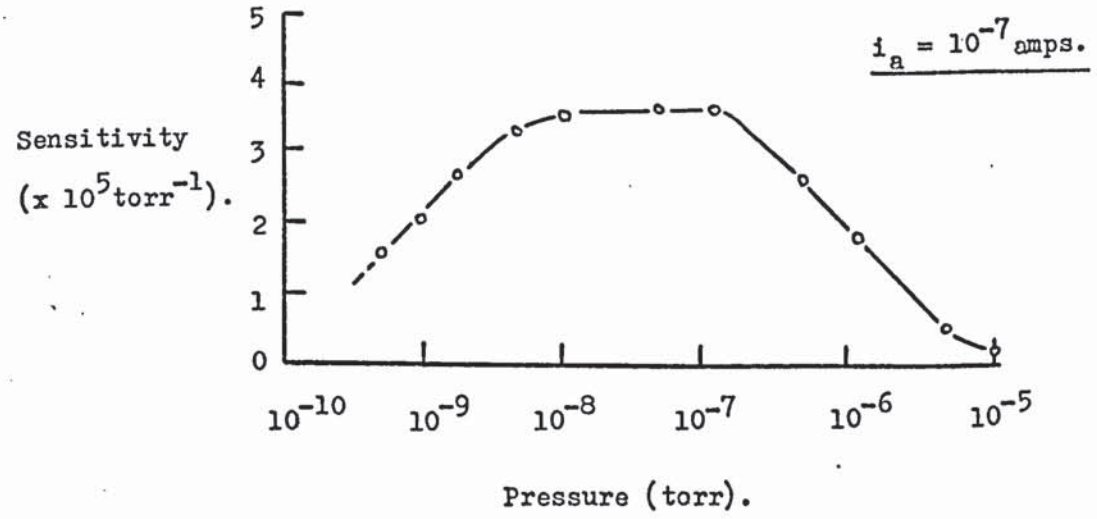

Figure 3.14. The variation of sensitivity with pressure.

the ionisation cross-section, n is the number of gas molecules per unit volume and I_e is the electron emission current from the filament. At pressures above the high pressure limit of the gauge, the average total electron path length is limited by collisions with gas molecules. Hence, the variables in equation (6) will be I_p, n and $\bar{l}$. Below the high pressure limit, for a linear variation of I_p with pressure to occur, the sensitivity S must be constant, that is $\bar{l}$ must be constant with pressure. Hence, for a linear response of the gauge below the high pressure limit, the only variables in equation (6) are I_p and n. Now it has been shown that if the sensitivity is too high, that is if $\bar{l}$ is too long, then electron space-charge problems will be encountered. However, if the number of electrons is reduced, that is if I_e is reduced, then these electron space-charge problems can be overcome. At first sight, by reducing I_e by an order of magnitude, the pressure at which electron-space problems occurred could be expected to be reduced by an order of magnitude also. However, if $\bar{l}$ is now constant with pressure, then this would probably not be the case. This is because the electron space-charge is dependent upon the number of electrons per unit volume, which is in turn dependent upon $\bar{l}$ and I_e. Thus, the electron density in the ionising volume will tend to remain constant with pressure. This is probably why only a single peak, with no space-charge oscillations, is present in the bias characteristics at any pressure when $i_a = 10^{-7}$ amps. Thus, in practise the electron space-charge problems develop far more slowly at $i_a = 10^{-7}$ amps than at $i_a = 1$ μA.

Measurements with the electron-orbit ionisation gauge were carried out down to pressures of 5×10^{-10} torr as measured by the IOG 13T gauge, that is 1.4×10^{-10} torr as measured by the Trigger gauge. However, at 5×10^{-10} torr, it was necessary to use an electron emission current of 10 mA for the IOG 13T gauge. This produced a residual electron current of 3.5×10^{-12} amps on the collector electrode of the electron-orbit ionisation gauge. With 1 mA emission for the IOG 13T gauge, the residual

electron current was 3×10^{-13} amps. These residual currents were measured when the filament in the electron-orbit ionisation gauge was switched off, but had a bias voltage V_B of +36 volts on it, whilst V_A = 1 kV. The true ion collector current i_c in the electron-orbit ionisation gauge is of the order of 10^{-12} amps at a pressure of 10^{-9} torr when using an anode current of 10^{-7} amps. Thus, the residual electron current at 5×10^{-10} torr resulting from the 10 mA electron emission for the IOG 13T gauge, will be of the same order as the true collector current i_c. A correction was made by adding the 3.5×10^{-12} amps onto the measured value of i_c obtained at 5×10^{-10} torr. No significant interference from the Trigger gauge with the electron-orbit ionisation gauge was observed.

Another problem encountered at very low pressures below 10^{-10} torr was due to positive ion emission from the tungsten filament of the electron-orbit ionisation gauge. This emission was very dependent upon filament temperature but independent of pressure. It was due to positive ions produced at the hot filament surface probably from alkali metal impurities in the tungsten. However, the positive ion emission reduces with filament age and this process was accelerated by operating the filament at a very high temperature prior to taking any measurements. However, when using a tungsten filament at pressures in the region of 10^{-11} to 10^{-12} torr, even after a period of operation of the filament at a high temperature as described above, the positive ion emission could still be a problem. For this reason, it would be advisable to use filaments that operate at lower temperatures, such as thoriated tungsten or lanthanum hexaboride (Jenkins[45]). Thus, measurements have not been taken below 10^{-10} torr, but no low pressure limit has been observed. Calculations (Appendix 2) show that the X-ray limit of the gauge should be in the region of 10^{-12} torr.

3.4. Discussion.

In any very high sensitivity device such as the electron-orbit ionisation gauge, electron space-charge oscillations will be a problem at low pressures, producing instabilities in the bias characteristics of the gauge if too large an emission current is used. In one series of experiments with the electron-orbit ionisation gauge, reducing the sensitivity of the gauge by removing rods from the collector electrode, also reduced the instabilities due to the electron space-charge oscillations. This is analogous to the observations reported by Meyer and Herb[26] with orbitrons of high and low sensitivities. In their high sensitivity orbitrons, they observed instabilities with dips to negative collector currents, which they attributed to electrons gaining sufficient energy to reach the collector electrode. In their low sensitivity orbitrons these instabilities were not observed in the bias characteristics. Gammon[27] reported instabilities at far higher pressures in the region of 10^{-5} torr and attributed these to electron interaction with the electrostatic field distortion produced by the filament. In the electron-orbit ionisation gauge, the field distortion associated with the filament is very small and removed from the orbiting electrons and no instabilities have been encountered at the pressures reported by Gammon[27]. However, if too many rods were removed from the collector electrode in order to reduce the sensitivity of the electron-orbit ionisation gauge, there were indications that instabilities were developing which were possibly due to electron interaction with the large field perturbations at the collector electrode. Thus, it is reasonable to assume that the instabilities reported by Meyer and Herb[26] and those reported by Gammon[27] are of a different nature from each other. The instabilities reported by Meyer and Herb[26] appear to be of the same nature as those encountered in the electron-orbit ionisation gauge at low pressures. It is essential to keep any perturbations of the anode field inside the ionising volume to a minimum,

in order to prevent any instabilities of the type reported by Gammon[27]. Also, in any very high sensitivity device, it is necessary to keep the electron emission current to a minimum in order to reduce the instabilities due to electron space-charge oscillations.

The results obtained with the electron-orbit ionisation gauge were of a very reproducible nature even when new filaments were used. The gauge should find useful application in the ultra high vacuum field due to its very high sensitivity. A mesh structure could replace the 32 rod structure of the collector electrode, so simplifying the construction of the gauge.

Finally, this design of ionising device may find application as the ioniser in radial electrostatic field ion pumps. The whole gauge including the filament could be raised by about + ½ kV above an earthed outer casing in a manner similar to that described by Bills[31] for the orbitron. This would ensure that ions passing through the collector electrode grid structure, have sufficient energy to be trapped efficiently by ion burial at the outer casing wall. It was observed that at V_A = 1 kV, only about 15% of the collector current i_c was lost due to ions passing through the collector. Thus, if this device is to be used in an ion pump, the collector electrode will probably have to be made more open in order to increase the number of ions passing through it, even if this means some loss in sensitivity. The titanium gettering material would preferably be obtained from a separate resistance heated sublimation filament. This method is preferred to having slugs of titanium mounted on the anode as described by Douglas et al[30], as these would lower the sensitivity of the device as a result of electron collision with the enlarged regions of the anode due to these slugs of titanium.

CHAPTER 4.

INVESTIGATION OF THE COLD CATHODE TWIN WIRE OSCILLATOR.

4.1. Introduction.

An investigation of the characteristics in terms of the geometry of the cold cathode twin wire oscillator is described in this Chapter. The influence of secondary electron yield from the collector electrode is also described. The construction of the oscillator was based on the design described by McIlraith[32] and Thatcher[34].

4.2. Experimental equipment.

4.2.1. Design of the oscillator.

The construction of the cold cathode twin wire oscillator is shown in the schematic diagram in Figure 4.1. The collector electrode consisted of a 5 cm internal diameter by 20 cm long stainless steel tube and two 'Dural' end-plates were positioned at the ends of the collector. Each end-plate contained six 0.95 cm diameter gas pumping ports. Anode wires of 0.25 mm diameter tungsten were used at a separation of 0.5 cm. These anodes were positioned in and electrically insulated from the end-plates by two ceramic bushes. Spring tensioning of the anode wires was employed in order to prevent them from bowing when heated by electron bombardment. The cold cathode oscillator was operated in the high vacuum system described in section 2.2.3.

4.2.2. The electrical circuit.

A schematic diagram of the electrical circuit is given in Figure 4.2. The tube voltage V_T was provided from a H.T. power unit capable of delivering an output of 50 mA at 12 kV. A $10^5 \Omega$ current

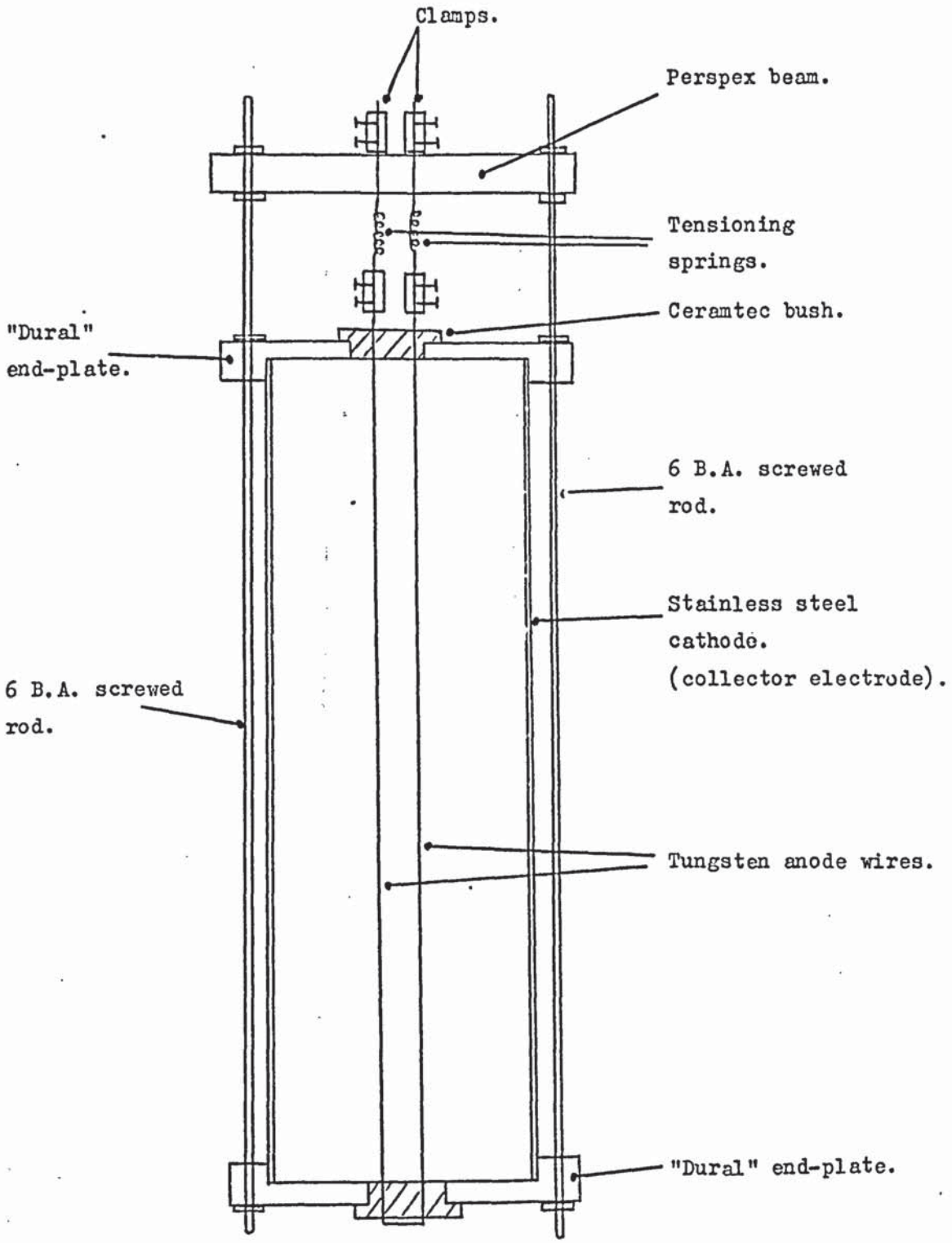

Figure 4.1. The cold cathode twin wire oscillator.

limiting resistor was placed between the anodes and the output of the H.T. unit. The tube current i_T was measured at the earthed collector electrode (which is now the cold cathode) by means of a microammeter capable of measuring from 0.2 μA to 120 mA.

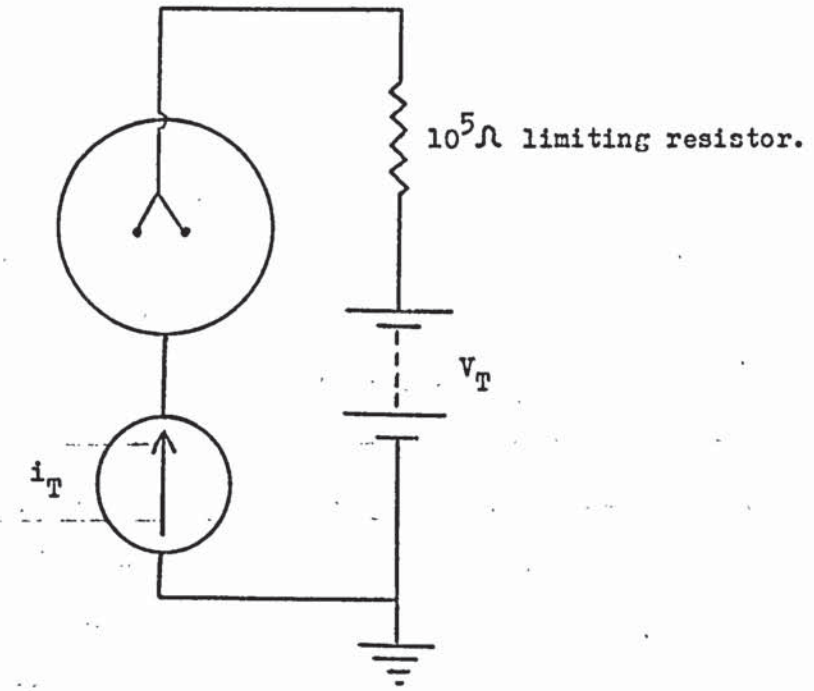

Figure 4.2. Circuit for the cold cathode twin wire oscillator.

4.3. The current - voltage characteristics.

The variation of tube discharge current i_T with anode voltage V_T was investigated at different pressures. It should be noted that V_A is the anode voltage with respect to the earthed collector electrode, where the voltage V_L across the $10^5\Omega$ limiting resistor has been taken into account. Thus, the applied tube voltage V_T from the output of the H.T. unit is equal to the sum of V_A and V_L.

The curves of i_T versus V_A were obtained by measuring i_T as V_A was decreased. In order to obtain reproducible results, the oscillator was operated for a period of time in order to outgas the materials before any

measurements were made. During these experiments with the cold cathode twin wire oscillator, it is the Penning gauge pressures that are quoted rather than the Bayard - Alpert pressures given in Appendix 1. The characteristics are given in Figure 4.3 and are very similar to those obtained by Thatcher[34], with the cut-off voltage for the discharge being dependent on the total gas pressure.

In order to test the efficiency of the plane end-plates for the end-reflection of the electrons along the z axis, three further oscillators were constructed with collector electrode tube lengths of 10 cm, 7.5 cm and 5 cm. Similar shaped characteristics were obtained as for the 20 cm long oscillator and these are given in Appendix 3. From the cleaning of the anode wires by heating due to electron bombardment, it was observed that the electrons only approached the end-plates to within approximately 1.8 cm. Hence, the active discharge region was approximately 3.6 cm shorter than the length of the oscillator. As the oscillator length was reduced, the tube current density was found to remain constant if these end-effects were taken into account.

The usual form of current - voltage characteristics were obtained down to pressures of 5×10^{-6} torr, but the cut-off voltage at 10^{-6} torr was less than at 5×10^{-6} torr, resulting in a cross-over in the characteristics as shown in Figure 4.3(b). The cause of this cross-over is uncertain, but it was observed that this cross-over did not always occur, as sometimes no discharge at all could be obtained at 10^{-6} torr. As the cross-over discharge current at 10^{-6} torr was dependent upon the collector electrode length, it appears that this current must be due to genuine oscillating electrons. The cross-over only occurred when the leak valve was fully closed and the high vacuum system was at its ultimate pressure of about 10^{-6} torr. Also, the discharge glow at 10^{-6} torr was only visible in the vicinity of the ceramic insulators. The existence of

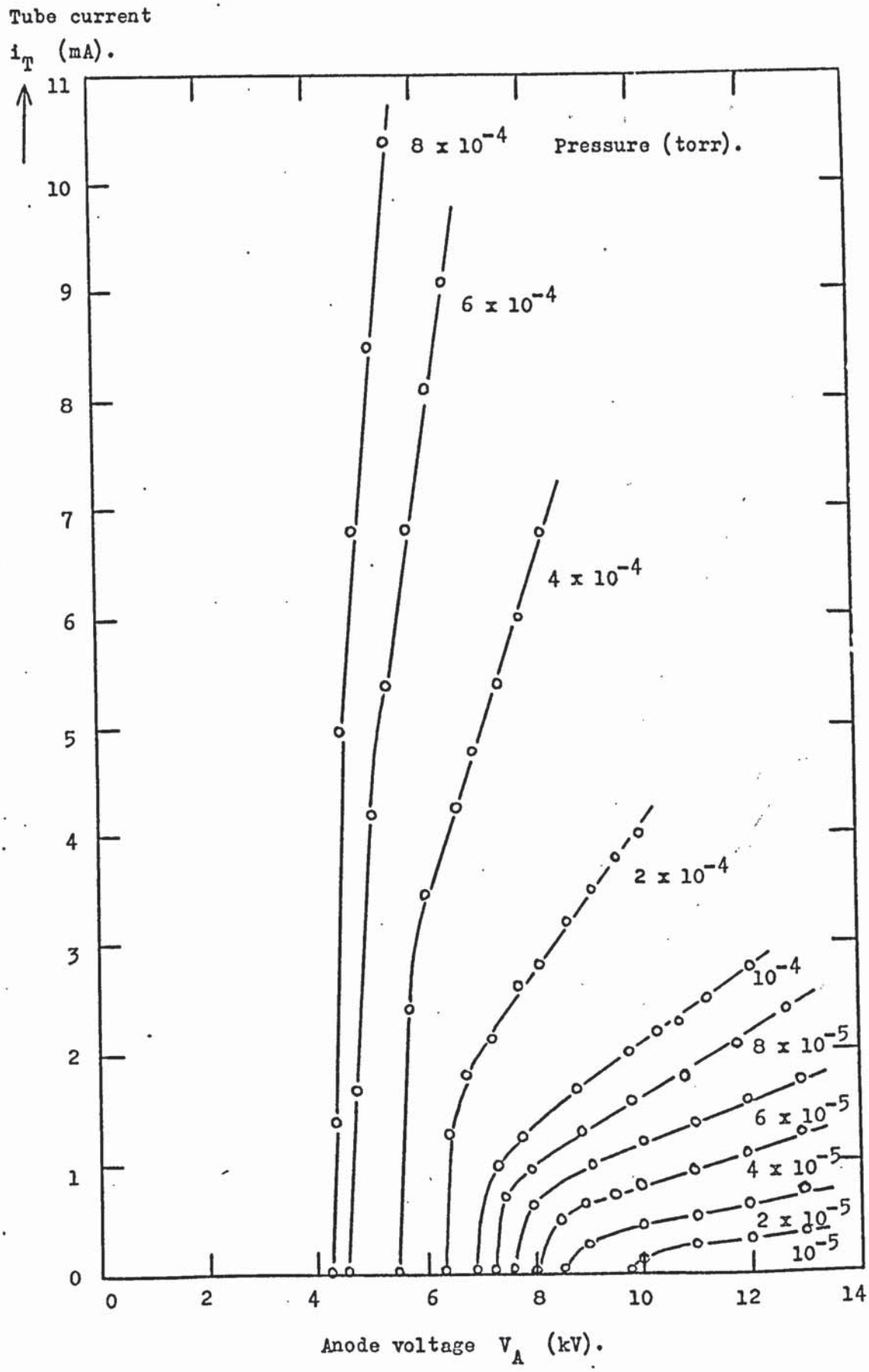

Figure 4.3(a). Characteristics of the cold cathode oscillator.

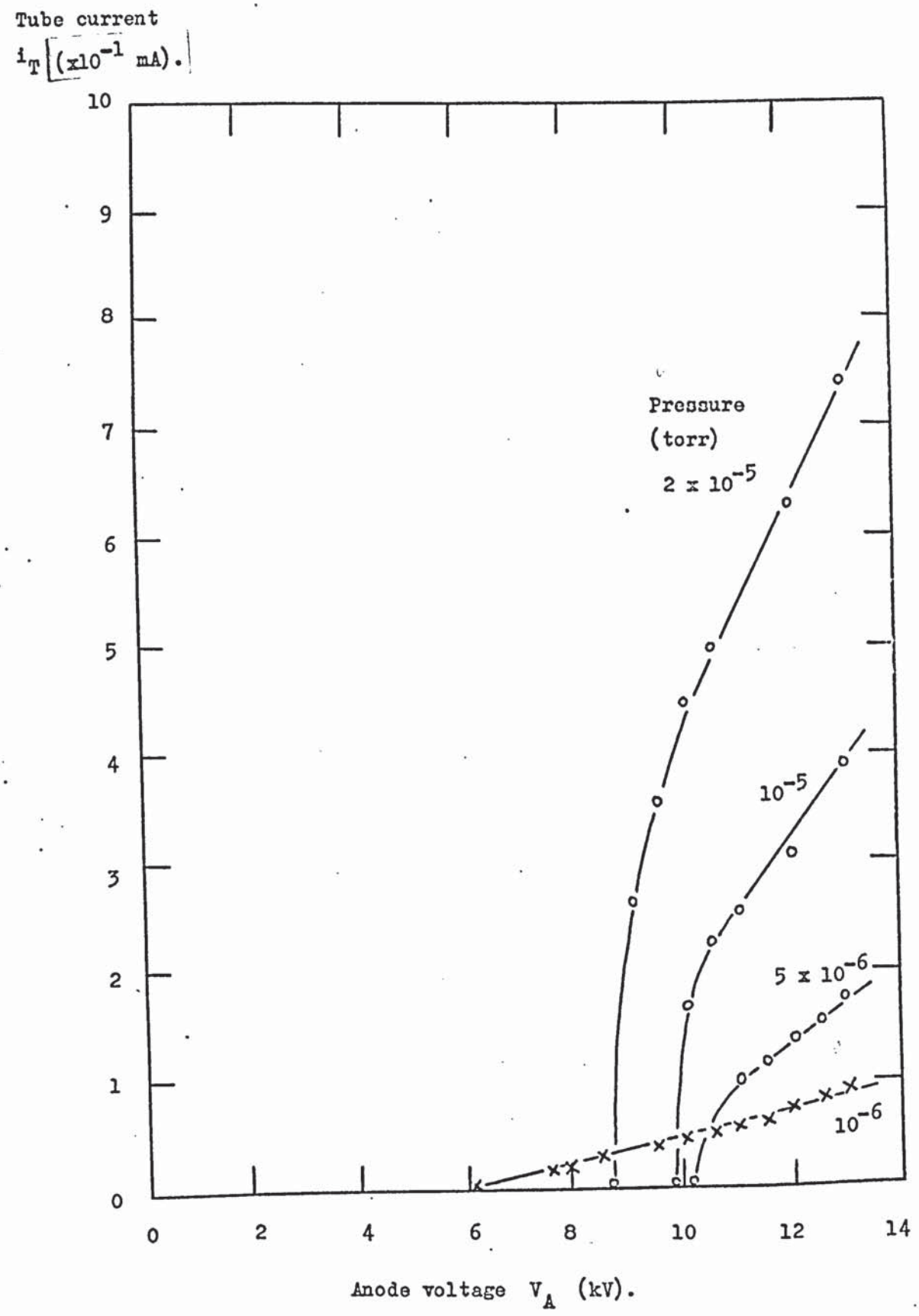
Tube current
i_T [(x10^{-1} mA).
10
9
8
7
6
5
4
3
2
1
0
0
2
4
6
8
10
12
14
Pressure
(torr)
2 x 10^{-5}
10^{-5}
5 x 10^{-6}
10^{-6}
Anode voltage V_A (kV).

Figure 4.3 (b).

the cross-over is suspected to be dependent upon the degree of contamination of the insulating bushes. This could possibly give rise to a supply of electrons or gas from the contaminated insulators, so initiating the discharge at this pressure.

4.4. The effects of variation of anode separation and anode diameter.

The variation of tube current i_T with anode centre to centre separation is given in Figure 4.4. for V_T = 9 kV. Similar information is given in Appendix 4 for values of V_T equal to 10 and 11 kV. The tube voltages V_T quoted in Figure 4.4 and Appendix 4 are not corrected for the voltage drop V_L across the $10^5 \Omega$ limiting resistor. Anode diameters of 0.15 mm, 0.25 mm and 0.4 mm were used and in all cases, as the anode separation is decreased, the value of i_T increases until a maximum is obtained at an anode separation of 5 mm to 6 mm. However, at anode separations of less than about 4 mm, it was not possible to obtain any discharge, so giving rise to a cut-off at this anode separation, (Rushton and Fitch[46]).

The electrostatic field in the xy plane of the electron-orbit ionisation gauge, which uses a single wire anode, is a true central force field. In the central force field, the angular momentum $\underline{L}$ of the individual electrons is conserved if $\underline{L}$ is defined relative to the centre of the field, since the line of action acting on the electron passes through the centre of the field and so the torque $\underline{K}$ on the electron is zero. Since $\frac{d\underline{L}}{dt} = \underline{K}$, then $\underline{L}$ is constant with time.

In the twin wire oscillator, the electrostatic field approximates to a central force field when the distance $\underline{r}$ of the electron from the origin (that is the saddle-point) is large compared with the anode separation. Hence, at large values of $\underline{r}$, the angular momentum of the electron about the origin will tend to be conserved. Hence, the electrons will follow the field lines if they have zero initial kinetic energy. However, if they

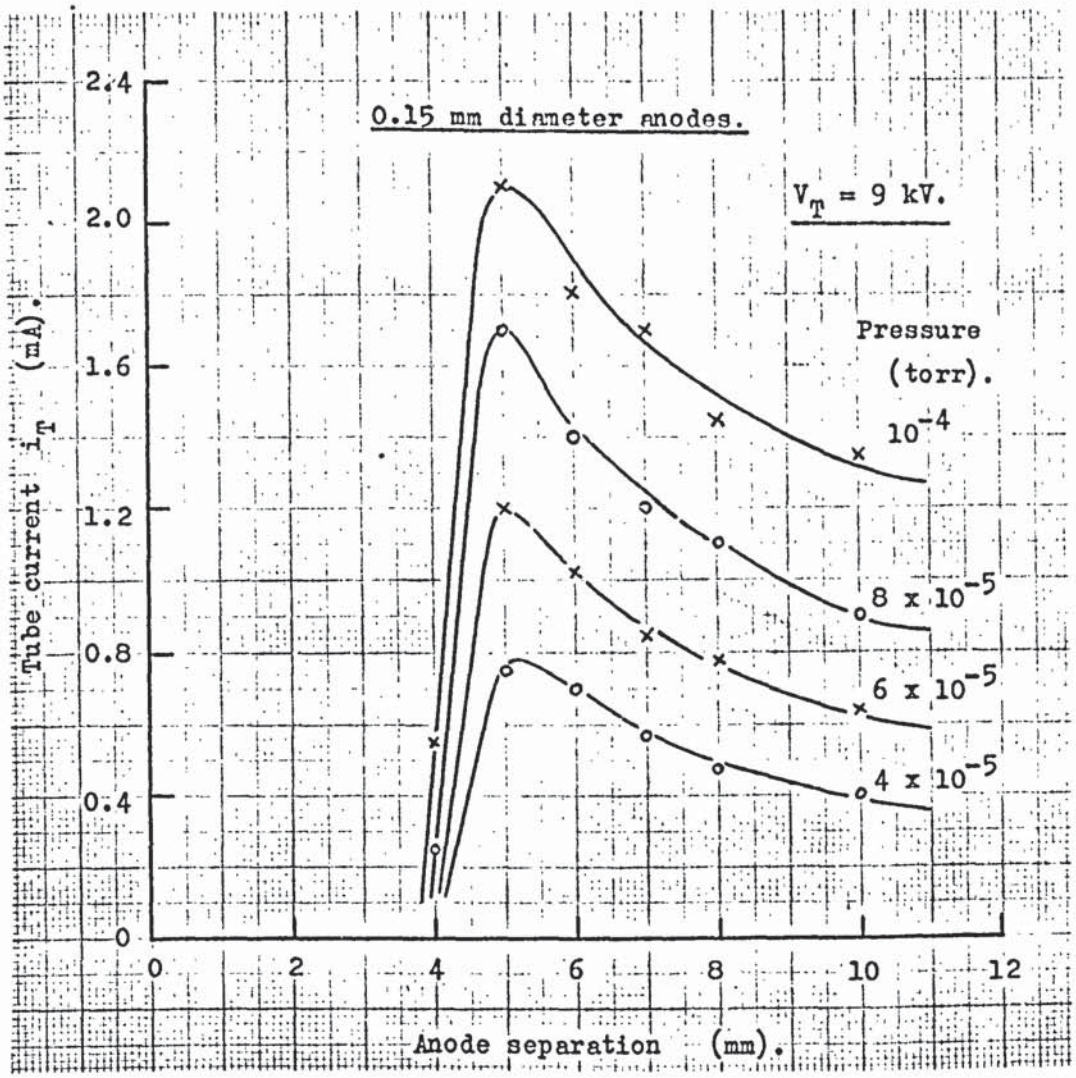

Figure 4.4 (a). The variation of tube current with anode separation.

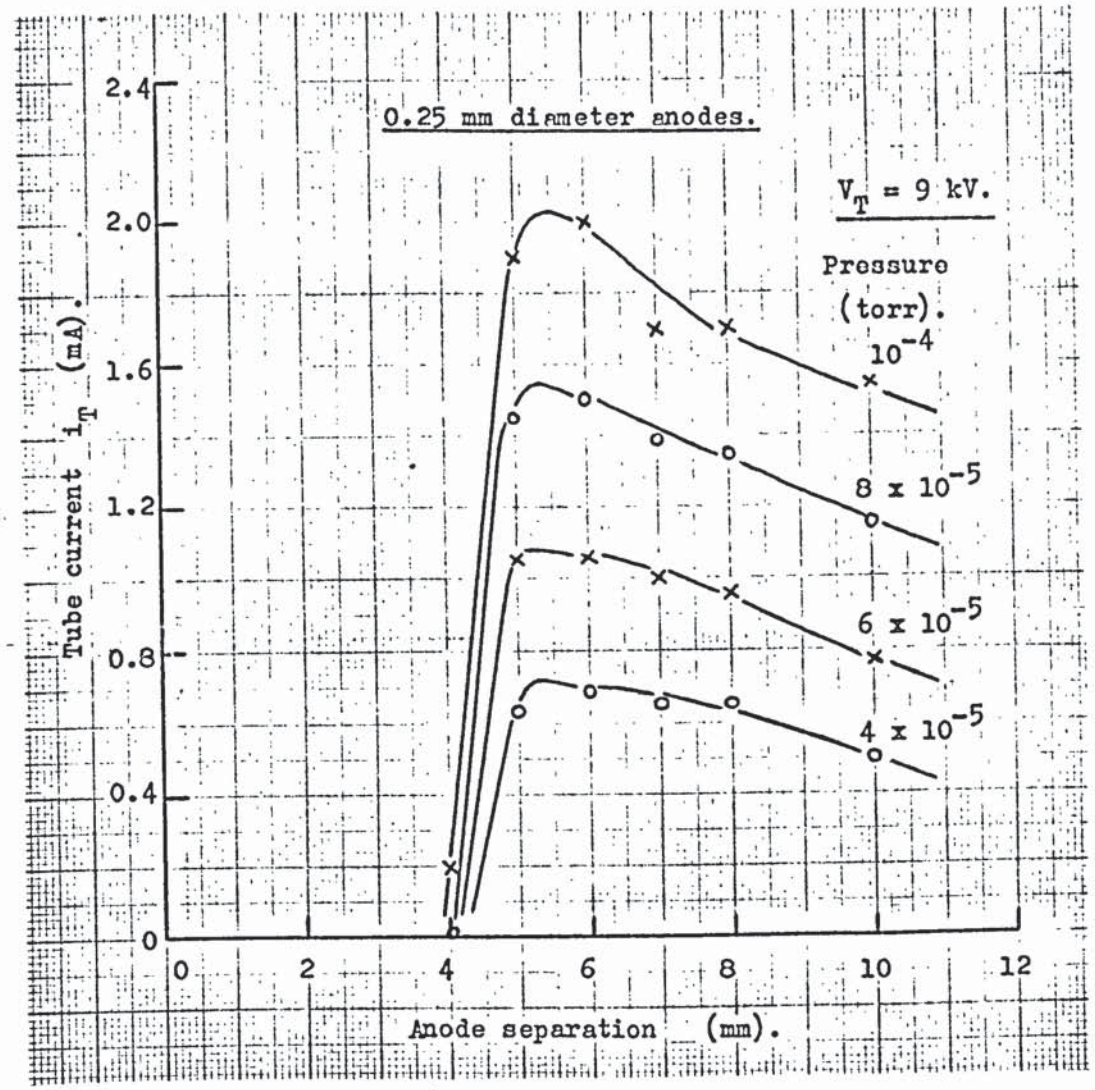
0.25 mm diameter anodes.
V_T = 9 kV.
Pressure (torr).
10^{-4}
8 x 10^{-5}
6 x 10^{-5}
4 x 10^{-5}
Tube current i_T (mA).
Anode separation (mm).
0
0.4
0.8
1.2
1.6
2.0
2.4
0
2
4
6
8
10
12

Figure 4.4 (b).

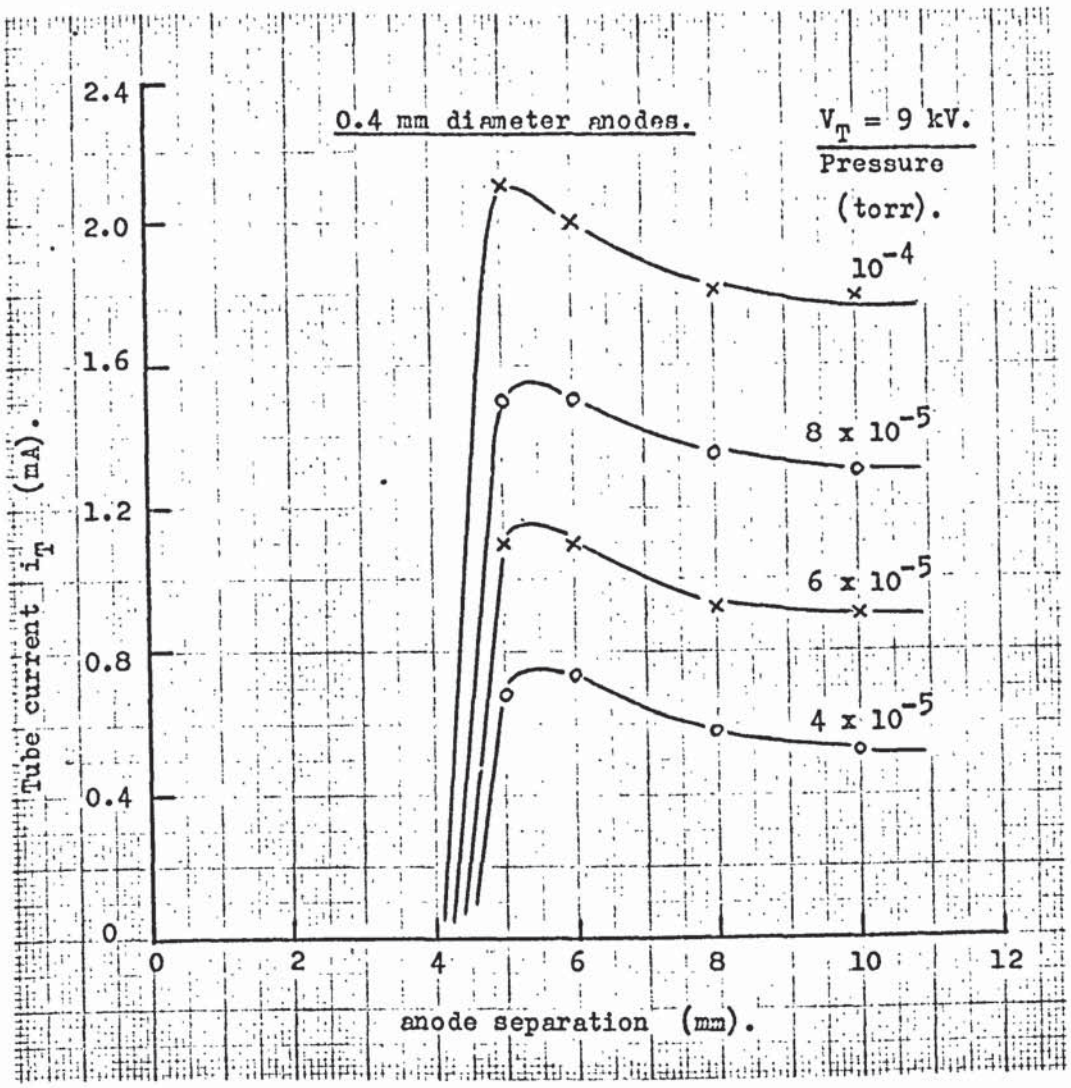
0.4 mm diameter anodes.
V_T = 9 kV.
Pressure (torr).
10^{-4}
8 x 10^{-5}
6 x 10^{-5}
4 x 10^{-5}
Tube current i_T (mA).
anode separation (mm).
0
0.4
0.8
1.2
1.6
2.0
2.4
0
2
4
6
8
10
12

Figure 4.4 (c).

have an initial kinetic energy, they will follow a trajectory where $\underline{L}$ is conserved and is given by :-

$$\underline{L} = m\,\underline{r} \times \underline{v} = m\,\underline{r}\,\underline{v}\sin\theta \quad \ldots\ldots\ldots (7)$$

where $\underline{v}$ is the electron velocity and m is the electron mass.

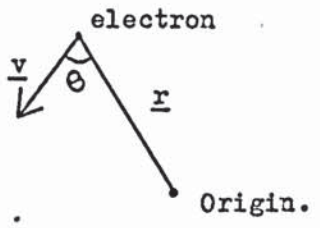

Figure 4.5.

Hence, the trajectory of the electron at large values of $\underline{r}$ will be given by :-

$$\underline{v} \times \underline{r} = \text{constant}$$

where the constant is determined by the initial kinetic energy of the electron.

However, as the electron approaches the vicinity of the anodes, the angular momentum of the electron about the saddle-point will no longer be conserved due to the anodes exerting a torque $\underline{K} = \underline{r} \times \underline{F}$ on the electron, where $\underline{F}$ is the resultant force exerted on the electron by the anodes.

At large anode separations, the potential of the saddle-point will be low and the electrons will experience a torque$\underline{K}$ exerted by the anodes at larger values of $\underline{r}$, giving rise to a relatively short average total electron path length. As the anode separation is decreased, the saddle-

point potential increases, so making the electrostatic field appear to be more like a true central force field. Hence, the total electron path length will tend to increase and so the discharge will build up. This increase in total electron path length with decrease in anode separation has been demonstrated when using the rubber model analogue of the twin wire oscillator. The discharge would continue to increase as the anode separation is decreased further, if it were not for the fact that electrons ejected from the collector electrode surface by positive ion bombardment, are ejected in random directions and with initial energies of up to several electron-volts (Hagstrum[47]).

Therefore, the initial velocity $\underline{v}_x$ in the direction of the x axis must be sufficiently large to cause the electron to be immediately captured by one of the anodes. As the anode separation is reduced, the electron velocity $\underline{v}_x$ which is necessary to cause the electron to be captured would also be reduced. Thus, an anode separation will probably exist where the majority of the electrons have sufficiently large velocity components $\underline{V}_x$ to cause them to be captured by one of the anodes. At this separation, very few electrons will oscillate between the anodes and a cut-off is observed.

A rough calculation can be made of energy required by the electron in order for it to be immediately captured. McIlraith[36] calculated the frequency of oscillation of the electrons along the y axis to be about 2×10^8 Hz when $V_A = 10$ kV, giving a period T of oscillation of about 5×10^{-9} seconds. Thus, the time taken for the electron to reach the plane of the anode wires is $T/4 = 1.25 \times 10^{-9}$ seconds. Assuming that the electrostatic field is a true central force field with its origin at the saddle-point, then the electron will travel along the field lines to the saddle-point, if it has zero initial velocity. Taking the anode separation of 0.4 cm (the separation at which the cut-off occurs), then to hit an anode immediately, the electron must have a velocity component $\underline{v}_x$ that is

sufficient to make it travel 0.2 cm along the x axis direction. Assuming that $\underline{v}_x$ remains constant as the electron approaches the anode plane, then,

$$\underline{v}_x = \frac{2 \times 10^{-3}}{1.25 \times 10^{-9}} \text{ m sec}^{-1} = 1.6 \times 10^{6} \text{ m sec}^{-1},$$

which is equivalent to an electron kinetic energy of 6.3 eV.

Thus, an electron emitted from the collector wall in the x axis direction with an energy of 6.3 eV will collide directly with an anode. With an anode separation of 0.5 cm, the equivalent electron energy will be about 11 eV, which about 1.7 times that of the required energy at 0.4 cm separation. The above calculation assumes that $\underline{v}_x$ is constant as the electron approaches the plane of the anodes. This is obviously not true, as the electrostatic field is not a true central force field and the electrons can only oscillate along the y axis if there is to be no resultant force on it in the x axis direction. However, this calculation does indicate that the initial energies required to explain the cut-off are within the range of energies expected for electrons ejected from a surface by positive ion bombardment.

However, it is not necessary for the electron to be captured immediately to produce a cut-off in the discharge. It is only necessary that $\underline{v}_x$ should be sufficiently large to enable the electron to be captured by an anode before a useful ionising collision with a gas molecule occurs. Thus, the electron may make several oscillations between the anodes before being captured and so the required value of $\underline{v}_x$ for the discharge cut-off may be less than the calculated value. Furthermore, as the mean free path between ionising collisions increases with decrease in pressure, the anode separation at which the discharge ceases will also be dependent upon pressure, as appears to be the case in Figure 4.4 and Appendix 4.

It can be seen from Figure 4.4, that the anode diameter has very little effect upon the performance of the oscillator. An oscillator that

employs two 2 mm diameter anodes has been constructed and little deterioration in the performance of the oscillator was observed. The use of these rigid anodes offer many advantages over the wire anodes and these were made use of in the improved version of the ion source application of the oscillator, as described in Chapter 6.

4.5. The influence of electron yield from the collector electrode.

In order to investigate the effects of the electron emission yield from the collector electrode surface, the material used for the collector electrode was changed to aluminium. The characteristics of tube current i_T versus anode voltage V_A are given in Figure 4.6. Similar shaped characteristics were obtained as when using the stainless steel collector electrodes, but due to the larger secondary electron emission yield from the aluminium collector surface, the characteristic curves for the aluminium collector were displaced from the curves for the stainless steel collector, to smaller values of V_A. This made the cut-off voltage with the aluminium collector occur at approximately half of the value of the cut-off voltage with the stainless steel collector. In addition, because of the larger electron yield from the aluminium collector surface, the tube current i_T becomes critically dependent upon anode voltage at the higher values of V_A.

In order to investigate the effects of the electron yield from the collector surface upon the low pressure limit of the oscillator, the oscillator first with the stainless steel collector and then with the aluminium collector, was put into the ultra high vacuum system described in section 3.3.2, with the mass spectrometer magnet removed for reasons explained in the next chapter. It was found that the low pressure limit of the device was lower by about a factor of two when using the aluminium collector at any given value of V_A. No indication of the cross-over mentioned in section 4.3 was observed during these experiments.

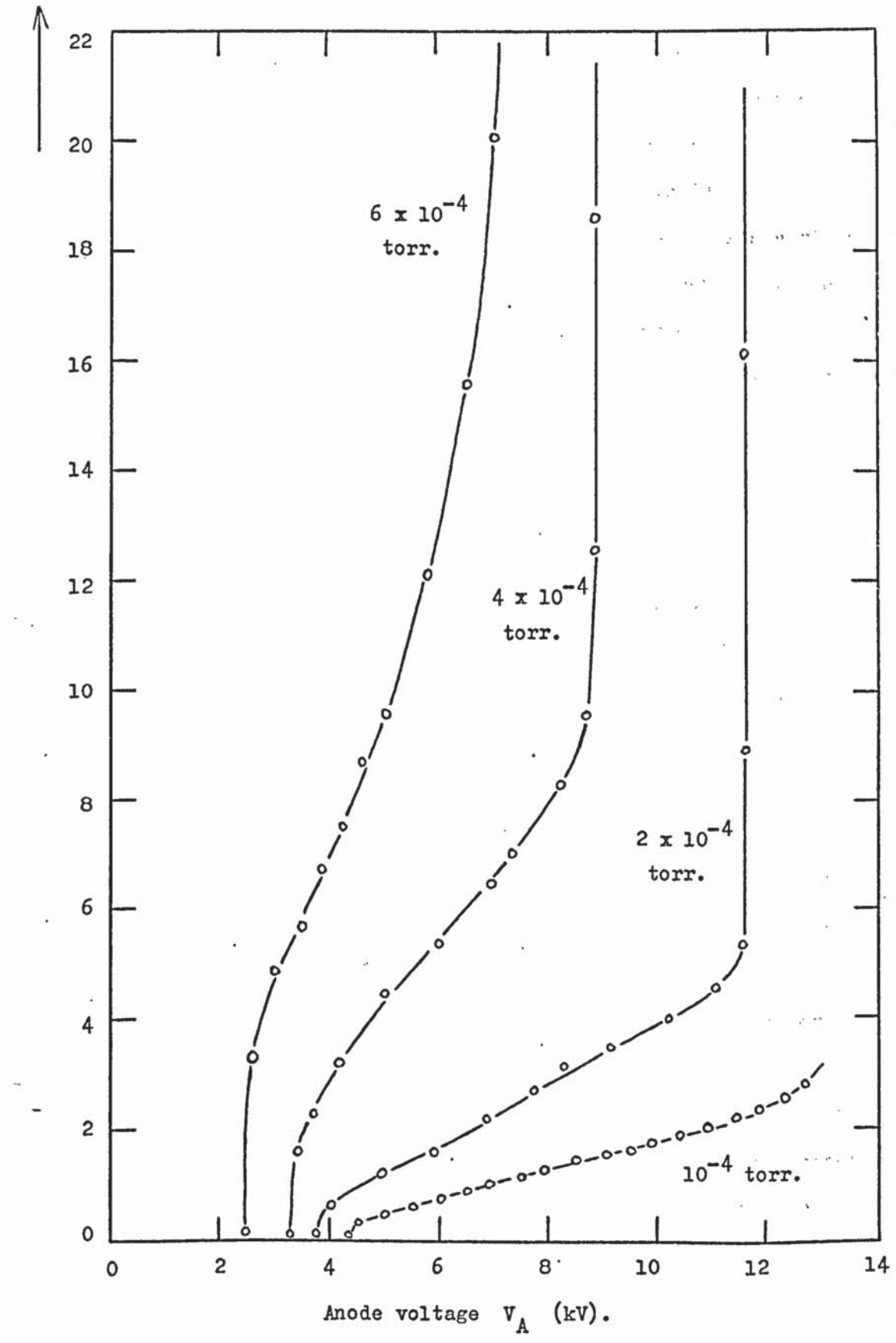

Figure 4.6. Discharge characteristics when using the aluminium collector.

It was found that when operating the oscillator with the aluminium collector in the high vacuum system, the performance of the oscillator fell off gradually. After a few hours operation, the performance of this oscillator was less than that obtained from the oscillator with the stainless steel collector. This is now believed to be due to the original aluminium collector having a considerable oxide layer on its surface which is known to have a high secondary yield. But during operation, the surface became cleaned by positive ion bombardment, so exposing the relatively clean aluminium surface from which the secondary electron yield is lower. Hence, aluminium appears to be an unsuitable material for the collector electrode, if reproducible results are to be obtained.

4.6. Discussion.

The anode separation is the important parameter to be considered when constructing the twin wire oscillator, as below a critical anode separation, no cold cathode discharge can be maintained. Anode diameter has little influence on the performance of the oscillator and 2 mm diameter anodes have been successfully used in an ion source based on this principle, as described in Chapter 6.

The twin wire oscillator is capable of sustaining a cold cathode discharge down to pressures of 10^{-6} torr, depending upon the value of the electron yield from the material used for the collector electrode. However, the experiments concerned with the geometrical changes in the device have not produced any significant reduction in the low pressure limit. Therefore, it was assumed that some other factor or factors were responsible for this low pressure limit. A possible reason is discussed in the next chapter which is concerned with the influence of magnetic fields upon the performance of the oscillator.

CHAPTER 5.

THE INFLUENCE OF MAGNETIC FIELDS UPON THE PERFORMANCE OF THE OSCILLATORS.

5.1. Introduction.

The cold cathode oscillator was put into the ultra high vacuum system, in order to carry out further investigations of its low pressure limit. However, it was found that a discharge could not be held at a pressure below about 10^{-4} torr, even with V_T up to 11 kV. Previously it was found that using the high vacuum system, a discharge could be maintained down to the region of between 10^{-5} and 10^{-6} torr. It was thought that the poorer low pressure limit in the ultra high vacuum system may have been due to the presence of stray magnetic fields; such as from the triode ion pump, mass spectrometer or Trigger gauge magnets. In order to test this theory, the mass spectrometer and Trigger gauge magnets were removed. The low pressure limit of the oscillator was then reduced by about an order of magnitude, to a pressure of about 10^{-5} torr at V_T = 11 kV. This was now of the same order as the low pressure limit obtained in the high vacuum system. It was eventually concluded that the stray magnetic field from the mass spectrometer magnet had the most influence. Thus, an investigation of the influence of magnetic fields was carried out on both the cold cathode and thermionic oscillators, (Rushton and Fitch[46]).

5.2. The influence of magnetic fields on the cold cathode twin wire oscillator.

A magnetic field $\underline{B}$ will exert a force $\underline{F}$ on an electron of charge e with velocity $\underline{v}$, where $\underline{F}$ is given by :-

$$\underline{F} = e(\underline{B} \times \underline{v}).$$

Magnetic fields in the x, y and z directions of the twin wire oscillator will give rise to forces :-

$$\underline{F}_z = e(\underline{B}_x \times \underline{v}_y) \quad \ldots\ldots\ldots\ldots (8).$$

$$\underline{F}_y = e(\underline{B}_x \times \underline{v}_z) \quad \ldots\ldots\ldots\ldots (9).$$

$$\underline{F}'_z = e(\underline{B}_y \times \underline{v}_x) \quad \ldots\ldots\ldots\ldots (10).$$

$$\underline{F}_x = e(\underline{B}_y \times \underline{v}_z) \quad \ldots\ldots\ldots\ldots (11).$$

$$\underline{F}'_y = e(\underline{B}_z \times \underline{v}_x) \quad \ldots\ldots\ldots\ldots (12).$$

$$\underline{F}'_x = e(\underline{B}_z \times \underline{v}_y) \quad \ldots\ldots\ldots\ldots (13).$$

It was concluded by McIlraith[36] that as $\underline{v}_y$ is large, $\underline{F}_z$ in equation (8) and $\underline{F}'_x$ in equation (13) are also large. Assuming efficient end-reflection of the electrons, $\underline{F}_z$ should be harmless as it is directed along the length of the oscillator tube. However, $\underline{F}'_x$ will produce a Larmor precession of the electron trajectory about $\underline{B}_z$ as illustrated in Figure 5.1.

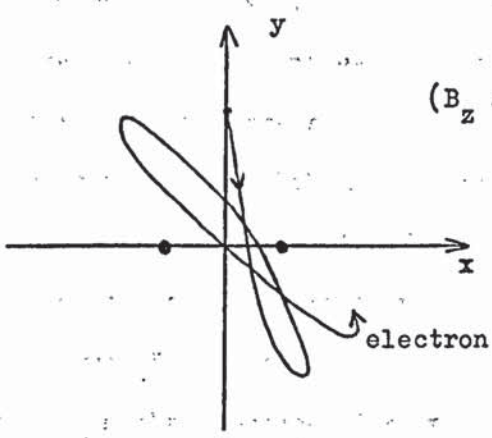

Figure 5.1. The Larmor precession.

Assuming that the electrostatic field were saucer shaped, the precession would continue indefinitely with a frequency, f, of rotation given by :-

$$f = \frac{e B_z}{4 \pi m} \quad \text{Hz} \qquad \ldots\ldots\ldots\ldots (14),$$

where m is the mass of the electron. The Larmor precession will eventually take the electron out of the discharge region and if the electron does not produce an ionising collision with a gas molecule before it leaves the discharge region, the discharge itself will be eventually destroyed if enough electrons are removed in this manner. As $\underline{v}_x$ and $\underline{v}_z$ are relatively small with respect to $\underline{v}_y$, then a magnetic field $\underline{B}_z$ will be the most damaging to the performance of the twin wire oscillator and this has been demonstrated experimentally to be the case.

In order to measure the effect of magnetic fields upon the performance of the cold cathode oscillator, the major component of the magnetic field of a permanent horse-shoe magnet was calibrated at various distances from the magnet using a Hall probe. The calibration curve for this magnet is given in Appendix 5. As it has been shown above that magnetic fields have their major influence upon the performance of the twin wire oscillator when they are applied along its z axis, various known magnetic fields from the calibrated magnet were then applied along this axis. Although the applied magnetic fields were not strictly uniform, it can be seen from the variation of tube current with applied magnetic field in Figure 5.2, that the performance of the oscillator rapidly deteriorates in the presence of magnetic fields. During these measurements, the oscillator was for convenience replaced into the high vacuum system with its z axis in the vertical position. The two curves in Figure 5.2 were obtained with the applied magnetic field being in opposite directions along the z axis. For curve A, the applied magnetic

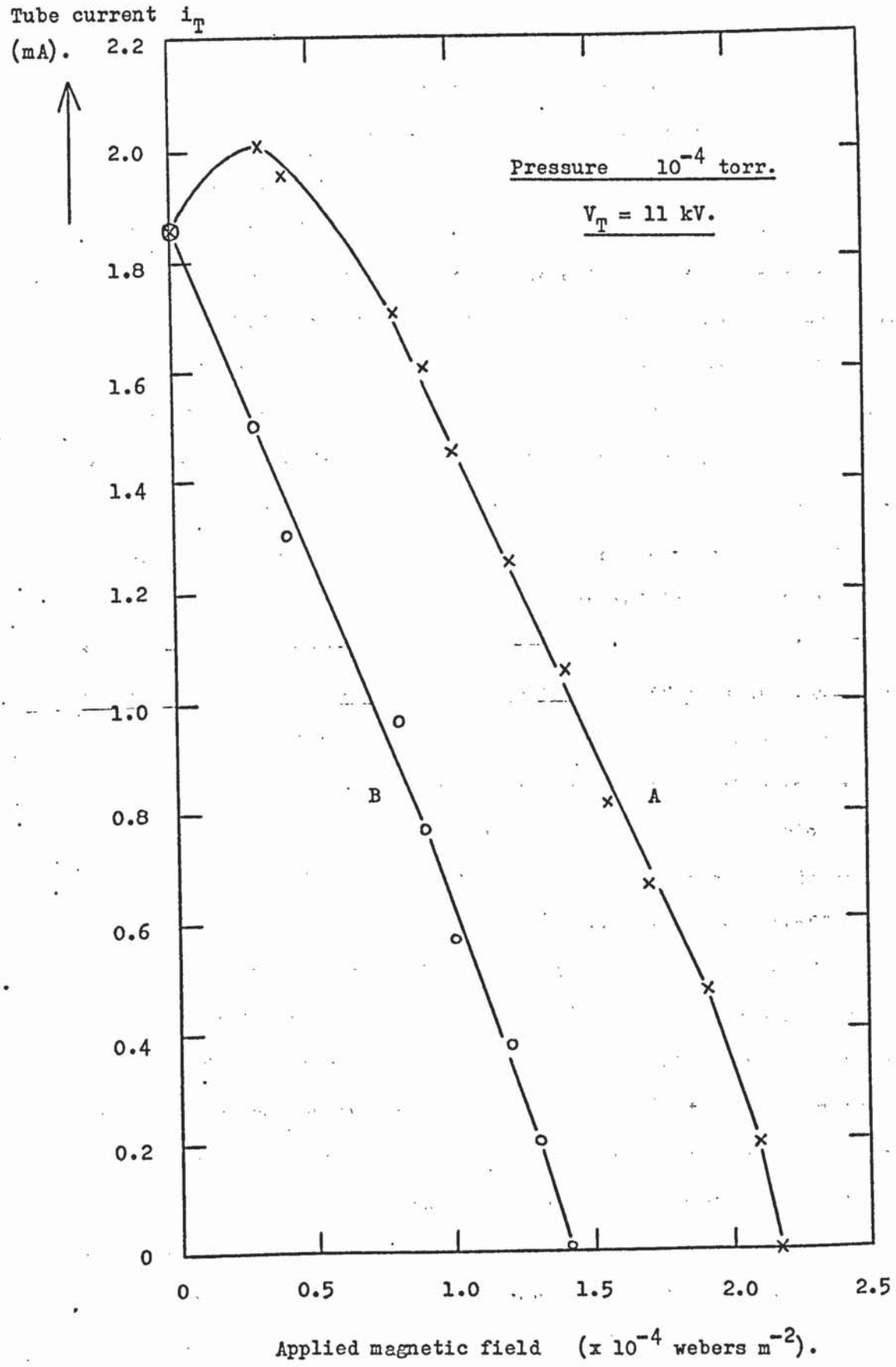

Figure 5.2. The variation of tube current with applied magnetic field.

field was in the opposite direction to the component of the earth's field along the z axis. At the maximum, the two fields cancel each other out. In curve B, there is a continual decrease in tube current i_T with increase in applied magnetic field, as in this case the earth's magnetic field and the applied magnetic field were in the same direction.

Figure 5.3 shows the variation of the oscillator's cut-off pressure with cut-off magnetic field with the oscillator's z axis in the horizontal position in the high vacuum system. The cut-off pressure is defined as the pressure at which a cold cathode disharge just ceases under certain conditions such as anode voltage and applied magnetic field. Conversely, the cut-off magnetic field $\underline{B}_c$ is the magnetic field applied along the oscillator's z axis, that is required to just cut out the discharge at a particular pressure and anode voltage. To obtain the results given in Figure 5.3, a particular cut-off pressure was obtained, first with the applied magnetic field and the earth's magnetic field in the same direction, and then with the two magnetic fields in opposition along the z axis. In this way, the earth's magnetic field along the z axis could be eliminated and the true cut-off magnetic field $\underline{B}_c$ determined at a particular cut-off pressure. It can be seen that the cut-off pressure of the oscillator is extremely dependent upon the presence of magnetic fields. At pressures in the region of 10^{-5} torr, the cut-off magnetic field is of the order of the earth's magnetic field. Hence, it is believed that the present low pressure limit of about 10^{-5} to 10^{-6} torr for the cold cathode twin wire oscillator could be due to the presence of stray magnetic fields in the laboratory, these stray magnetic fields being of the order of the earth's magnetic field.

From the simplified theory described, it might be expected that there would be a linear variation of cut-off pressure with magnetic field $\underline{B}_c$. Figure 5.3 does not show a linear variation between cut-off pressure and the cut-off magnetic field $\underline{B}_c$. This could be due to the applied

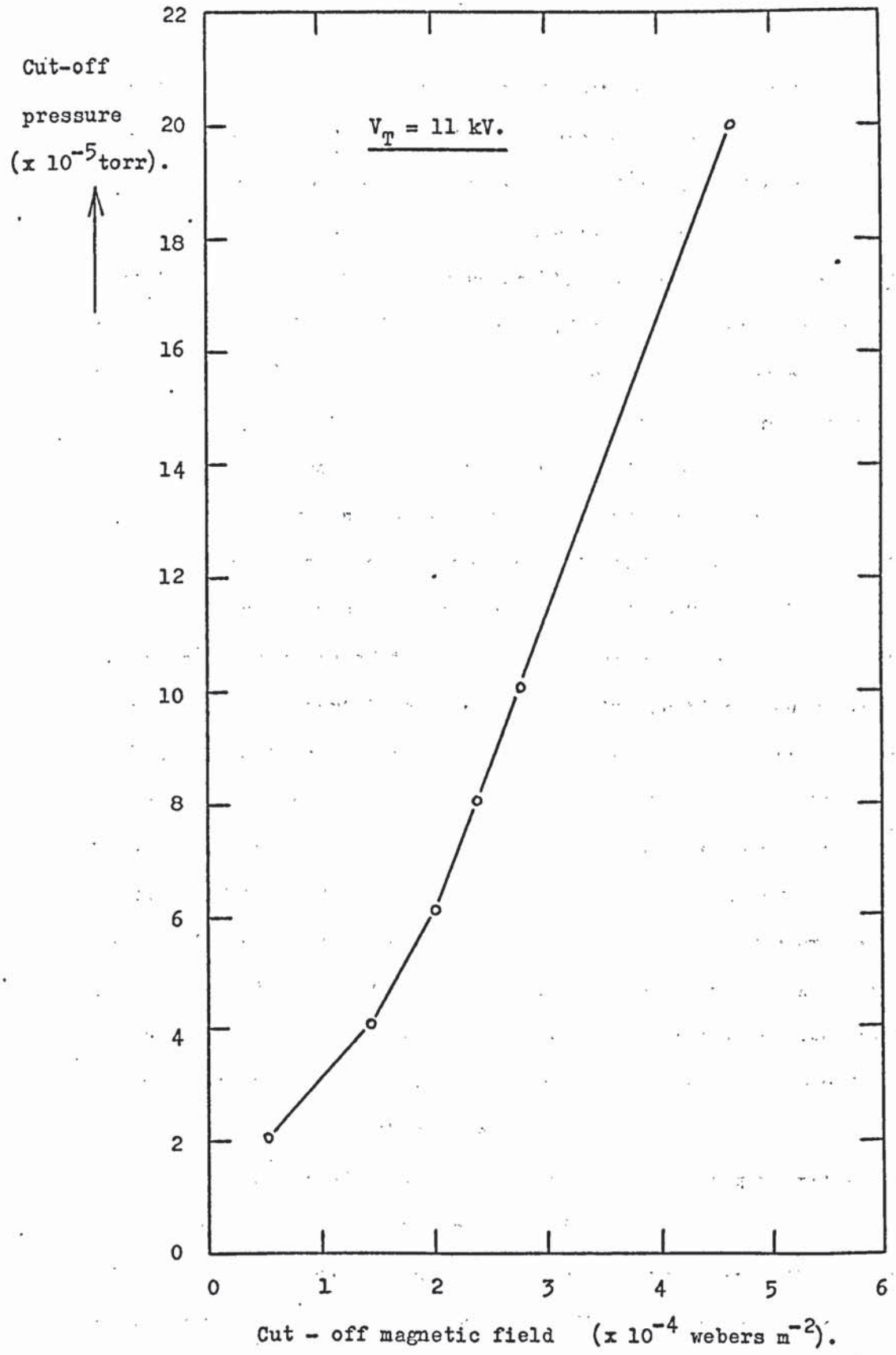

Figure 5.3. The variation of cut-off pressure with cut-off magnetic field.

magnetic field being much more non-uniform at small distances from the magnet - that is for large values of magnetic field $\underline{B}_c$. Also, at large distances from the magnet, that is at small values of magnetic field $\underline{B}_c$, stray magnetic field components in the laboratory, along directions other than the z axis of the twin wire oscillator may be significant. Thus, deviations from linearity in Figure 5.3 can be expected at both large and small values of $\underline{B}_c$ with this present experimental technique.

Having determined $\underline{B}_c$, an estimate of the stray magnetic field along the z axis can then be calculated. In the high vacuum system with the oscillator having its z axis in the horizontal position, the stray magnetic field along the z axis was estimated to be between 5×10^{-6} and 10^{-5} webers m^{-2}. This was later measured with a Hall probe as 8×10^{-6} webers m^{-2}, which is of the order to be expected for the horizontal component of the earth's magnetic field. In the high vacuum system with the oscillator's z axis in the vertical position, the stray field along the z axis was estimated to be between 3.5×10^{-5} and 4×10^{-5} webers m^{-2}. Measurements with the Hall probe confirmed this as being 4×10^{-5} webers m^{-2} which is of the order to be expected for the vertical component of the earth's field. With the oscillator in the ultra high vacuum system in the vertical position and with the mass spectrometer and Triggor gauge magnets removed, the stray field was determined as about 3×10^{-5} webers m^{-2}. Measurements with the Hall probe showed this to vary between 3×10^{-5} and 4×10^{-5} webers m^{-2} in this direction.

It was observed that with the oscillator in its normal position, that is with its z axis in the horizontal position in the high vacuum system, a better low pressure limit was achieved than with the oscillator's z axis being in the vertical position. This is due to the larger component of the earth's magnetic field being in the vertical direction. This again demonstrates that magnetic fields along the z axis of the oscillator, of the order of the earth's field, will affect the performance of the cold

cathode oscillator. At one stage during these magnetic field experiments, the 6 B.A. stainless steel screwed rods employed to hold the end-plates onto the collector electrode tube, became very slightly magnetised and this reduced the tube current. Replacing the stainless steel rods with brass rods restored the tube current to its normal value. An improvement was also obtained in the low pressure limit when using the brass rods. With the brass rods, the best low pressure limit for the cold cathode discharge was about 10^{-5} torr in the vertical position and about 5×10^{-6} torr in the horizontal position when V_T = 11 kV.

5.3. The influence of magnetic fields on the thermionic oscillators.

As a result of the experiments carried out with the cold cathode oscillator, investigations of the influence of magnetic fields on the thermionic twin-wire oscillator were carried out in the high-vacuum system for both the orbiting and oscillating mode electrons. With a filament bias V_B of +12 volts for the orbiting mode and +96 volts for the oscillating mode when V_A = 1 kV, the effects of magnetic fields along the z axis upon these two modes were observed. In Figure 5.4, the variation of the ion collector current i_c with applied magnetic field along the z axis is shown for both the orbiting and the oscillating modes. With the oscillating mode, the collector current i_c is reduced by an order of magnitude with the application of a magnetic field of only 10^{-4} webers m^{-2}. With the orbiting mode, over the region CD in Figure 5.4, a general decrease in collector current i_c occurs when the orbiting mode electrons are disturbed by the relatively large magnetic fields. However, even in the orbiting mode condition, some electrons are emitted from the tip of the filament and thus go into oscillation between the anodes. It is the disturbance of these oscillating electrons by the magnetic field that gives rise to the region AB.

By replacing the twin anode wires with a single anode wire, as in

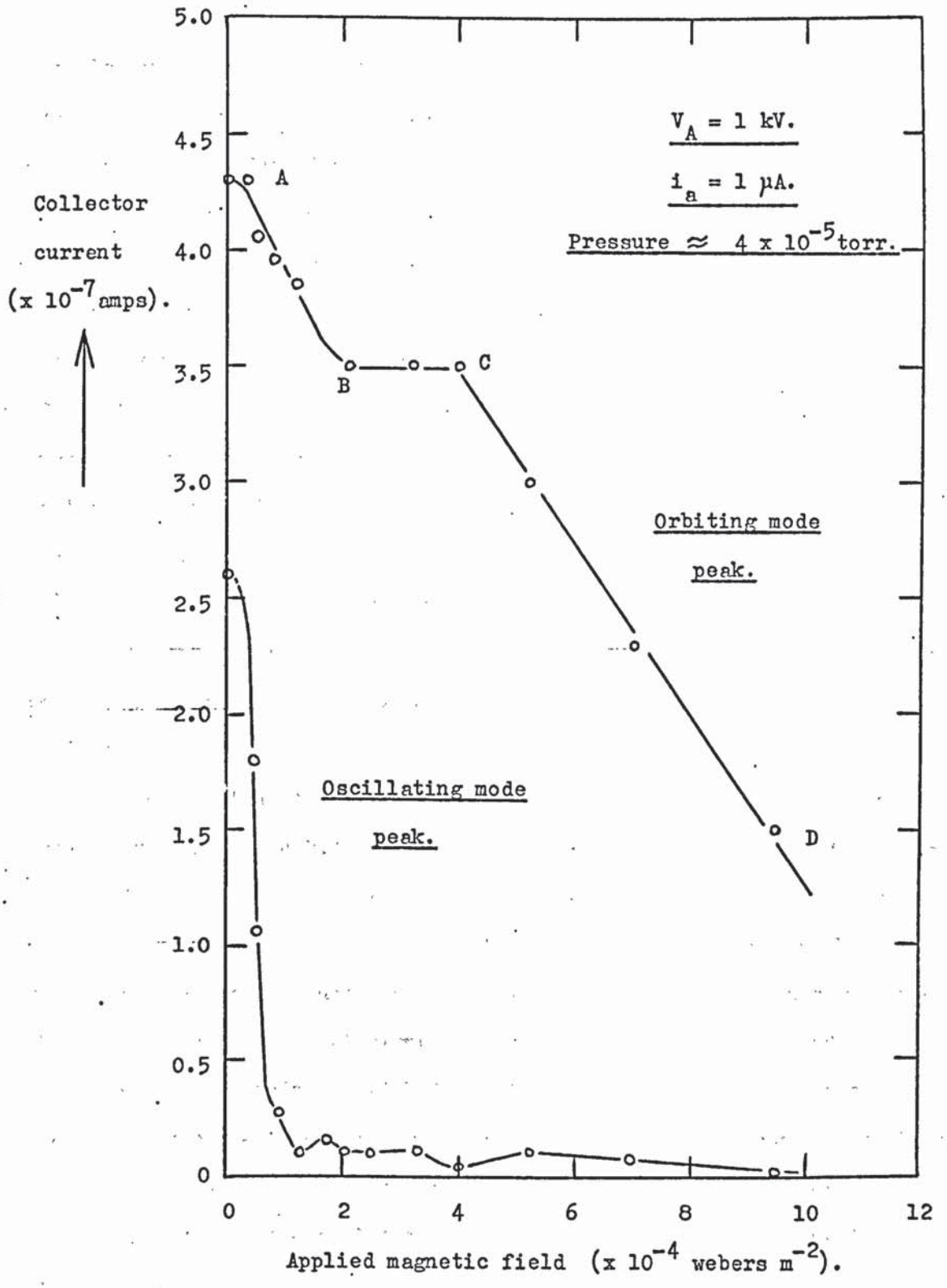

Figure 5.4. The variation of collector electrode current with applied magnetic field for the thermionic twin wire oscillator.

the electron-orbit ionisation gauge, only orbiting electrons are possible. It can be seen in Figure 5.5 that the orbiting electrons are only seriously affected by magnetic fields greater than 10^{-4} webers m^{-2}. As would be expected, no region AB is obtained when using the single anode wire. Whether the magnetic field was applied along the x, y or z axes made no observeable difference on the influence of the magnetic field upon the orbiting mode electrons. However, due to the very high sensitivity of greater than 10^{5} $torr^{-1}$ for the electron-orbit ionisation gauge, at low pressures in the region of 10^{-8} torr, very high electron densities exist in the ionising volume of the device, giving rise to electron space-charge oscillations. With the application of magnetic fields of the order of 10^{-4} webers m^{-2} or more, the electrons can be made to leave the ionising volume and go to the anode more quickly, so reducing the electron density and the associated electron space-charge oscillations, as described in Chapter 3.

When operating the thermionic twin wire oscillator in the high vacuum system, four 4 B.A. mild steel screwed rods were employed to tension the anodes. At one stage during these experiments, the oscillating mode peak in the bias characteristics could not be obtained whereas the orbiting mode peak was unaffected. It was later found that this was due to the presence of a residual magnetic field that had been produced in the 4 B.A. mild steel rods. As with the cold cathode oscillator, these mild steel rods were replaced with brass rods and the oscillating mode peak was restored. All of the magnetic field measurements quoted here for the thermionic twin wire oscillator have been carried out when using these brass rods.

5.4. Discussion.

McIlraith[36] had originally predicted that small magnetic fields of the order of the earth's field would have little effect upon the

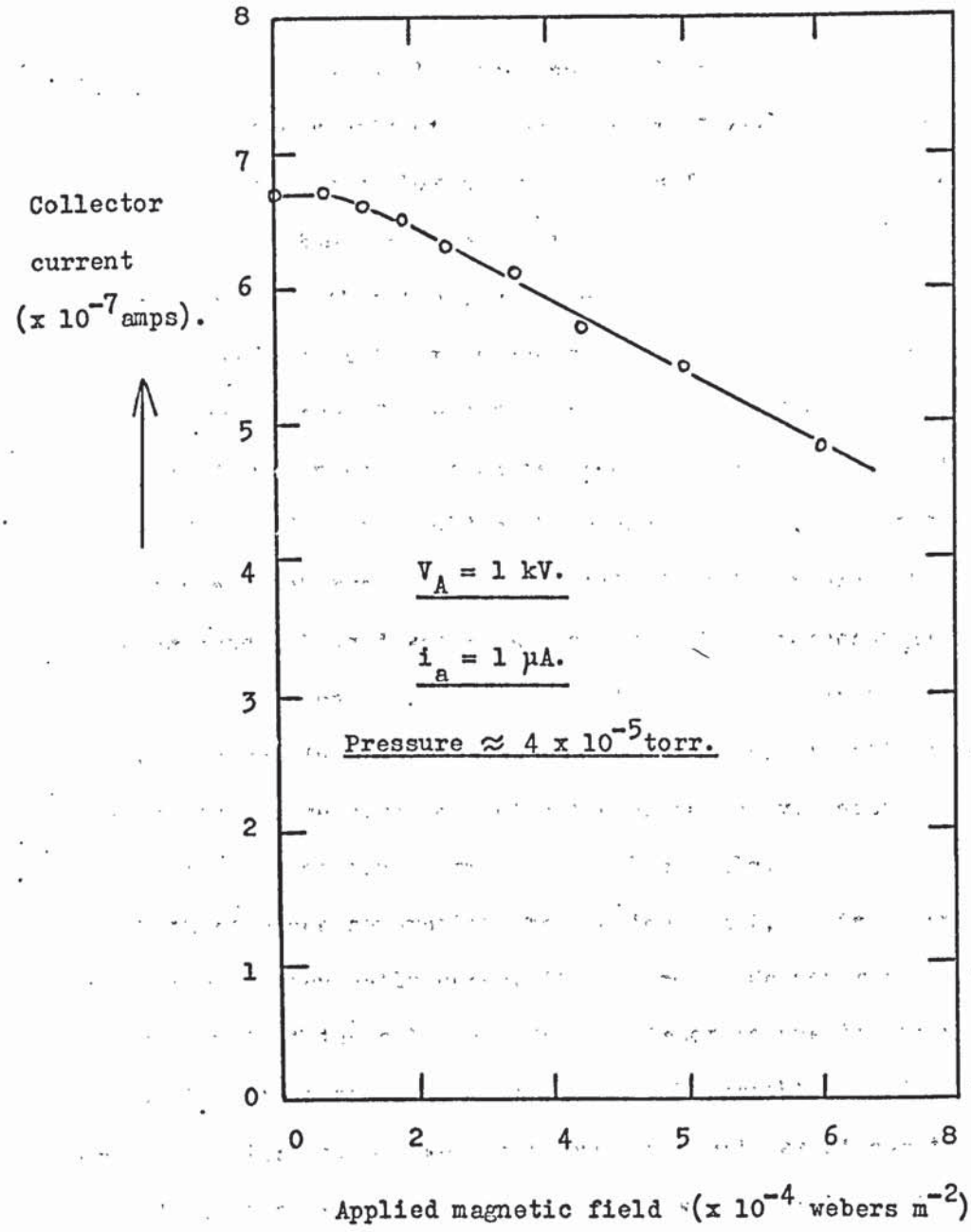

Figure 5.5. The variation of collector electrode current with applied magnetic field when using a single anode wire.

performance of the twin wire oscillator. However, these experiments have demonstrated that magnetic fields have a much more significant influence upon the oscillating mode electrons, whether in the cold cathode or the thermionic twin wire oscillator, especially when the magnetic field is applied along the z axis of the oscillator. These experiments have shown that magnetic fields as low as the earth's field will produce a deterioration in the performance of the twin wire oscillator. It is therefore believed that the low pressure limit of 10^{-5} to 10^{-6} torr for the cold cathode oscillator is due to stray magnetic fields in the laboratory which are of the order of the earth's field. Experiments have been carried out in which attempts have been made to shield these stray magnetic fields from the cold cathode oscillator, in order to see if a cold cathode discharge could be maintained at lower pressures. The shielding material used was an alloy with a high permeability at low magnetic field strengths, but the results of these experiments proved to be inconclusive. In order to obtain any evidence, it will be necessary to cancel out these stray magnetic fields in the vicinity of the oscillator by using some form of Helmholtz coils.

With an anode separation that is too small, it is known that the discharge will eventually cease. If at 5 mm anode separation, the low pressure limit of the cold cathode oscillator is due to stray magnetic fields, then it is possible that even if the earth's field is screened from the oscillator, a lower pressure limit will exist due to the anode separation. This is because the electrons will be able to travel further in the x axis direction due to the increased mean free path between ionising collisions at lower pressures. If the anode separation is made larger, then the average total electron path length $\bar{l}$ within the oscillator will be shortened, so reducing the discharge efficiency.

Due to the destructive influence of magnetic fields upon the oscillating mode electrons, care must be taken to avoid the presence of

large magnetic fields when operating both the cold cathode and thermionic twin wire oscillators.

CHAPTER 6.

THE IMPROVED ION SOURCE.

6.1. Introduction.

The cold cathode twin wire oscillator was first employed as an ion source by Fitch et al[37]. This was done by allowing positive ions formed within the discharge to escape through an aperture positioned in the collector electrode on the y axis. Ion beam current densities of about 100 $\mu A\ cm^{-2}$ were observed at pressures in the region of 5×10^{-4} torr. The major problem with this ion source was due to the fragile nature of the thin anode wires, which were very easily burned out if there was a sudden rise in gas pressure. However, it was shown in section 4.4, that the anode wire diameter had little influence upon the performance of the oscillator, whereas the value of the anode spacing was rather critical. It was therefore realised that advantage could be taken of this phenomenon by designing an ion source with much larger diameter anodes at an appropriate anode separation. In this chapter, an ion source using 2mm diameter anodes is described, which has a performance equal to the original ion source, but which is much simpler in construction and more reliable in operation.

6.2. Description and performance of the improved ion source.

The construction of the improved ion source[48] is illustrated in Figure 6.1. The ion collector electrode was again of stainless steel, 20 cm long by 5 cm internal diameter with a rectangular aperture, 2.5 cm long by 0.5 cm wide. End-plates of the usual design were used, but were now constructed of stainless steel. The anodes were made from 2 mm diameter tungsten rods and were free to move in the ceramic insulating bushes during thermal expansion caused by electron bombardment. It was

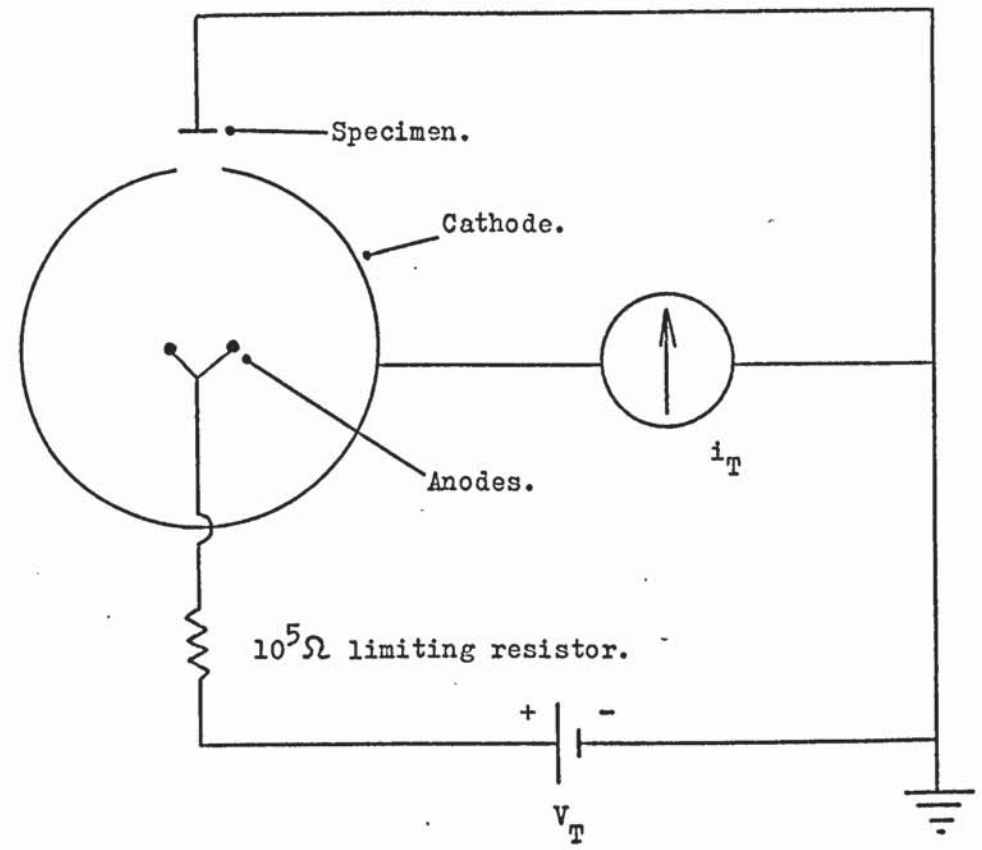

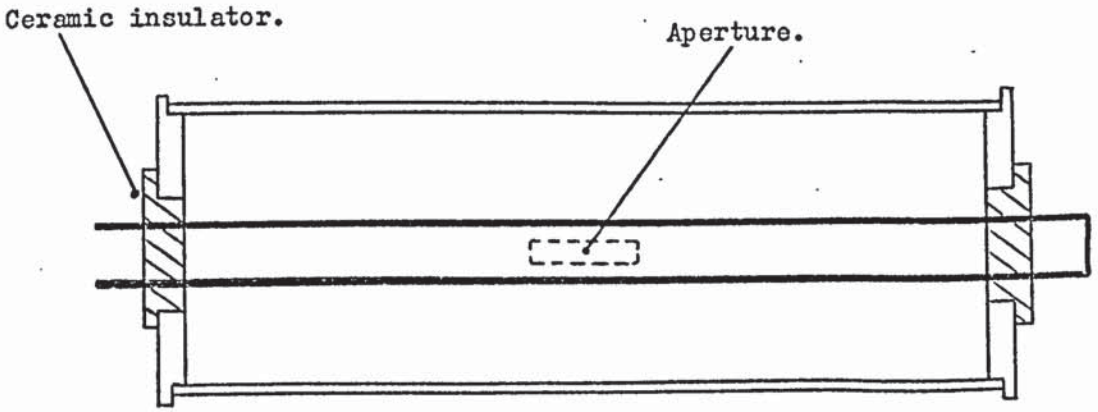

Figure 6.1. Schematic diagram of the improved ion source.

therefore not necessary to incorporate any spring tensioning of the anodes.

The performance of this ion source was investigated for several values of anode separation and it was found to compare favourably with the oscillators that employed finer anodes. Again, if the anode separation was too small, no discharge could be maintained. However, the optimum anode centre to centre separation was found to be about 8 to 9 mm. This is larger than the value of 5 to 6 mm separation for the optimum performance obtained with the wire anodes. It thus appears that the surface to surface anode spacing rather than the centre to centre separation as illustrated in Figure 6.2, is the important parameter in optimising the performance of the oscillator. Thus, the optimum surface to surface spacing is about 6 to 7 mm, which is not very different from that for the wire anodes. This is to be expected, as the anode separation at which the discharge ceases due to the initial kinetic energies of the electrons, will to a first approximation, depend upon the surface to surface spacing rather than the centre to centre separation.

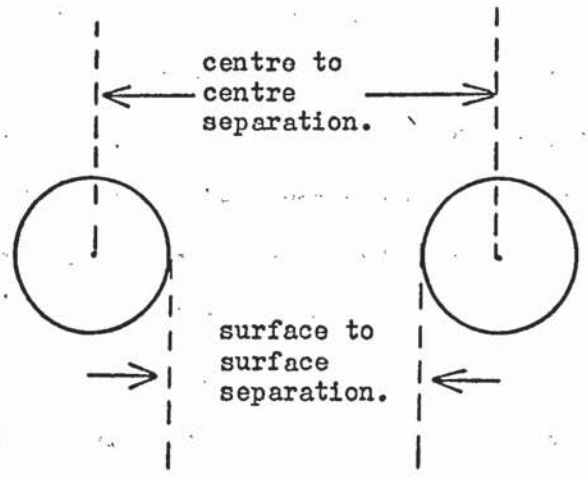

Figure 6.2.

At centre to centre separations larger than 9 mm, the fall in tube current i_T was not drastic and so an anode centre to centre separation of 10 mm

was used in the ion source. The variation of tube current i_T with tube voltage V_T for this anode separation, is given in Figure 6.3 for the pressure range 6×10^{-4} torr to 1×10^{-4} torr. It was observed that the tube current reduced by as much as 30% after an initial period of outgassing and the results in Figure 6.3 were obtained after this period when the tube current was constant with time.

During normal operating conditions, the 2 mm diameter anodes reached temperatures in excess of 1000° C, but this was considerably cooler than when using the wire anodes because of the increased surface area. The performance of the ion source was reduced by about 50% when 6 mm diameter stainless steel tubular anodes were employed. This suggested that it should be possible to incorporate water cooling of the anodes if it is necessary to reduce the anode temperature.

6.3. The radial distribution of positive ions emerging from the discharge.

The radial distribution of positive ions emerging from the discharge in the cold cathode oscillator was determined by scanning a Faraday cage around the outside of the ion collector electrode. A 120° aperture was milled into the collector electrode midway along its length, as illustrated by the dashed line in Figure 6.4(a). The aperture had a width of 3 mm and a nickel cleat was placed around the oscillator's collector electrode, so producing an effective aperture of about 1 cm by 3 mm in size in the collector. In this way, this effective aperture could be rotated around the oscillator tube relative to the plane of the anodes. The Faraday cage was constructed mainly from nickel sheet and had a 1 mm diameter limiting aperture in front of the collector cup, as shown in Figure 6.5. This Faraday cage was scanned from -10° to 90° rotation from the y axis, as illustrated in Figure 6.4(a). The distance along the y axis between the limiting aperture and the collector electrode was maintained constant at approximately 5 cm. Inside the vacuum chamber, the

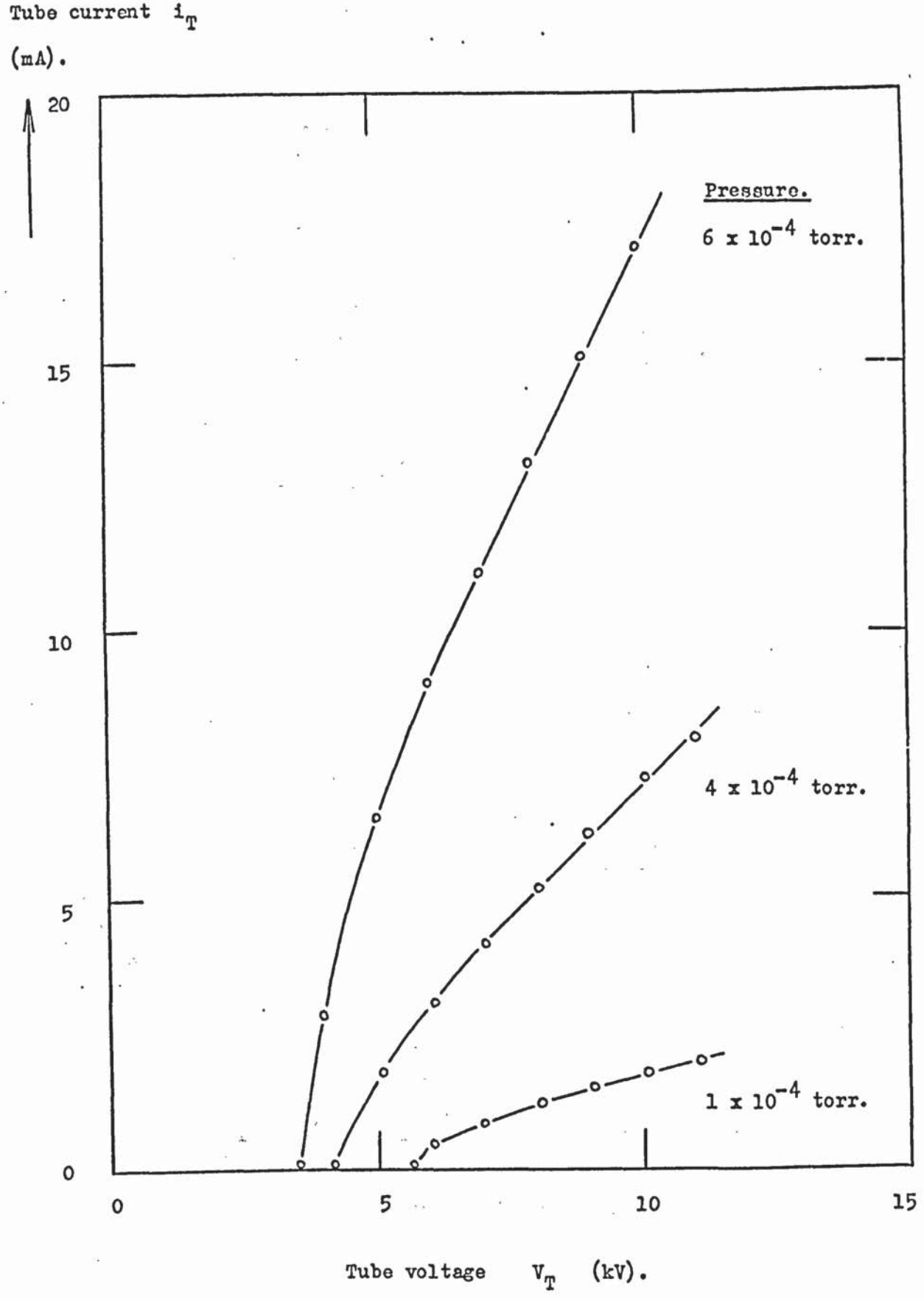

Figure 6.3. The variation of tube current with tube voltage for the improved ion source.

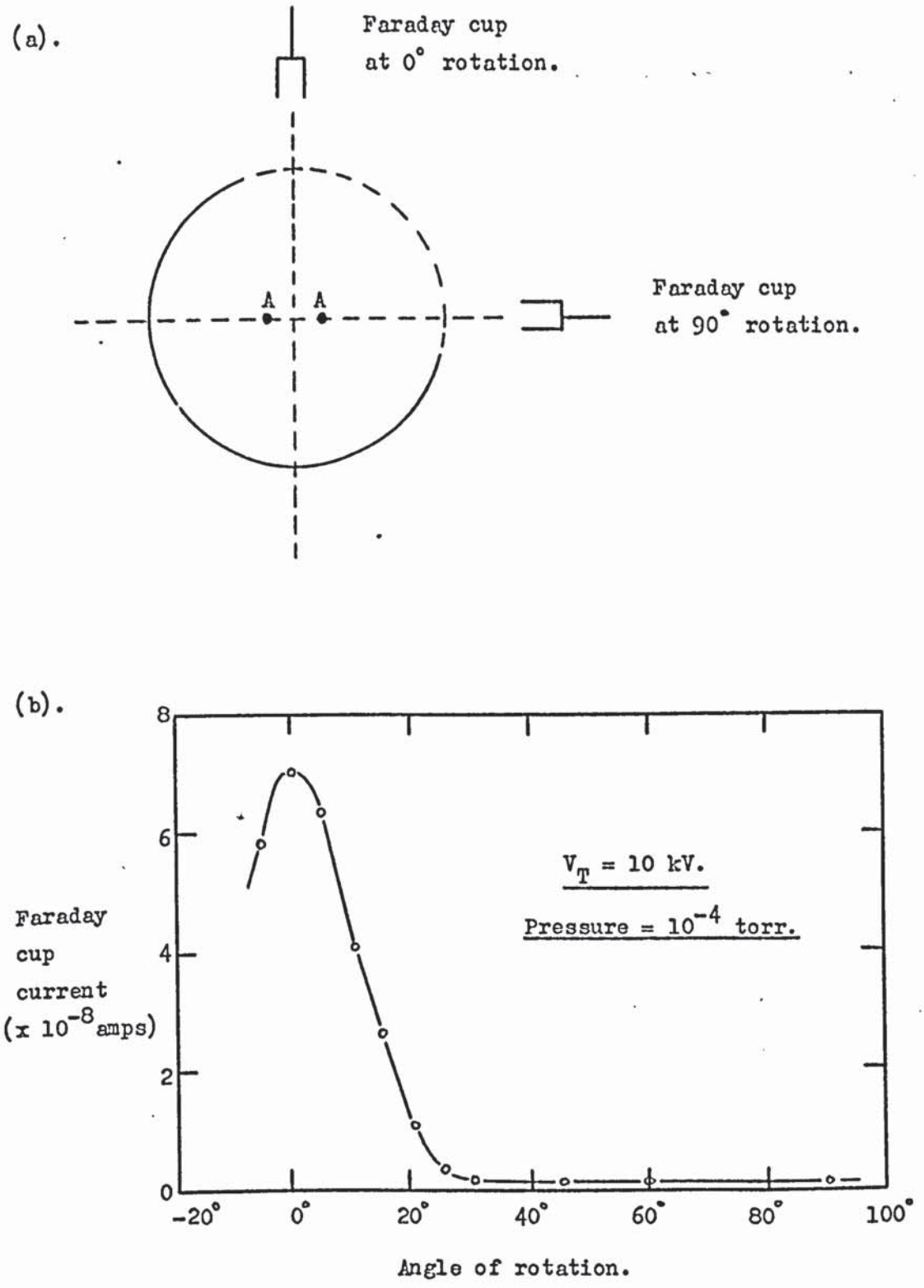

Figure 6.4. The positive ion current distribution from the cold cathode discharge.

electrical lead to the Faraday cup collector was completely screened in order to prevent it collecting any ions scattered from the glass bell jar.

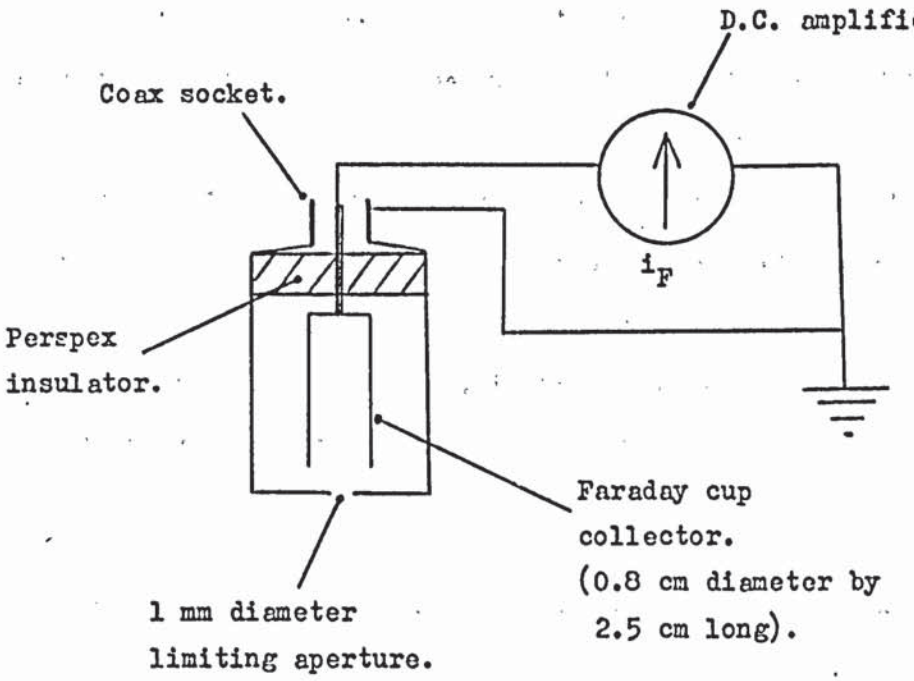

Figure 6.5. The Faraday cage.

The variation of Faraday cup current i_F with angle of rotation is given in Figure 6.4(b). The ion current density falls off quite rapidly with angle of rotation and the discharge subtends an angle of about 50° at the cylinder axis. This agrees with the widths of the observed ion etched regions on the interior of the collector electrode surface.

6.4. Current density of the ion beam.

The variation of ion beam current density with distance along the y axis from the ion source aperture is given in Figure 6.6. The diameter of the limiting apeture in the Faraday cage was 1 mm and its area is therefore 7.8×10^{-3} cm^2. At V_T = 10 kV and i_T = 7 mA, the ion beam current density at the aperture is about 90 μA cm^{-2}.

Assuming that the current densities obtained by the Faraday cage

are due to singly positively charged ions, a knowledge of the secondary electron emission from the collector electrode wall can be obtained by extrapolation of the measured ion densities back to the position of the collector. These can then be compared with the average current densities obtained from a knowledge of the tube current i_T and the area of the ion etched regions on the interior surface of the collector electrode. Thus, as the total area of the two ion etched regions is 80 cm^2, then the values obtained for the current densities from the two methods agree very closely, indicating a secondary electron emission coefficient of zero from the collector electrode wall. However, it has been shown in Figure 6.4(b) that the ion density falls off quite rapidly with angle of rotation.

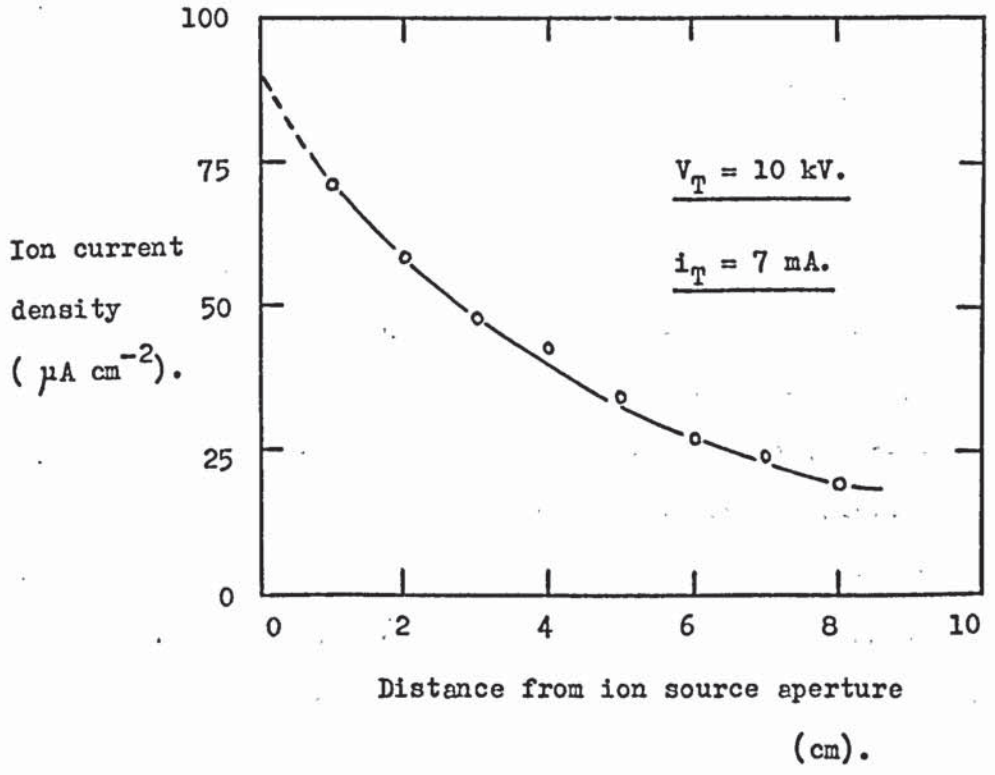

Figure 6.6. The variation of ion beam current density with distance from the ion source aperture.

From this distribution, it can be seen that the average ion current density will be approximately half of that measured by the Faraday cage at 0° rotation on the y axis. Thus, the secondary electron emission coefficient from the collector wall will be in the region of unity, assuming that these electrons are produced purely by positive ion bombardment of the collector electrode surface.

The results given in Figure 6.6 were obtained when using 0.25 mm diameter anodes in the ion source. The variation of ion beam current density with distance from the aperture was also investigated when using the rigid 2 mm diameter anodes in the improved ion source and these results are given in Appendix 6. It was found that the ion beam current densities obtained with the improved ion source under given conditions of V_T and i_T were the same as obtained from the original wire anode ion source. However, the improved ion source gave completely reliable operation when delivering ion beam current densities in excess of 300 $\mu A\ cm^{-2}$ due to the more robust nature of the rigid anodes.

6.5. Energy distribution of the ion beam.

An attempt was made to determine the energy distribution of the ion beam emerging from the ion source, by putting a positive retarding voltage on the collector cup in the Faraday cage. It was found that the Faraday cup collector current i_F went negative when a retarding voltage of only +3 volts was applied to the cup. This negative current increased with increase in retarding voltage. This was attributed to electrons being ejected from the surface of the limiting aperture by positive ion bombardment and then being attracted into the Faraday cup collector due to the positive voltage on the cup.

The positive retarding voltage was then put onto the limiting aperture structure, with the cup being maintained at earth potential. The positive Faraday current i_F began to increase with the application of a

positive potential on the limiting aperture. This was attributed to electrons being produced in the collector cup by positive ion bombardment and then being attracted out of the cup by the positive potential on the limiting aperture structure. These unsatisfactory results indicate some of the problems associated with ion energy analysis, which are even more serious than in electron energy analysis.

The design of various types of retarding field energy analysers is dealt with by Simpson[49]. Due to the problems encountered with the Faraday cage when it was used as an ion energy analyser, it was decided to separate the analyser and detector systems, as shown in Figure 6.7. Aperture 1 was the 1 mm diameter limiting aperture that had the positive retarding potential V_R applied to it. Aperture 2 was 3 mm in diameter and was maintained at earth potential so screening the Faraday cup collector from the retarding voltage V_R on aperture 1. The Faraday cup was maintained at earth potential and a D.C. amplifier was used to measure i_F. Aperture 3 was 3 mm in diameter and was earthed in order to shield aperture 1 from most of the ion beam leaving aperture 4 in the ion source. This was necessary, as when aperture 1 was at a fairly high positive voltage, instabilities within the analyser system were observed if aperture 3 was not employed.

The variation of i_F with retarding potential V_R is given in Figure 6.8, for V_T = 10 kV and i_T = 7 mA. With the $10^5 \Omega$ limiting resistor at the output of the H.T. power supply, the actual voltage across the tube, V_A, was 9.3 kV. Then, by plotting di_F/dV_R versus V_R, the energy distribution of the ion beam is obtained as given in Figure 6.9, where di_F/dV_R is proportional to the number of ions per unit energy N(E) and V_R is proportional to the ion energy in electron-volts.

In the ion energy spectrum, ions are present at energies of about 20 eV and above, 20 eV being in the region of the first ionisation potential. The ion population density N(E) rises to a maximum at somewhere

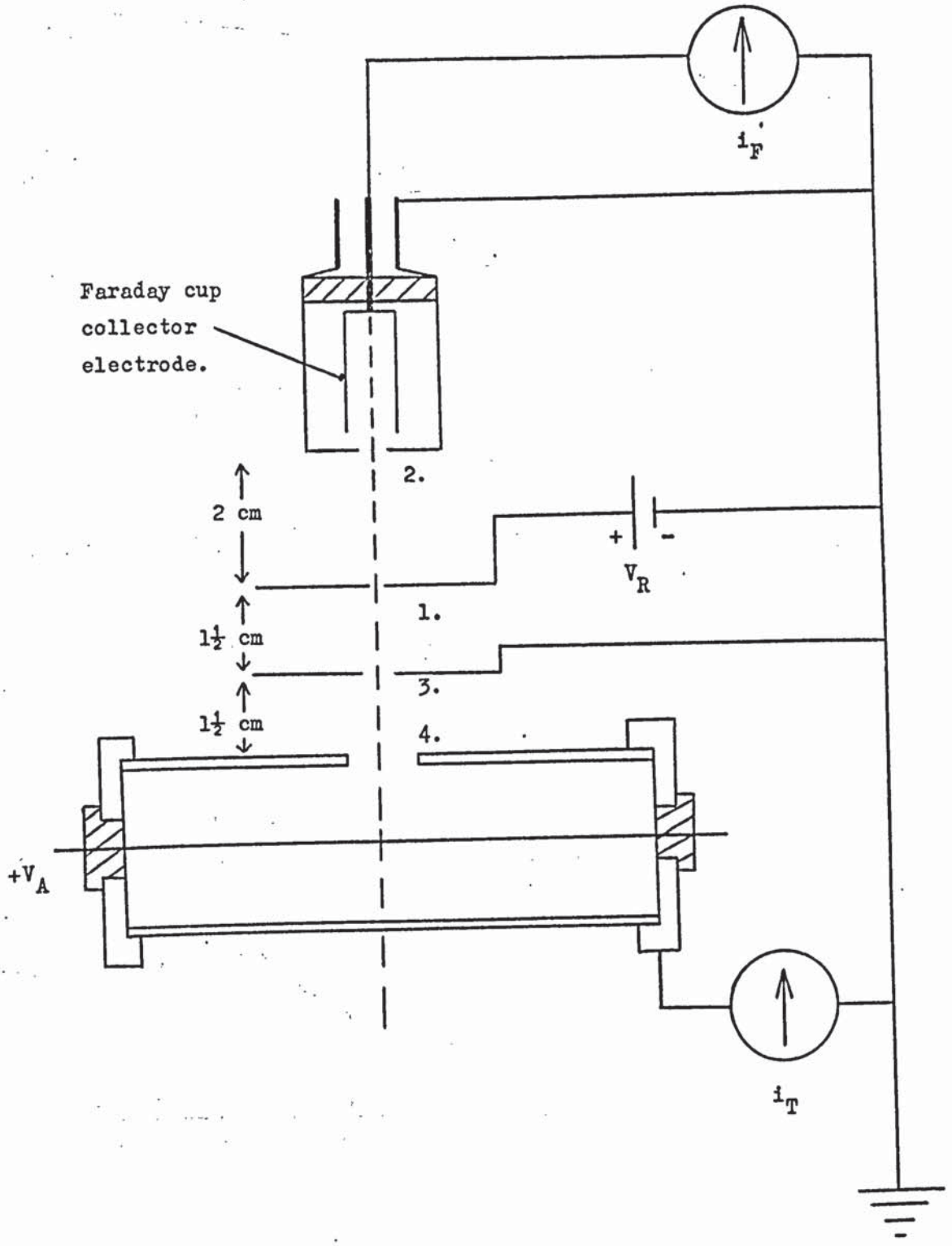

Figure 6.7. The electrode arrangement for the ion energy analysis.

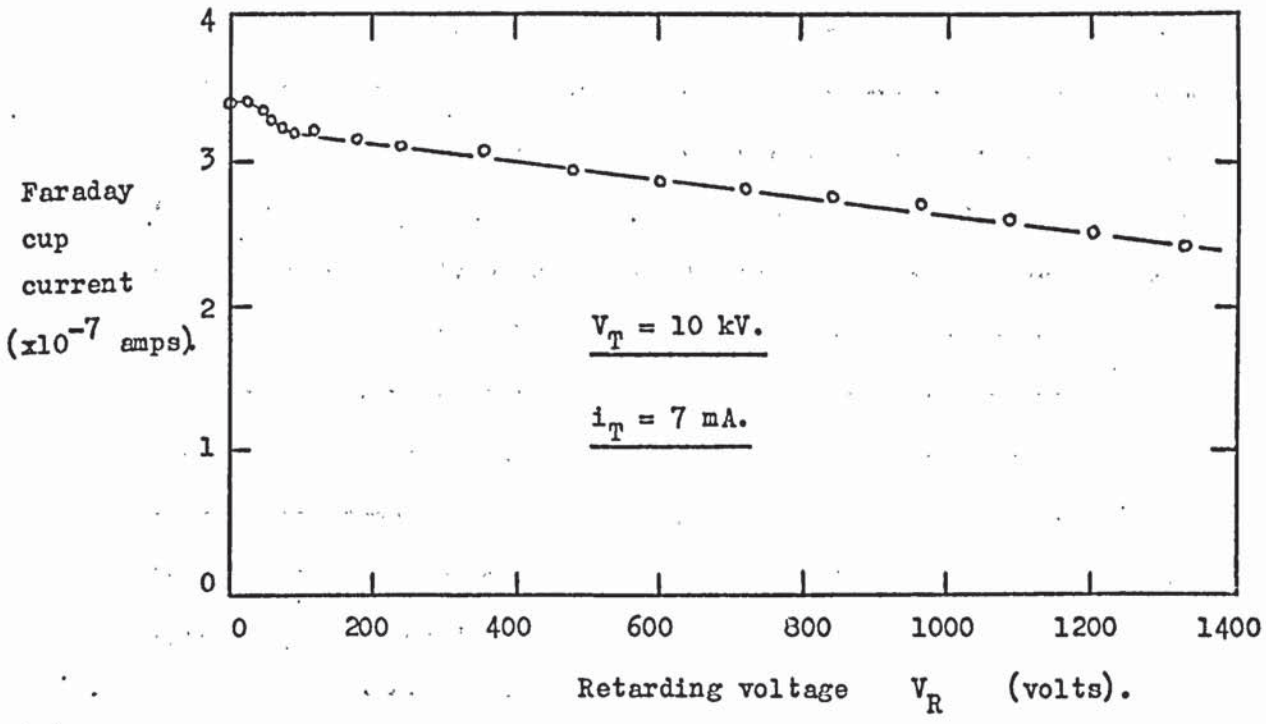

Figure 6.8. The variation of Faraday cup current with retarding voltage.

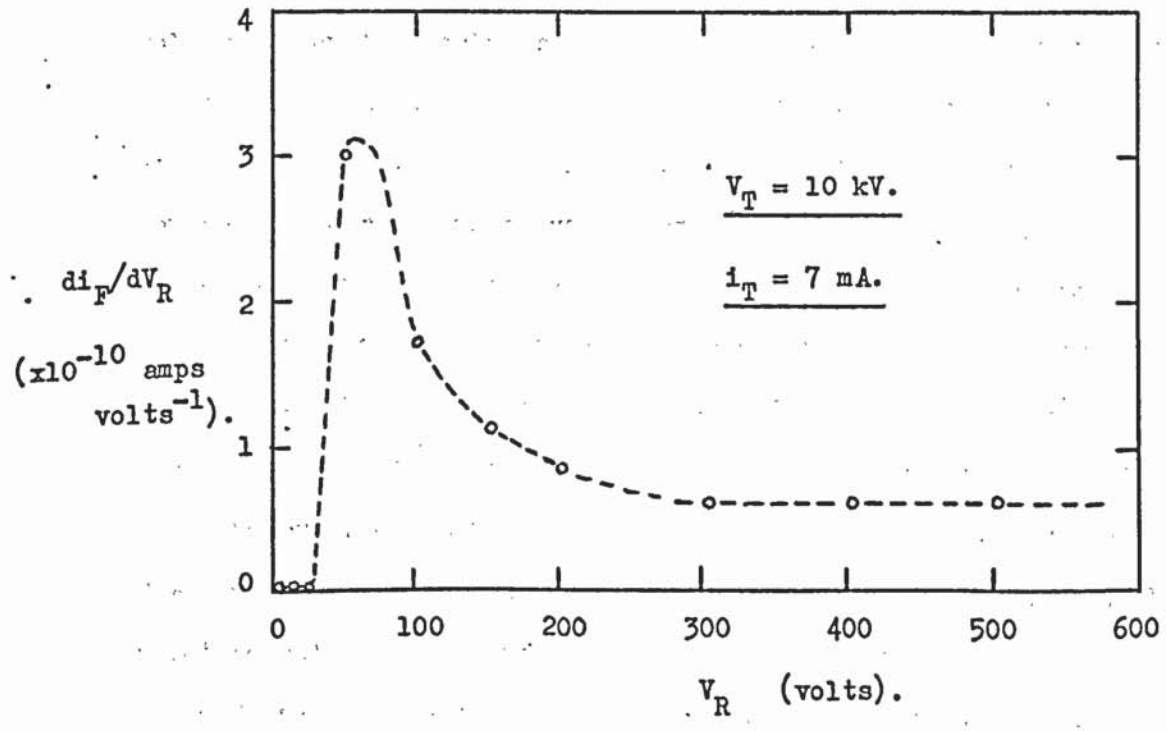

Figure 6.9. The resulting ion energy spectrum.

between 50 and 100 eV. This is in the energy region where the maximum ionisation cross-section for nitrogen occurs and so will most likely be due to ions that have been produced by electrons that have been ejected from the collector electrode by positive ion bombardment. This low energy peak represents only about 6% of the total number of ions in the ion beam and so the exact shape of this low energy peak is uncertain. Above the low energy peak, there appears to be a broad distribution of ion energies. However, it was found to be difficult to make very high ion energy measurements of several keV with the present system, due to instabilities occurring in the analyser system when using these very high retarding voltages V_R.

In order to investigate the form of the high energy end of the spectrum, the applied tube voltage was reduced to 4 kV with i_T = 7 mA. Thus, the anode voltage V_A was 3.3 kV when taking into account the voltage drop across the current limiting resistor. In this way, the retarding voltage V_R on the analyser could be made to approach the value of V_A. The variation of i_F with V_R is given in Figure 6.10, for values of V_R up to about 1300 volts. At values for V_R of 1500 volts and greater, the Faraday cup current i_F showed an excessive drop and at V_R = 2.5 kV, i_F was completely negative. This could be due to an increase in ion population density in this energy region, but due to the negative current at V_R = 2.5 kV, it is suspected that it is more likely due to electrons produced within the analyser system, entering the Faraday cup collector.

However, extrapolation of the graph in Figure 6.10 gives zero Faraday cup current i_F at a value for V_R of about 2.5 kV. Now, the saddle-point potential is in the region of 70% to 80% of V_A and as V_A is 3.3 kV, the saddle-point potential is within the region of 2.3 to 2.6 kV. This corresponds closely to the intercept when i_F = 0 in Figure 6.10. Thus, it seems reasonable that the ion energies should extend up to energies corresponding to the region of the saddle-point potential. Extrapolation

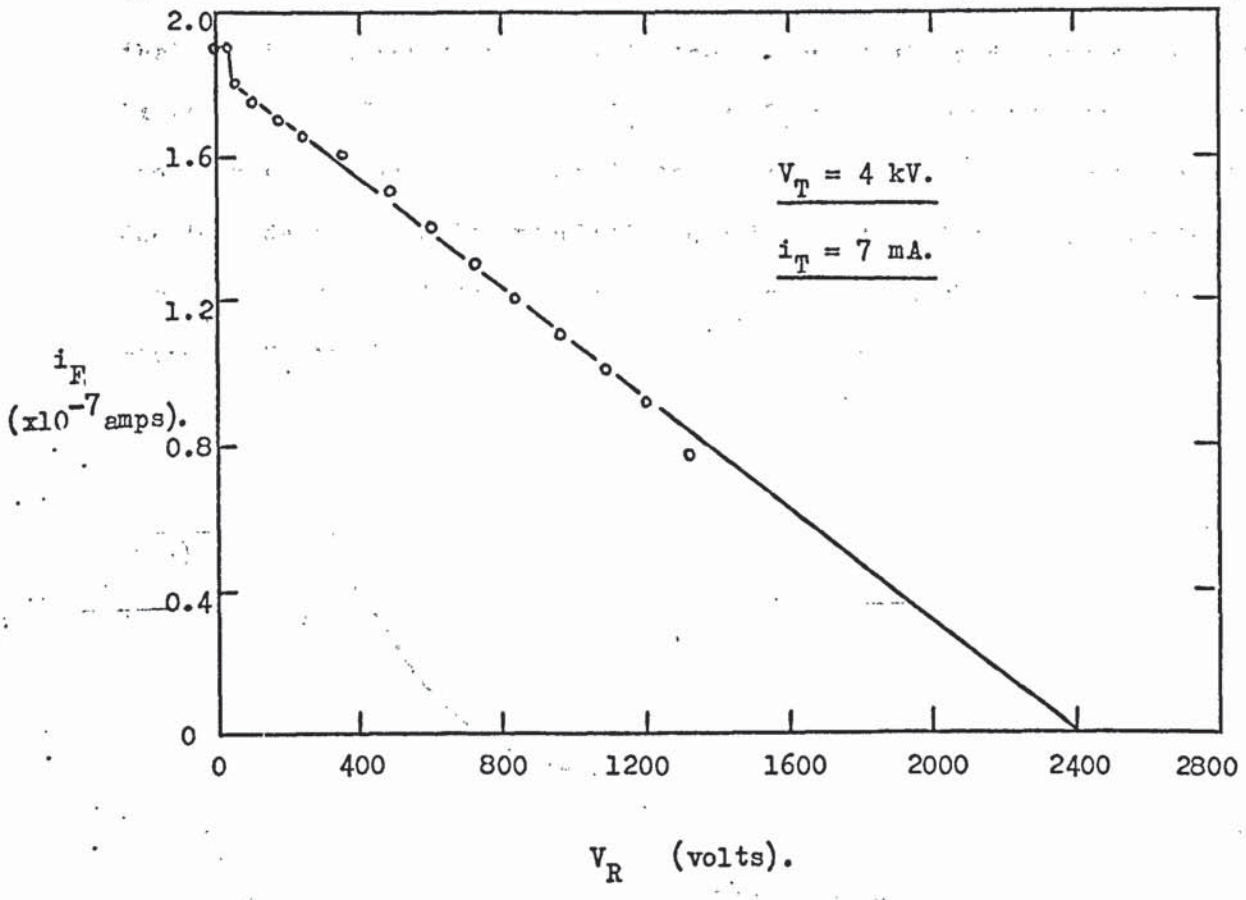

Figure 6.10. The variation of Faraday cup current with retarding voltage when using a tube voltage of 4 kV.

of the graph of i_F versus V_R in Figure 6.8 will give zero i_F at a value of V_R in the region of 5200 volts. With an applied tube voltage V_T of 10kV and i_T = 7 mA, the anode voltage V_A is 9.3 kV and the saddle-point potential will be in the region of 6.5 to 7.5 kV. This supports the theory that the ion energies extend up to the region of the saddle-point potential. Extrapolation of the graphs of i_F versus V_R is only a rough approximation, probably giving an intercept with the V_R axis at too small a value of V_R, due to a decrease in ion population density at the higher ion energies. The ion energy spectrum will probably be similar to the illustration given in Figure 6.11.

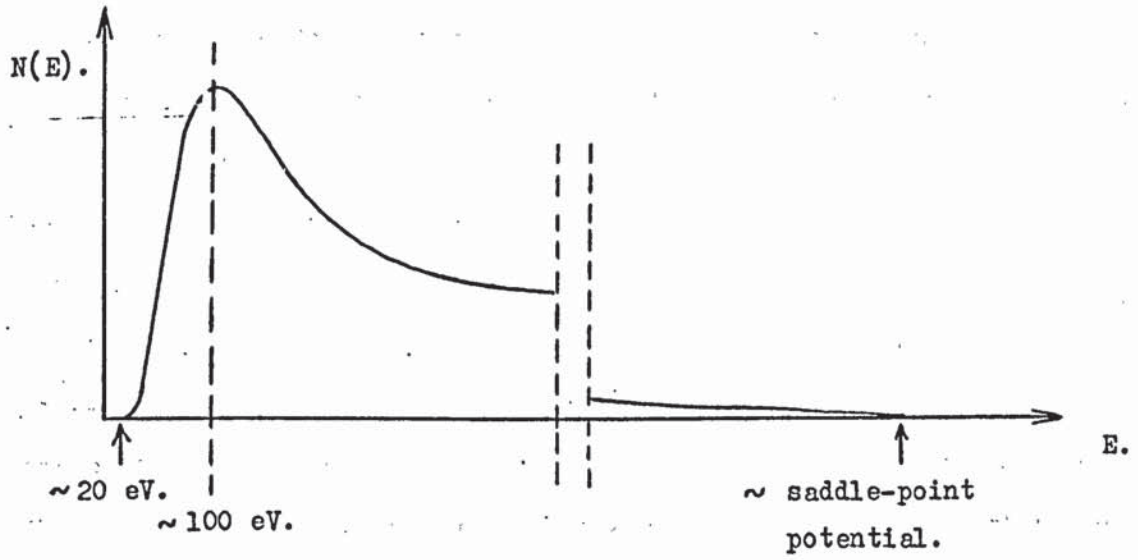

Figure 6.11. The possible ion energy spectrum.

The ion energy measurements have only been carried out with the analyser positioned on the y axis of the oscillator. However, the ion source aperture has its own ion optical properties. The low energy ions will tend to be deviated to the sides of the ion beam more than the high energy ions, by the electrostatic field distortion at the aperture in the

collector electrode. Thus, the ion energy spectrum will be modified to some extent at positions away from the y axis.

6.6. Examples of ion etching using the improved ion source.

Atoms can be removed from the surface of a solid material at a useful rate by bombarding it with a beam of ions whose mass is greater than a few atomic units and energy is greater than about 100 eV (Spencer and Schmidt[50]). When preparing thin foil specimens by ion bombardment, it is necessary to keep their temperature low in order to avoid structural changes and so ion current densities in excess of about 200 $\mu A\ cm^{-2}$ are not necessary (Barber[51]). Thus, this improved ion source should find many applications such as in specimen preparation for both optical and electron microscopy and in device fabrication by ion beam machining.

Several specimens have been etched by bombarding them with positively charged argon ions using the improved ion source (Fitch and Rushton[48]). The specimens were mounted in turn as shown in Figure 6.1 at a distance of 2 cm from the ion source aperture. All of the specimens were approximately 1 cm square and the bombarding argon ions arrived at normal incidence to the specimen surface. Scanning electron micrographs of some of the specimens that have been ion etched are given in Figure 6.12.

Figures 6.12(a), (b) and (c) show micrographs of polycrystalline nickel, molybdenum and O.F.H.C. copper specimens respectively. In order to make the effects of the ion etching more obvious, half of the specimen was shielded using aluminium foil. In all of the micrographs, the etched regions are on the right. The nickel and molybdenum specimens were in sheet metal form whereas the copper was in the form of a metal stub. Mechanical polishing to a $\frac{1}{4}\ \mu$ finish was employed for both the molybdenum and copper specimens. In all three cases, the applied tube voltage V_T was 10 kV and the tube current i_T was maintained at between 10 and 15 mA. The nickel and molybdenum specimens were bombarded with

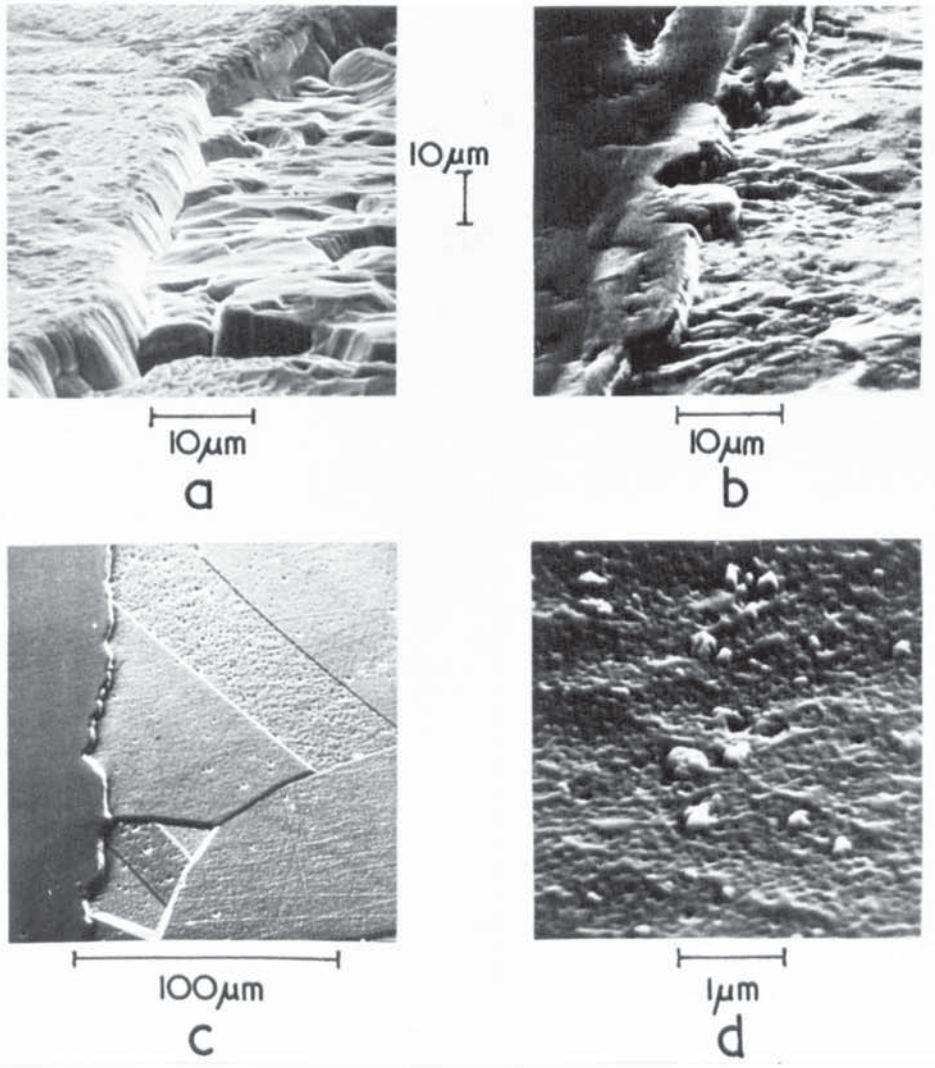

Figure 6.12. Examples of ion etching using the improved ion source.

argon ions of approximately 100 $\mu A\ cm^{-2}$ for 8 hours each. Due to the higher sputtering yield of copper, the copper specimen was only exposed to the ion beam for $1\frac{1}{2}$ hours. Figure 6.12(d) shows the surface of an acrilonitrile butadiene styrene (ABS) plastic specimen after bombardment with argon ions at 50 $\mu A\ cm^{-2}$ for 4 hours. This plastic is a two phase polymer and consists of small particles of graft rubber in a styrene acrilonitrile (SAN) matrix. The ion etching has revealed the distribution and size of the rubber particles. Other specimens that have been successfully etched are aluminium, tungsten and soda glass.

The successful ion etching of the glass and plastic specimens is interesting in that some process must be preventing a positive charge build up on these non-conducting specimens. This process preventing the charge build up may be due to leakage of charge across the specimen surfaces from earth due to the relatively small dimensions of the specimens. On the other hand, it is possible that this charge build up is neutralised by negatively charged particles such as electrons present in the ion beam emerging from the ion source. Thus, it will require further investigation to establish the nature of this process.

6.7. Small volume ion sources.

The tube current density was maintained when collector electrode tube lengths of 10 cm and 7.5 cm were employed, when using the 2mm diameter anodes. Figure 6.13 is a colour photograph of the inside surface of the 10 cm long collector electrode. This collector has been split and rolled out flat. The two regions that have been etched by positive ion bombardment can be clearly seen in the photograph. Thin film colour fringes can be seen over the rest of the surface, but the material comprising these films and the mechanism of their formation is uncertain. They could be a result of oil contamination or of material that has been removed from the ion etched regions of the collector electrode surface.

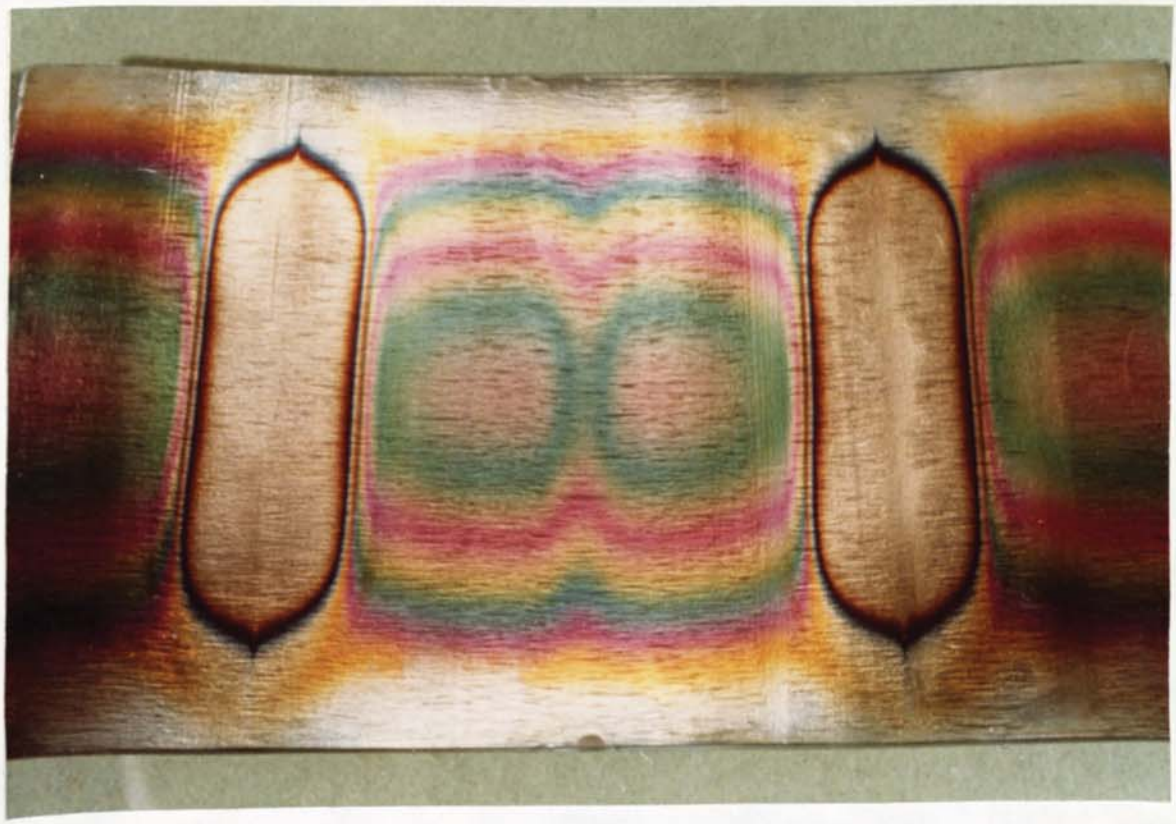

Figure 6.13.

However, these colour fringes disappear after a period of operation, due to the deposition of a relatively thick layer of material that has been removed from the ion etched regions of the collector electrode.

An oscillator was set up with a stainless steel collector electrode that was approximately 2.5 cm in diameter by 7.5 cm long. Two 2 mm diameter tungsten anodes were employed and at an applied tube voltage V_T of 10 kV and a pressure of 6×10^{-4} torr, a tube current of about 3 mA was obtained with an anode centre to centre separation of 7 mm. The ion etched regions on the collector electrode were about 1 cm wide, which suggests that the positive ion current densities were comparable to those obtained with the larger diameter oscillator. With this small diameter oscillator, experiments were carried out to determine what size of circular aperture could be tolerated. With circular apertures of 5 mm diameter or more, no discharge could be maintained. With a 4mm diameter circular aperture, a discharge could only be held at pressures above 4×10^{-4} torr. With circular apertures of 3 mm and 2 mm diameter, satisfactory discharges could be maintained in both cases. Thus, the maximum size of aperture that could be tolerated in this small diameter oscillator was 3 mm. The loss in performance of the oscillators with bigger apertures was most likely due to the field distortion produced by these relatively large apertures, interfering with the oscillating electrons. However, a 6 mm diameter aperture at the side of the oscillator, that is away from the discharge region, did not have any influence upon the performance of the oscillator. Hence, gas pumping ports in the collector electrode at the side of the oscillator away from the discharge region are a feasible proposition.

6.8. Multiple beam and wide beam ion sources.

Experiments with the rubber model analogue have shown that oscillating electron trajectories can be obtained when using any even

number of anodes. Figure 6.14 shows the case of 4 anodes in which the oscillations are in the directions XX' and YY'. Independently, McIlraith[52] predicted the same phenomenon by using a computer to investigate the electron trajectories in the oscillator. The ion source was reconstructed using four 2 mm diameter tungsten rods at a separation of 8.5 mm and positioned as shown in Figure 6.14, inside the stainless steel cylindrical collector electrode of 20 cm length and 5 cm diameter. This anode spacing was found from the rubber model analogue to give the largest number of oscillations. Glow discharges were obtained in the tube as indicated by the shaded areas in Figure 6.14 and the characteristics were similar in form to those of the twin anode device, but the actual tube currents i_T at a given tube voltage V_T and pressure were somewhat lower. However, the widths of the ion etched regions inside the collector cylinder were narrower than in the twin anode case, indicating that the ion density may be only slightly reduced. With this multiple beam ion source, it should be possible to etch a large number of specimens at the same time.

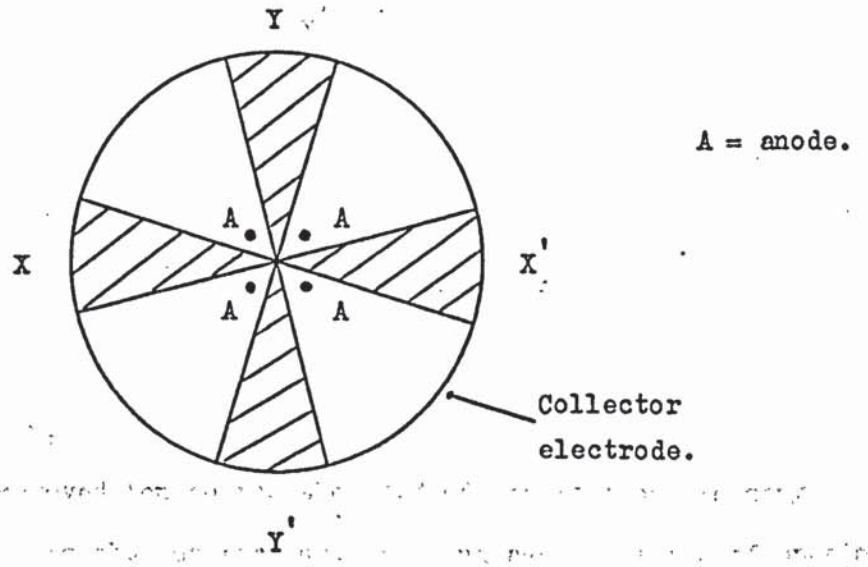

Figure 6.14. The multiple beam ion source.

It has also been observed from the rubber model analogue experiments that the cylindrical collector electrode can be replaced by a collector of square or rectangular cross-section. Using a square stainless steel collector electrode 5 cm wide and 20 cm long, the full width of the ion beam YY' can be used to etch a large area specimen by using the specimen itself as one side of the collector electrode, as indicated in Figure 6.15.

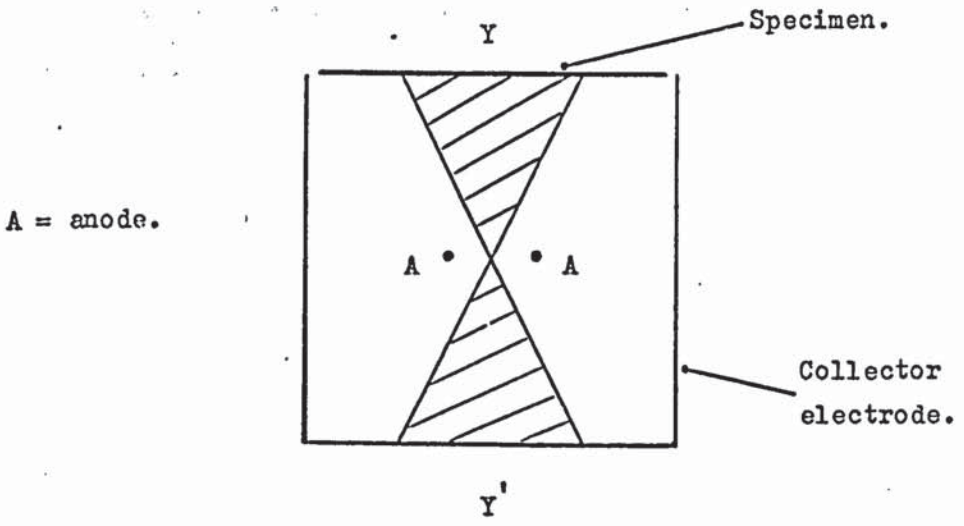

Figure 6.15. The wide beam ion source.

6.9. Discussion.

The improved ion source should find applications in many techniques, such as the ion etching, thinning and polishing of specimens and also in device fabrication by ion beam machining. Both metallic and non-metallic specimens have been successfully ion etched using this ion

source. The source is simple to construct and it was found to be completely reliable in operation. The length of the collector electrode could be reduced below 20 cm in order to reduce the power consumption of the ion source.

With the smaller diameter ion sources, it should be possible to use them to ion etch specimens in situ, such as in the specimen stage of the electron microscope. Introducing gas directly into the ion source tube rather than flooding the whole chamber may have several advantages, such as reducing the gas load requirements of the system and may also give some degree of pressure differential between the inside and outside of the ion source. This would allow the specimen stage to be maintained at a lower pressure than that in the discharge region.

CHAPTER 7.

CONCLUSIONS AND SUGGESTIONS FOR FUTURE WORK.

This investigation has shown that when electrons are injected into the twin wire electrostatic charged particle oscillator from a hot "V" shaped filament, two principal modes of electron oscillation can occur. If a low positive bias voltage with respect to the collector electrode is applied to the filament, then the electrons will orbit around the anodes in the "orbiting mode". On the other hand, when a high positive bias voltage is applied to the filament, the electrons will oscillate between the anodes in the "oscillating mode". The orbiting mode was always very reproducible and this method of electron injection has been successfully used in the development of the electron-orbit ionisation gauge. This gauge has a very high sensitivity in excess of 10^{5} $torr^{-1}$, giving it a low pressure limit due to X-rays in the region of 10^{-12} torr. However, in order to overcome the electron space-charge oscillations arising at low pressures due to this very high sensitivity, the gauge has to be operated at an electron current of 10^{-7} amps or less. This method of electron injection into the electron-orbit ionisation gauge should find useful application in the ioniser of a radial field ion pump. The oscillating electron mode produces a directed beam of ions and thus the X-ray limit of an ionisation gauge that uses the oscillating electron mode, could be eliminated by deflecting the ion beam onto a collector which is shielded from the X-rays generated at the anodes. However, the filament has to be run at a much higher temperature for the oscillating mode than for the orbiting mode. This is due to the restricted area of electron emission from the filament when operated under the high bias voltage conditions.

Magnetic fields have been shown to have a considerable destructive

influence upon the oscillating electron mode in both the thermionic and cold cathode forms of the twin wire oscillator, whereas the orbiting mode is only affected by relatively large magnetic fields. It is believed that the low pressure limit of about 10^{-6} torr for the discharge in the cold cathode oscillator is due to the presence of the earth's magnetic field. Further investigation of the influence of magnetic fields should be carried out using techniques that cancel out the earth's magnetic field in the vicinity of the oscillator, in order to confirm that the present low pressure limit of the self-sustained discharge is determined by the earth's magnetic field.

When constructing the twin wire oscillator, it was found that the anode separation was the important parameter to be considered, as when this was too small, no cold cathode discharge could be maintained. This is believed to be due to the initial velocity of the electrons having sufficiently large components along the x axis to cause the electrons to collide with one of the anodes before a useful ionising collision with a neutral gas molecule occurs. The variation of anode diameter has much less influence upon the performance of the oscillator and this has led to the use of larger diameter anodes and hence an improvement in the design of the ion source application of the oscillator. With the larger diameter anodes, the ion source can be operated at higher ion beam current densities with complete reliability. Ion beam current densities in excess of 100 $\mu A\ cm^{-2}$ at the specimen surface can be easily obtained with pressures in the region of 5×10^{-4} torr. The ion energy spectrum is broad with ion energies ranging from a few electron-volts up to energies equivalent to the region of the saddle-point potential. Future work directed towards the ion energy measurements should take into account any multiply charged ions or electrons that may be present in the ion beam.

A closer investigation of the influence of the electron yield from

the collector electrode should be carried out with a view to increasing the ionisation current, by using a material for the collector electrode that has a high secondary electron yield. Some form of specimen cooling or cooling of the anodes should be attempted in order to reduce the effects of radiation heating of the specimen from the anodes. In future, it may be advantageous to introduce the gas directly into the ion source tube rather than flooding the whole vacuum chamber. In this way, the gas load on the system would be reduced and may also allow the specimen stage to be maintained at a relatively low pressure with respect to the actual discharge region.

The improved ion source is very easy to construct and is entirely reliable in operation. It should find many applications in fields such as ion etching and polishing of specimens. Furthermore, the absence of magnetic fields would allow this ion source to be used in situations where the use of a Penning type ion source would be undesirable.

APPENDIX 1.

COMPARISON OF THE PENNING GAUGE AND IOG 13T GAUGE PRESSURES.

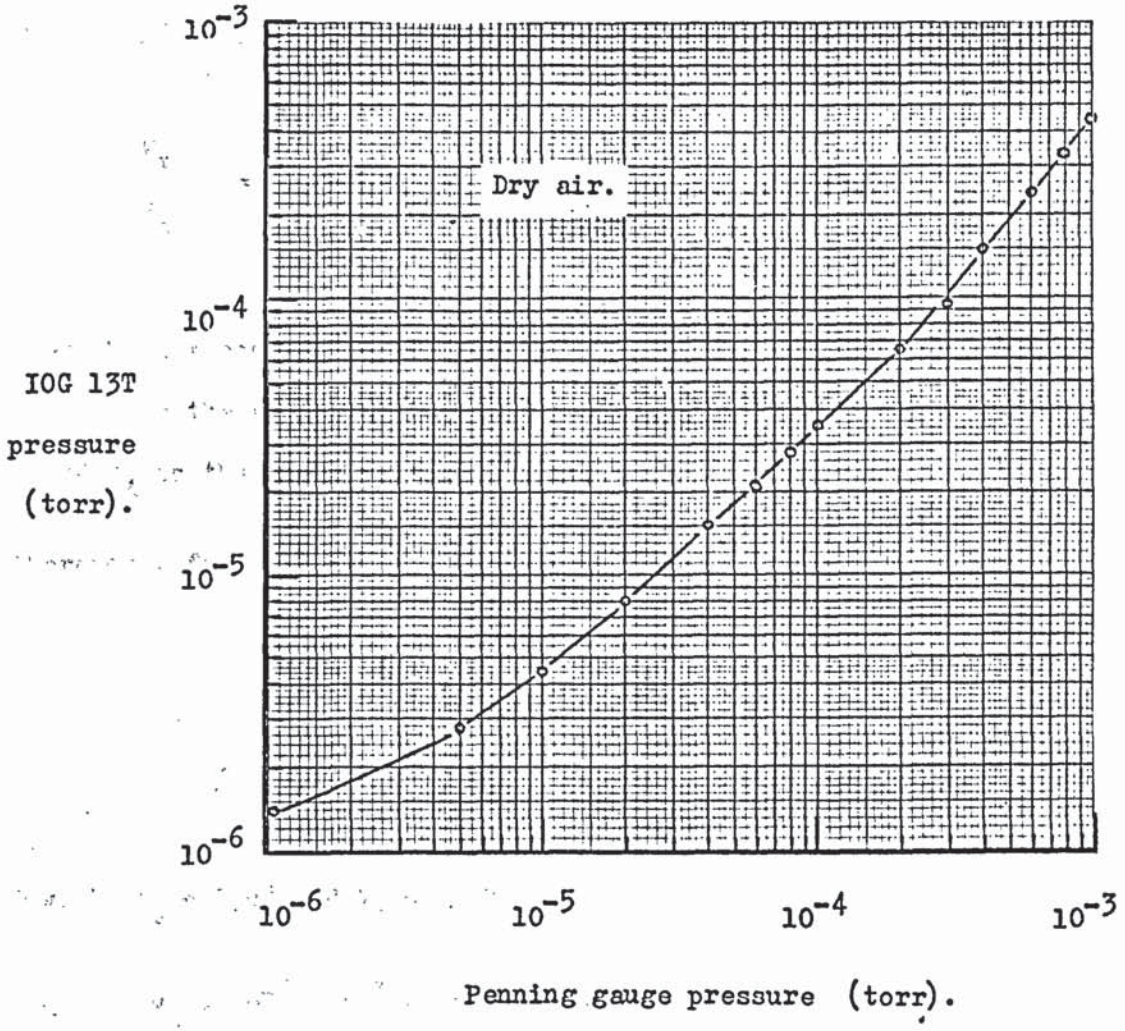

APPENDIX 2.

CALCULATION OF THE LOW PRESSURE LIMIT DUE TO X - RAYS OF THE ELECTRON - ORBIT IONISATION GAUGE.

The efficiency ϵ of producing X-rays at the anode by electron bombardment is given by :-

$$\epsilon = \frac{\text{Rate of energy loss due to X-ray emission from the anode.}}{\text{Rate of energy gain due to electron collection at the anode.}}$$

$$= \frac{W_X}{W_e} = K Z V_A \quad \ldots\ldots\ldots\ldots\ldots\ldots \text{(i)}.$$

where K is a constant = 10^{-9} volts^{-1},

Z is the atomic number = 74 for tungsten

and V_A is the anode voltage = 1 kV.

Therefore, from (i) :-

$$W_X = \epsilon W_e$$

$$\therefore W_X = K Z V_A W_e$$

Now, if i_a = 1 μA and V_A = 1 kV,

then $W_e = 10^{-6} \times 10^{3} = 10^{-3}$ watts.

$\therefore W_X = 10^{-3} \times 10^{-9} \times 74 \times 10^{3}$

$\therefore \underline{W_x = 7.4 \times 10^{-8} \text{ watts.}}$

Assuming that the electrons produce X-rays & transfer all of their energy eV_A into photon energy, then the number n_x of X-ray photons ejected per second is given by :-

$$n_x = \frac{W_X}{\text{X-ray photon energy}} = \frac{7.4 \times 10^{-8}}{1.6 \times 10^{-19} \times 10^3}$$

$$\therefore \underline{n_x = 4.6 \times 10^8 \text{ X-rays sec}^{-1}.}$$

Now, if all of the X-rays strike the collector, then the number of electrons n_e ejected from the collector will be :-

$$n_e = Q \cdot n_x \quad \text{electrons sec}^{-1},$$

where Q is the quantum efficiency of a material for a particular photon energy.

For X-rays of 1000 volts energy, Q for tungsten is 10^{-2}. Hence,

$$n_e = 10^{-2} \times 4.6 \times 10^8 \text{ electrons sec}^{-1}.$$

$$\therefore \underline{n_e = 4.6 \times 10^6 \text{ electrons sec}^{-1}.}$$

Therefore, the residual X-ray current $i_x = e\, n_e$, where e is the electronic charge.

$$\therefore i_x = 1.6 \times 10^{-19} \times 4.6 \times 10^6$$

$$\therefore \underline{i_x = 7.4 \times 10^{-13} \text{ amps.}}$$

The collector electrode and end-plates will intercept approximately 50% of the X-rays. Therefore, i_x for the open collector will be :-

$$\underline{i_x = \frac{7.4}{2} \times 10^{-13} = 3.7 \times 10^{-13} \text{ amps.}}$$

The low pressure limit due to X-rays is when $i_p \longrightarrow i_x$. Now, the sensitivity S is given by :-

$$S = \frac{i_p}{i_a} \times \frac{1}{P} \quad \text{torr}^{-1}$$

where i_p = the ion current,

i_a = the anode current $\simeq i_e$

and P = the total gas pressure.

Therefore, letting $i_p = i_x$ and taking S as 3×10^5 torr^{-1}, the low pressure limit P_x due to X-rays will be given by :-

$$P_x = \frac{i_x}{i_a} \times \frac{1}{S} = \frac{3.7 \times 10^{-13}}{10^{-6}} \times \frac{1}{3 \times 10^5}$$

$$\therefore \underline{P_x \simeq 10^{-12} \text{ torr.}}$$

Thus, the low pressure limit due to X-rays will be in the region of 10^{-12} torr, which will be independent of i_a. This low pressure limit due to X-rays can be reduced further by electrically isolating the end-plates from the collector electrode.

Appendix 3.

CHARACTERISTICS OF THE COLD CATHODE OSCILLATOR.

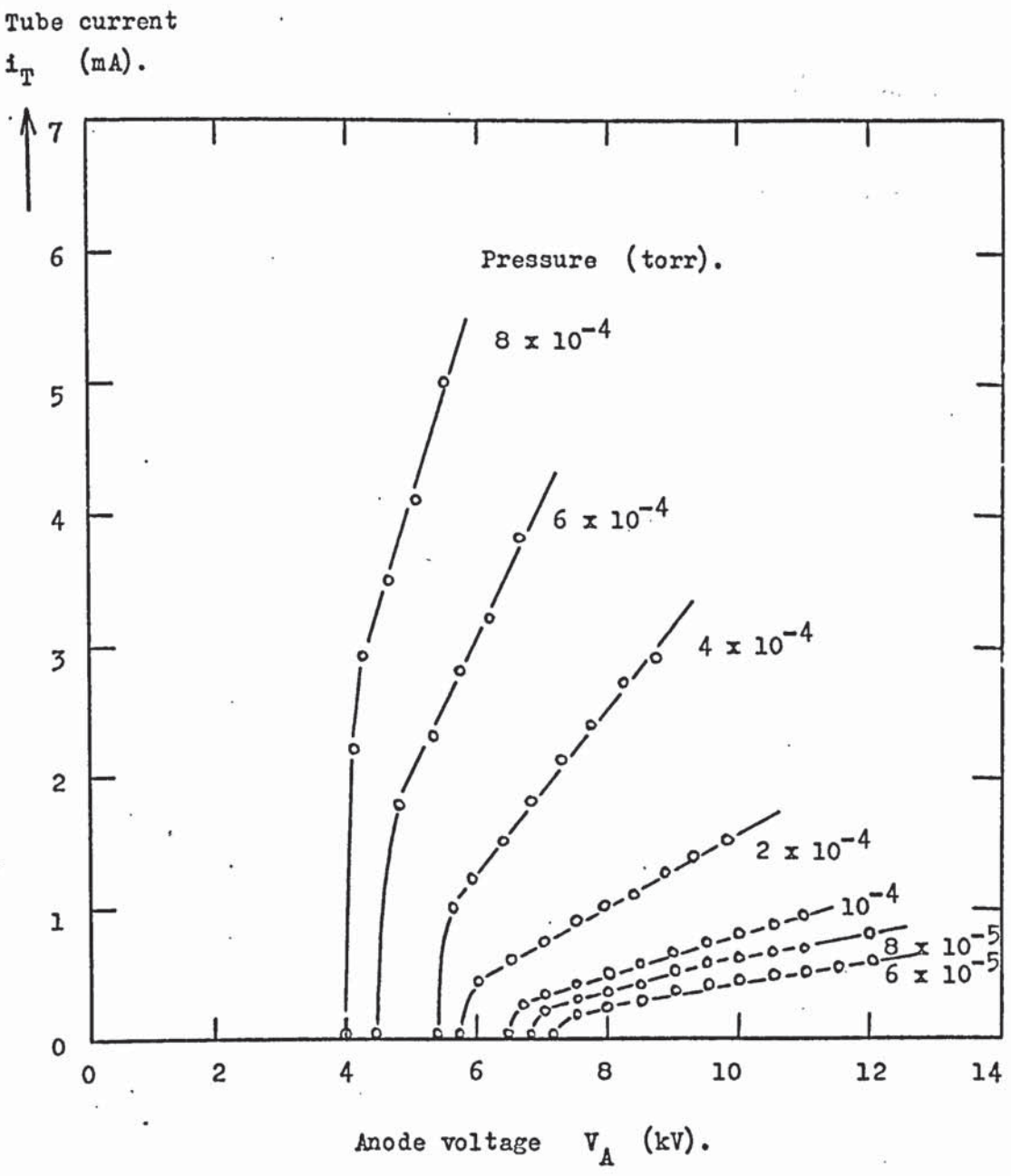

Collector electrode tube length = 10 cm.

Appendix 3. (continued).

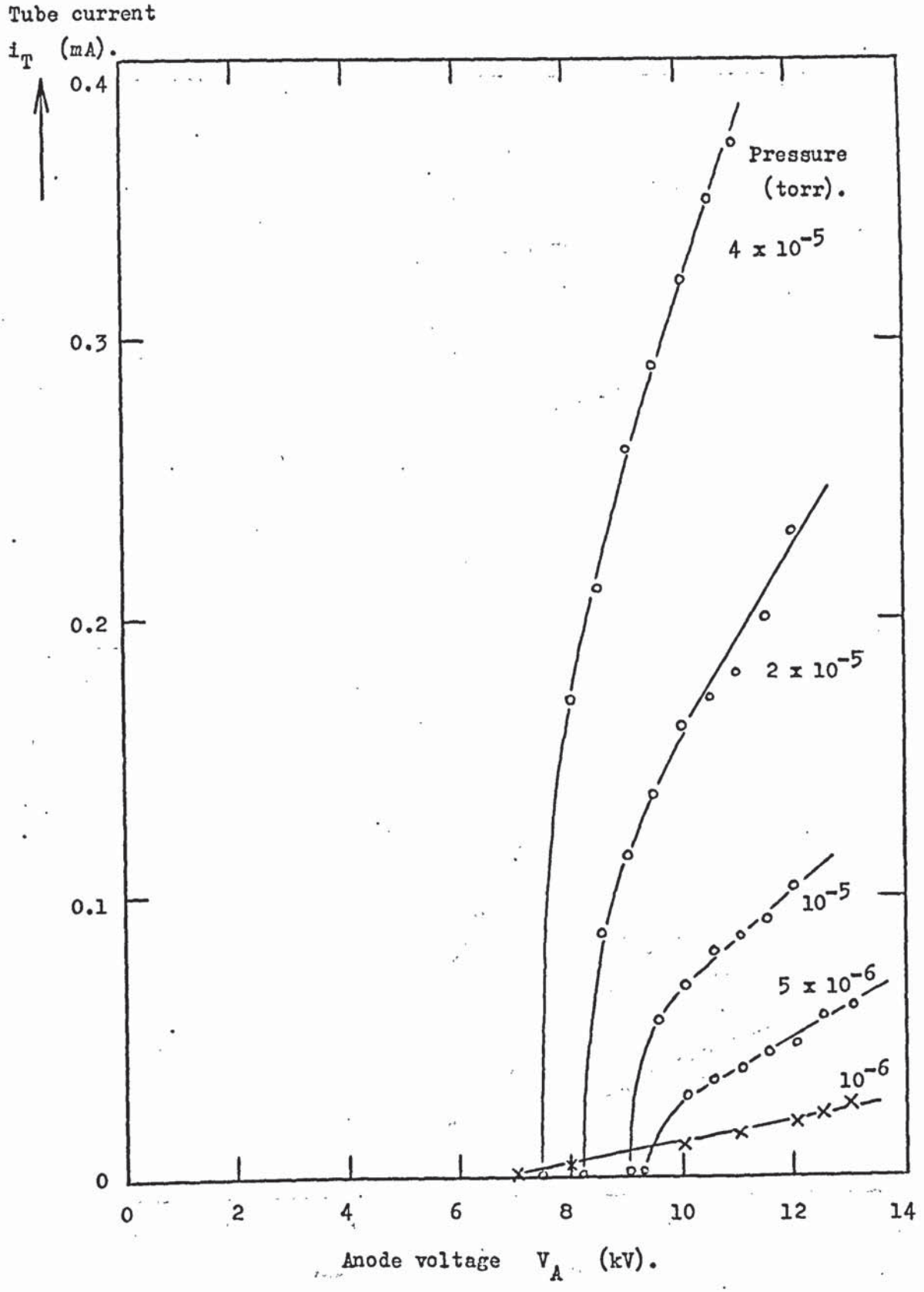

Collector electrode tube length = 10 cm.

Appendix 3. (continued).

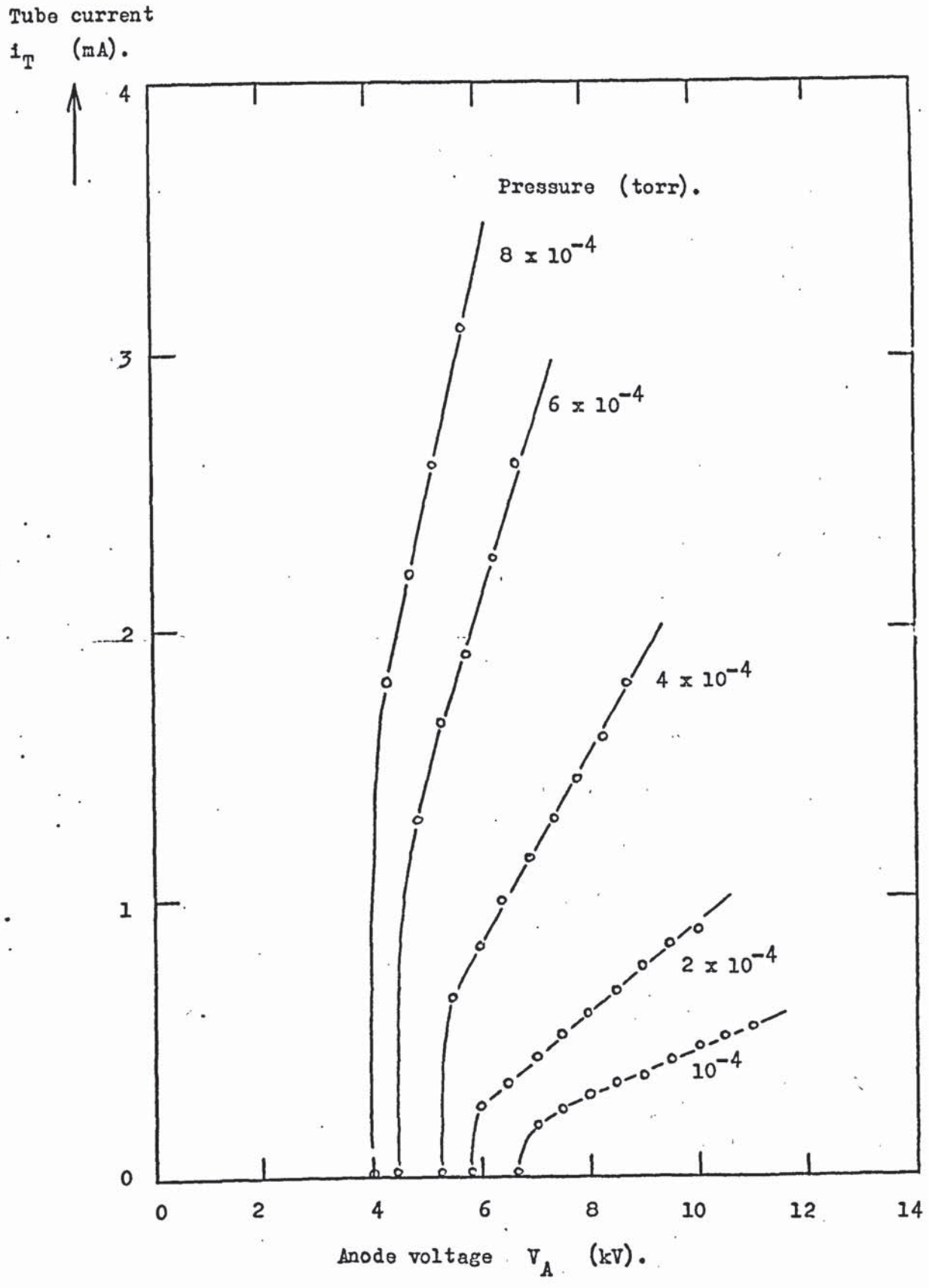

Collector electrode tube length = 7.5 cm.

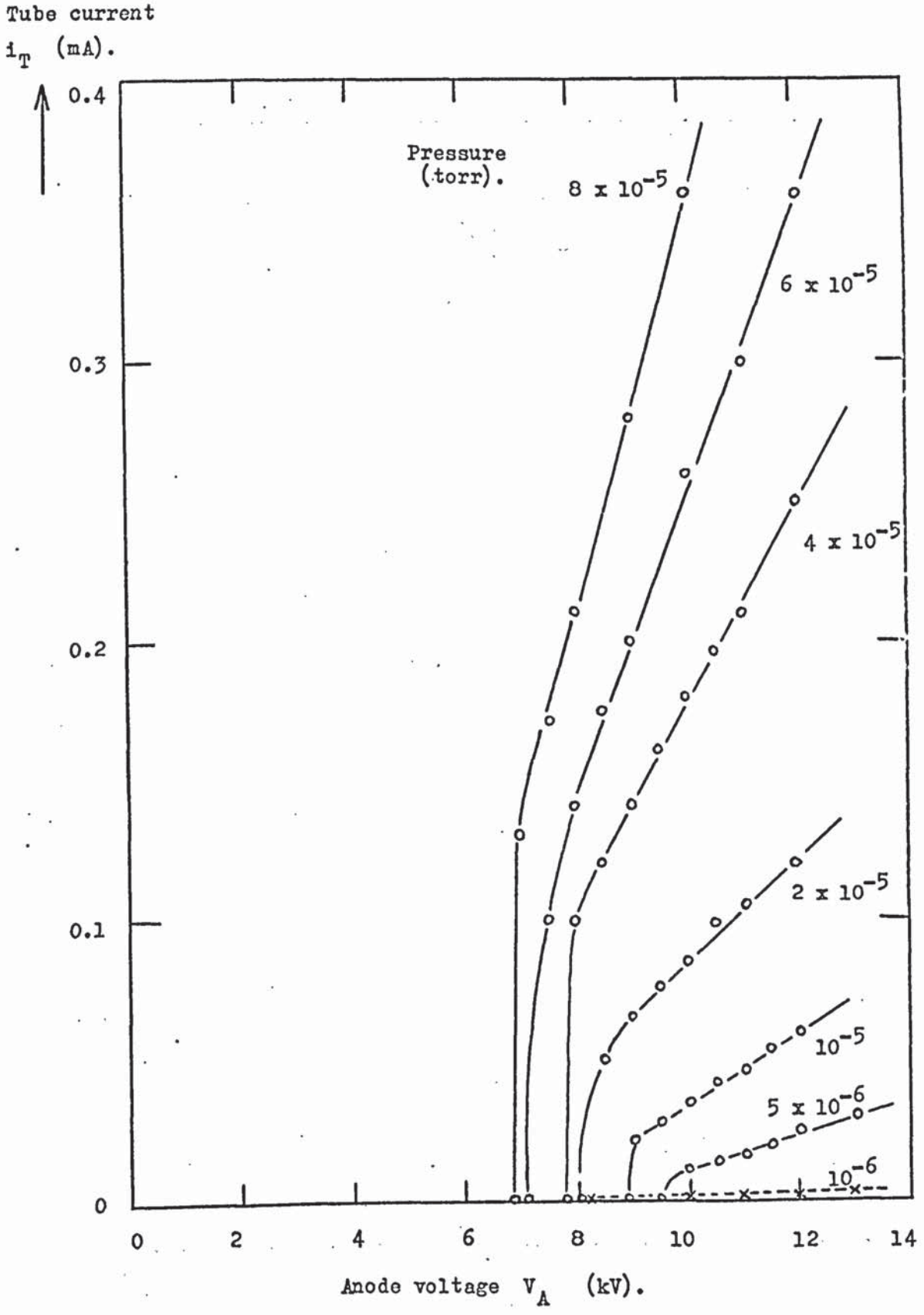

Collector electrode tube length = 7.5 cm.

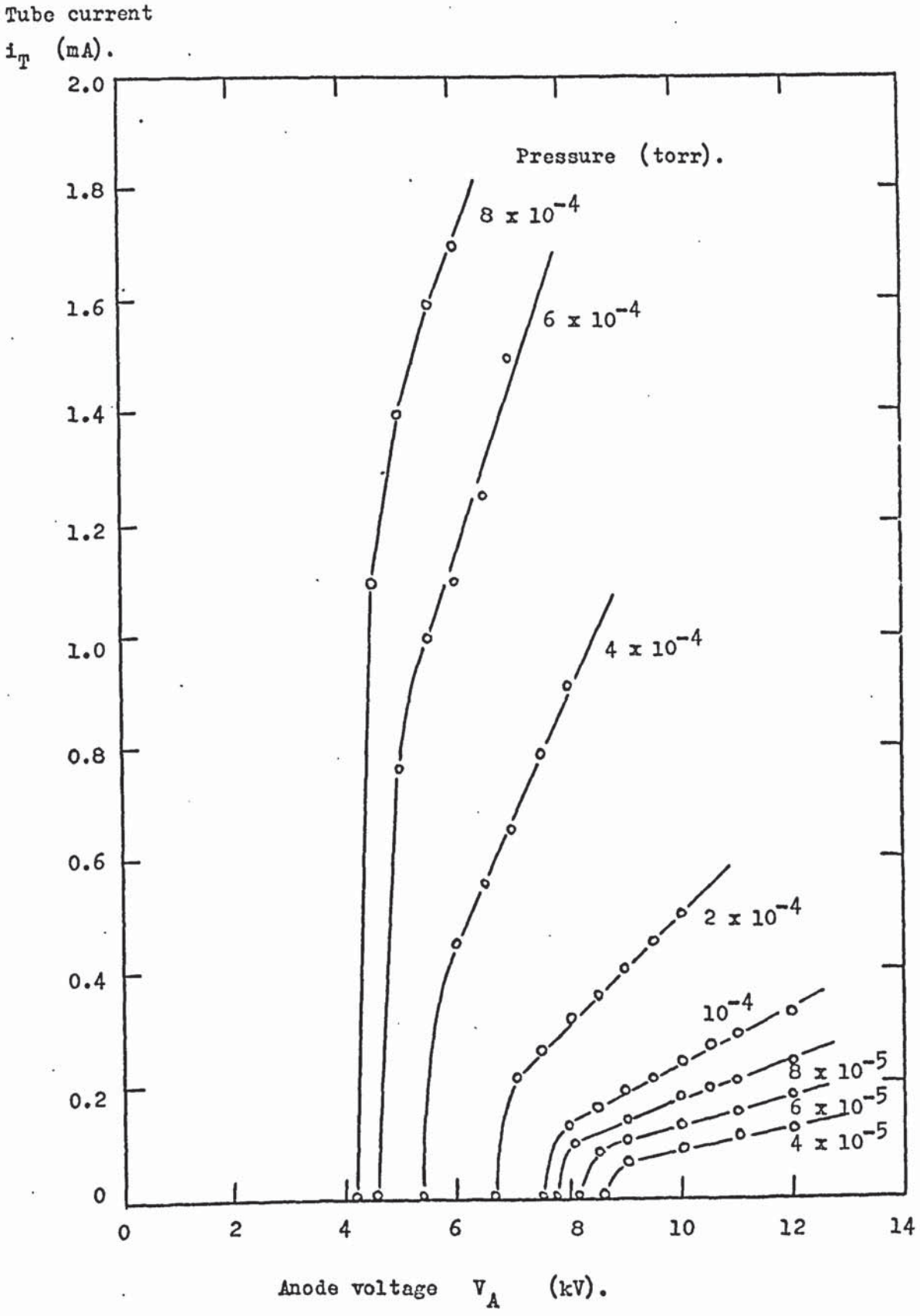

Collector electrode tube length = 5 cm.

APPENDIX 4.

THE VARIATION OF TUBE CURRENT WITH ANODE SEPARATION.

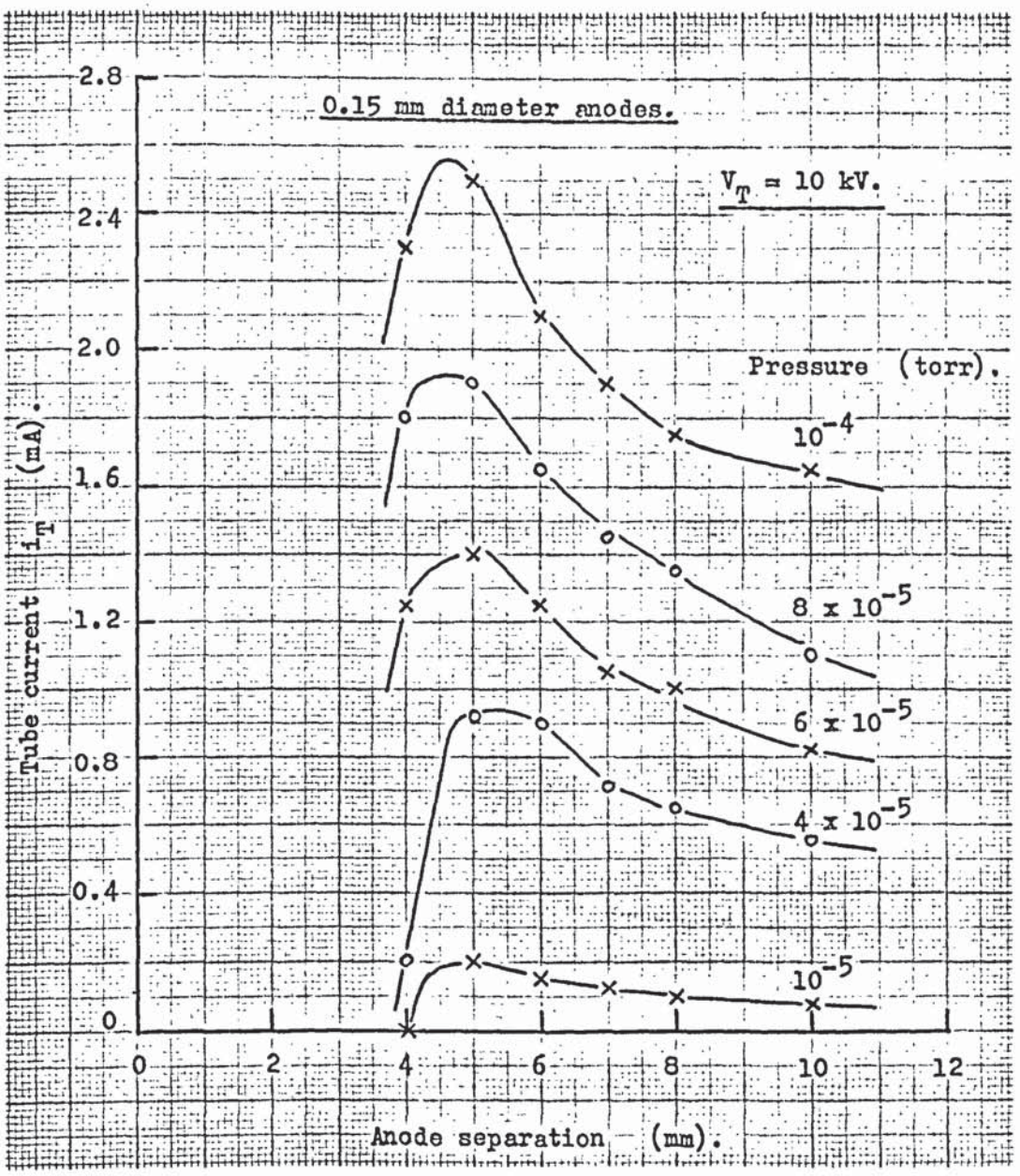

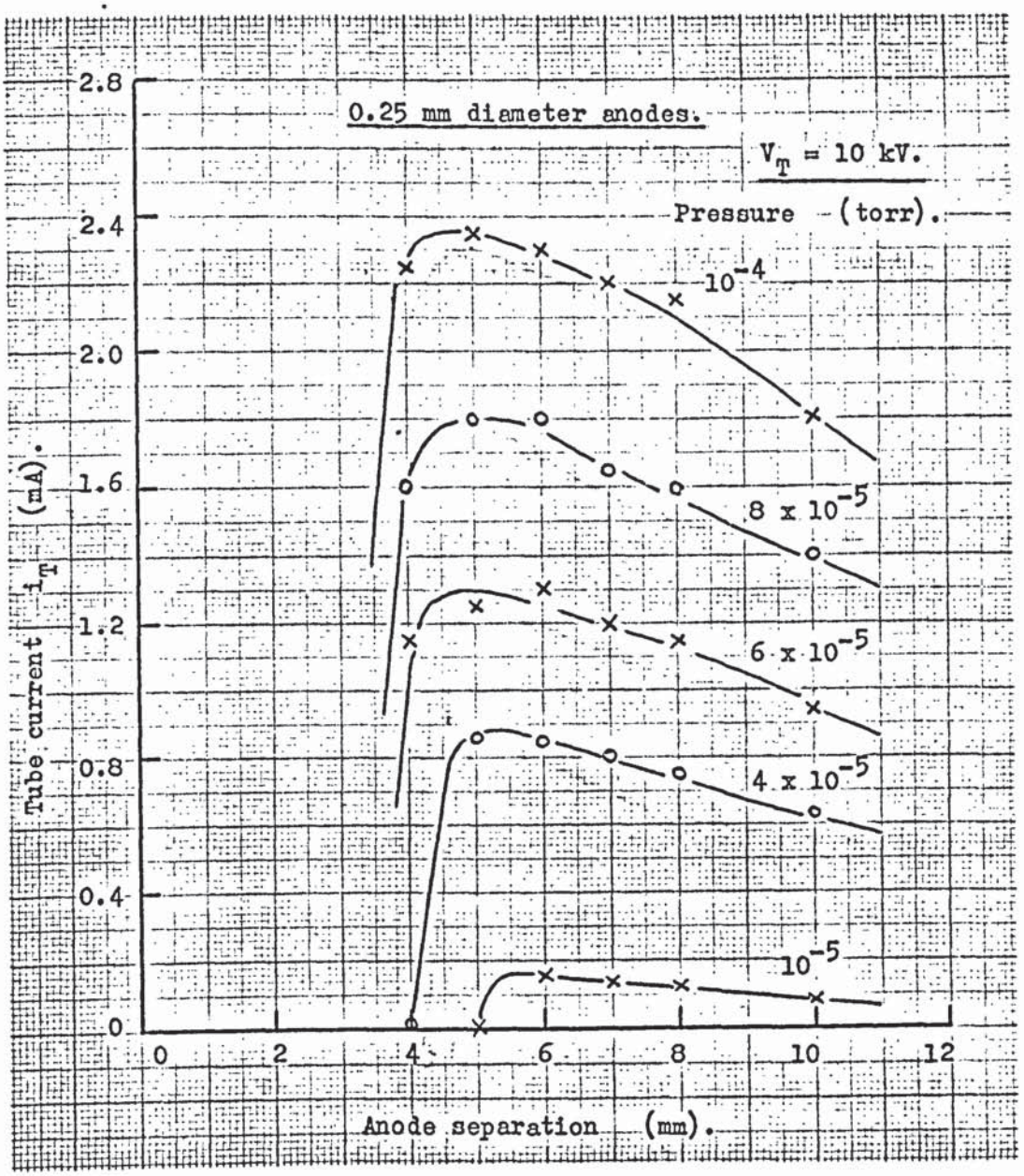
0.25 mm diameter anodes.
V_T = 10 kV.
Pressure (torr).
10^{-4}
8×10^{-5}
6×10^{-5}
4×10^{-5}
10^{-5}
Tube current i_T (mA).
Anode separation (mm).
0
0.4
0.8
1.2
1.6
2.0
2.4
2.8
0
2
4
6
8
10
12

Appendix 4. (continued).

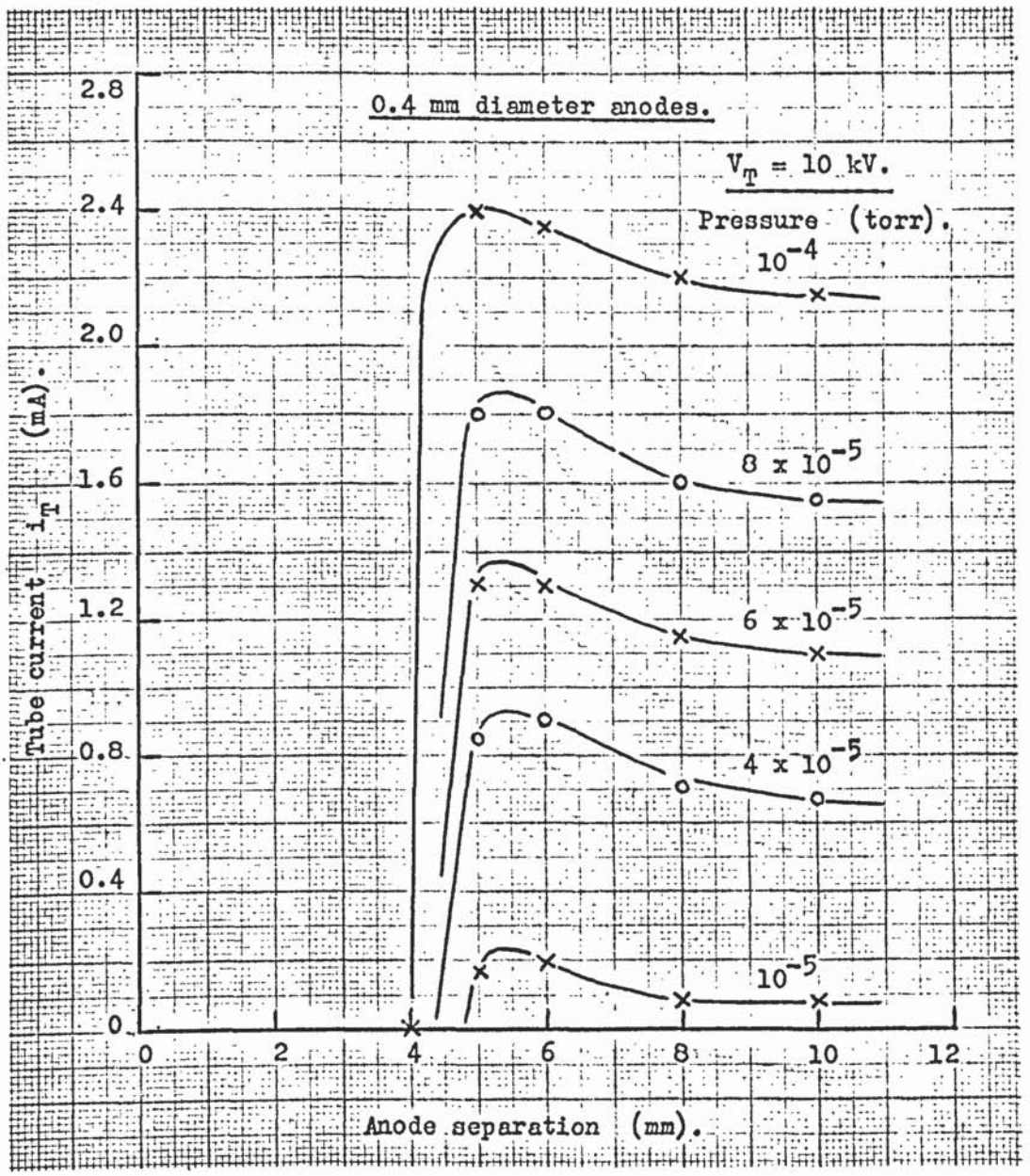

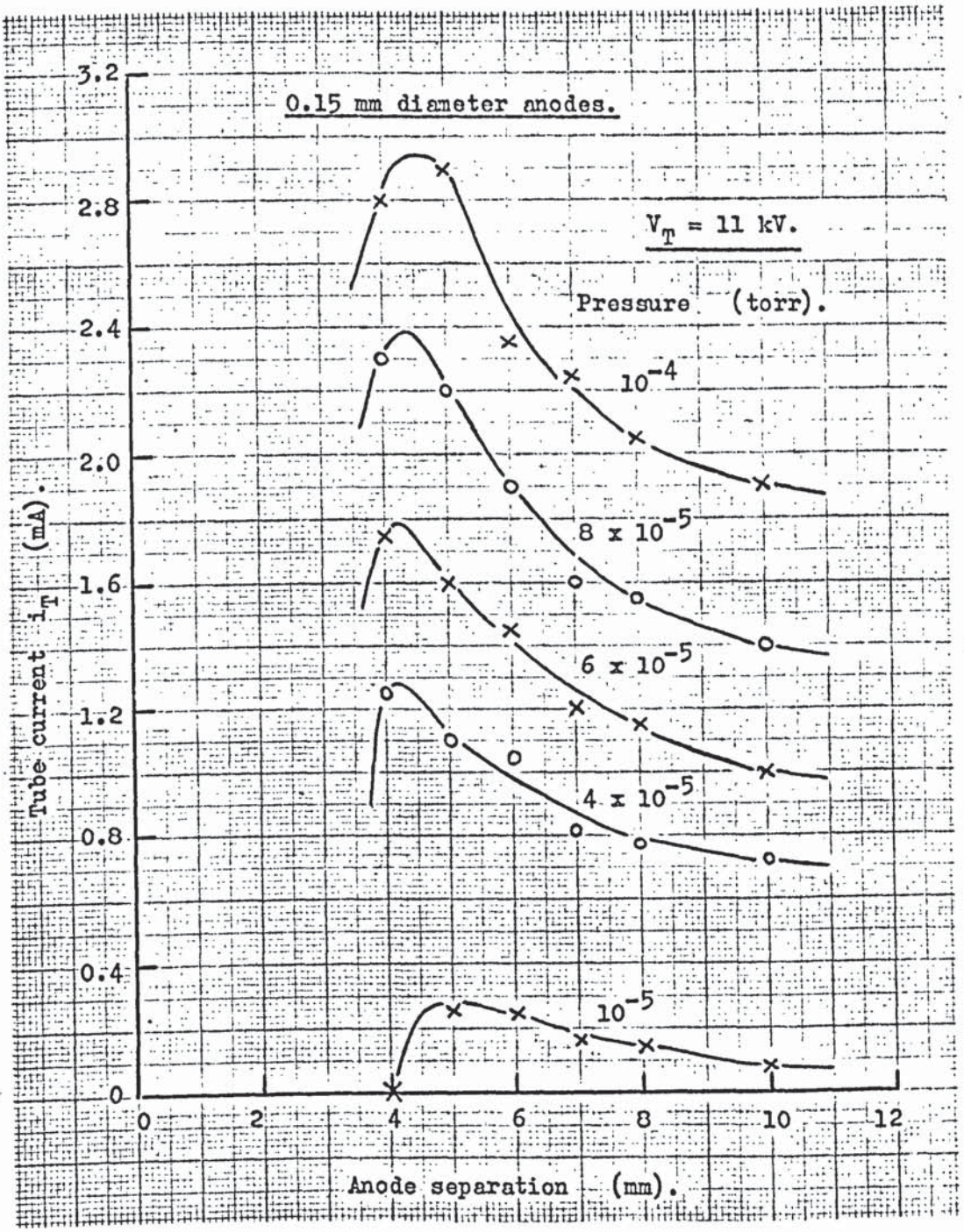
0.15 mm diameter anodes.
V_T = 11 kV.
Pressure (torr).
10^{-4}
8×10^{-5}
6×10^{-5}
4×10^{-5}
10^{-5}
Tube current i_T (mA).
Anode separation (mm).
0
0.4
0.8
1.2
1.6
2.0
2.4
2.8
3.2
0
2
4
6
8
10
12

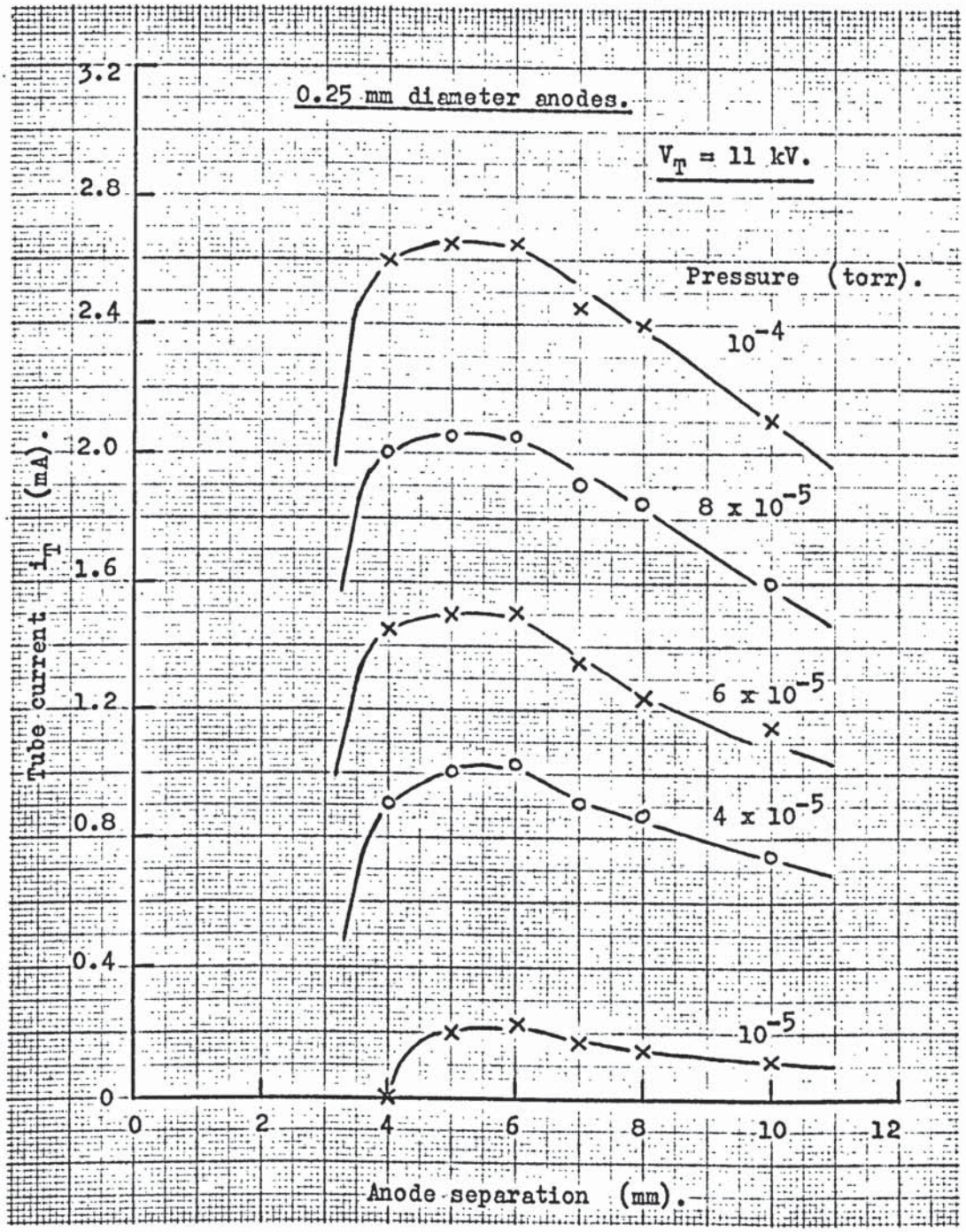
0.25 mm diameter anodes.
V_T = 11 kV.
Pressure (torr).
10^{-4}
8×10^{-5}
6×10^{-5}
4×10^{-5}
10^{-5}
Tube current i_T (mA).
Anode separation (mm).
0
0.4
0.8
1.2
1.6
2.0
2.4
2.8
3.2
0
2
4
6
8
10
12

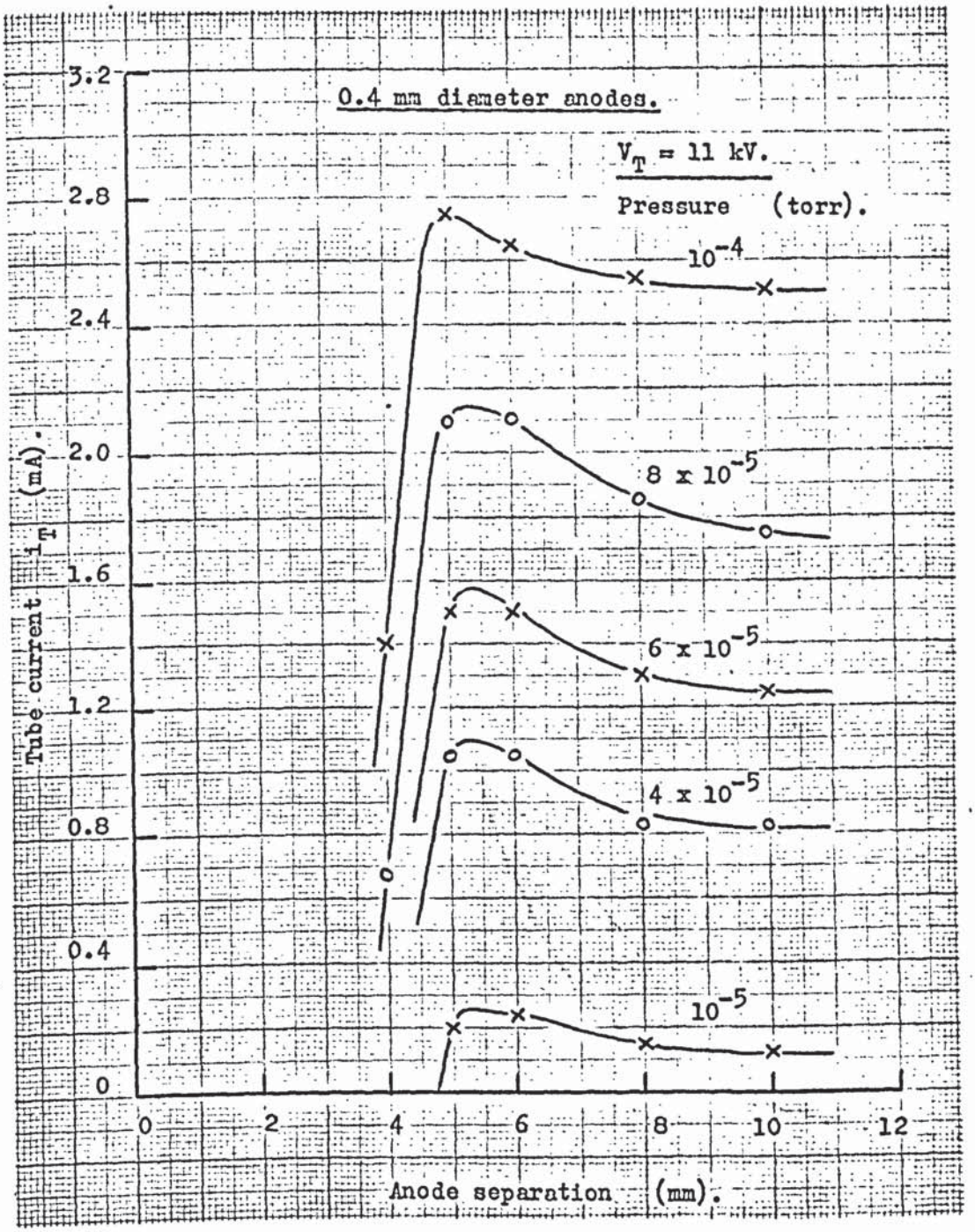
0.4 mm diameter anodes.
V_T = 11 kV.
Pressure (torr).
10^{-4}
8×10^{-5}
6×10^{-5}
4×10^{-5}
10^{-5}
Tube current I_T (mA).
3.2
2.8
2.4
2.0
1.6
1.2
0.8
0.4
0
0
2
4
6
8
10
12
Anode separation (mm).

APPENDIX 5.

THE MAGNET CALIBRATION CURVE.

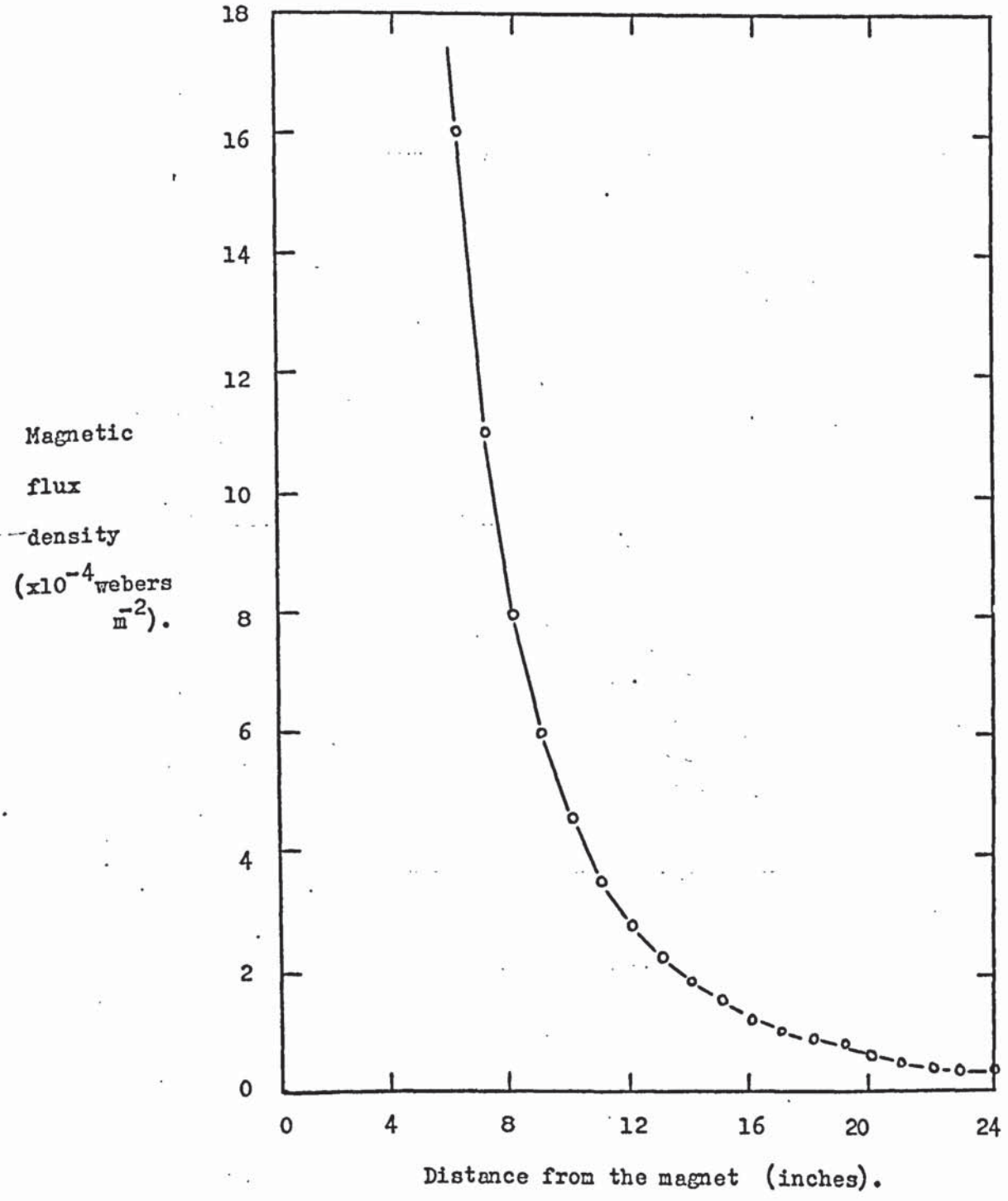

APPENDIX 6.

ION BEAM CURRENT DENSITIES OBTAINED FROM THE IMPROVED ION SOURCE.

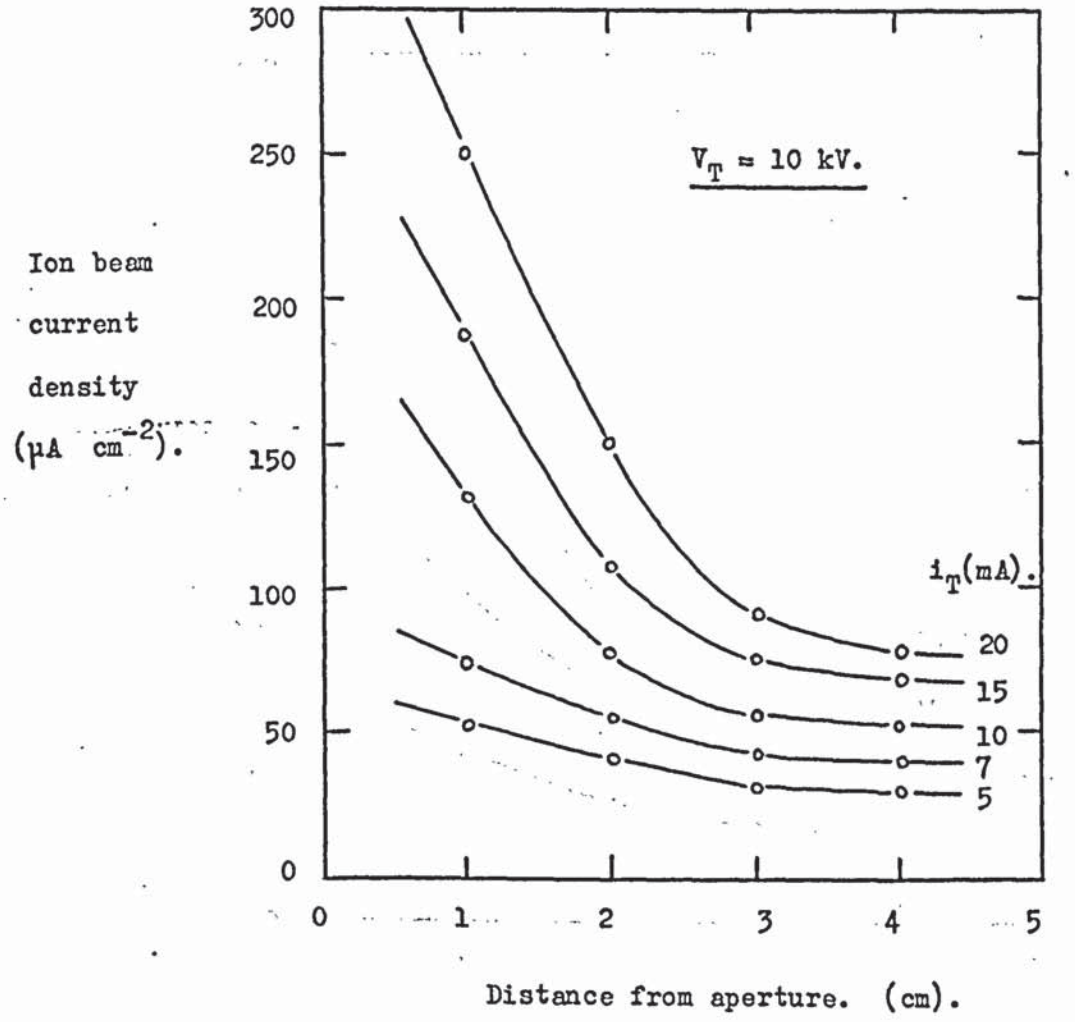

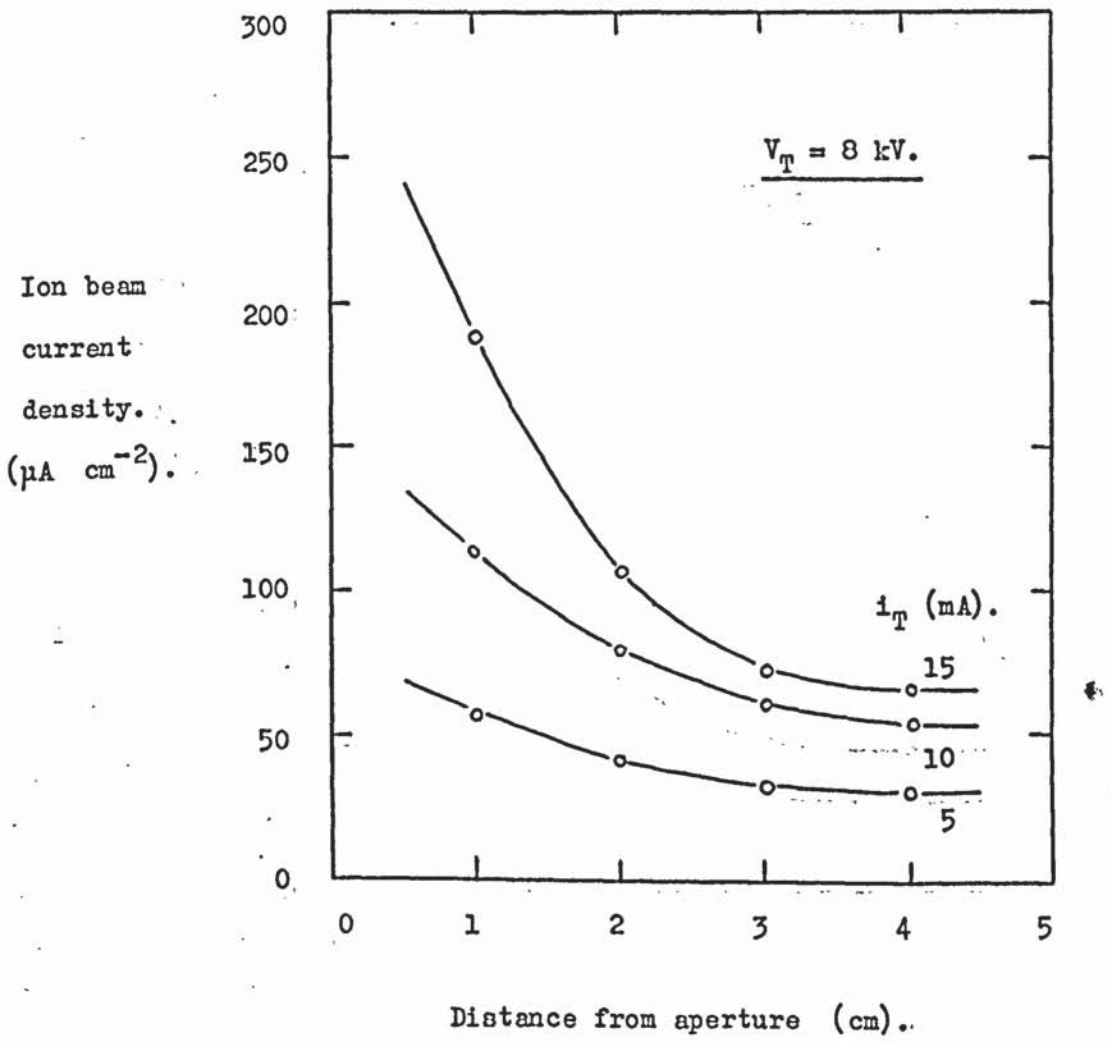
300
250
200
150
100
50
0
0
1
2
3
4
5
V_T = 8 kV.
i_T (mA).
15
10
5
Ion beam current density. (μA cm^{-2}).
Distance from aperture (cm).

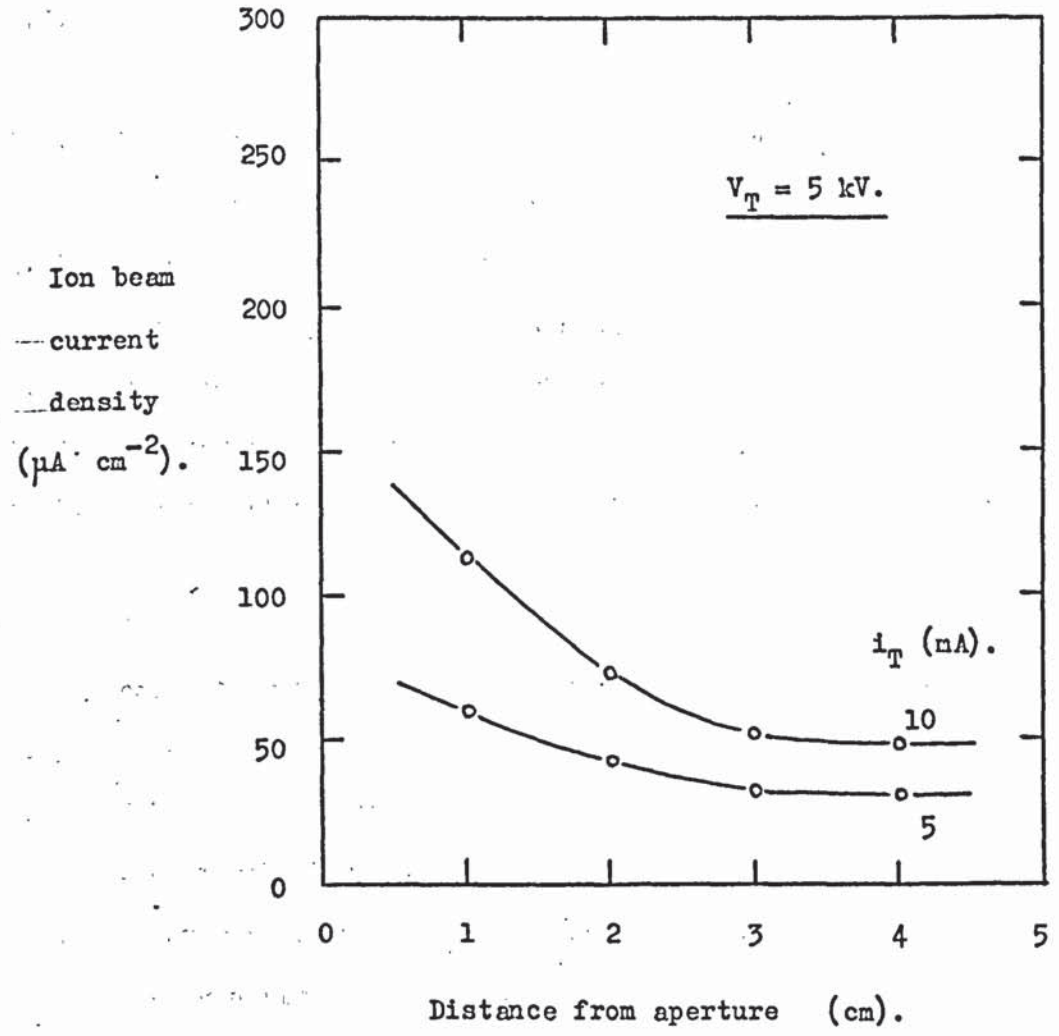
300
250
200
150
100
50
0
V_T = 5 kV.
Ion beam current density ($\mu A \cdot cm^{-2}$).
i_T (mA).
10
5
0
1
2
3
4
5
Distance from aperture (cm).

List of Figures.

1.1. Electrode structure for the Penning discharge.

1.2. Cutaway diagram of the inverted magnetron gauge.

1.3. The Lafferty gauge.

1.4. The Nielsen ion source.

1.5. The Bayard-Alpert ionisation gauge.

1.6. The radial field electrostatic ion pump.

1.7. The orbitron ionisation gauge.

1.8. Electron trajectories.

1.9. Variation of sensitivity with the ratio V_B/V_A.

1.10. Schematic diagram of the twin wire oscillator in the xy plane.

1.11. Potential at a point P(x,y).

1.12. Schematic diagram of the twin wire oscillator in the xz plane.

1.13. The ion etched regions on the collector surface.

1.14. The variation of sensitivity with V_B/V_A.

1.15. The variation of sensitivity with V_B/V_A for the nude oscillator.

2.1. The thermionic twin wire oscillator with a collector electrode consisting of 32 tungsten rods.

2.2. End-plate for the twin wire oscillator.

2.3. Schematic diagram of the twin wire oscillator and the associated electrical circuit.

2.4. The variation of collector current with filament bias voltage in the twin wire oscillator.

2.5. The distribution of the lines of equipotential in the various collector electrode geometries.

2.6. The distribution of the lines of equipotential in the single plate anode device.

2.7. The variation of collector electrode current with filament bias voltage in the single plate anode device.

2.8. The variation of the lines of equipotential in the field around the filament with change in filament bias voltage.

2.9. The effect of filament rotation about the anode wires.

2.10. Modes of operation in the twin wire oscillator.

2.11. Demonstration of the dependence of the oscillating mode upon the anode voltage.

2.12. Variation of the maximum value of i_c for the orbiting peak with change of filament immersion depth.

2.13. Composite electron modes.

3.1. The electron-orbit ionisation gauge and its electrical circuit.

3.2. The potential distribution inside the electron-orbit ionisation gauge.

3.3. The variation of collector electrode current with filament bias voltage at a pressure of 1.4×10^{-5} torr.

3.4. The variation of sensitivity with pressure.

3.5. Filament orientations.

3.6. Schematic diagram of the electron-orbit ionisation gauge for use in ultra high vacuum.

3.7. The electron-orbit ionisation gauge for use in ultra high vacuum.

3.8. Schematic diagram of the ultra high vacuum system.

3.9. The ultra high vacuum system.

3.10. The bias characteristics of the electron-orbit ionisation gauge in ultra high vacuum.

3.11. Modification of the low pressure bias characteristic by the presence of a magnetic field.

3.12. The bias characteristics for the electron-orbit ionisation gauge using a reduced electron emission current.

3.13. The variation of collector current with pressure.

3.14. The variation of sensitivity with pressure.

4.1. The cold cathode twin wire oscillator.

4.2. Circuit for the cold cathode twin wire oscillator.

4.3. Characteristics of the cold cathode oscillator.

4.4. The variation of tube current with anode separation.

4.5. Conservation of angular momentum of an electron.

4.6. Discharge characteristics when using the aluminium collector.

5.1. The Larmor precession.

5.2. The variation of tube current with applied magnetic field.

5.3. The variation of cut-off pressure with cut-off magnetic field.

5.4. The variation of collector electrode current with applied magnetic field for the thermionic twin wire oscillator.

5.5. The variation of collector electrode current with applied magnetic field when using a single anode wire.

6.1. Schematic diagram of the improved ion source.

6.2. Definition of the surface to surface anode separation.

6.3. The variation of tube current with tube voltage for the improved ion source.

6.4. The positive ion current distribution from the cold cathode discharge.

6.5. The Faraday cage.

6.6. The variation of ion beam current density with distance from the ion source aperture.

6.7. The electrode arrangement for the ion energy analysis.

6.8. The variation of Faraday cup current with retarding voltage.

6.9. The resulting ion energy spectrum.

6.10. The variation of Faraday cup current with retarding voltage when using a tube voltage of 4 kV.

6.11. The possible ion energy spectrum.

6.12. Examples of ion etching using the improved ion source.

6.13. The interior surface of the 10 cm long collector electrode.

6.14. The multiple beam ion source.

6.15. The wide beam ion source.

List of main symbols.

a	=	Anode radius.
b	=	Collector electrode radius.
$\underline{B}, B_x$	=	Magnetic field.
d	=	Half the anode centre to centre separation.
D	=	Filament immersion depth.
e	=	Electron charge.
E, E_x	=	Electrostatic field.
$\underline{F}, F_x$	=	Force on an electron.
i_a	=	Anode current.
i_c	=	Collector electrode current.
i_e	=	Emission current.
i_F	=	Faraday cup current.
i_T	=	Tube current.
$\underline{L}$	=	Angular momentum.
m	=	Mass of electron.
P, p	=	Pressure.
q	=	Charge per unit length.
T	=	Period of electron oscillation.
V_A	=	Anode voltage.
V_B	=	Filament bias voltage.
V_R	=	Retarding voltage.
V_T	=	Tube voltage.
$V_{x,y}$	=	Potential at a point P(x,y).
$\underline{v}, v_x$	=	Electron velocity.
x, y, z	=	Co-ordinate axes.
ϵ	=	Dielectric constant.
ϵ_o	=	Permitivity of free space.

References.

1. Penning, F.M. — Physica, 4, 71, (1937).

2. Penning, F.M. and Nienhuis, K. — Philips Tech. Rev., 11, 116, (1949).

3. McIlwraith, C.G. — Rev. Sci. Inst., 18, 683, (1947).

4. Chernatony, L. de and Crawley, D.J. — Vacuum, 20, 389, (1970).

5. Redhead, P.A. — Canad. J. Phys., 37, 1260, (1959).

6. Hobson, J.P. and Redhead, P.A. — Canad. J. Phys., 36, 271, (1958).

7. Hall, L.D. — Rev. Sci. Inst., 29, 367, (1958).

8. Jepsen, R.L., Francis, A.B., Rutherford, S.L. and Kietzmann, B.E. — Trans. 7th. A.V.S. Vacuum Symp. 1960, Pergamon Press (New York), p.45,1961.

9. Brubaker, W.M. — Trans. 6th. A.V.S. Vacuum Symp. 1959, Pergamon Press (New York), p.302, 1960.

10. Andrew, D., Sethna, D.R. and Weston, G.F. — Proc. 4th. Internl. Vacuum Congress, p. 337, (1968).

11. Stuart, P.R., Osborn, J.S. and Lewis, S.M. — Vacuum, 19, 503, (1969).

12. Lamar, E.S., Buechner, W.W. and Van de Graaff, R.J. — J. App. Phys., 12, 133, (1941).

13. Barnett, C.F., Stier, P.M. and Evans, G.E. — Rev. Sci. Inst., 24, 394, (1953).

14. Houston, J.M. — Bull. Am. Phys. Soc. II, 1, 301, (1956).

15. Lafferty, J.M. — J. App. Phys., 32, 424, (1961).

16. Nielsen, K.O. — Proc. Int. Conf. on Applications of Ion Beams to Semiconductor Technology, Grenoble, France, p.27, (1967).

17. Bayard, R.T. and Alpert, D. — Rev. Sci. Inst., 21, 571, (1950).

18. Redhead, P.A. — Rev. Sci. Inst., 31, 343, (1960).

19. Schuemannn, W.C. — Rev. Sci. Inst., 34, 700, (1963).

20. Khan, M. and Schroeer, J.M. — Rev. Sci. Inst., 42, 1348, (1971).

21. Gabor, D. — British Patent 887 251, (1962).

22. Herb R.G., Pauly, T. and Fisher, K.J. — Bull. Am. Phys. Soc., 8, 336, (1963).

23. Mourad, W.G., Pauly, T. and Herb, R.G. — Rev. Sci. Inst., 35, 661, (1964).

24. Hooverman, R.H. — J. App. Phys., 34, 3505, (1963).

25. White, A.D. and Perry, D.L. — Rev. Sci. Inst., 32, 730, (1961).

26. Meyer, E.A. and Herb, R.G. — J. Vac. Sci. Tech., 4, 63, (1967).

27. Gammon, R.B. — Vacuum, 17, 379, (1967).

28. Fitch, R.K., Norris, T.J. and Thatcher, W.J. — Vacuum, 19, 227, (1969).

29. Gosselin, C.M., Beitel, G.A. and Smith, A. — J. Vac. Sci. Tech., 7, 233, (1970).

30. Douglas, R.A., Zabritski, J. and Herb, R.G. — Rev. Sci. Inst., 36, 1, (1965).

31. Bills, D.G. — J. Vac Sci. Tech., 4, 149, (1967).

32. McIlraith, A.H. — Nature, 212, 1422, (1966).

33. McIlraith, A.H. — Paper submitted to 5th. Int. Vacuum Conf., (1971).

34. Thatcher, W.J. — Ph.D. Thesis, University of Aston in Birmingham, (1970).

35. McIlraith, A.H. — Notes on the initiation of a self-sustained discharge (unpublished), 1969.

36. McIlraith, A.H. — Notes on a charged particle oscillator (unpublished).

37. Fitch, R.K., Mulvey, T., Thatcher, W.J. and McIlraith, A.H. — J. Phys. D : App. Phys., 3, 1399, (1970).

38. Fitch, R.K., Mulvey, T., Thatcher, W.J. and McIlraith, A.H. — J. Phys. E : Sci. Inst., 4, 553, (1971).

39. Haine, M.E. and Einstein, P.A. — Brit. J. App. Phys., 3, 40, (1952).

40. Fitch, R.K. and Rushton, G.J. — Vacuum, 20, 445, (1970).

41. Fitch, R.K. and Rushton, G.J. — British Patent Application (1970), No. 31142/70.

42. Fitch, R.K. and Rushton, G.J. — Vacuum, 20, 535, (1970).

43. Fitch, R.K. and Rushton, G.J. — Vacuum, 21, 453, (1971).

44. Dushman, S. Scientific Foundations of Vacuum Technique, 2nd. Ed., John Wiley and Sons, p.301, (1962).

45. Jenkins, R.O. Vacuum, 19, 353, (1969).

46. Rushton, G.J. and Fitch, R.K. Vacuum, 21, 449, (1971).

47. Hagstrum, H.D. Phys. Rev., 89, 244, (1953).

48. Fitch, R.K. and Rushton, G.J. J. Vac Sci. Tech., 9, 379, (1972).

49. Simpson, J.A. Rev. Sci. Inst., 32, 1283, (1961).

50. Spencer, E.G. and Schmidt, P.H. J. Vac. Sci. Tech., 8, 52, (1971).

51. Barber, D.J. J. Mat. Sci., 5, 1, (1970).

52. McIlraith, A.H. Private Communication, (1971).

Acknowledgements.

I would like to thank my supervisor Dr. R. K. Fitch for his continual help, advice and encouragement throughout the course of this work. Thanks are also due to Dr. T. Mulvey for many helpful discussions.

Acknowledgements are due to Mr. F. Lane and the staff of the Physics Department Workshop, for their assistance in the construction of many of the devices described in this thesis.